UNIVERSITA' VITA-SALUTE SAN RAFFAELE

CORSO DI DOTTORATO DI RICERCA INTERNAZIONALE IN MEDICINA MOLECOLARE

Curriculum in Cellular and Molecular Biology

PATHOGENETIC EVENTS LEADING TO TUBULOINTERSTITIAL RENAL DAMAGE IN UROMODULIN-ASSOCIATED KIDNEY DISEASE

DoS: Prof. Luca Rampoldi

Second Supervisor: Prof. Irina Udalova

Tesi di DOTTORATO di RICERCA di Mariapia Giuditta Cratere

Matr. 015557

Ciclo di dottorato XXXV

SSD MED/03

Anno Accademico 2021/2022

UNIVERSITA' VITA-SALUTE SAN RAFFAELE

CORSO DI DOTTORATO DI RICERCA INTERNAZIONALE IN MEDICINA MOLECOLARE

Curriculum in Cellular and Molecular Biology

PATHOGENETIC EVENTS LEADING TO TUBULOINTERSTITIAL RENAL DAMAGE IN UROMODULIN-ASSOCIATED KIDNEY DISEASE

DoS: Prof. Luca Rampoldi

Second Supervisor: Prof. Irina Udalova

Tesi di DOTTORATO di RICERCA di Mariapia Giuditta Cratere

Matr. 015557

Ciclo di dottorato XXXV

SSD MED/03

Anno Accademico 2021/2022

RELEASE OF PHD THESIS

Il/la sottoscritto/a / *I, the undersigned*	**Mariapia Giuditta Cratere**
Matricola / *registration number*	**015557**
nat_ a/ *born in*	**Venosa (PZ)**
il/*on*	**24/04/1992**

autore della tesi di Dottorato di ricerca dal titolo/ *author of the PhD Thesis titled*

PATHOGENETIC EVENTS LEADING TO TUBULOINTERSTITIAL RENAL DAMAGE IN UROMODULIN-ASSOCIATED KIDNEY DISEASE

☐ AUTORIZZA la Consultazione della tesi / *AUTHORIZE the public release of the thesis*

☒ NON AUTORIZZA la Consultazione della tesi per **12 mesi** /*DO NOT AUTHORIZE the public release of the thesis for **12 months***

a partire dalla data di conseguimento del titolo e precisamente */ from the PhD thesis date, specifically*

Dal/from …/…/… Al/to …/…/…

Poiché/*because:*

☐ l'intera ricerca o parti di essa sono potenzialmente soggette a brevettabilità/ *The whole project or parts of it may be the subject of a patent application;*

☒ci sono parti di tesi che sono già state sottoposte a un editore o sono in attesa di pubblicazione/ *Parts of the thesis have been or are being submitted to a publisher or are in the press;*

☐la tesi è finanziata da enti esterni che vantano dei diritti su di esse e sulla loro pubblicazione/ *the thesis project is financed by external bodies that have rights over it and its publication.*

È fatto divieto di riprodurre, in tutto o in parte, quanto in essa contenuto / *reproduction of the thesis in whole or in part is forbidden*

Data /*Date* **22/12/2022** Firma /Signature

Mariapia G Cratere

DECLARATION

This thesis has been

- composed by myself and has not been used in any previous applicationfor a degree. Throughout the text I use both 'I' and 'We' interchangeably.
- has been written according to the editing guidelines approved by the University.

Permission to use images and other material covered by copyright has been sought and obtained. For the image in *Figure 50*, it was not possible to obtain permission and is therefore included in thesis under the "fair use" exception (Italian legislative Decree no. 68/2003).

All the results presented here were obtained by myself, except for:

1) Preliminary data on $Tg^{UmodC147W}$ mice at one day post-natal (*Introduction, 1.6 Preliminary data, Figure 9*) were produced by Matteo Trudu, Molecular Genetics of Renal Disorders Unit, Division of Genetics and Cell Biology, San Raffaele Scientific Institute, Milan (present address Age related diseases Unit, Division of Genetics and Cell Biology, San Raffaele Scientific Institute, Milan).

2) Characterization of $Tg^{UmodC147W}$ /$Ccr2^{-/-}$ mouse line at eight day post-natal and 24-weeks of age (*Results, Figure 10-12 and 21-24*) was performed in collaboration with Francesca Nicola, Molecular Genetics of Renal Disorders Unit, Division of Genetics and Cell Biology, San Raffaele Scientific Institute, Milan (present address Emerging bacterial pathogens Unit, Division of Immunology, Transplantation and Infectious Disease, San Raffaele Scientific Institute, Milan) during her Master thesis internship.

3) Histology staining (*Results, Figure 43D, 44D; Appendix Figure I.4D, I.5D*) were performed in collaboration with Dr. Barbara Canciani (Laboratory of Regenerative Medicine and Biomaterials, San Raffaele Scientific Institute, IRCSS Istituto Ortopedico Galeazzi, Milan).

4) Urea biochemistry analyses (*Results Figure 47.B; Appendix Figure I.8B*) were processed by Dr. Micol Ravà, Core Facility of Animal Biochemistry, San Raffaele Scientific Institute, Milan.

All sources of information are acknowledged by means of reference.

ACKNOWLEDGEMENTS

I am grateful to my Director of Study Prof. Luca Rampoldi for the precious mentoring, guidance and support he gave me during these years.

I acknowledge my second supervisor Prof. Irina Udalova and my tutor Dr. Giovanna Musco.

I acknowledge Prof. Matteo Iannacone (Dynamics of immune responses unit, Immunology, Transplantation and Infectious Diseases, San Raffaele Scientific Institute, Milan) for kindly providing us the $Ccr2^{-/-}$ mouse line.

I thank Micol Ravà (Core Facility of Animal Biochemistry, San Raffaele Scientific Institute, Milan) for biochemistry analyses.

I thank Barbara Canciani (Laboratory of Regenerative Medicine and Biomaterials, San Raffaele Scientific Institute, IRCSS Istituto Ortopedico Galeazzi, Milan) for precious help in setting up histology staining protocol and shared reagents.

I am grateful to all the past and present members of Molecular Genetics of Renal Disorders Unit. I particularly thank Matteo Trudu that generated the results that served as preliminary data for this project and Francesca Nicola for her collaboration on the Ccr2 project part. I thank my colleagues Céline, Claudia, Francesco, Maurizio and Elena for scientific discussion, suggestions, and shared time during these years.

I would like to acknowledge “FCSR-Fronzaroli” for supporting my research fellowship.

ABSTRACT

Mutations in *UMOD*, encoding uromodulin, lead to *UMOD*-related Autosomal Dominant Tubulointerstitial Kidney Disease (ADTKD-*UMOD*), a rare cause of end-stage kidney disease, characterized by interstitial fibrosis and inflammation. The hallmark of *UMOD* mutations is endoplasmic reticulum (ER) retention of misfolded uromodulin, but downstream molecular mechanisms of pathogenesis are still unclear, and no therapeutic strategy is currently available.

In a mouse model, expressing C147W mutant uromodulin ($Tg^{Umod\text{C147W}}$) and modelling human disease, we reported induction of pro-inflammatory chemokines already at one day-*post natal*, in absence of any histological sign of kidney damage. Since all up-regulated chemokines are ligands of the same receptor Ccr2, we generated a $Tg^{Umod\text{C147W}}/Ccr2^{-/-}$ mouse line to evaluate the role of Ccr2 axis in disease onset and progression. $Tg^{Umod\text{C147W}}/Ccr2^{-/-}$ mice were characterized at different stages of disease. Our results showed that targeting of Ccr2 does not block disease onset nor it delays disease progression, as no significant differences were detected between $Tg^{Umod\text{C147W}}$ mice carrying $Ccr2^{-/-}$ or $Ccr2^{+/+}$ genotype.

Stemming from the serendipitous observation of full rescue of mutant uromodulin ER retention in a $Tg^{Umod\text{C147W}}$ mouse which showed at sacrifice low body weight and malocclusion due to incisors overgrowth, we hypothesized that such effect was due to reduced food intake. A proof-of-concept experiment of calorie restriction (CR) regimen, mimicking food intake reduction, indeed recapitulated the effect on mutant uromodulin trafficking observed in the "rescued" mouse. To assess the therapeutic potential of reducing the intracellular load of mutant uromodulin, we tested the effect of a milder and prolonged CR protocol. Also such milder protocol led to a drastic reduction of mutant uromodulin ER retention and aggregation in epithelial expressing cells. Our data point at restored autophagic flux and consequent degradation of mutant uromodulin intracellular aggregates as a mechanism of action of CR. This, in turn, relieves cell stress and downstream activation of inflammation and fibrosis, ameliorating disease phenotype of $Tg^{Umod\text{C147W}}$ mice. Overall, our results establish the proof of principle that rescuing the primary effect of *UMOD* mutations can prevent ADTKD-*UMOD* onset and progression and provide evidence for a possible therapeutic strategy.

TABLE OF CONTENT

ACRONYMS AND ABBREVIATIONS **1**

LIST OF FIGURES AND TABLES **4**

1. INTRODUCTION **6**

1.1 Uromodulin **6**

1.2 Biochemical properties and structure of uromodulin **7**

1.2.1 Protein and domains ***7***

1.2.2 Maturation, polymerization and polarized secretion ***9***

1.3 Physiological roles of uromodulin **13**

1.3.1 Protection against urinary tract infections (UTIs) ***13***

1.3.2 Protection against kidney stones ***14***

1.3.3 Kidney sodium transport ***15***

1.3.4 Kidney calcium and magnesium transport ***17***

1.3.5 Modulation of kidney immunity ***18***

1.3.6 Roles of circulating uromodulin ***19***

1.4 Relevance of uromodulin in common kidney diseases **21**

1.4.1 Chronic kidney disease ***22***

1.4.2 Hypertension ***24***

1.5 Autosomal Dominant Tubulointerstitial Kidney Disease (ADTKD) **26**

1.5.1 ADTKD-UMOD ***28***

1.5.1.1 ADTKD-UMOD in vitro studies 31

1.5.1.2 ADTKD-UMOD in vivo models 33

1.5.2 ADTKD-MUC1 ..... ***38***

1.5.3 ADTKD-REN ***40***

1.5.4 ADTKD-HNF1β ***42***

1.5.5 ADTKD-SEC61A1 ..... *44*

1.5.6 Atypical forms of ADTKD *46*

1.6 Preliminary data **48**

2. AIMS OF THE WORK **51**

3. RESULTS **52**

3.1 Generation and characterization of Tg$^{Umod\text{C147W}}$/*Ccr2*$^{-/-}$ mouse line **52**

3.1.1 Characterization of 1-week-old Tg^{UmodC147W}/Ccr2$^{-/-}$ mice *53*

3.1.2 Characterization of 6-week-old Tg^{UmodC147W}/Ccr2$^{-/-}$ mice *56*

3.1.3 Characterization of 14-week-old Tg^{UmodC147W}/Ccr2$^{-/-}$ mice *60*

3.1.4 Characterization of 24-week-old Tg^{UmodC147W}/Ccr2$^{-/-}$ mice *64*

3.1.5 Summary of Tg^{UmodC147W}/Ccr2$^{-/-}$ mouse line characterization *68*

3.2 Rescue of mutant uromodulin ER retention **70**

3.3 Proof-of-concept calorie restriction in Tg$^{Umod\text{wt}}$ and Tg$^{Umod\text{C147W}}$ mice **71**

3.3.1 Effect of calorie restriction on uromodulin biology *73*

3.3.2 Effect of calorie restriction on inflammation and fibrosis *75*

3.3.3 Effect of calorie restriction on tubular damage *78*

3.3.4 Effect of calorie restriction on autophagy *80*

3.3.6 Effect of calorie restriction on kidney physiology *84*

3.4 Testing the efficiency of a milder and prolonged calorie restriction protocol on Tg$^{Umod\text{C147W}}$ mice **85**

3.4.1 Influence of sex on disease severity in Tg^{UmodC147W} mice *86*

3.4.2 Effects of CR-30 on ADTKD-UMOD phenotype in female Tg^{UmodC147W} mice *89*

3.4.2.1 Effect of CR-30 on uromodulin biology 89

3.4.2.2 Effect of CR-30 on kidney inflammation 93

3.4.2.3 Effect of CR-30 on kidney fibrosis 95

3.4.2.4 Effect of CR-30 on tubular damage 97
3.4.2.5 Effect of CR-30 on lipid metabolism 99
3.4.2.6 Effect of CR-30 on kidney physiology 100
3.4.2.7 Molecular mechanisms induced by CR-30 101
4. DISCUSSION 106
4.1 C-C chemokine receptor type 2 and chemokines 107
4.2 Calorie restriction 112
5. MATERIALS AND METHODS 120
5.1 Animal models 120
5.1.1 $Tg^{UmodC147W}$ and Tg^{Umodwt} mouse lines 120
5.1.2 Generation of $Tg^{UmodC147W}/Ccr2^{-/-}$ mouse line 120
5.1.3 Protocol of 55% calorie restriction 121
5.1.4 Protocol of 30% calorie restriction 121
5.1.5 Metabolic cage for urine collection 121
5.1.6 Serum samples collection 122
5.1.7 Mouse tissues collection 122
5.2 Genomic DNA extraction and genotyping 122
5.2.1 Uromodulin genotyping 123
5.2.2 Ccr2 genotyping 124
5.3 Purification of PCR product from agarose gel and sequencing 125
5.4 Protein extraction 125
5.5 Endo Hf Digestion 126
5.6 Western blot 126
5.7 Immunofluorescence 126
5.8 Histological staining 127
5.9 RNA extraction and isolation 128

5.10 Reverse transcription and Real-Time qPCR analysis 128

5.11 Semiquantitative RT-PCR analysis 129

5.12 Antibodies 129

5.13 Primers 130

5.14 Statistical Analysis 132

6. REFERENCES 133

APPENDIX 152

I. Effects of CR-30 on ADTKD-UMOD phenotype in male $Tg^{UmodC147W}$ mice .. 152

I.1 Effect of CR-30 on uromodulin biology 152

I.2 Effect of CR-30 on kidney inflammation 155

I.3 Effect of CR-30 on kidney fibrosis 156

I.4 Effect of CR-30 on tubular damage 157

I.5 Effect of CR-30 on kidney autophagy 159

I.6 Effect of CR-30 on kidney physiology 160

ACRONYMS AND ABBREVIATIONS

4-PBA	4-phenylbutyrate
ADPKD	Autosomal dominant polycystic kidney disease
ADTKD	Autosomal dominant tubulointerstitial kidney disease
AKI	Acute kidney injury
ATF4	Activating transcription factor 4
ATF6	Activating transcription factor 6
BIP	Binding immunoglobulin protein
BP	Blood pressure
Ca^{2+}	Calcium
CAB39	Calcium-binding protein 39
CAKUT	Congenital anomalies of the kidney and urinary tract
CaO	Calcium oxalate
CaP	Calcium phosphate
CasR	Calcium-sensing receptor
CCL12	C-C Motif Chemokine Ligand 12
CCL2	C-C Motif Chemokine Ligand 2
CCL7	C-C Motif Chemokine Ligand 7
CCL8	C-C Motif Chemokine Ligand 8
CCR1	C-C chemokine receptor 1
CCR2	C-C chemokine receptor 2
CCR5	C-C chemokine receptor 5
CD45	Cluster of differentiation 45
CD68	Cluster of differentiation 68
CHOP	C/EBP Homologous Protein
CKD	Chronic kidney disease
CNT	Connecting tubules
CR	Calorie restriction
CR-30	30% calorie restriction
CR-55	55% caloric restriction
CRELD2	Cysteine-rich EGF-like domains 2
CVD	Cardiovascular disease
DAMP	Danger-associated molecular patterns
DCT	Distal convoluted tubule
E. Coli	Escherichia coli
EGF	Epidermal growth factor
eGFR	Estimated glomerular filtration rate
EHP	External hydrophobic patch
EMT	Epithelial-to-mesenchymal transition
ENU	N-ethyl-N-nitrosourea
ER	Endoplasmic reticulum

ERAD	ER-associated degradation
ERGIC	ER-to-Golgi compartment
ESKD	End stage kidney disease
FJHN1	Familial juvenile hyperuricemic nephropathy 1
GAlNAc	N-acetilgalactosamine
GAPDH	Glyceraldehyde-3-Phosphate Dehydrogenase
GFR	Glomerular filtration rate
GPI	Glycosylphosphatidylinositol
GRP78	Glucose regulated protein 78
GWAS	Genome-wide association study
HA	Hemagglutinin
HNF1B	Hepatocyte nuclear factor 1β
HPRT1	Hypoxanthine Phosphoribosyl Transferase 1
HTN	Hypertension
IHP	Internal hydrophobic patch
IRE1	Inositol-requiring enzyme 1
IRI	Ischemia-reperfusion injury
K^+	Potassium
KDIGO	Kidney Disease: Improving Global Outcomes
KIM-1	Kidney Injury Molecule 1
LCN2	Lipocalin-2
MAMs	Mitocondria-associated membranes
MCKD2	Medullary cystic kidney disease type 2
Mg^{2+}	Magnesium
MITKD	Mitochondrial inherited tubulointerstitial kidney disease
MLPA	Multiplex Ligation-dependent Probe Amplification
MOBY	Maturity onset diabetes of the young
MS	Multiple sclerosis
mTOR	Mammalian target of rapamycin
MUC1	Mucin 1
MUC1-fs	Mucin 1 frameshifted protein
NCC	Na^+/Cl^- cotransporter
NKCC2	Na^{2+}-K^+-$2Cl^-$ cotransporter
NLRP3	NACTH, LRR and PYD domains-containing protein 3
NOS	Not otherwise specified
OSR1	Oxidative stress–responsive kinase 1
PERK	Protein kinase RNA-like ER kinase
PKD	Polycystic kidney disease
PMN	Polymorphonuclear leukocytes
RAAS	Renin-Angiotensin-Aldosterone System
RAS	Renal artery stenosis
RCAD	Renal cyst and diabetes

REN	Renin
ROMK	Renal outer medullary K^+ channel
ROS	Reactive Oxygen Species
SDS-PAGE	Sodium Dodecyl Sulphate - PolyAcrylamide Gel Electrophoresis
SEC61A1	α1 subunit of the SEC61 translocon
SMRT	Single molecule real-time sequencing
SNP	Single nucleotide polymorphism
SORL1	Sorting protein-related receptor with A-type repeats 1
SPAK	STE20/SPS1-related proline/alanine-rich kinase
TAL	Thick ascending limb
TBP	TATA-Box Binding Protein
THP	Tamm-Horsfall protein
TLR4	Toll-like receptor 4
TNFα	Tumor necrosis factor-α
TRPM2	Transient receptor potential cation channel subfamily M, member 2
TRPV5	Transient receptor potential cation channel subfamily V member 5
TRPV6	Transient receptor potential cation channel subfamily V member 6
UMOD	Uromodulin
UPR	Unfolded protein response
UUO	Unilateral ureteral obstruction
VNTR	Variable number tandem repeats
ZP	Zona pellucida

LIST OF FIGURES AND TABLES

Figure 1. Schematic representation of the nephron.
Figure 2. Schematic representation of human uromodulin domain architecture.
Figure 3. Summary of uromodulin functions and polarized secretion.
Figure 4. Common genetic variants of *UMOD* associated with increased risk for complex traits.
Figure 5. Clinical features of ADTKD.
Figure 6. Summary of ADTKD mutations in *UMOD*.
Figure 7. Endoplasmic reticulum retention of mutant uromodulin in Tg$^{Umod\text{C147W}}$ mice and in ADTKD-*UMOD* patients.
Figure 8. Cellular effects induced by mutations in ADTKD genes.
Figure 9. Early events induced by mutant uromodulin expression in kidneys of Tg$^{Umod\text{C147W}}$ mice at one day post-natal.
Figure 10. Characterization of 1-week-old Tg$^{Umod\text{C147W}}$/*Ccr2*$^{-/-}$ mice.
Figure 11. Inflammation in kidneys of 1-week-old Tg$^{Umod\text{C147W}}$/*Ccr2*$^{-/-}$ mice.
Figure 12. Tubular damage in kidneys of 1-week-old Tg$^{Umod\text{C147W}}$/*Ccr2*$^{-/-}$ mice.
Figure 13. Characterization of 6-week-old Tg$^{Umod\text{C147W}}$/*Ccr2*$^{-/-}$ mice.
Figure 14. Inflammation in kidneys of 6-week-old Tg$^{Umod\text{C147W}}$/*Ccr2*$^{-/-}$ mice.
Figure 15. Fibrosis in kidneys of 6-week-old Tg$^{Umod\text{C147W}}$/*Ccr2*-/- mice.
Figure 16. Tubular damage in kidneys of 6-week-old Tg$^{Umod\text{C147W}}$/*Ccr2*$^{-/-}$ mice.
Figure 17. Characterization of 14-week-old Tg$^{Umod\text{C147W}}$/*Ccr2*$^{-/-}$ mice.
Figure 18. Inflammation in kidneys of 14-week-old Tg$^{Umod\text{C147W}}$/*Ccr2*$^{-/-}$ mice.
Figure 19. Fibrosis in kidneys of 14-week-old Tg$^{Umod\text{C147W}}$/*Ccr2*$^{-/-}$ mice.
Figure 20. Tubular damage in kidneys of 14-week-old Tg$^{Umod\text{C147W}}$/*Ccr2*$^{-/-}$ mice.
Figure 21. Characterization of 24-week-old Tg$^{Umod\text{C147W}}$/*Ccr2*$^{-/-}$ mice.
Figure 22. Inflammation in kidneys of 24-week-old Tg$^{Umod\text{C147W}}$/*Ccr2*$^{-/-}$ mice.
Figure 23. Fibrosis in kidneys of 24-week-old Tg$^{Umod\text{C147W}}$/*Ccr2*$^{-/-}$ mice.
Figure 24. Tubular damage in kidneys of 24-week-old Tg$^{Umod\text{C147W}}$/*Ccr2*$^{-/-}$ mice.
Figure 25. Rescue of mutant uromodulin ER retention in a Tg$^{Umod\text{C147W}}$ mouse.
Figure 26. Calorie restriction protocol and mouse body weight during the diet.
Figure 27. Effect of calorie restriction on mutant uromodulin ER retention and uromodulin expression.
Figure 28. Effect of calorie restriction on uromodulin trafficking.
Figure 29. Effect of calorie restriction on mutant uromodulin ER aggregation.
Figure 30. Effect of calorie restriction on inflammation and fibrosis.
Figure 31. Effect of calorie restriction on tubular damage.
Figure 32. Lc3 ratio in kidneys and liver of Tg$^{Umod\text{wt}}$ and Tg$^{Umod\text{C147W}}$ AL and CR mice.
Figure 33. p62 levels in kidneys of Tg$^{Umod\text{wt}}$ and Tg$^{Umod\text{C147W}}$ mice.
Figure 34. Effect of calorie restriction on blood urea nitrogen levels.
Figure 35. Schematic protocol of milder, prolonged calorie restriction experiment and mice body weight during the diet.
Figure 36. Uromodulin expression in male and female mice.
Figure 37. Mutant uromodulin ER retention and aggregation in male and female Tg$^{Umod\text{C147W}}$ mice.
Figure 38. Inflammation, fibrosis and tubular damage in male and female Tg$^{Umod\text{C147W}}$ mice.

Figure 39. Effect of CR-30 on uromodulin protein and transcript levels in female Tg$^{Umod\text{C147W}}$ mice.
Figure 40. Effect of CR-30 on mutant uromodulin ER retention in female Tg$^{Umod\text{C147W}}$ mice.
Figure 41. Effect of CR-30 on mutant uromodulin aggregation in female Tg$^{Umod\text{C147W}}$ mice.
Figure 42. Effect of CR-30 on kidney inflammation in female Tg$^{Umod\text{C147W}}$ mice.
Figure 43. Effect of CR-30 on kidney fibrosis in female Tg$^{Umod\text{C147W}}$ mice.
Figure 44. Effect of CR-30 on tubular damage in female Tg$^{Umod\text{C147W}}$ mice.
Figure 45. Effect of CR-30 on lipid metabolism in female Tg$^{Umod\text{C147W}}$ mice.
Figure 46. Effect of CR-30 on kidney physiology of female Tg$^{Umod\text{C147W}}$ mice.
Figure 47. Effect of CR-30 on autophagy in kidney of female Tg$^{Umod\text{C147W}}$ mice.
Figure 48. Calorie restriction reduces mTOR activation in Tg$^{Umod\text{C147W}}$ mice.
Figure 49. Effect of CR-30 on ER-phagy in female Tg$^{Umod\text{C147W}}$ mice.
Figure 50. Chemokine receptor and ligand pairings.
Figure 51. Early and late compensatory effects induced by *Ccr2* deletion in kidneys of Tg$^{Umod\text{C147W}}$ mice.
Figure 52. Cellular and molecular mechanisms controlled by calorie restriction.
Figure 53. Working model: effect of calorie restriction on ADTKD-*UMOD* pathogenesis.
Figure 54. Uromodulin genotyping.
Figure 55. *Ccr2* genotyping.
Figure I.1. Effect of CR-30 on uromodulin protein and transcript levels in male Tg$^{Umod\text{C147W}}$ mice.
Figure I.2. Effect of CR-30 on mutant uromodulin ER retention in male Tg$^{Umod\text{C147W}}$ mice.
Figure I.3. Effect of CR-30 on mutant uromodulin aggregation in male Tg$^{Umod\text{C147W}}$ mice.
Figure I.4. Effect of CR-30 on kidney inflammation in male Tg$^{Umod\text{C147W}}$ mice.
Figure I.5. Effect of CR-30 on kidney fibrosis in male Tg$^{Umod\text{C147W}}$ mice.
Figure I.6. Effect of CR-30 on tubular damage in male Tg$^{Umod\text{C147W}}$ mice.
Figure I.7. Effect of CR-30 on autophagy in kidney of male Tg$^{Umod\text{C147W}}$ mice.
Figure I.8. Effect of CR-30 on kidney physiology of male Tg$^{Umod\text{C147W}}$ mice.

Table 1. ADTKD-*UMOD* mouse models.
Table 2. Characterization of Tg$^{Umod\text{C147W}}$/*Ccr2*$^{-/-}$ mouse line.
Table 3. PCR protocol reaction for transgene detection.
Table 4. PCR protocol reaction for *Ccr2* genotyping.
Table 5. Protocol of semiquantitative RT-PCR reaction.
Table 6. List of antibodies used for western blot and/or immunofluorescence experiments.
Table 7. List and sequences of primers used for *UMOD* and *Ccr2* genotyping.
Table 8. List and sequences of primers used for gene expression analysis.

1. INTRODUCTION

1.1 Uromodulin

In 1950, Igor Tamm and Frank Horsfall by using salt-precipitation on urine of healthy individuals, isolated a mucoprotein that demonstrated potent inhibitory effects on viral haemagglutination induced by influenza, mumps and Newcastle disease viruses (Tamm & Horsfall, 1950). Additional investigations on this feature demonstrated that this ability was abolished by treatment with neuraminidase, an enzyme of viral envelope able to remove sialic acid-residues on the host cells (Tamm & Horsfall, 1952). Biochemical characterization of that protein, that was named Tamm-Horsfall protein (THP), revealed a high carbohydrate content (accounting for about 30% of its molecular weight) and a complex glycosylation pattern (Gottschalk, 1952). Further electron microscopy studies revealed its filamentous structure with small fibres (diameters of 4-24 nm) capable to attach viral particle at several sites (Bayer, 1964).

Some years later, in 1985, Muchmore and Decker isolated a glycoprotein with a potent inhibitory effect on human T cells activation and monocyte cytotoxicity by using lectin-based affinity chromatography on urine of pregnant women. For its marked immunomodulatory properties, they proposed to name this glycoprotein "uromodulin" (Muchmore & Decker, 1985).

In 1987, a seminal work from Pennica *et al*, by comparing several similarities between the two previously described proteins, i.e., tissue localization, cDNA sequence, aminoacidic and carbohydrate composition, molecular weight, and immunosuppressive activity, demonstrated that THP and uromodulin were the same protein (Pennica *et al*, 1987).

Today, this protein is acknowledged as the most abundant protein in physiological urine and its excretion is estimated at a rate of about 30-60 mg/day (Pruijm *et al*, 2016). Despite its biological functions are not yet fully elucidated (discussed below), its role in kidney physiology and disease has raised interest from both translational and basic research.

In this thesis, we will refer to the protein using the term uromodulin.

1.2 Biochemical properties and structure of uromodulin

1.2.1 Protein and domains

Uromodulin (encoded by the *UMOD* gene, located on human chromosome 16p12.3) is a kidney specific protein (Pennica *et al*, 1987), predominantly produced by epithelial cells of the thick ascending limb of Henle's loop (TAL, 90%) and in a minor amount by tubular epithelial cells of the initial portion of the distal convoluted tubule (DCT1, 10%) (Tokonami et al, 2018) (**Figure 1**).

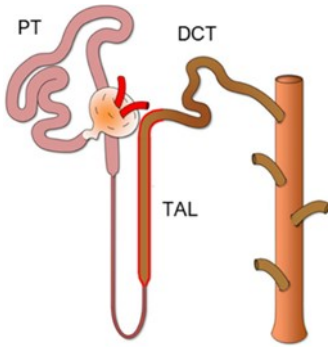


Figure 1. Schematic representation of the nephron. *The portions of the nephron where uromodulin is expressed are indicated in red. PT, proximal tubule; DCT, distal convoluted tubule; TAL, tick ascending limb of Henle's loop. (Adapted from* Schaeffer et al, 2021. *Reproduced with permission from the Annual Review of Physiology, Volume 83 © 2021 by Annual Reviews, http://www.annualreviews.org).*

Uromodulin is synthetized as a 640 amino acids precursor. Predicted protein domains (**Figure 2**) include an N-terminal leader peptide (residues 1-24) driving co-translational insertion in the endoplasmic reticulum (ER) and removed during protein maturation. It also contains four epidermal grow factor (EGF)-like domains which are thought to mediate uromodulin interaction with other proteins, that are EGF-I (residues 31-64), EGF-II (residues 65-107) and EGF-III (residues 108-149) which are predicted to be Ca^{2+} binding, and EGF-IV (residues 295-319). The protein also includes a central cysteine-rich domain of unknown function whose structural resolution was recently improved through a combined approach using AlphaFold2 prediction, X-ray crystallography and cryo-EM data. This central region contains a bipartite decoy module, composed by a beta-

hairpin (β) (residues 150-171) stabilized by a disulphide bridge and a D10C domain (residues 172-291) containing five intramolecular disulphide bonds (Stsiapanava *et al*, 2022). The C-terminus of uromodulin contains a bipartite Zona Pellucida (ZP) domain (residues 324-587), composed of an N-terminal (ZP-N) and a C-terminal (ZP-C) subdomain, separated by a short linker region. ZP domains are found in eukaryotic proteins forming extracellular filaments that share a similar supramolecular structure, among which zona pellucida sperm receptors ZP1, ZP2 and ZP3. As for all these proteins, the ZP domain of uromodulin is essential for uromodulin polymerization. It contains an internal hydrophobic patch (IHP, residues 430-462) that interact with an external hydrophobic patch (EHP, residues 598-607), located at the C-terminus of the ZP-C domain, thus inhibiting uromodulin premature polymerization (Jovine *et al*, 2002; Schaeffer *et al*, 2009). The hydrophobic stretch constituted by ammino acids 614-640 serves as a signal for the attachment of a glycosylphosphatidylinositol (GPI) anchor on Ser614, important for uromodulin localization at plasma membrane of expressing cells (Cavallone *et al*, 2001).

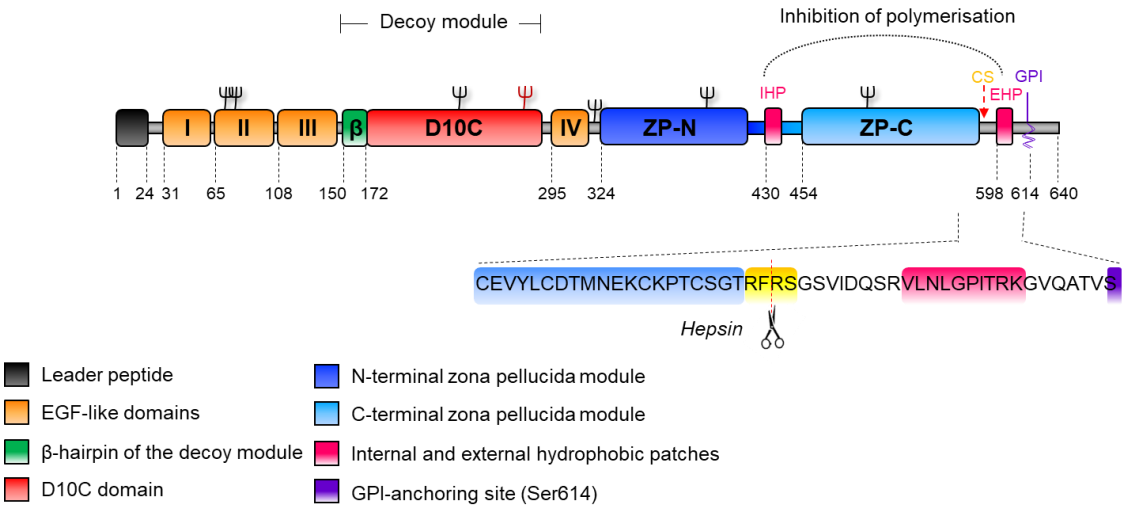


Figure 2. Schematic representation of human uromodulin domain architecture. *Starting from N-terminus, it contains a leader peptide (in black); three Epidermal Growth Factor (EGF)-like domains; the decoy module composed by a beta-hairpin (β) domain and a cysteine rich domain (D10C); a fourth EGF-like domain and a bipartite zona pellucida domain, formed by the ZP-N and the ZP-C domains connected by an interdomain linker. The GPI-anchoring site, predicted at Ser614 is shown in purple. Also shown are the internal (IHP) and external (EHP) hydrophobic patches whose interaction maintains uromodulin in a polymerization incompetent status during protein maturation along the secretory pathway. The seven sites of N-glycosylation are indicated*

with Ψ and the red one represents Asn275 which retains a high-mannose moiety. The inset reports protein sequence from the C-terminal part of the ZP-C to Ser614. Hepsin cleavage site (CS) is reported in yellow (adapted from Schaeffer et al, 2021 and Stsiapanava et al, 2022).

Uromodulin sequence contains 48 conserved cysteines, all involved in the formation of 24 intramolecular disulphide bridge, an essential requirement for proper protein folding (Serafini-cessi *et al,* 1993).

Uromodulin is a heavily glycosylated protein, a posttranslational modification that strongly impacts on its functions and physicochemical properties and that occurs at seven (Asn76, Asn80, Asn232, Asn275, Asn322, Asn396, Asn513) of the eight putative N-glycosylation sites (Asn38, being close to the N-terminus, is not used) (van Rooijen *et al*, 1999). Except for Asn275 which retains a high-mannose moiety, all glycan chains are matured to complex ones (poly-antennary sialic acid-terminated carbohydrates) in the Golgi, where they are modified through sialylation, fucosylation or sulfation (van Rooijen *et al*, 1999). Uromodulin was also reported to be O-glycosylated with a mechanism that is reversible and under hormonal control (Easton *et al*, 2000). Uromodulin carries the Sd^a antigen a pentasaccharide composed by GalNAcβ(1,4)[Neu5Acα(2,3)]Galβ(1,4)GlcNAc sequence on terminal sugars with immunodominant functions as blood group determinant (Donald *et al*, 1983).

1.2.2 Maturation, polymerization and polarized secretion

Uromodulin maturation process along the secretory pathway starts with co-translational insertion of the 640 amino acids precursor in the ER where folding, glycosylation and the attachment of a preformed GPI-anchor occur. Membrane-bound uromodulin is then sorted to the Golgi apparatus, where high-mannose residues are trimmed and complex glycans are added (except for chain at Asn275). Acquisition of the correct tertiary structure is a rate-limiting step in uromodulin maturation. Indeed, when expressed in different types of transfected cells, uromodulin can be detected as an immature ER-resident precursor form of about 85 kDa that after glycan processing shows an apparent increase in molecular mass to about 110 kDa corresponding to the fully glycosylated isoform (Serafinicessi *et al*, 1993; Rampoldi *et al*, 2003; Schaeffer *et al*, 2017). Once in

the trans Golgi, uromodulin is partitioned into lipid rafts thanks to its GPI-anchor, and it is directed to the apical membrane of epithelial cells (Benting *et al*, 1999; Simons & Ikonen, 1997).

Once on the plasma membrane, uromodulin is released in the urine upon proteolytic cleavage. Cleavage occurs at a conserved phenylalanine residue flanking the ZP domain (Phe587 in human corresponding to Phe588 in the murine protein sequence) (Santambrogio *et al*, 2008), and is mediated by hepsin, a membrane-bound serine-protease that is co-expressed and co-localises with uromodulin at apical membrane of TAL cells (Brunati *et al*, 2015).

In the urine uromodulin is found predominantly as high molecular weight polymers (M*r* 1-10 x 10^6) (Serafini-Cessi *et al*, 2003) whose formation is mediated by ZP domains (Jovine *et al*, 2002). Cleavage by hepsin is a key event for protein polymerization to occur. Indeed, during intracellular trafficking uromodulin is maintained in a polymerization-incompetent state due to the interaction between EHP and IHP hydrophobic patches (Schaeffer *et al*, 2009). Hepsin cleavage releases the EHP, allowing the exposure of a highly hydrophobic interface of the ZP-N domain, due to dissociation of interaction with IHP (Bokhove *et al*, 2016). Consistently, hepsin knockout mice show dramatic reduction of uromodulin urinary levels, that still retains the EHP, and it does not assemble into filaments (Brunati *et al*, 2015).

Purified urinary uromodulin observed by electron microscopy (EM) appears as a three-dimensional net-like matrix, formed by long filaments, composed of smaller fibrils, having a width of about 100 Å and an average length of 25,000 Å (Porter & Tamm, 1955). The formation of uromodulin homodimers, mediated by the ZP-N domain, is an indispensable intermediate phase of filament formation (Bokhove *et al*, 2016). Cryo-electron tomography allowed to determine low-resolution structure of uromodulin filaments revealing a zigzag-organized backbone, composed by ZP domains, with laterally protruding arms, composed by the EGF and D10C domains (Weiss *et al*, 2020). An additional cryo-EM study at higher resolution clarified the peculiar molecular mechanism of uromodulin polymers assembly that occurs with a four-step proposed model starting with 2 homodimers (from 4 monomers) that are GPI-anchored to the apical membrane. Cleavage at the consensus site from hepsin in only one of the moieties,

displaces EHP-IHP interaction inducing rearrangement on its ZP-N/ZP-C linker allowing the formation of head-to-tail interaction between ZP-C from one homodimer with ZP-N from the other homodimer, leading to the link of three consecutive uromodulin monomers (Stsiapanava *et al*, 2020). This structure explains the resistance of uromodulin polymers to proteolysis and chemical denaturation. This model agrees with previously published crystallography data and was corroborated by another cryo-EM study, proposing a similar process of polymerization starting from two pro-uromodulin (Stanisich *et al*, 2020).

The determinants controlling polarized targeting and apical release of uromodulin have been intensively studied (**Figure 3**). Studies in an *in vitro* model of polarized epithelial cells, demonstrated that rather than GPI-anchor, the apical sorting of uromodulin to plasma membrane is mediated by N-glycans (Pang *et al*, 2004). A role in the control of uromodulin urinary excretion is played by the G protein-coupled calcium-sensing receptor (CaSR), localized at the basolateral membrane of TAL cells and involved in paracellular Ca^{2+} reabsorption. Receptor antagonists or its genetic deletion led to increased apical localization and urinary levels of uromodulin while, on the contrary, CasR pharmacological activation is associated with diffuse intracellular localization and a decreased release in the urine (Tokonami *et al*, 2018). Genome wide association studies (GWAS) revealed association between uromodulin urinary levels and common variants in *KCNJ1*, *SORL1* and *CAB39* (Olden *et al*, 2014). Among these, *KCNJ1* encodes for the renal outer medullary K^+ channel ROMK, expressed in the apical membrane of TAL cells and activated by uromodulin itself. Studies on *Kcnj1* deficient mice and *in vitro* pharmacological analysis using both non-selective and selective ROMK inhibitors demonstrated defective apical excretion of uromodulin and its intracellular accumulation, due to alteration of the membrane potential of TAL cells downstream to ROMK decreased activity. This is further confirmed in humans as, carriers of loss-of-function mutation in *KCNJ1*, causing Bartter syndrome type 2 show decreased urinary uromodulin concentrations (Schiano *et al*, 2019). *CAB39* encodes for the scaffolding protein calcium-binding 39, involved in the activation of SPS1-related proline and alanine-rich kinase (SPAK) and oxidative stress-responsive kinase (OSR1), while *SORL1* encodes for sortilin-related receptor 1, and mediates SPAK membrane sorting, where it phosphorylates and activates the Na^{2+}-K^+-$2Cl^-$ cotransporter (NKCC2). Both these proteins are highly enriched in the TAL and DCT segments, where uromodulin is

expressed and their activity likely affects uromodulin maturation and secretion via regulation of NKCC2 or Na^+/Cl^- cotransporter (NCC) (Olden *et al*, 2014). Recently, a new meta-GWAS revealed association with urinary excretion of uromodulin and common variants in *KRT40* and *WDR72* (Joseph *et al*, 2022). *WDR72* encodes for a tryptophan-aspartate repeat domain protein, highly expressed in the kidney, although not colocalizing with uromodulin, that has been recently implicated in the regulation of vesicle trafficking and associated with kidney function, urinary acidification and kidney stones (Katsura *et al*, 2022). *KRT40* encodes for a type I keratin implicated in the formation of intermediate filament in epithelial cells. *In vitro*, silencing of *KRT40* is reflected by decreased excretion of uromodulin, that accumulates intracellularly and altered ROMK sorting at the plasma membrane, suggesting a role of this protein in the polarized trafficking of proteins to the apical membrane (Joseph *et al*, 2022). Furthermore, a role for Myh9 and Myh10, two actin-associated non-muscle myosins associated with vesicle biogenesis and endocytosis, has been proposed in uromodulin trafficking and proper localization. Indeed, the conditional inactivation of both these motor proteins in renal tubules of adult mice results in intracellular accumulation of uromodulin within ER tubules followed by activation of ER stress and unfolded protein response (UPR) eventually leading to progressive renal tubulointerstitial disease (Otterpohl *et al*, 2020).

In the last years, growing interest has emerged around circulating uromodulin that is present in the serum at a concentration that is at least 1000-fold lower than in the urine (20-50 ng/ml vs. 20-50 µg/ml) (Thornley *et al*, 1985; Scherberich *et al*, 2018). Serum uromodulin concentration decreases upon nephrectomy, and it is essentially absent in anephric subject, reflecting its kidney origin (Dawnay & Cattell, 1981). As opposed to the polymeric urinary form, circulating uromodulin is monomeric and it displays a higher molecular weight than its urinary counterpart in SDS-PAGE (Micanovic *et al*, 2018). This excludes reuptake of urinary uromodulin and rather points at basolateral release from epithelial expressing cells as the source of circulating uromodulin. Consistently, despite predominant apical localization, different reports described uromodulin localization at the basolateral membrane of expressing cells (Bachmann *et al*, 1985; El-Achkar & Wu, 2012; Scherberich *et al*, 2018). The pathways governing uromodulin basolateral localization and release are still unknown. Recently, genome-wide association studies of circulating uromodulin identified a loss-of-function variant in the *B4GALNT2* gene, encoding a Sd^a

synthetizing β-1,4-N-acetyl-galactosaminyltransferase, associated with increased serum uromodulin levels (Li *et al*, 2022).

Of note, using a specific antibody directed against uromodulin EHP, thus recognising the polymerization-incompetent form of the protein, Micanovic *et al* demonstrated that the nonpolymerizing form of the protein is not only present in the circulation but also in the urine. This suggests the existence of two different mechanisms for the release of uromodulin in its polymeric and monomeric forms (Micanovic *et al*, 2022).

1.3 Physiological roles of uromodulin

The functions of uromodulin are only partly elucidated, mostly thanks to studies in *Umod* knockout mice (**Figure 3**) (Schaeffer *et al*, 2021).

1.3.1 Protection against urinary tract infections (UTIs)

Several *in vivo* and *in vitro* evidence established that uromodulin exerts a direct protective action against urinary tract infections (UTIs) (**Figure 3**), commonly caused by *Escherichia coli* (*E. coli*). Bacterial adhesion to uroepithelial cells is the first and critical step for recurrent and persistent bladder colonization. The binding of *E. coli* to the surface of urothelial cells is mediated by lectin-like adhesins present on fimbriae or pili, classified according to their sugar specificity. Type 1 fimbriae are composed of the structural subunit FimA and expose the lectin-like protein FimH that binds high-mannose-rich uroplakin Ia receptor, a membrane protein expressed by epithelial bladder cells. *In vitro* studies demonstrated the ability of uromodulin to act as a competing inhibitor, by directly and specifically binding with type-1 fimbriated *E. coli* hence preventing its adhesion to uroplakin Ia receptor (Serafini-Cessi *et al*, 2005). *In vivo* studies on *Umod* knockout mice demonstrated their increased susceptibility to type-1 fimbriated (but not P-fibriated) *E. coli* bladder colonization, further corroborating the protective role of uromodulin against UTIs (Mo *et al*, 2004; Bates *et al*, 2004). The resolution of the three-dimensional structure of uromodulin filaments explained such inhibitory role. Uromodulin filaments arrange in a “fishing net” structure, exposing high mannose glycans at position Asn275 that act as

binding sites for lectin-like FimH, trapping uropathogenic bacteria and thus competing with uroplakin Ia interaction (Weiss *et al*, 2020; Stsiapanava *et al*, 2022). The flexibility of uromodulin polymers allows the encapsulation of entire bacteria and facilitates their elimination by micturition (Ørskov *et al*, 1980; Weiss *et al*, 2020).

These *in vitro* and *in vivo* data are supported by genetic studies in humans. Higher uromodulin urinary concentrations at baseline have been associated with lower risk of UTI, independently of other UTI risk factors, in a cohort of older community-residing subject (Garimella *et al*, 2017). This is consistent with results obtained in a study comparing UTI patients with or without bacteriemia and revealing that bacteriemia correlates with extremely low uromodulin urinary levels (van der Starre *et al*, 2015).

The protective role of uromodulin against UTI has likely been the driving selective pressure that has kept variants in the *UMOD* promoter, associated with increased uromodulin expression, at high frequency in all populations worldwide. Interestingly, such variants are correlated with UTI markers and prevalence of antibiotic resistant UTIs (Ghirotto *et al*, 2016).

1.3.2 Protection against kidney stones

Nephrolithiasis (or kidney stones) is one of the most common urological diseases (Alelign & Petros, 2018). Stone formation is caused by the precipitation of oversaturated crystals from the urine in the kidney, in a multistep process, that comprises nucleation, crystal growth, aggregation and crystal adherence to the kidney epithelial cells. Supersaturation and the presence of macromolecules with inhibitory effect are two critical factors regulating the propensity to form stones. The supersaturation of urine with crystal-forming compounds such as calcium oxalate (CaOx) and calcium phosphate (CaP) continuously expose the kidney to crystallization. However, kidney microenvironment contains both pro- and anti-crystallization molecules that are generally balanced to prevent crystal formation. Two of the macromolecules with crystal-formation inhibitory effect are osteopontin (OPN) and uromodulin (Grant *et al*, 1973; Jang *et al*, 2021).

In vitro and *in vivo* experiments demonstrated the ability of uromodulin to directly inhibit stone crystallization (**Figure 3**). *In vitro*, uromodulin shows an inhibitory role on

crystallization since its sialylated and negatively charged glycans prevent aggregation of CaOx and CaP crystals (Serafini-Cessi *et al*, 2005). Consistently, oxidative modification of urinary uromodulin, that can be induced under oxidative stress conditions and that affects protein folding, can promote CaOx crystallization and crystal growth without affecting crystal aggregation (Chaiyarit & Thongboonkerd, 2022).

In vivo studies on *Umod* knockout models confirmed the relevance of these biological properties. As compared to wild type littermates, *Umod* knockout mice show urines that are supersaturated with CaP and contain reduced levels of citrate (Liu *et al*, 2010). These animals display increased susceptibility to spontaneous kidney stone formation, independently from genetic background or gender and with a penetrance that increases with age (at 15 months of age 85-100% of *Umod* knockout mice present intrarenal crystals). Moreover, this susceptibility is clearly dependent on gene dosage, with *Umod* heterozygous mice showing an intermediate severity (Mo et al, 2004, 2007; Liu et al, 2010). Different case-control studies supported this direct protective ability also in humans, reporting lower uromodulin urinary levels in kidney stone formers (Romero *et al*, 1997; Lau *et al*, 2008). Moreover, a GWAS in Icelandic and Dutch cohorts reported the association of reduced risk of kidney stone formation with an *UMOD* variant (SNP rs4293393-allele T) linked with higher uromodulin urinary levels (Gudbjartsson *et al*, 2010).

The protective effect of uromodulin against renal stones formation may also be indirect, via modulation of Ca^{2+} handling (see also *Paragraph 1.3.4*). Uromodulin has indeed been demonstrated to stabilize the Ca^{2+} channel transient receptor potential cation channel subfamily V member 5 and 6 (TRPV5/6) in the DCT, indirectly decreasing Ca^{2+} excretion and hence reducing urinary concentration of CaOx and CaP (Wolf *et al*, 2013). Studies in a rat model of induced nephrolithiasis support this hypothesis, showing that activation of the Uromodulin/TRPV5 axis reduces intrarenal CaOx deposition (Cui *et al*, 2022).

1.3.3 Kidney sodium transport

Uromodulin plays a critical role in urine concentration, as shown for instance by impaired ability to concentrate urine under water deprivation that was observed in *Umod* knockout mice (Bachmann *et al,* 2005). The TAL segment plays a key role in water concentration,

since it is water impermeable, but it allows ion absorbance. This diluting function is essential to generate a hyperosmotic interstitium that drives water reabsorption in the collecting ducts. The role of uromodulin in water homeostasis could be direct, by contributing to TAL water impermeability, and/or indirect by regulating urinary sodium intake (**Figure 3**).

Early studies described uromodulin ability to form hydrophobic gel-like structure and to change its polymeric form under different physicochemical conditions. Uromodulin polymerization increases with increasing concentration of Ca^{2+} and Na^{2+}, reaching its maximum at concentrations similar to the ones measured in the lumen of TAL segment. In this conditions, uromodulin polymers are impermeable to water while they allow ion movement (Wiggins, 1987).

The connection between uromodulin and salt absorption in the TAL and DCT was first suggested by dietary studies showing increased uromodulin at both protein and mRNA levels in male Sprague-Dawley rats after hight-salt diet (Ying & Sanders, 1998). These results were later confirmed in humans, with the observation that high salt intake results in increased uromodulin urinary levels, whereas the opposite is seen with low salt diets (Torffvit *et al*, 2004). *Umod* knockout mice showed altered expression at baseline of key ion transporters and channels (Bachmann *et al,* 2005).

About 30% of filtered Na^{+} is reabsorbed in the TAL primarily via the apical NKCC2 co-transporter. *Umod* knockout mice showed decreased levels of active (i.e., phosphorylated) NKCC2 at the cell apical membrane and its accumulation in intracellular vesicles. Reduction of the activity of the transporter was also confirmed by reduced response to furosemide, a loop diuretic specifically inhibiting NKCC2. *In vitro* analysis on TAL cells and oocytes clarified that NKCC2 phosphorylation, necessary for its intracellular trafficking and stabilization at the plasma membrane, only occurs after uromodulin transfection (Mutig *et al*, 2011). Studies on a second, independently generated *Umod* knockout mouse line, confirmed these findings, demonstrating that defects of NKCC2 activity are exacerbated in aged KO mice that were unresponsive to furosemide due to complete absence of NKCC2 translocation to the apical surface of TAL cells. These mice also displayed increased levels of serum uric acid likely downstream of up-regulation of Na^{+}-coupled urate transporters (*Slc5a8* and *Slc22a12*) and sodium-hydrogen exchanger 3

(NHE3) in the proximal tubules, suggesting that NKCC2 dysfunction in *Umod* knockout mice induces the activation of compensatory pathways in other nephron segments (Liu *et al*, 2018).

Uromodulin could also impact on TAL function by modulating ROMK activity and hence K^+ homeostasis in this segment. As already described, ROMK affects uromodulin trafficking and polarized secretion, as both mice and patients with ROMK inactivating mutation show decreased uromodulin urinary levels (Schiano *et al*, 2019). Conversely, *in vitro*, uromodulin was shown to increase membrane trafficking and stabilization of ROMK, possibly explaining why in TAL segments of *Umod* knockout mice it accumulates in intracellular vesicles with reduced membrane levels (Renigunta *et al*, 2011).

1.3.4 Kidney calcium and magnesium transport

A role of uromodulin in calcium and magnesium homeostasis has been described (*Figure 3*). While filtered magnesium (about 50-60%) and calcium (20%) are reabsorbed via the paracellular pathway in the TAL, their uptake is fine-tuned in the DCT via an active transcellular pathway (Nie *et al,* 2018; Boder *et al,* 2021).

Active Ca^{2+} uptake from the urine is mediated by TRPV5 and TRPV6, two Ca^{2+} selective channels enriched on the apical membrane of late segments of DCT (DCT2) and connecting tubules (CNT) (Loffing *et al*, 2001; Nijenhuis *et al*, 2003). *In vitro* studies demonstrated the ability of uromodulin to decrease caveolin-mediated endocytosis of TRPV5 and TRPV6, hence increasing channel abundance at the plasma membrane. Consistently, *Umod* knockout mice show a marked reduction of TRP5 levels on the surface of DCT cells (Wolf *et al*, 2013).

Mg^{2+} transcellular reabsorption from the urine is instead mediated by the Mg^{2+} channel transient receptor potential melastin 6 (TRPM6), localized at the apical membrane of DCT cells. The role of uromodulin in Mg^{2+} homeostasis, was initially suggested from transcriptional profiling of DCT tubules isolated from mice under low-magnesium diet, detecting *Umod* as one of the most up-regulated genes (de Baaji *et al*, 2013). Further *in vitro* studies elucidated the ability of uromodulin to decrease dynamin-mediate

endocytosis of TRPM6, thus stabilizing it at cell surface (Nie *et al*, 2018). *In vivo*, under low-magnesium *Umod* knockout mice displayed reduced urinary uromodulin levels, decreased apical staining of TRPM6 in DCT cells and increased urinary Mg^{2+} wasting (Nie *et al*, 2018)

Of note, the regulation of TRPV5 and TRPV6 abundance was proposed to be mediated by extracellular uromodulin released by TAL cells, suggesting a paracrine control on DCT2 and CNT (Wolf *et al*, 2013). However, for TRPM6, that is co-expressed with uromodulin in DCT1, an autocrine mechanism of control cannot be excluded (Kemter *et al*, 2013; Wolf *et al*, 2019).

1.3.5 Modulation of kidney immunity

Several studies investigated the ability of uromodulin to modulate immune response, depicting it both as a pro- or an anti-inflammatory molecule (**Figure 3**).

Uromodulin pro-inflammatory role remains debated and yet to be elucidated. Several *in vitro* studies reported that uromodulin can activate different types of innate immunity cells such as neutrophils (Horton *et al*, 1990; Schmid *et al*, 2010; Thomas *et al*, 1993), monocytes (Thomas *et al*, 1993) and dendritic cells (Pfistershammer *et al*, 2008). All these studies were performed by using polymeric, urine-purified uromodulin, likely providing a model for its pro-inflammatory role as a danger-associated signalling molecule (DAMP) when, in conditions of altered uroepithelial integrity, it contacts immune cells in the kidney interstitium. This is in line with the observation that uromodulin aggregates activate monocytes by binding to Toll-like receptor 4 (TLR4) and inducing NF-kB pathway, or can be phagocytosed activating the NLRP3 (NACTH, LRR and PYD domains-containing protein 3) inflammasome. This eventually induces secretion of pro-inflammatory cytokine (IL-1β) and cell death (Darisipudi *et al*, 2012). Consistently, in a murine model of unilateral ureteral obstruction (UUO), *Umod* knockout mice developed a milder inflammatory response, characterized by reduced infiltration of $F4/80^{+}$ macrophages in the kidney interstitium, suggesting a role of uromodulin in monocyte recruitment (Maydan et al, 2018).

In other settings, uromodulin was instead demonstrated to exert an anti-inflammatory function. A possible protective role of uromodulin emerged from studies in a mouse model of acute kidney injury (AKI) induced by renal ischemia-reperfusion injury (IRI). In this context, *Umod* knockout mice were more susceptible to functional and histological kidney damage, as demonstrated by higher levels of inflammatory cell infiltrate and tubular cell necrosis (El-Achkar *et al*, 2008). Given that protected cells are mainly localized in S3 proximal tubule segment, a crosstalk between TAL cells and adjacent nephron segments has been hypothesized (El-Achkar *et al*, 2013). During the recovery phase after IRI, uromodulin seems to relocate from apical to basolateral side of epithelial cells and this associated with increased release in the circulation, pointing at serum uromodulin as a possible prognostic biomarker in the recovery phase from AKI (El-Achkar *et al*, 2008, 2013). In *Umod* knockout mice, delayed kidney recovery from AKI has been also associated with impaired M1 (pro-inflammatory) to M2 (healing phenotype) transition of kidney macrophages, indicating a role of uromodulin in modulating their number, plasticity and activity (Micanovic *et al*, 2018). The protective effect of uromodulin might reside on its ability to trap cytokines (IFN-γ, IL-1, TNF-α, IL-6, CXCL1 and IL-13) and influence their clearance through urine (Liu *et al*, 2012). Uromodulin was also reported to bind complement 1q, inhibiting the activation of the classical complement pathway (Rhodes, 2006). Finally, the observation that *Umod* knockout mice show increased number of neutrophils, also systemically and in the liver, suggested a broader role of uromodulin the regulation of neutrophil homeostasis. Further characterization of this phenotype revealed that it is due to activation of the IL-23/IL-17 axis in tubular S3 epithelium leading to enhanced granulopoiesis in the bone marrow and suggesting a role of uromodulin and the kidney as modulator of the hematopoietic system (Micanovic *et al*, 2015).

1.3.6 Roles of circulating uromodulin

A small proportion of uromodulin can reach the bloodstream via basolateral release from epithelial expressing cells (**Figure 3**). Little is known about the biological function of circulating uromodulin.

In patients with surgery-induced AKI, concentration of circulating uromodulin dropped and inversely correlated with oxidative damage at systemic level. Studies to characterize this association revealed a role of uromodulin in modulating both kidney and systemic oxidative stress by inhibiting the activity of transient receptor potential cation channel subfamily M, member 2 (TRPM2), a multifunctional and non-selective calcium ion channel implicated in increased reactive oxygen species (ROS) production during AKI (LaFavers *et al*, 2019). Circulating uromodulin also exerts an anti-inflammatory role, as described in a preclinical mouse model of sepsis without severe kidney injury (cecal ligation and puncture). In this context, basolateral secretion of uromodulin is increased, and it acts at systemic level on macrophages to enhance bacterial phagocytosis and clearance. Consistently, *Umod* knockout mice show increased mortality and bacterial burden that are ameliorated upon administration of a monomeric form of uromodulin (LaFavers *et al*, 2022). In addition, uromodulin has been shown to inhibit vascular calcification in the context of CKD. *Umod* knockout mice were indeed more susceptible to induced vascular calcification than wild type mice. *In vitro* studies on primary aortic smooth muscle cells suggest that uromodulin can interfere with and block cytokine-dependent pro-calcific signaling. This anti-calcific effect is quenched by uromodulin carbamylation and, interestingly, increased levels of carbamylated uromodulin was measured in serum of CKD patients (Alesutan *et al*, 2021).

All these findings expand the immunomodulatory role of uromodulin beyond the kidney, revealing its function as a systemic anti-inflammatory molecule and suggest the therapeutic potential of modulating circulating uromodulin levels.

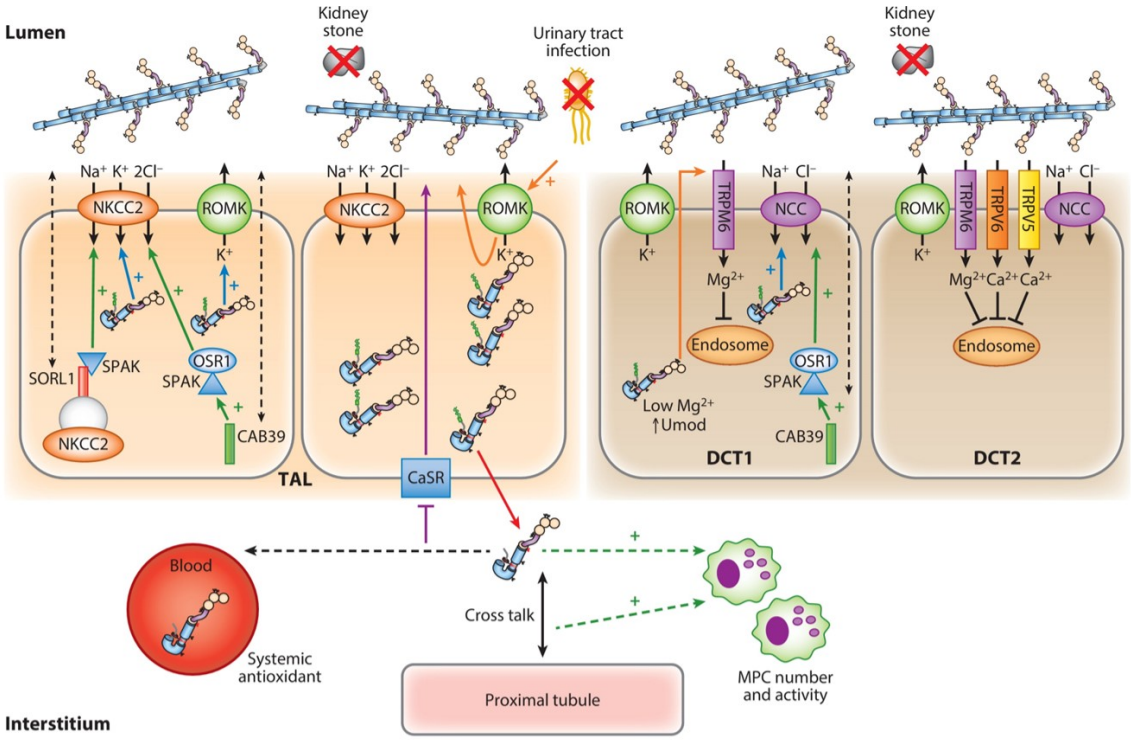


Figure 3. Summary of uromodulin functions and polarized secretion. *Uromodulin has a protective role against UTIs and kidney stone. It is also able to modulate renal sodium transport due to its ability to activate NKCC2 and ROMK in the TAL, and NCC in the DCT. CaSR and ROMK have a role in regulating apical uromodulin secretion. NKCC2 and NCC activation is contributed by scaffold proteins CAB39 and SPAK/OSR1, also associated with uromodulin urinary levels (dashed arrow). Calcium and magnesium transport in the DCT are enhanced by urinary uromodulin that is able to block endocytosis of TRPM6, TRPV5 and TRPM6. Circulating uromodulin released through the basolateral side of epithelial cells acts as an antioxidant molecule and regulates number and activity of polymorphonuclear cells (From* Schaeffer et al, 2021. *Reproduced with permission from the Annual Review of Physiology, Volume 83 © 2021 by Annual Reviews, http://www.annualreviews.org).*

1.4 Relevance of uromodulin in common kidney diseases

In recent years, extensive efforts have been made to understand the clinical relevance and the role of uromodulin in both systemic and kidney diseases. The *UMOD* gene appears to be involved in a *continuum* of genetic risk of kidney disease, ranging from common to rare disorders. Indeed, while common low-impact variants are strongly associated in the general population with increased risk for complex traits, as CKD, hypertension and kidney stones, rare variants with large-effect size are the major cause

of a Mendelian disease known as Autosomal Dominant Tubulointerstitial Kidney Disease (ADTKD) *(Paragraph 1.5)*.

1.4.1 Chronic kidney disease

Chronic kidney disease (CKD) is defined as reduced glomerular filtration rate (GFR, <60 mL/min/1.73 m^2) persisting for more than 3 months or kidney damage, of any primary cause. CKD is a common disease, with a worldwide prevalence in the general population of about 10%. Its burden on public health is associated with metabolic syndromes, ESKD and multi-systemic complications, such as increased risk to develop cardiovascular diseases (CVD). No specific cure is currently available and renal replacement therapy (kidney transplant or dialysis) represents the only therapeutical option.

Besides estimated GFR (eGFR), uromodulin, being a kidney-specific product, is considered a marker of kidney functioning mass. Several studies have indeed demonstrated the correlation between urinary or circulating uromodulin with eGFR and its clinical relevance for the identification of early-stage CKD (Fedak *et al*, 2016; Schulz *et al*, 2019; Steubl *et al*, 2016; Thornley *et al*, 1985).

CKD is a multifactorial disorder whose risk is contributed both by acquired (environmental) and inherited (genetic) factors. Common aetiologies of CKD are hypertension, diabetes mellitus, atherosclerosis, and nephrotoxic drugs, while its genetic architecture is only partially understood.

A seminal GWAS comparing about 2,000 CKD patients and non-CKD controls with European ancestry, identified the common variant rs12917707 located in the *UMOD* promoter associated with kidney function and CKD risk (Köttgen *et al*, 2009). This finding was later confirmed on a larger study in a total of about 7,000 CKD European patients (Köttgen *et al*, 2010). The minor T allele (with a frequency of 0.18 in the population) is associated with 20% reduced risk to develop CKD, independently from other main risk factors of the disease such as systolic blood pressure, hypertension medication, diabetes mellitus, age, and male gender (Köttgen *et al*, 2010). Complementarily, a meta-analysis of uromodulin urinary levels in the general population

reported higher uromodulin levels in urine of carriers of the rs12917707-G risk allele and its association with increased risk of CKD (Olden *et al*, 2014)

Several subsequent studies on different ethnic background replicated the association of *UMOD* variants, all mapping in gene promoter within the same linkage *disequilibrium* block, with kidney function and CKD (**Figure 4**) (Devuyst *et al*, 2017; Gudbjartsson *et al*, 2010; Morris *et al*, 2019; Akwo *et al*, 2022).

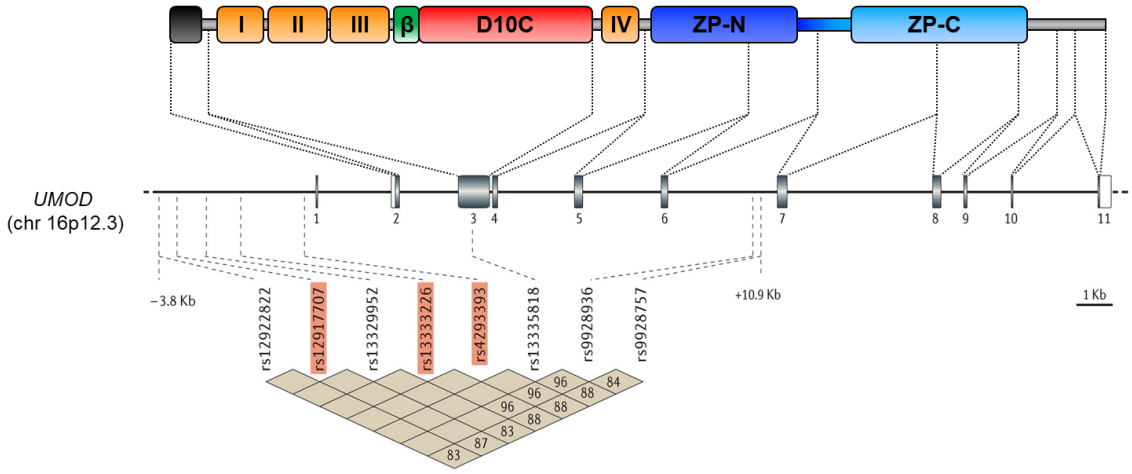


Figure 4. Common genetic variants of UMOD associated with increased risk for complex traits. *Correspondence between exon (in grey) and intron structure of the human UMOD gene (central panel) and encoded protein domains (upper panel). The lower panel shows the position of the top SNPs (indicated in red) identified in several GWAS. These variants are within a region of complete linkage disequilibrium spanning the UMOD promoter and extending to intron 6, as indicated by the r^2 values between the indicated SNPs (those without number represent the maximum value 100) (from Devuyst et al, Nat Rev, 2017*; license number 5444130816248*).*

Recently, the CKD Genetics Consortium reported a trans-ancestry GWAS meta-analysis with about one million individuals which identified 264 loci, explaining about 20% of genetic predisposition to CKD. This large study confirmed that the *UMOD* locus shows the largest effect size on kidney function and CKD (Wuttke *et al*, 2019). This study also revealed independent association of CKD risk with a SNP, rs77924615, mapping within the *UMOD*-flanking gene *PDILT*. This variant, that is not in *linkage disequilibrium* with *UMOD* promoter variants, is associated with uromodulin urinary levels but not with the expression of *PDILT* itself (Wuttke *et al*, 2019). A similar finding was obtained from

expression studies on kidney tissue from 260 healthy individuals, pointing out that *PDILT* acts as a quantitative trait locus for *UMOD* expression (Morris *et al*, 2019).

The biological effect of *UMOD* promoter variants was clarified by analyzing nephrectomy samples from homozygous carriers of either risk or protective alleles at *UMOD* promoter variant rs12917707 and rs4293393. The analysis of *UMOD* transcript levels revealed two-fold increased *UMOD* expression in kidney samples of individuals bearing the *UMOD* promoter risk variants compared to carriers of the protective haplotype. This effect was modeled in transgenic mice overexpressing wild type uromodulin ($Tg^{Umod\text{wt/wt}}$) (Trudu *et al*, 2013). Increased age-associated kidney damage, as tubular damage and kidney inflammation was observed in $Tg^{Umod\text{wt/wt}}$ mice at 24 months of age, relative to age-matched wild type controls. Interestingly, similar increased focal lesions were observed in human nephrectomy samples from individuals older than 65 years of age and with preserved renal function who carried homozygous *UMOD* risk haplotype, as compared to carriers of protective alleles. This is in line with previous demonstration that the effect of *UMOD* genetic variants on kidney function is age-dependent, becoming significantly stronger in individuals with over 65 years of age (Gudbjartsson *et al*, 2010; Pattaro *et al*, 2012). In the context of UUO-induced kidney injury, considered an animal model of CKD, *Umod* knockout mice develop milder tubular injury and inflammation response, compared to wild type littermates (Maydan *et al*, 2018). This observation corroborates, in a setting complementary to $Tg^{Umod\text{wt/wt}}$ mice, the link between increased *UMOD* gene dosage and CKD risk. Further studies are warranted to understand the molecular bases of such association.

1.4.2 Hypertension

As mentioned above, *UMOD* promoter risk haplotype was also associated with higher risk of hypertension. Hypertension (HTN) is a major cause of CVD morbidity and mortality, with a global estimated prevalence of about 31% of adults (1.39 billion) worldwide (Mills *et al*, 2020). Hypertension is a complex trait, with both genetic and environmental factors concurring to determine susceptibility. In order to identify new pharmacological targets to regulate BP and treat HTN, extensive effort has been accomplished to identify its genetic bases as high BP is heritable for 30-60% of cases.

The association of hypertension with *UMOD* was demonstrated in 2010 by Padmanabhan et al through a GWAS analysis comprising 1,621 hypertensive cases and 1,699 controls and validated in 19,845 cases and 16,541 controls. The associated SNP rs13333226 is localised in the *UMOD* promoter. The minor G allele associated with a reduced risk of develop HTN (OD = 0.6) and CVD is also associated with lower urinary levels and with increased eGFR (Padmanabhan *et al*, 2010). Another polymorphism rs12917707, also in the *UMOD* promoter and in linkage *disequilibrium* with rs13333226 has been associated with cardiorenal function in patients with arterial HTN and CVD. Homozygous carriers of the protective allele indeed show significantly higher eGFR values and smaller left atrial diameter (Algharably *et al,* 2017).

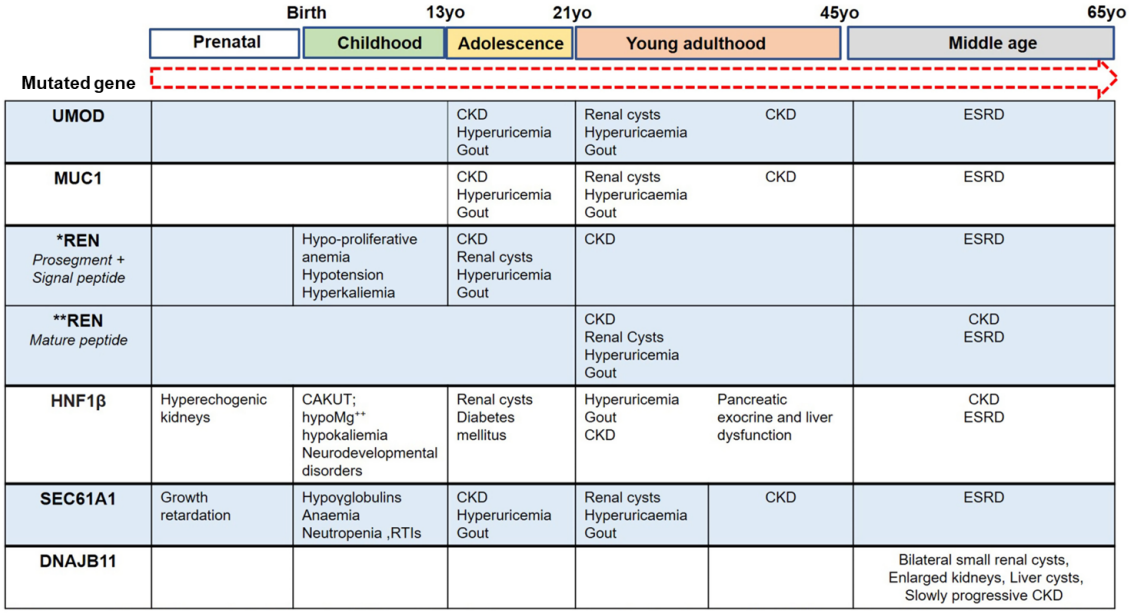
As mentioned above, studies on homozygous carriers of *UMOD* risk alleles and on a mouse model overexpressing uromodulin demonstrated that the biological effect of *UMOD* promoter variants is higher gene expression leading to increased protein production and excretion in the urine (Trudu *et al*, 2013). Thus, increased uromodulin levels that are protective against UTIs and kidney stones, are independently associated with higher risk of CKD and HTN.

The causal link between the level of uromodulin expression and HTN has been demonstrated in $Tg^{Umodwt/wt}$ mice. These mice overexpressing uromodulin spontaneously develop salt sensitive hypertension that can be normalized by reducing dietary NaCl. This phenotype is due to hyperactivation of NKCC2, demonstrated by increased phosphorylation of the transporter and enhanced response to furosemide. Such mechanism is conserved in hypertensive patients homozygous for *UMOD* risk variants, for whom furosemide treatment is more effective in lowering BP (Trudu *et al*, 2013). The causative role of uromodulin in BP regulation is further corroborated by the observation that at baseline, *Umod* knockout mice show significantly lower blood pressure as compared to wild type counterparts and show resistance of BP increase with increased salt intake (Graham *et al*, 2014). Uromodulin regulates NKCC2 through a mechanism that is only partly understood, involving tumor necrosis factor-α (TNFα) and SPAK and OSR1 kinases (Trudu *et al*, 2013; Graham *et al*, 2014). Based on these preclinical findings a clinical trial (BHF UMOD) is currently ongoing to test the efficiency on BP regulation of torasemide, an inhibitor of NKCC2, in hypertensive patients based on their *UMOD* genotype (McCallum *et al*, 2021).

1.5 Autosomal Dominant Tubulointerstitial Kidney Disease (ADTKD)

Autosomal Dominant Tubulointerstitial Kidney Disease (ADTKD) is a group of rare and genetically heterogenous disorders inherited in an autosomal dominant manner. They are mainly characterized by interstitial fibrosis with tubular atrophy in the absence of significant glomerular lesions, normal urinary parameters and progressive loss of kidney function leading to ESKD in the adulthood (**Figure 5**) (Devuyst *et al*, 2019; Mabillard *et al*, 2021; Econimo *et al*, 2022). The age at ESKD can range from 20 to 80 years and the rate of progression to kidney failure is highly variable within and between families for yet unknown reasons (Bleyer *et al*, 2017; Kidd *et al*, 2020; Olinger *et al*, 2020a). Mutations in 5 genes are the cause of ADTKD: *UMOD* (Hart, 2002), *MUC1* (Kirby et al, 2013), *REN* (Živná *et al*, 2009), *HNF1B* (Bingham *et al*, 2003) and *SEC61A1* (Bolar *et al*, 2016) (**Figure 5**). In addition, mutations in *DNAJB11* have been reported to cause a rare and atypical form of ADTKD (Cornec-Le Gall *et al*, 2018). Additional causative genes are likely to be identified, as mutations in the already reported genes have not been found in at least 20-30% of individuals with criteria for definite ADTKD (Cormican *et al*, 2019).

More than one term has been used when referring to the disease, including Medullary Cystic Kidney Disease (MCKD) type 1 and 2 and Familial Juvenile Hyperuricemic Nephropathy (FJHN) type 1 and 2 (Eckardt *et al*, 2015). The variety of these terms and the fact that cysts are not a common hallmark in patients prompted a Kidney Disease: Improving Global Outcomes (KDIGO) consensus study which proposed the term autosomal dominant tubulointerstitial kidney disease (ADTKD) to collectively describe these disorders. According to the gene carrying the pathogenic variant, the disease is subclassified as ADTKD-*(mutated gene)*. ADTKD patients with no identified causative gene are referred to as ADTKD-NOS, for “not otherwise specified” (Eckardt *et al*, 2015).



UMOD			CKD Hyperuricemia Gout	Renal cysts Hyperuricaemia Gout	CKD	ESRD
MUC1			CKD Hyperuricemia Gout	Renal cysts Hyperuricaemia Gout	CKD	ESRD
***REN** *Prosegment + Signal peptide*		Hypo-proliferative anemia Hypotension Hyperkaliemia	CKD Renal cysts Hyperuricemia Gout	CKD		ESRD
****REN** *Mature peptide*				CKD Renal Cysts Hyperuricemia Gout		CKD ESRD
HNF1β	Hyperechogenic kidneys	CAKUT; hypoMg^{++} hypokaliemia Neurodevelopmental disorders	Renal cysts Diabetes mellitus	Hyperuricemia Gout CKD	Pancreatic exocrine and liver dysfunction	CKD ESRD
SEC61A1	Growth retardation	Hypoyglobulins Anaemia Neutropenia ,RTIs	CKD Hyperuricemia Gout	Renal cysts Hyperuricaemia Gout	CKD	ESRD
DNAJB11						Bilateral small renal cysts, Enlarged kidneys, Liver cysts, Slowly progressive CKD

Figure 5. Clinical features of ADTKD. *The table recapitulates kidney and extra-kidney manifestations of each ADTKD subtype. Age at onset of chronic kidney disease (CKD) and end stage renal disease (ESRD) are indicated. ADTKD, autosomal dominant tubulointerstitial kidney disease; CAKUT, congenital anomalies of the kidney and urinary tract; RTI, respiratory tract infections (from Econimo et al, 2022. Open access).*

Genetic testing is the first-line approach for ADTKD diagnosis and characterization. It is carried out by panel testing with next generation sequencing (NGS) of the reported causative genes, even though exome sequencing is becoming increasingly common (Groopman *et al*, 2019). These new molecular diagnosis approaches and different large international cohort studies have led to an increase in reported cases. Nowadays ADTKD is considered one of the most common monogenic causes of CKD (Mabillard *et al*, 2021; Econimo *et al*, 2022), although its precise prevalence is difficult to be established due to high heterogeneity of clinical presentation and difficulties in screening for *MUC1* mutations (see *Paragraph 1.5.2*).

There is no specific cure for ADTKD other than kidney replacement therapy. The disease does not recur after kidney transplantation that hence represents a definitive option for patients reaching ESKD (Eckardt *et al*, 2015).

1.5.1 ADTKD-UMOD

Mutations in *UMOD* lead to ADTKD-*UMOD* (OMIM #162000), which was defined as a disease with juvenile onset of hyperuricemia, gout and progressive kidney failure and previously identified as FJHN1 or MCKD2. *UMOD* was identified as the causative gene in 2002 (Hart, 2002).

Different genetic studies point at ADTKD-*UMOD* as the most common ADTKD form. A study on 726 patients from two large registries calculated its prevalence at 37% of all ADTKD cases (Olinger *et al*, 2020). Data from a single center study in United Kingdom based on family history and *UMOD* sequencing, established ADTKD-*UMOD* as the most frequent kidney monogenic disease after Autosomal Dominant Polycystic Kidney Disease (ADPKD), accounting for 3% of all ESKD cases (Gast *et al*, 2018). This high prevalence was further confirmed by exome sequencing data obtained from a cohort of more than 3,000 patients with ESKD, reporting *UMOD* mutation in 1% of all patients with a monogenic diagnosis of CKD and describing ADTKD-*UMOD* as the third most frequent kidney monogenic disorder after ADPKD and Alport syndrome (Groopman *et al*, 2019). More recently, a study on 221 Taiwanese families presenting with CKD identified *UMOD* missense mutations in 1.36% of all the cases (Chen *et al*, 2022).

Patients with *UMOD* mutation present with impaired urinary concentration ability, bland urinalysis, normal or elevated blood pressure, normal or small-sized kidneys, and progressive loss of kidney function leading to ESKD (**Figure 5**). Data on kidney survival suggests a variable decline in kidney function. A large cooperative international work on 722 affected individuals from 249 families estimated the median age at ESKD onset at 47 years (ranging from 18 to 87) (Kidd *et al*, 2020), while in a second study including patients from the ADTKD American and European registries, age at ESKD was estimated at 54 years (range 25 to 70) (Olinger *et al*, 2020). Both these studies described significantly better prognosis and kidney survival in female patients compared to males (Kidd *et al*, 2020; Olinger *et al*, 2020). The only extrarenal presentation and characteristic hallmark of ADTKD-*UMOD* is hypouricosuric hyperuricemia, caused by decreased fractional excretion of urate, that leads to early onset gout. Gout is described in 83% of affected men and 74% of affected women, with a median age at presentation of 27 years (Olinger *et al*, 2020) and it is reported as the most common feature in paediatric presentation (Bleyer *et al*, 2021). Hyperuricemia is likely due to defective ion transport

as a consequence of TAL cell damage. Reduced NKCC2 activity in this segment could induce an hypovolemic state and compensatory up-regulation of Na^{2+} transporters in the proximal tubule, where Na^{2+} transport is indirectly coupled with uric acid reabsorption, eventually leading to lower fractional excretion of urate, hyperuricaemia and gout (Scolari *et al*, 2004; Ayasreh *et al,* 2018; Bernascone *et al,* 2010).

Kidney histology of ADTKD-*UMOD* patients is characterized by diffuse tubulointerstitial damage, with moderate inflammatory infiltrate, interstitial fibrosis, thickening and lamellation of the tubular basement membrane and tubular atrophy and cysts at the cortico-medullary junction in one third of the cases (Olinger *et al,* 2020). Uromodulin staining in kidney specimen of ADTKD-*UMOD* patients reveals the presence of large intracellular aggregates, as opposite to the predominant localization at the cell apical membrane observed in control kidneys (Rampoldi *et al*, 2003). Intracellular accumulation is associated with significantly reduced apical and basolateral uromodulin secretion as shown by its reduced concentration in urine and blood of ADTKD-*UMOD* patients compared to healthy individuals (Dahan *et al,* 2003; Bleyer *et al,* 2004; Satanovskij *et al,* 2017).

As for other ADTKD forms, no specific therapy is currently available for ADTKD-*UMOD*. Transplantation is effective and shows no evidence of disease recurrence (Cormican *et al,* 2019). Allopurinol and xanthine oxidase inhibitors can be used to control hyperuricemia and prevent gout (Eckardt *et al*, 2015).

To date, more than 170 ADTKD-*UMOD* mutations have been reported (**Figure 6**) (Devuyst *et al*, 2017; Olinger *et al*, 2020; Kidd *et al*, 2020; Econimo *et al*, 2022). The vast majority are private mutations, usually described in members from one or few families only. However, a recent analysis of 12 apparently unrelated pedigrees from a geographically contiguous UK region, presenting familiarity of CKD, identified a rare *UMOD* pathogenic variant c.278_289delTCTGCCCCGAAG insCCGCCTCCT (Indel rs878855325, indicated in **Figure 6** as V93-G97 del4ins) in 88 probands. Further analysis of this variant in the UK 100K Genomes Project and from UK Biobank increased to 117 the number of CKD patients harbouring the Indel rs878855325 variant. A shared haplotype between carriers was demonstrated, suggesting a founder effect for this variant in the British population (Valluru *et al*, 2022).

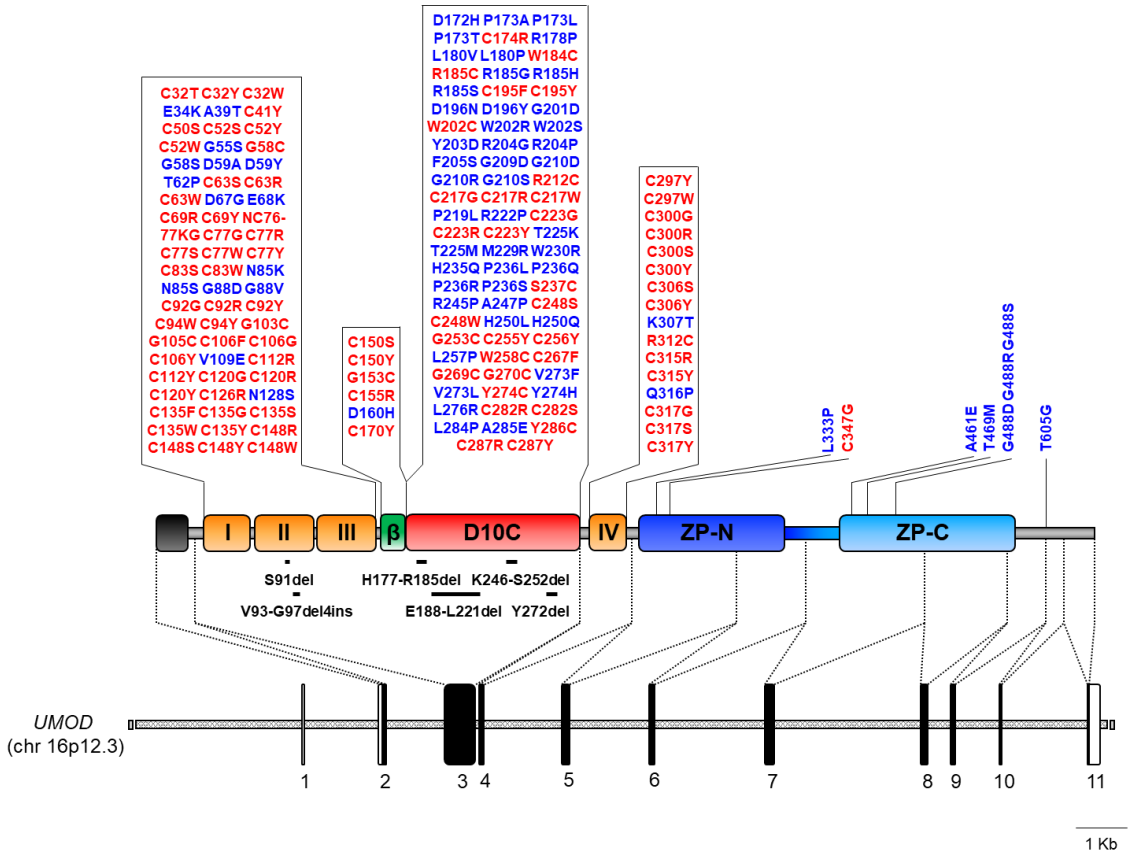


Figure 6. Summary of ADTKD mutations in UMOD. *The upper panel shows the localization on the protein sequence and the amino acid substitution induced by all the reported UMOD mutations. The exon (in black) and the intron (in grey) structure of the human UMOD gene is reported in the lower panel. Most of the mutations are clustered in exon 3 and exon 4. In red mutations involving a cysteine residue are reported. The six in-frame deletions are indicated in black. Mutations reported in blue are missense changes affecting residues other than cysteines (adapted and updated from Devuyst et al, 2017; Olinger et al, 2020; Kidd et al, 2020).*

Apart from six in-frame deletions, all reported mutations are missense changes, mostly (95.5%) mapping in exons 3 and 4, corresponding to the N-terminal part of the protein and encoding for the four EGF-like and the D10C domains. The majority of these mutations directly involve a disulphide bond, either by replacing or introducing a cysteine residue (Devuyst *et al*, 2019; Olinger *et al*, 2020). As discussed above, the formation of the 24 intramolecular disulphide bonds of uromodulin is necessary for the acquirement of the proper protein structure (Serafinicessi *et al*, 1993). Thus, the common effect of *UMOD* mutations, due to their impact on protein folding, is retention of misfolded mutant protein in the ER of TAL epithelial cells, a feature observed in kidney biopsies from

patients (Bernascone *et al,* 2010), and recapitulated by several *in vitro* and *in vivo* models of mutant uromodulin expression (see below).

Evidence of genotype-phenotype correlation between *UMOD* mutation and ADTKD onset and progression has been reported. Studies on patients bearing different *UMOD* mutations suggested that mutation types have no impact on disease prognosis as no significant differences in age at ESKD or gout onset are observed for patients carrying mutations on cysteine residues compared with mutations in polar residues (Bollée *et al*, 2011; Olinger *et al*, 2020). In contrast, mutation position is correlated with clinical features as demonstrated by the observation that patients carrying mutations in N-terminal EGF-like domains II and III developed earlier onset of ESKD (45-52 years) compared to carriers of mutations affecting the D10C or other C-terminal domains (60-65 years) (Moskowitz *et al*, 2013).

UMOD mutations usually segregate as heterozygous alleles. Nevertheless, the few reported homozygous carriers of *UMOD* mutations consistently showed a more severe phenotype (Rezende-Lima *et al*, 2004; Edwards *et al*, 2017). This gene dosage effect was confirmed in two different mouse models of the disease with animals homozygous for *Umod* mutation showing more severe kidney dysfunction and morphological alteration (Kemter *et al*, 2013).

1.5.1.1 ADTKD-UMOD in vitro studies

Different *in vitro* studies carried out by expressing several uromodulin mutants in a variety of cellular systems characterized the effect of ADTKD associated *UMOD* mutations and identified ER retention of mutant uromodulin as the primary effect. (Bernascone *et al*, 2006; Choi *et al*, 2005; Vylet'al *et al*, 2006; Schaeffer *et al*, 2017).

Intracellular gain-of-(toxic)-function of *UMOD* mutation was demonstrated by transcriptional profiling of immortalized mouse TAL (mTAL) cells expressing p.Cys150Ser uromodulin mutant isoform revealing induction of the unfolded protein response (UPR). UPR is a stress response induced by the cell in presence of ER engulfment. This response is aimed at restoring ER homeostasis by reducing ER load through decreased general protein synthesis, increased folding through induction of ER

chaperones and increased degradation by activation of the endoplasmic reticulum-associated degradation (ERAD). This response can be activated via three different sensors localized in the ER membrane i.e., IRE1, PERK and ATF6 (Walter & Ron, 2011). In mTAL cells, the specific induction of the IRE1 pathway was observed, with no activation of the other two UPR sensors. Consistent with UPR activation, mutant uromodulin was shown to interact with the main ER chaperones Bip and calnexin, suggesting that uromodulin is folded in the ER through the calnexin-calreticulin cycle (Schaeffer *et al*, 2017).

Although defective ER to Golgi protein transport is the leading effect of all *UMOD* mutations, the extent of ER retention varies among different mutants. Based on this observation, an *in vitro* score dividing *UMOD* mutations in four classes was proposed and, interestingly, it was found to be a promising predictor of age at ESKD as the amount of intracellular retention induced by the mutation correlates with the severity of the disease in patients (Kidd *et al*, 2020). Of note, the *UMOD* missense variant p.Thr62Pro was recently reported as a variant with an intermediate biological effect. This variant has been detected in about 1/1000 individuals of European ancestry and associated with kidney failure in the 100K Genomes Project. *In vitro* characterization revealed an intermediate *UMOD* trafficking defect and ER stress induction when compared with wild type and with the prototypical ADTKD-*UMOD* mutant p.Cys150Ser. This correlates with intermediate decrease of uromodulin levels in the urine and reduced disease severity (i.e., slower progression of kidney failure with ESKD delayed by about 20 years) observed in p.Thr62Pro carriers compared to patients bearing canonical ADTKD-*UMOD* mutations (Olinger *et al*, 2022). The identification of such an intermediate-effect *UMOD* variant completes the spectrum of *UMOD*-associated kidney diseases, ranging from frequent variants with low effect size to very rare variants associated with the Mendelian disease.

Studies in Madin-Darby canine kidney (MDCK) cells demonstrated that mutant uromodulin escaping the ER quality control and reaching the plasma membrane forms large extracellular aggregates, as opposed to the assembly in filamentous polymers of the wild type protein. Interestingly, when co-expressed with wild type uromodulin, mimicking the patient condition, mutant uromodulin induces a dominant negative effect on wild type protein polymerization, suggesting that the gain-of-function effect of mutant

uromodulin can be exerted both intracellularly (due to ER retention) and extracellularly (Schaeffer *et al*, 2012).

Some *in vitro* studies reported induction of apoptosis in cells expressing different mutant uromodulin isoforms (Choi *et al*, 2005; Ma *et al*, 2012). Improvement of cell viability has been observed upon treatment of cells with the low molecular weight chemical chaperones 4-PBA, with concomitant increase in uromodulin trafficking and secretion (Choi *et al*, 2005; Ma *et al*, 2012). Unfortunately, these data were not reproduced *in vivo*, as 4-PBA did not rescue mutant uromodulin trafficking in a mouse model of ADTKD-*UMOD* (Kemter *et al*, 2014).

1.5.1.2 ADTKD-UMOD in vivo models

Several mouse models, carrying different *UMOD* mutations and generated with various strategies of mutagenesis, have been reported so far (**Table 1**) (Bernascone *et al*, 2010; Kemter *et al*, 2013, 2017; Piret *et al*, 2017; Johnson *et al*, 2017; Ma *et al*, 2017). The first ADTKD-*UMOD in vivo* model was generated in our laboratory and is the murine model that has been used during my PhD thesis. It is a transgenic mouse line expressing HA-tagged, p.Cys147Trp mutant uromodulin isoform ($Tg^{Umod\text{C147W}}$), homologous to the patient mutation p.Cys148Trp previously identified and characterized *in vitro* (Rampoldi *et al*, 2003). $Tg^{Umod\text{C147W}}$ mice recapitulate most of the features of the human disease, as remarkable retention and accumulation of mutant protein within the ER of TAL cells (**Figure 7** and **Table 1**), tubular dilation and atrophy, kidney inflammation (characterized by the presence of markers of inflammatory cells as macrophages and granulocytes), interstitial fibrosis and progressive kidney injury leading to mild kidney failure around 24 weeks of age. Hyperuricemia was not detected, likely due to the presence of the hepatic enzyme uricase, expressed in mice but not in humans, able to catalyze the conversion of uric acid (with low solubility) to allantoin (with high solubility) (Bernascone *et al*, 2010). As observed in ADTKD-*UMOD* patients, $Tg^{Umod\text{C147W}}$ mice showed a reduction in urinary uromodulin excretion, polyuria, polydipsia and reduced urine osmolarity. Urinary concentration defect results from TAL dysfunction as mutant mice display defective expression of some key ion transporters of this segment (NKCC2, ROMK and the chloride channel Kb, ClC-Kb) necessary for urine concentration. This is possibly due to

necrotic TAL cell death observed at a later time point (24 weeks of age) (Bernascone *et al*, 2010). Of note, transgenic mice for the wild type protein (Tg^{Umodwt}) do not develop any of the described disease phenotypes, excluding an effect due to uromodulin overexpression (Bernascone *et al*, 2010). Further characterization of this model at earlier time points of pathogenesis will be presented in the section "*1.6 Preliminary results*".

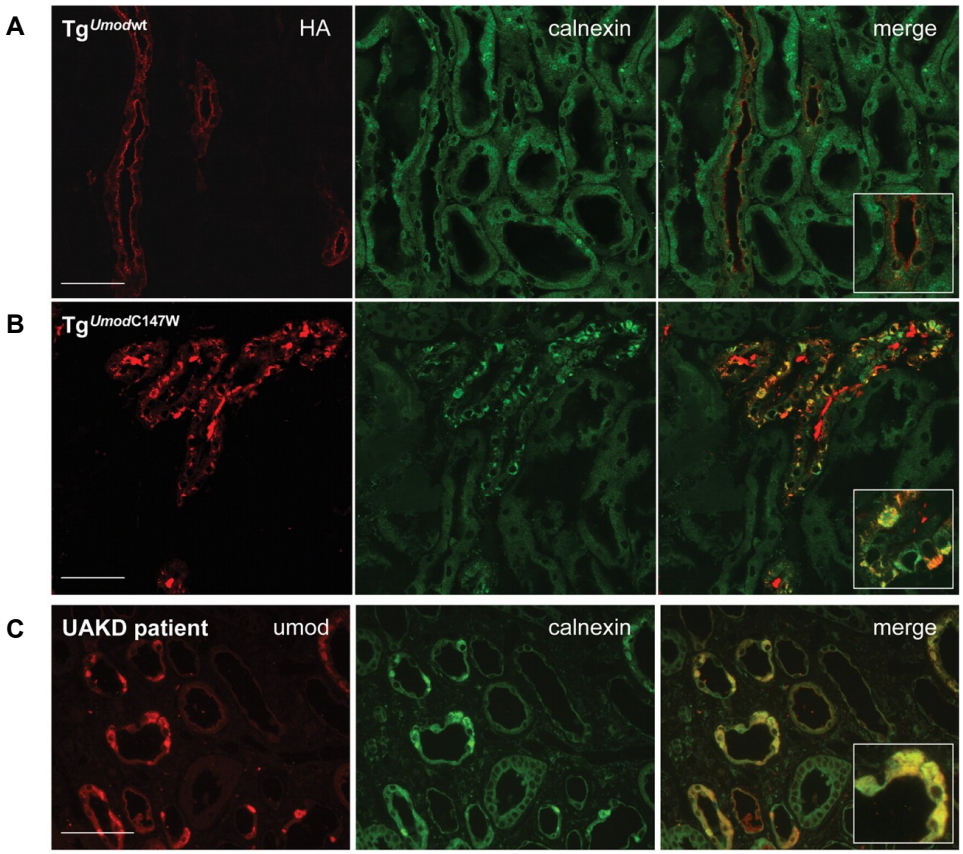


Figure 7. Endoplasmic reticulum retention of mutant uromodulin in $Tg^{UmodC147W}$ mice and in ADTKD-UMOD patients. *Immunofluorescence analysis for transgenic uromodulin (anti-HA, in red) and the ER chaperone calnexin (in green) in A) $Tg^{Umodwtt}$ and B) $Tg^{UmodC147W}$ mice. C) Staining for uromodulin (in red) and calnexin (in green) on a kidney biopsy from an ADTKD-UMOD patient (UAKD, uromodulin associated kidney disease). Uromodulin in Tg^{Umodwt} is enriched at the apical plasma membrane, while in $Tg^{UmodC147W}$ mice it is retained in the ER, similarly to what observed in ADTKD-UMOD patient (data from Bernascone et al, 2010).*

Two mouse models expressing p.Cys93Phe and p.Ala227Thr uromodulin isoforms have been generated by N-ethyl-N-nitrosourea-induced mutagenesis ($Umod^{C93F}$, $Umod^{A227T}$). While the two *Umod* variants have not been identified in ADTKD patients, both models

develop the main features of ADTKD, including defects in urine concentration, reduced fractional excretion of urate and kidney morphological alterations suggesting tubulointerstitial damage (**Table 1**). Interestingly, they show different degrees of mutant uromodulin ER retention that are reflected by differences in the onset and progression of the disease, with *Umod*^{C93F} mice showing a more severe phenotype. Proteomic analysis on outer medulla kidney samples (enriched in TAL segments) from *Umod*^{C93F} mice revealed modification in the composition of ER, mitochondria and peroxisomes, as well as in cellular energy metabolism (Kemter *et al*, 2017). In *Umod*^{C93F} mice, retention of mutant uromodulin alters ER homeostasis, causing ER stress and leading to UPR, as demonstrated by increased phosphorylation of eIF2α and increased expression of *Atf4*, *Atf6* and CHOP. A decreased number of mitochondria with altered morphology was also observed in TAL cells of mutant mice, likely because of reduction of mitochondrial fission. Mitochondrial dysfunction could be secondary to ER stress, affecting ER-mitochondria communication, as suggested by altered levels of proteins of the mitochondria-associated membranes (MAMs) (Kemter *et al*, 2017). Interestingly, kidney transcriptomic analysis of *Umod*^{C93F} and *Umod*^{A227T} mice revealed the up-regulation of *Scd1*, encoding for the stearoyl-coenzyme A desaturase 1, a highly regulated lipogenic enzyme specifically expressed in the S3 segment of the proximal tubule, a portion of the nephron in close proximity of the TAL (Horsch *et al*, 2014). This gene has been associated with inflammation and cellular stress (Liu *et al*, 2011b) and its induction might indicate that kidney damage propagates from TAL segments to neighboring proximal tubules (Horsch *et al*, 2014).

A knock-in ADTKD model was obtained by homologous recombination in murine embryonic stem cells. This mouse line carries the p.Cys125Arg *UMOD* mutation (*Umod*^{C125R}), corresponding to the mutation p.Cys126Arg reported in humans . By 24 weeks of age, mutant mice develop all ADTKD-*UMOD* main features (**Table 1**) (Piret *et al*, 2017). Recently, high-resolution spatial transcriptomics analysis on kidney slides from 24-week-old homozygous *Umod*^{C125R} mice identified, specifically into the kidney medulla, increased expression of UPR genes and presence of a subpopulation of Trem2^{+} macrophages in proximity of epithelial TAL cells. Trem2 is a membrane receptor expressed on resident macrophages that has been involved in immunomodulation and

damage sensing. This inflammatory cell may expand in response to injury of neighbouring epithelial cells (Marshall *et al*, 2022).

A second ADTKD knock-in mouse line, expressing the p.Cys147Trp missense mutation (*Umod*^{C147W}) was generated using the CRISPR-Cas9 technology. As the other models previously reported, *Umod*^{C147W} mice recapitulate the main features of the disease (**Table 1**) (Johnson *et al*, 2017). At 24 weeks, *Umod*^{C147W} mice display features of autophagy deficiency, demonstrated by accumulation of p62, reduction of active Lc3b and deregulation of key autophagy genes in uromodulin-positive epithelial cells. *In vitro*, treatment of human tubular epithelial cells expressing p.Cys147Trp mutant uromodulin with mTOR inhibitors rapamycin or torkinib, that increase autophagy flux, lead to a reduction of intracellularly aggregated mutant uromodulin (Johnson *et al*, 2017). Inflammation and particularly induction of the TNF signalling pathway was observed at all the analysed time points. Interestingly, the administration of a recombinant fusion protein TNFR:Fc to block TNF-α signalling slowed disease progression highlighting the importance of inflammation in ADTKD-*UMOD* onset and progression and the potential therapeutic relevance of its targeting (Johnson *et al*, 2017).

Study	Bernascone et al, *Hum Mol Genet.* 2010	Kemter et al, *AJP Renal Physiol.* 2009	Kemter et al, *Hum Mol Genet.* 2013	Johnson et al, *J Clin Invest.* 2017	Piret et al, *Dis Model Mech.* 2017	Ma et al, *PLoS One.* 2017
Type	Transgenic	ENU	ENU	Knock-in	Knock-in	Knock-in
Mutation	C147W	A227T	C93F	C147W	C125R	C217G
Background	FVB	C3HeB/FeJ (C3H)	C3HeB/FeJ (C3H)	C57BL/6J	C57BL/6J	FVB
Umod ER accumulation	Yes	Yes	Yes	Yes	Yes	Yes
Umod urinary secretion	↓	↓	↓	↓	↓	↓
Body weight	=	↓	↓	↓	=	=
Plasma Ur Ac	=	↑	NR	NR	=	↑
Renal Failure	Yes	Yes	Yes	Yes	Yes	Yes
Urinary concentration	↓	↓	↓	↓	↓	↓ young mice (↑ old mice)
Urinary pH	↓	NR	NR	NR	↓	↓
Urinary Ur Ac	NR	↓	↓	NR	↓	↓
Urinary Ca	↑	↑	↑	NR	↑	(↑)
Fibrosis	Yes	Yes	Yes	Yes	Yes	Yes
Immune infiltration	Yes	Yes	Yes	Yes	Yes	(Yes)
Tubular dilation	Yes	No	Yes	NR	No	Yes
ER stress/ UPR	Yes	Yes	Yes (PERK, ATF6)	Yes (IRE1, PERK)	Yes (IRE1, PERK)	Yes (IRE1)
Autophagy	↓	NR	↑ (mitophagy)	↓	NR	NR
Mitochondria	NR	↓	↓	NR	NR	NR
Apoptosis	No (necrosis, 24w)	No	No	Yes	No	Yes

Table 1. ADTKD-UMOD mouse models. *The table recapitulates the main features of the different mouse models carrying uromodulin mutations reported so far. Mutagenesis approach, type of mutations and effects induced by mutations on uromodulin biology, kidney function and morphology and at cellular levels are reported. ER, Endoplasmic Reticulum; Ur Ac, Uric Acid; UPR, Unfolded protein response; NR, not reported (Bernascone et al, 2010; Kemter et al, 2013; Kemter et al, 2017; Piret et al, 2017; Johnson et al, 2017; Ma et al, 2017).*

In summary, patient data and several different *in vitro* and *in vivo* models of mutant uromodulin expression clearly established retention of mutant uromodulin within the ER as the primary cellular effect induced by *UMOD* mutations. This is likely due to protein misfolding, ascribing ADTKD-*UMOD* to the family of ER storage diseases. Uromodulin ER retention leads to ER stress and UPR induction that have been described in cell and animal models, and also detected in patient samples (Adam *et al*, 2012; Kim *et al*, 2021; Olinger *et al*, 2022; Kim *et al*, 2017). Other phenotypes proposed to be secondary to ER stress have been reported as mitochondrial dysfunction, defective protein homeostasis and impaired autophagy in TAL cells (**Figure 8**). A gain-of-toxic-function effect of *UMOD* mutations is supported by evidence that *Umod* knockout mice do not show any sign of the disease (Raffi *et al*, 2006).

1.5.2 ADTKD-MUC1

Mutations in *MUC1* (human chromosome 1q22) cause the second most recurrent form of ADTKD, ADTKD-*MUC1* (OMIM #174000), which together with ADTKD-*UMOD* accounts for about 50% of all ADTKD cases (Olinger *et al*, 2020). The main clinical features of the disease are very similar to ADTKD-*UMOD*, including autosomal dominant pattern of inheritance, non-significant urinalysis, hyperuricemia with gout and slowly progressive tubulointerstitial kidney disease leading to ESKD (**Figure 5**) (Bleyer *et al*, 2017; Olinger *et al*, 2020).

A large collaborative study on an International ADTKD cohort (comprising two large cohorts from Europe and USA) including 726 patients from 585 pedigrees compared the phenotype and disease progression in ADTKD due to *UMOD* or *MUC1* mutations. This study revealed that kidney disease is more severe in patients with ADTKD-*MUC1* showing higher prevalence (58% in ADTKD-*MUC1* vs 44% in ADTKD-*UMOD*) and earlier age of onset of ESKD (mean age 36 years in ADTKD-*MUC1* vs 46 years in ADTKD-*UMOD*) (Olinger *et al,* 2020). Another discriminating feature is gout which is significantly less frequent (26% vs 79%) and appears at later age (45 vs 27 years) in ADTKD-*MUC1* compared to ADTKD-*UMOD* (Olinger *et al,* 2020). These results were confirmed in a second study on a smaller cohort composed of 131 affected individuals showing more severe disease and lower hyperuricemia prevalence in ADTKD-*MUC1* patients vs. ADTKD-*UMOD* ones (Ayasreh *et al*, 2018).

MUC1 encodes for mucin-1 (MUC1), a single-pass transmembrane protein expressed on the apical membrane of epithelial cells in many tissues including lungs, digestive tract, mammary glands, uterus, prostate and in the kidney, where it is expressed in TAL, DCT and CD cells (Hanisch & Muller, 2000; Patton *et al*, 1995). By forming a protective mucous barrier, MUC1 is involved in cell signaling events, cell-cell adhesion, modulation of immune function, lubrication, cell surface hydration and protection from degradative enzymes (Chen *et al*, 2021). The mucinous properties of MUC1 are contributed by an extracellular domain constituted by repetitive segments of 20 amino acids with high threonine and serine content that are heavily O-glycosylated. These repeats are encoded

by a GC-rich VNTR (variable number of tandem repeats) containing 60 nucleotide- long repeats (Hanisch & Muller, 2000; Kirby *et al*, 2013).

All but one reported mutations map in the *MUC1* VNTR. The most common is the insertion of a cytosine residue in a tract of seven cytosine within one of the 20-125 copies of the VNTR (Kirby *et al*, 2013; Wopperer *et al*, 2022) while the few other mutations consist in the insertion of a guanosine residue or the deletion of two cytosine residues (Živná *et al*, 2018). The only mutation outside the VNTR consists in a 2 bp (AG) deletion located upstream of the VNTR (Yamamoto *et al*, 2017). Importantly, all the described mutations lead to the same frameshift within the VNTR, and to the consequent production of a mutant frameshifted mucin 1 (MUC1fs) that presents a new repetition of 20 amino acids and a premature stop codon soon after the VNTR. The newly encoded sequence is cysteine-rich, highly positively charged and is predicted to be natively unfolded (Devuyst *et al*, 2019). Since MUC1fs still contains the physiological leader peptide but lacks the protein C-terminus, important for post-translational processing, membrane anchoring and recycling, it enters the secretory pathway but accumulates in the ER-to-Golgi (ERGIC) compartment (Kirby *et al,* 2013; Dvela-Levitt *et al*, 2019).

Owing to their genomic context, *MUC1* mutations cannot be detected by Sanger sequencing, whole genome or whole exome sequencing. An alternative method of detection, based on MUC1fs acquired resistance to restriction enzyme Mwol, followed by a probe-extension assay coupled with mass spectrometry or capillary electrophoresis (SnaPshot minisequencing) has been developed (Kirby *et al*, 2013; Blumenstiel *et al*, 2016; Ekici *et al*, 2014). However, this assay is limited to one type of mutation, i.e., cytosine insertion within the VNTR. To overcome this problem, an alternative method based on long read single molecule real-time sequencing (SMRT) targeted to *MUC1* has been reported (Wenzel *et al*, 2018). To date these techniques are carried out in few laboratories worldwide. The technical difficulties in developing standardized methods for *MUC1* mutation detection have stimulated the development of non-genetic alternative approaches, currently used on research base only, as detection of MUC1fs by immunochemistry on kidney biopsies specimen or on urinary exfoliated cells from patients (Knaup *et al*, 2018; Živná *et al*, 2018) or the measurement of MUC1 circulating levels (Vylet'al *et al*, 2021).

Regarding ADTKD-*MUC1* pathophysiology, the absence of any histopathological abnormalities in kidneys of *Muc1* knockout mice suggests a toxic gain-of-function effect of *MUC1* mutations (Spicer *et al*, 1995). A recent seminal paper demonstrated that the primary effect of *MUC1* mutations is the retention and accumulation of MUC1fs in the ERGIC. This is due to its interaction with the cargo receptor TMED9, a member of the p24 protein family, implicated in the regulation of vesicle trafficking along the secretory pathway (Dvela-Levitt *et al*, 2019). In turn, this leads to the activation of the ATF6 branch of the UPR, whose chronic induction eventually results in epithelial cell injury and death, a mechanism that could explain the disease late-onset (**Figure 8**), (Dvela-Levitt *et al*, 2019).

In the same study, the authors carried out a high-content small molecule screening and identified a lead compound, BRD4780, able to specifically remove MUC1fs intracellular accumulation with consequent rescue of ATF6 activation both in cellular and murine models. From a molecular point of view, BRD4780 acts by binding to TMED9, releasing MUC1fs that is then rerouted into endosomes and finally targeted to lysosomal degradation. BRD4780 seems to act on other misfolded proteins, such as mutant uromodulin and mutant rhodopsin, hence representing an interesting lead for ADTKD and other proteinopathies associated with mutant protein accumulation in the cell secretory pathway (Dvela-Levitt *et al*, 2019).

1.5.3 ADTKD-REN

REN (human chromosome 1q32.1) encodes for renin, a secreted aspartyl protease that catalyzes the cleavage of angiotensinogen to angiotensin I during the first step of the Renin-Angiotensin-Aldosterone System (RAAS) cascade regulating multiple biological functions, including kidney Na^{2+} and K^{+} handling, blood pressure homeostasis, modulation of erythropoiesis, nephrogenesis and kidney tubulogenesis (Sparks *et al*, 2014; Almeida *et al*, 2020; Imai *et al*, 1983). In the kidney, renin is mainly synthesized in the juxtaglomerular cells as an inactive precursor, preprorenin, composed of 406 amino acids. It contains a 23 amino acid N-terminal signal peptide that directs co-translational import in the ER where it is cleaved to prorenin, formed by a 43 amino acid pro-segment regulating renin activity and by the mature part of the protein (340 amino acids)

containing the enzymatic catalytic site (Imai *et al*, 1983). Once in the Golgi apparatus, prorenin is glycosylated and then secreted as such via constitutive exocytosis or it can be directed to the regulated secretory pathway where it is stored in granules, matured to active renin by cleavage of the N-terminal pro-segment and secreted via regulated exocytosis.

Homozygous or compound heterozygous loss-of-function *REN* mutations causing complete loss of renin synthesis are the cause of renal tubular dysgenesis (RTD), a very rare and severe disorder of kidney tubular development leading to perinatal mortality (Gribouval *et al*, 2005).

Instead, heterozygous dominant *REN* mutations lead to ADTKD-*REN* (OMIM #613092). So far, 111 individuals from 30 families have been reported for a total of 16 mutations (all missense changes and one in-frame deletion) mapping in all protein domains (Živná *et al*, 2020). A clear genotype-phenotype correlation is observed, as position of the affected amino acid in the protein sequence correlates with the severity of the clinical manifestations (**Figure 5**). Patients harboring pathogenic variants in the leader peptide (8 mutations) or pro-segment region (3 mutations) display a more severe phenotype, characterized by very early (probably prenatal) onset, slowly progressive decline of kidney function, childhood/adolescence anemia, hyperkalaemia and acidosis and early-onset gout. Mutations in the mature protein (5 reported so far) have been associated with a milder phenotype characterized by adult-onset of gout and decreased kidney function and absence of anemia, hyperkalaemia and acidosis, with a clinical picture resembling ADTKD-*UMOD* (Schaeffer *et al*, 2019; Živná *et al*, 2020). Kidney biopsy analyses are reported only for mutations mapping in renin leader peptide and revealed periglomerular fibrosis, tubular atrophy, thickening of Bowman's capsule and of tubular basement membranes and interstitial fibrosis with focal mild interstitial inflammatory infiltrate (Bleyer *et al*, 2010). Renin and prorenin signals show a strong decrease both in the juxtaglomerular and tubuloepithelial cells and are even absent at an advanced stage of the disease (Živná *et al*, 2009).

The precise molecular mechanisms leading to kidney damage, inflammation and fibrosis are not yet elucidated, but different studies clarified the cellular effects induced by different mutant renin isoforms (**Figure 8**). The localization of the mutations is associated

with a different effect on renin processing along the secretory pathway. Mutations in the leader peptide interfere with ER translocation and processing of nascent preprorenin leading to induction of mild ER stress (Živná *et al*, 2009; Bleyer *et al*, 2010; Beck *et al*, 2011), mutations in the pro-segment result in protein accumulation in the ERGIC compartment (Živná *et al*, 2020), and mutations mapping in the mature part cause full retention of prorenin in the ER, likely due to protein misfolding, with consequent induction of UPR (Schaeffer *et al*, 2019). All types of mutations result in a reduced amount of secreted renin. Low renin activity due to reduced renin biosynthesis and secretion could indeed explain anemia and other symptoms observed in these patients, as mild hypotensive state, hyperkalaemia and acidosis, and decreased fractional excretion of urate (Schaeffer *et al*, 2019; Živná *et al*, 2020). However, several evidence suggests that ADTKD-related *REN* mutations have a common gain-of-function effect. Despite their different cellular phenotypes, expression in zebrafish of renin mutants in the leader peptide (p.Leu16del) or mature part (p.Leu381Pro) are both associated with a similar kidney phenotype, i.e. defective pronephros development (Schaeffer *et al*, 2019). Moreover, heterozygous carriers of RTD-associated loss-of-function *REN* mutations do not exhibit any sign of ADTKD (Schaeffer *et al*, 2020). Consistently, expression in zebrafish of a renin loss-of-function mutant affecting the enzymatic site (D104N) and associated with RTD does not lead to defective pronephros development (unpublished data from our lab).

As for other ADTKD forms, no specific treatment is available, although fludrocortisone treatment, tested in a relatively low number of patients, was shown to be effective in ameliorating hyperkalaemia and acidosis and improving eGFR by increasing aldosterone levels and hence decreasing mutant renin production (Bleyer *et al*, 2010; Živná *et al*, 2020).

1.5.4 ADTKD-HNF1β

HNF1B (human chromosome 17q12) encodes for hepatocyte nuclear factor 1β, a transcription factor belonging to the POU-homeodomain containing superfamily. HNF1β regulates tissue specific expression of developmental target genes, acting as a homodimer or forming heterodimers with HNF1α. It plays a critical role in embryogenic development

of kidney, pancreas, liver, and genitourinary tract (Saji *et al*, 2008; Liu *et al*, 2011; Mendel *et al*, 1991) and full knockout of *Hnf1b* in mouse is embryonic lethal (Gresh *et al*, 2004).

The most common reported mutations are whole *HNF1B* gene deletions but heterozygous missense, frameshift, splice affecting, or nonsense point mutations have also been reported (Izzi *et al*, 2020). About 50% of cases are due to *de novo* pathogenic variants, while when a positive family history is present, the way of inheritance is autosomal dominant (Heidet *et al*, 2010). Incomplete penetrance of clinical features has been reported as well as a preponderance of dominant maternal inheritance, suggesting epigenetic modifiers or defect in male fertility (Heidet *et al*, 2010; Okorn *et al*, 2019). Regarding genotype-phenotype correlation, the contrasting results reported in literature suggest a more severe phenotype in carriers of point mutations compared with whole gene deletions (Dubois-Laforgue *et al*, 2018; Nagano *et al*, 2019). ADTKD-*HNF1B* molecular diagnosis is performed by combining conventional sequencing to detect point mutations and copy number variation analysis and multiplex ligation-dependent probe amplification to identify whole gene deletion (Devuyst *et al*, 2019). *HNF1B* mutations are associated with a multi-systemic disorder, characterized by both kidney and extra-kidney manifestation (**Figure 5**). *HNF1B* mutations were first reported to be associated with maturity-onset diabetes of the young type 5 (MODY5) and nephropathy (Horikawa *et al*, 1997). The association of cysts and diabetes led to propose the name renal cyst and diabetes (RCAD) syndrome (Heidet *et al*, 2010). Kidney involvement is the earliest and most prevalent (more than 60% of patients) clinical manifestation that includes cystic abnormalities, chronic tubulointerstitial nephritis, hyperuricemia, congenital abnormalities of kidney and urinary tract (CAKUT), hypomagnesemia and hypokalaemia, and slowly progressive CKD. Within this spectrum, only patients presenting with tubulointerstitial fibrosis as leading cause of kidney damage should be classified as ADTKD-*HNF1B* (OMIM #137920) (Eckardt *et al*, 2015). In those cases, the clinical picture mimics the one observed in ADTKD-*UMOD* patients.

Molecular pathogenesis leading to kidney phenotypes can be imputed to *HNF1B* haploinsufficiency and loss of regulated expression on its target genes (**Figure 8**). In murine models, kidney specific deletion of *Hnf1b*, heterozygous splicing mutation associated with reduced functional Hnf1β or expression of dominant negative mutant

forms of Hnf1β, recapitulate the phenotype of human patients with *HNF1B* mutation, resulting in kidney cysts and renal failure (Hiesberger *et al*, 2004; Niborski *et al*, 2021). The molecular characterization of this phenotype revealed the key role of Hnf1β in activating transcription of different cystic disease genes, including *Pkhd1*, *Pkd2*, *Umod*, *Glis2* and *Kif12* (Gresh *et al*, 2004; Ferrè & Igarashi, 2019). HNF1β has been also implicated in the regulation of the expression of genes encoding for ion transport channels as *FXYD2* encoding for the γ subunit of Na^+-K^+-ATPase, *SLC12A1* (encoding for NKCC2) in the TAL (Ferrè & Igarashi, 2019) and *KCNJ10* (that encodes the K^+ channel Kir4.1) in the DCT (Kompatscher *et al*, 2017). Insights into the mechanisms that link *HNF1B* mutations and tubulointerstitial fibrosis have been reported. Fibrotic phenotype could be contributed by decreased expression of miR-200, part of a long noncoding RNA under the transcriptional control of HNF1β, whose inactivation *in vitro* in renal epithelial cells results in increased epithelial-to-mesenchymal transition (EMT) (Hajarnis *et al*, 2015). Moreover, HNF1β is a transcriptional repressor of *Twist2*. Over-activation of *Twist2* in renal epithelial cells lacking *Hnf1b* triggers a transcriptional program eventually leading to EMT and Tgf-β secretion by epithelial cells. This results in the activation of interstitial cells stimulating fibrogenesis and resulting in kidney fibrosis (Chan *et al*, 2018).

No specific therapy is currently available for the management of ADTKD-*HNF1B* patients. However, treatments should target extrarenal manifestations, including pancreatic dysfunction and neuropsychiatric symptoms (Econimo *et al*, 2022).

1.5.5 ADTKD-SEC61A1

ADTKD-*SEC61A1* (OMIM #617056) is an ultrarare disease, described in two families bearing the missense pathogenic mutations p.Val67Gly and p.Thr185Ala in *SEC61A1* (human chromosome 3q21.3) (Bolar *et al*, 2016). Patients presented autosomal dominant progressive loss of kidney function, associated with congenital anemia, hyperuricemia, and various extra-kidney manifestations including growth and mild cognitive impairment, cleft palate, bifid uvula, and polydactyly. Kidney biopsies revealed periglomerular fibrosis, focal glomerular sclerosis and multiple tubulointerstitial areas consistent with ADTKD (**Figure 5**) (Bolar *et al*, 2016). *SEC61A1* disease-causing

mutations have been reported in two additional families with hematological disorders (primary antibody deficiency) with unclear kidney phenotype (Schubert *et al*, 2018).

SEC61A1 encodes for the α1 subunit of the SEC61 translocon that together with subunits β (*SEC61B*) and γ (*SEC61G*) forms a heterotrimeric protein-conducting complex, responsible for the co-translational import of newly synthesized proteins into the ER (Linxweiler *et al*, 2017). ADTKD-related mutations in *SEC61A1* affect the plug domain (p.Val67Gly) or the constriction ring (p.Thr185Ala) resulting in altered selectivity and permeability of the pore of the translocon channel (Bolar *et al*, 2016). While wild type protein exclusively localizes in the ER, *in vitro* expression of mutant SEC61α isoforms demonstrated its aggregation in the ER with partial mislocalization to the Golgi apparatus, reproducing SEC61α localization in kidney sections from an affected individual (Bolar *et al*, 2016). The resulting *SEC61A1* channelopathy affects folding and post-translational modification of secretory proteins (as, for instance, renin) and alters Ca^{2+} homeostasis (reducing expression of regulatory Ca^{2+} transporters Ora1 and SERCA2). These dysfunctions could directly induce ER-stress or could modify cell susceptibility to ER stress, leading to apoptosis and ultimately to interstitial fibrosis (Bolar *et al*, 2016; Sicking *et al*, 2022). Activation of the UPR was indeed reported in cells expressing Sec61α p.Val67Gly mutant (**Figure 8**). Functional studies *in vivo*, suggested that SEC61 complex is necessary for normal renal development as *Sec61a1* morpholino-based silencing in zebrafish leads to tubular atrophy and pronephros alteration (Bolar *et al*, 2016). This phenotype is fully rescued by injection of human mRNA encoding for wild type Sec61α, while it is not by ADTKD mutants, providing evidence that they are not functional (Bolar *et al*, 2016). Interestingly, the phenotype observed is similar to pronephros development defects described in renin zebrafish mutants (Schaeffer *et al*, 2019). Of note, a recent study on cellular models expressing ADTKD-*SEC61A1* mutants showed that treatment with the molecular chaperone phenylbutyrate restores normal calcium levels and can rescue the signal-peptide dependent defect of renin ER translocation (Sicking *et al*, 2022).

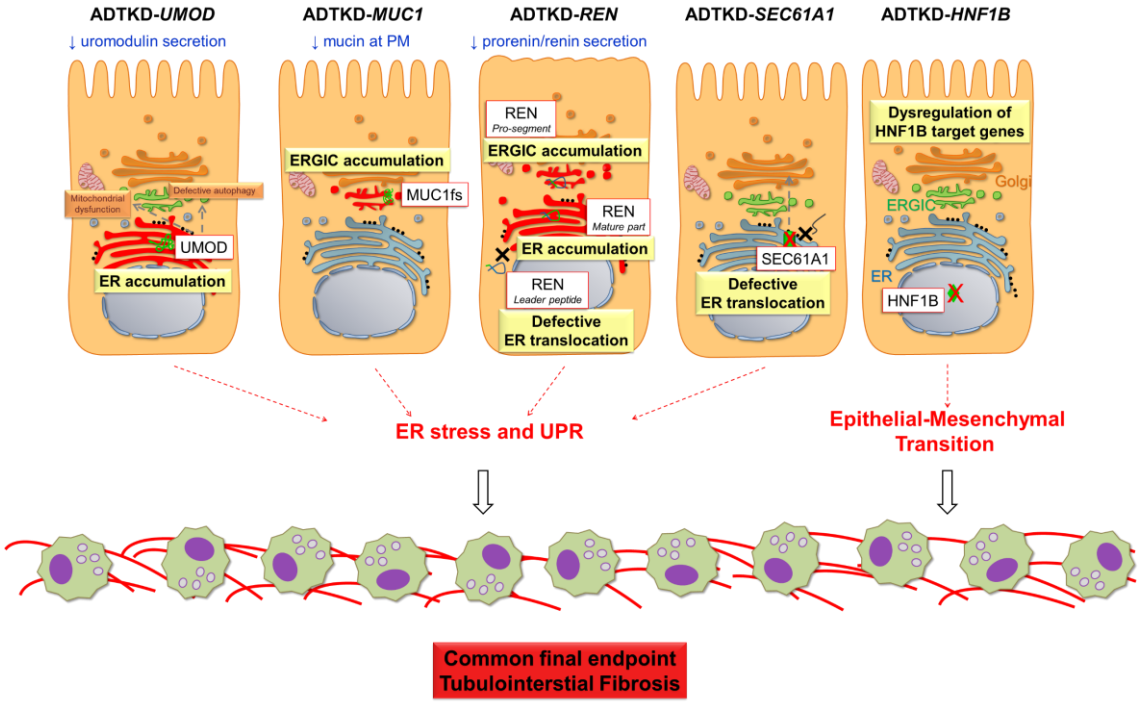


Figure 8. Cellular effects induced by mutations in ADTKD genes. *Mutated uromodulin accumulates in the ER leading to ER stress and induction of the Unfolded Protein Response (UPR). Secondary mitochondrial dysfunction and defective autophagy have also been reported. ER retention is reflected by decreased uromodulin urinary secretion. Mutations in MUC1 result in the synthesis of a frameshifted protein (MUC1fs) that accumulates in the ERGIC, reducing mucin1 abundance at the plasma membrane. MUC1fs expression activates the ATF6 branch of the UPR. Their localization within protein sequence influences cellular effects of renin mutations. Leader peptide mutations interfere with protein ER translocation, mutations in the pro-segment led to ERGIC accumulation, while mutations in the mature part cause ER retention. All these effects result in decreased secretion of renin/prorenin in the blood. UPR is induced by mutation in the leader peptide and in the mature part, while no data are yet available for mutations in the pro-segment. SEC61A1 mutations lead to the synthesis of a non-functional protein partly misrouting to the Golgi and activate the UPR. Common endpoints of these ADTKD forms are defective protein trafficking, ER stress and UPR activation. Although still not formally proved, it is likely that such stress response could be pathogenic, playing a key role in the activation of inflammation and fibrosis in the kidney. Mutations in HNF1B are loss-of-function mutations resulting in the reduction of expression of HNF1B target genes. Loss of HNF1B induces epithelial-mesenchymal transition in vitro and in vivo, a mechanism that could be at the bases of kidney fibrosis.*

1.5.6 Atypical forms of ADTKD

DNAJB11 (human chromosome 3q27.3) encodes for DnaJ heat shock protein family (Hsp40) member B11, a soluble glycoprotein playing a role in ER homeostasis as it acts as the main cofactor of Bip. Five different heterozygous *DNAJB11* mutations, mostly truncating, with autosomal dominant inheritance pattern have been reported in seven

unrelated multigenerational families (Cornec-Le Gall *et al*, 2018). Affected patients show a phenotype partially overlapping with ADTKD and Autosomal Dominant Polycystic Kidney Disease (ADPKD), presenting slightly enlarged kidneys with bilateral small cysts, liver cysts, tubulointerstitial fibrosis and slowly progressive kidney failure (**Figure 5**) (Cornec-Le Gall *et al*, 2018). From a molecular point of view, *in vitro* studies on human cortical tubular epithelial cells knockout for *DNAJB11* described defective trafficking and maturation process of polycystin-1 (encoded by *PKD1*), explaining the ADPKD-like phenotype (Cornec-Le Gall *et al*, 2018). Moreover, in kidney specimens from two unrelated patients carrying *DNAJB11* heterozygous mutations abnormal intracellular accumulation of mucin1 and uromodulin were observed, linking DNAJB11 with tubulointerstitial pathogenesis (Cornec-Le Gall *et al*, 2018).

In 2017, a peculiar type of tubulointerstitial kidney disease with maternal inheritance has been described. Mutations were identified in mitochondrial DNA (mtDNA) and led to the introduction of the terminology mitochondrial inherited tubulointerstitial kidney disease (MITKD). Causative homoplasmic variants were identified in the mtDNA control region (m.547A>T) in a family and in the mitochondrial $tRNA^{Phe}$ encoding sequence (m.616T>C) in other two pedigrees (Connor *et al*, 2017). Of note, these patients do not present multi-organ disease, as usually reported in mitochondrial disorders. Studies in patient fibroblasts carrying m.547A>T mutation revealed reduced levels of $tRNA^{Phe}$ leading to defective mitochondrial protein synthesis thus affecting multiple components of the respiratory chain. These data suggest susceptibility of the kidney to specific alterations in $tRNA^{Phe}$ and consequent initiation of tubulointerstitial damage (Connor *et al*, 2017).

Recent literature reports the identification of mutations in genes usually associated with Alport syndrome, such as *COL4A4* and *COL4A5,* in individuals that were assigned to ADTKD-NOS (Popp *et al*, 2022) or with CKD of unknown origin, with no specific clinical findings but tubulointerstitial fibrosis (Popp *et al*, 2022). Such unexpected associations are not restricted to ADTKD, as *COL4A4* and *COL4A5* have been associated with an increasing number of kidney diseases, as cystic kidney diseases after exclusion of *PKD1* and *PKD2*, focal segmental glomerular sclerosis, familial IgA glomerulonephritis as well as kidney failure of unknown etiology (Savige & Harraka,

2021). Although the role of these genes in disease pathophysiology is not yet clear, they should be considered in individuals with no mutations in established ADTKD genes.

1.6 Preliminary data

As already mentioned, different studies clarified some aspects of ADTKD-*UMOD* molecular genetics, establishing a gain-of-function effect of *UMOD* mutations and highlighting the central role of their common effect on uromodulin trafficking and TAL cell homeostasis for disease pathogenesis. Still, little is known about downstream mechanisms leading to renal disease or how to counteract the effect of *UMOD* mutations.

To gain insight into the molecular mechanisms leading to the clinical manifestations of the disease, the transcriptional profiling of kidneys from young $Tg^{Umod\text{C147W}}$ mice (4 and 8 weeks of age) was previously generated in our laboratory and compared to the one of expression-matched mice transgenic for wild type uromodulin ($Tg^{Umod\text{wt}}$) (Trudu *et al*, 2017). At 4 weeks, $Tg^{Umod\text{C147W}}$ mice are in a pre-symptomatic stage of the disease, showing no major histological sign of kidney damage and normal renal function, although strong accumulation of mutant uromodulin in TAL cells is evident. Pathway enrichment analysis identified strong induction of pathways related to inflammation and fibrosis, while a reduced expression was observed for genes associated with metabolism of amino acids, fatty acids and lipids (Kang *et al*, 2015). Down-regulation of amino acid and lipid metabolism has been linked with progression of kidney damage in murine and human models of tubulointerstitial fibrosis and confirmed metabolic alterations described in others ADTKD-*UMOD* models (Kemter *et al*, 2017). As compared to 4-week-old mice, inflammation and inflammatory response-related genes showed increased expression in kidneys of 8-week-old $Tg^{Umod\text{C147W}}$ mice, suggesting a role of these pathways in disease progression (Trudu *et al*, 2017).

Interestingly, at 8 days *post-natal* (p8), some chemokines (*Ccl5* and *Ccl12*) and markers of innate immunity such as leukocytes (*Cd45*) and macrophages (*Cd68*) are already induced in kidneys of mutant mice, while no up-regulation was observed for fibrosis related genes (*Vim1*, *Tgfb1*, *Acta2*) (Trudu *et al*, 2017). At this time point, when mutant

uromodulin retention in the ER is already evident, an increased expression of *Atf3* and *Lcn2* was also observed (Trudu *et al*, 2017). *Atf3* is a stress-responsive gene that can be induced by different stressors among which ER stress, cytokines, genotoxic and cytotoxic agents (Hai *et al*, 1999). It encodes a transcription factor described to exert anti-apoptotic and anti-inflammatory functions in the context of kidney IRI (Yoshida *et al*, 2008). Thus, its up-regulation specifically in TAL nuclei of $Tg^{Umod\text{C147W}}$ mice at p8 can be regarded as evidence of early stress induction in cells expressing mutant uromodulin (Trudu *et al*, 2017). *Lcn2* encodes for lipocalin-2, a glycoprotein produced by different cell types such as neutrophils, macrophages, adipocytes, hepatocytes and tubular epithelial cells. It is regarded as a marker of distal tubule lesions, participating in proinflammatory and chemotactic mechanisms, reported to play a crucial role for CKD progression both in mouse and humans (Paragas *et al*, 2011; Viau *et al*, 2010; Marakala *et al*, 2022). Contrary to *Havrc1* (encoding for Kidney Injury Molecule-1 (Kim1)), a well-established marker of proximal tubular damage (Han *et al*, 2002) that appears up-regulated only in kidneys of adult $Tg^{Umod\text{C147W}}$ mice, induction of *Lcn2* at p8 suggests that tubular damage initiates in distal nephron, where uromodulin is expressed and then propagates to other segments as the disease progresses (Trudu *et al*, 2017). Overall, these data demonstrated that in $Tg^{Umod\text{C147W}}$ mice inflammation is an early event of pathogenesis, preceding fibrosis induction and occurring concomitantly with TAL cell stress and tubular damage (Trudu *et al*, 2017).

Aiming at better clarifying the significance of inflammation in disease onset, we tested the expression of 84 pro-inflammatory genes in kidneys of $Tg^{Umod\text{C147W}}$ mice at an earlier time point, p1. We detected significant up-regulation of the transcript for some key chemokines such as *Ccl2*, *Ccl7* and *Ccl12* (**Figure 9A**).

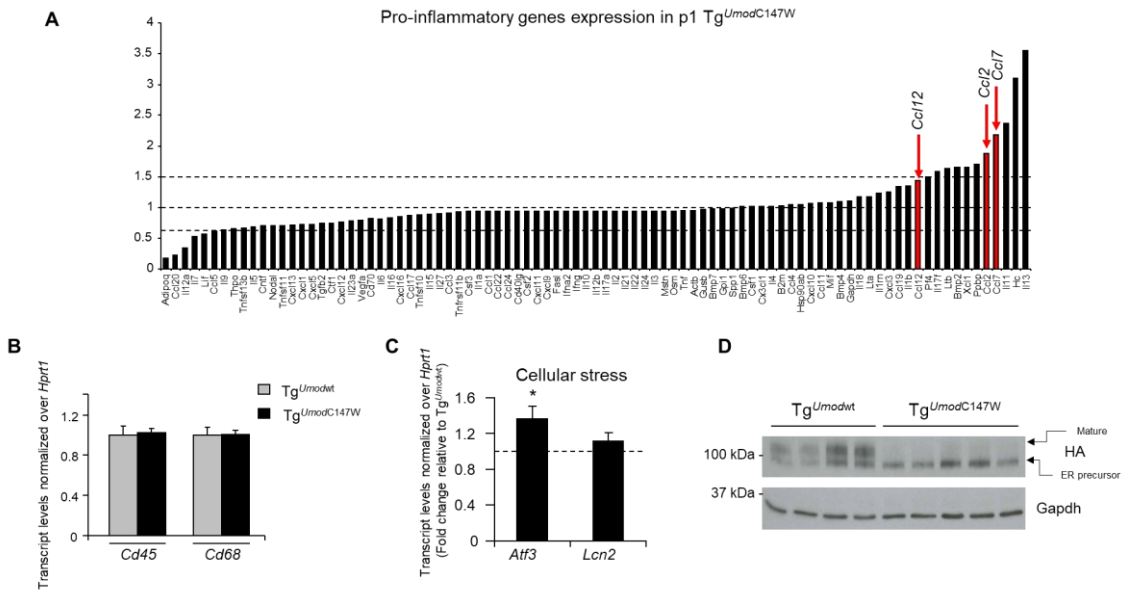


Figure 9. Early events induced by mutant uromodulin expression in kidneys of Tg^{UmodC147W} mice at one day post-natal. *A) Analysis by RT-qPCR of a panel of chemokines/cytokines (RT^2 Profiler PCR Arrays, Qiagen) in p1 Tg^{UmodC147W} mice relative to age- and sex-matched Tg^{Umodwt} (n = pool of 4 mice/group). Red arrow indicates chemokine genes whose induction was significant and confirmed by real-time RT-qPCR. B) Analysis by real-time RT-qPCR of markers of infiltrating cells (Cd45, pan-leucocytes marker, Cd68 macrophage marker) in p1 Tg^{UmodC147W} mice relative to age- and sex-matched Tg^{Umodwt}. C) Western blot analysis showing ER retention of mutant uromodulin (HA), evidenced as enrichment of the lower molecular weight (90 kDa) band corresponding to immature ER precursor compared to the upper (120 kDa) band corresponding to mature, fully glycosylated uromodulin in kidneys from Tg^{UmodC147W} mice at p1. D) Analysis by real-time RT-qPCR reveals Atf3 (cell stress) up-regulation, while no up-regulation of distal tubular damage marker (Lcn2) is detected (right panel). Data are expressed as mean ± s.e.m. *P < 0.05 (unpaired t-test). N=5/6 mice/genotype.*

This result strongly supports the hypothesis that induction of inflammation plays a key role in disease onset. It is also worth to note that these pro-inflammatory signals are observed in the absence of increased infiltrating inflammatory cells (**Figure 9B**), while ER retention of mutant uromodulin (**Figure 9C**) and cellular stress (i.e., *Atf3* induction) are already present (**Figure 9D**). TAL epithelial cells could directly be the source of pro-inflammatory signals, or could express signals activating resident inflammatory cells that, in turn, express pro-inflammatory chemokines.

2. AIMS OF THE WORK

Building on the interesting results obtained from the analysis of expression of pro-inflammatory genes in kidneys of Tg$^{Umod\text{C147W}}$ mice at p1, we planned to carry out a proof-of-concept study to investigate the role of inflammation in ADTKD-*UMOD* pathogenesis. Starting from the observation that all the up-regulated chemokines (*Ccl2*, *Ccl7* and *Ccl12*) are ligands of the same receptor, C-C chemokine receptor type 2 (Ccr2), we decided to assess the effect of its ablation on disease onset and progression. To do so, we adopted a genetic approach to generate Tg$^{Umod\text{C147W}}$/*Ccr2*$^{-/-}$ mice. These mice were characterized at different time points (1 week, 6 weeks, 14 weeks, and 24 weeks of age) corresponding to different and previously characterized stages of the disease in mice expressing mutant uromodulin. Characterization was carried out by studying the effect of *Ccr2* targeting on markers of inflammation, fibrosis, and tubular damage, previously shown to be up-regulated in Tg$^{Umod\text{C147W}}$ mice at these time points.

The serendipitous finding of rescue of mutant uromodulin ER retention in the kidneys of a Tg$^{Umod\text{C147W}}$ mouse that at sacrifice was significantly smaller compared to its littermates and presented with incisors overgrowth, led us to hypothesize that this effect was due to reduced food intake during its life. To test our hypothesis and to validate the effect of dietary restriction on mutant uromodulin ER retention and aggregation, we performed a proof-of-concept experiment on Tg$^{Umod\text{C147W}}$ mice, using a severe calorie restriction (55%) protocol, starting from weaning (p21) for 4 weeks, to mimic food intake reduction observed in the "rescued" mouse.

To assess the therapeutic potential of reducing the intracellular load of mutant uromodulin, we also tested the effect of a milder (30%) and prolonged (15 weeks) calorie restriction protocol. This experiment was performed on Tg$^{Umod\text{C147W}}$ mice starting from 8 weeks of age until 23 weeks, when they develop a fully blown kidney disease. To characterize the effect of calorie restriction on disease progression and to assess its possible role on disease recovery, 23-week-old calorie restricted Tg$^{Umod\text{C147W}}$ mice were compared with both age-matched and 8-week-old Tg$^{Umod\text{C147W}}$ mice fed *ad libitum*, respectively.

3. RESULTS

3.1 Generation and characterization of Tg$^{Umod\text{C147W}}$/*Ccr2*$^{-/-}$ mouse line

We decided to test the role of Ccr2 axis in ADTKD-*UMOD* onset and progression using a genetic approach. We generated a Tg$^{Umod\text{C147W}}$/*Ccr2*$^{-/-}$ mouse line, by crossing Tg$^{Umod\text{C147W}}$ mice with a previously reported *Ccr2*$^{-/-}$ mouse line (Boring *et al*, 1997). Tg$^{Umod\text{C147W}}$/*Ccr2*$^{-/-}$ mice were characterized at different time points (1 week, 6 weeks, 14 weeks and 24 weeks of age) by comparing them with Tg$^{Umod\text{C147W}}$/*Ccr2*$^{+/+}$ littermates. Tg$^{Umod\text{C147W}}$ animals are on the FVB background, while *Ccr2*$^{-/-}$ animals are on the C57BL/6J. Since C57BL/6J mice have been reported to be more resistant to kidney disease (Laouari *et al*, 2011; Zaidan *et al*, 2020) we could not exclude *a priori* that the parameters used to monitor ADTKD-*UMOD* progression in Tg$^{Umod\text{C147W}}$ mice on pure FVB background could be affected by the mixed genetic background. For this reason, Tg$^{Umod\text{C147W}}$/*Ccr2*$^{-/-}$ and Tg$^{Umod\text{C147W}}$/*Ccr2*$^{+/+}$ mice were also compared to their non-transgenic littermates, herein referred to as Ctr/*Ccr2*$^{+/+}$ (N=3-5 animals/group, all females).

Time points were chosen corresponding to different and previously characterized stages of disease in Tg$^{Umod\text{C147W}}$ mice.

At 1 week of age, Tg$^{Umod\text{C147W}}$ mice already displayed increased kidney expression of markers of leukocytes (*Cd45*), macrophages (*Cd68*) and of some pro-inflammatory chemokines (*Ccl5*, *Ccl12*) (Trudu *et al*, 2017). At 4 weeks of age, although Tg$^{Umod\text{C147W}}$ mice are still in a pre-symptomatic phase of the disease, as indicated by normal kidney histological parameters, we already reported induction of genes related to inflammation, fibrosis and tubular damage (Trudu *et al*, 2017). At 14 weeks of age, Tg$^{Umod\text{C147W}}$ mice show histological evidence of disease with signs of kidney interstitial fibrosis and inflammatory cell infiltrate (Bernascone *et al*, 2010). At 24 weeks mutant mice exhibit fully-blown disease, with marked tubulointerstitial damage, dilated and cystic tubules, dramatic increase of interstitial inflammation and fibrosis, and mild renal failure (Bernascone *et al*, 2010).

At each time point, Tg$^{Umod\text{C147W}}$/*Ccr2*$^{-/-}$ mice were systematically characterized by assessing ER retention of mutant uromodulin and by measuring the expression level of well-established markers of inflammation (*Cd68*, *Cd45*, *Ccl2* and *Ccl12*). To evaluate the effect of Ccr2 ablation on macrophage infiltration in kidneys of Tg$^{Umod\text{C147W}}$ mice, we also quantified F4/80^{+} area. Moreover, we studied kidney fibrosis by analyzing the fibrosis marker vimentin (*Vim1*) and tubular damage by assessing Lipocalin-2 (*Lcn2*) levels.

3.1.1 Characterization of 1-week-old Tg^{UmodC147W}/Ccr2$^{-/-}$ mice

As reported above, inflammation is an early event of pathogenesis occurring in kidneys of Tg$^{Umod\text{C147W}}$ mice (Trudu *et al*, 2017).

To test the role of Ccr2 axis in triggering inflammation and its significance in ADTKD-*UMOD* onset, we characterized Tg$^{Umod\text{C147W}}$/*Ccr2*$^{-/-}$ mice at 1 week of age.

Ccr2 ablation in kidneys from Tg$^{Umod\text{C147W}}$/*Ccr2*$^{-/-}$ mice was confirmed through semiquantitative RT-PCR (**Figure 10A**).

We then tested *Umod* transcript levels by real-time RT-qPCR and observed similar levels of expression in kidneys of mutant mice regardless of the *Ccr2* genotype, demonstrating that genetic ablation of the receptor does not affect uromodulin expression. As expected, Tg$^{Umod\text{C147W}}$ animals showed increased *Umod* expression levels compared to non-transgenic Ctr/*Ccr2*$^{+/+}$ mice, due to the presence of transgenic mutant uromodulin (**Figure 10B**).

Western blot analysis confirmed the presence of mutant uromodulin ER retention in kidneys of Tg$^{Umod\text{C147W}}$/*Ccr2*$^{-/-}$ and Tg$^{Umod\text{C147W}}$/*Ccr2*$^{+/+}$ mice, as demonstrated by the enrichment of the lower molecular weight band, corresponding to the immature isoform carrying ER-type glycans, as compared to non-transgenic mice (**Figure 10C**) (Bernascone *et al*, 2010). Mutant uromodulin trafficking is not affected by *Ccr2* expression, as demonstrated by comparable ratio ER precursor/mature uromodulin forms in kidneys of mutant mice of both *Ccr2* genotype (**Figure 10D**).

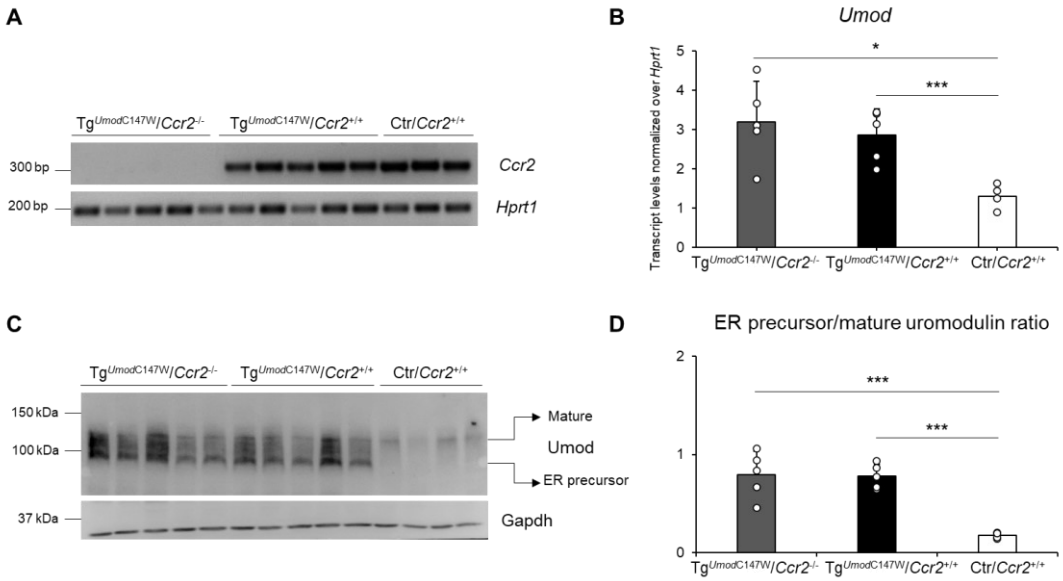


Figure 10. Characterization of 1-week-old Tg^{UmodC147W}/Ccr2$^{-/-}$ mice. *A) Semiquantitative RT-PCR to test Ccr2 expression. The expected 300 bp amplification product, corresponding to Ccr2 wild type transcript, was present only in Tg^{UmodC147W}/Ccr2$^{+/+}$ and Ctr/Ccr2$^{+/+}$ kidneys. Hprt1 (Hypoxanthine guanine phosphoribosyl transferase 1) is shown as a normalizer. B) Analysis by real-time RT-qPCR of Umod expression. C) Western blot using anti-uromodulin antibody shows a lower molecular weight (90 kDa) band corresponding to immature ER precursor and an upper (120 kDa) band corresponding to mature, fully glycosylated uromodulin. Gapdh is reported as loading control. D) Quantification of the ratio ER precursor/mature uromodulin form. N=3-5 animals/group. Data are expressed as mean ± s.d. *P<0.05; ***P<0.005 (unpaired t-test).*

We then measured expression levels of chemokines and markers of inflammatory cells. The analysis revealed significant up-regulation of pan leucocyte marker *Cd45*, macrophage marker *Cd68* and pro-inflammatory chemokines *Ccl2* and *Ccl12* in kidneys of mutant mice, irrespective of *Ccr2* genotype, compared to wild type mice. However, no significant differences are observed in kidneys of Tg^{Umod}C147W/*Ccr2*$^{-/-}$ mice compared to Tg^{Umod}C147W/*Ccr2*$^{+/+}$ litters (**Figure 11A**). We also studied kidney macrophage infiltration, by quantifying F4/80^{+} area, a murine monocytes/macrophage-restricted cell surface glycoprotein. This analysis revealed an increased F4/80^{+} area in kidneys of Tg^{Umod}C147W/*Ccr2*$^{-/-}$ and Tg^{Umod}C147W/*Ccr2*$^{+/+}$, compared to the control group, that however is not decreased by *Ccr2* ablation (**Figure 11B, C**).

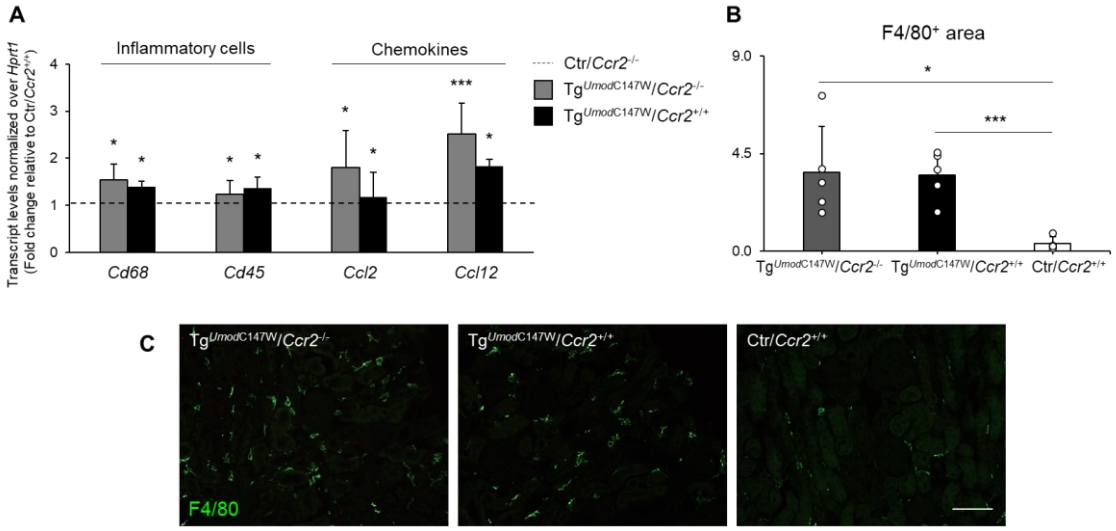


Figure 11. Inflammation in kidneys of 1-week-old $Tg^{UmodC147W}/Ccr2^{-/-}$ mice. *A) Analysis by real-time RT-qPCR of the expression of Cd68 (encoding for the macrophage marker Cluster of Differentiation 68 antigen), Cd45 (also known as Ptprc, encoding for the leukocyte common antigen), Ccl2 and Ccl12 (pro-inflammatory chemokines). $Tg^{UmodC147W}/Ccr2^{-/-}$ mice were compared to age-matched $Tg^{UmodC147W}/Ccr2^{+/+}$ and $Ctr/Ccr2^{+/+}$ animals. The histograms represent transcript levels normalized over Hprt1 and are reported as fold changes compared to $Ctr/Ccr2^{+/+}$ mice (dashed line). B) Quantification of F4/80^{+} area in kidneys of $Tg^{UmodC147}/Ccr2^{-/-}$, $Tg^{UmodC147W}/Ccr2^{+/+}$ and wild type mice. C) Representative pictures of immunofluorescence staining for F4/80 (monocyte/macrophage marker) in kidneys of $Tg^{UmodC147}/Ccr2^{-/-}$, $Tg^{UmodC147W}/Ccr2^{+/+}$ and wild type mice (Bar=100 µm). N=3-5 animals/group. Data are expressed as mean ± s.d. *P<0.05; ***P<0.005 (unpaired t-test).*

All together these results demonstrate that *Ccr2* targeting is not effective to prevent early induction of inflammation in kidneys of Tg^{Umod}C147W mice.

In the Tg^{Umod}C147W mouse model, early induction of inflammation at 1 week of age is associated with tubular damage, as demonstrated by previous evidence of increased kidney expression of distal tubule damage marker Lipocalin-2 (Lcn2, also called neutrophil gelatinase-associated lipocalin or Ngal) (Trudu *et al,* 2017). This is confirmed in the Tg^{Umod}C147W mouse lines, irrespective of *Ccr2* genotype, since we detected up-regulation of Lcn2 both at transcript and protein level relative to controls.

The lack of significant differences in Tg$^{Umod\text{C147W}}$/*Ccr2*$^{-/-}$ mice compared to Tg$^{Umod\text{C147W}}$/*Ccr2*$^{+/+}$ suggests that *Ccr2* inactivation has no effect in preventing tubular damage in mice expressing mutant uromodulin (**Figure 12**).

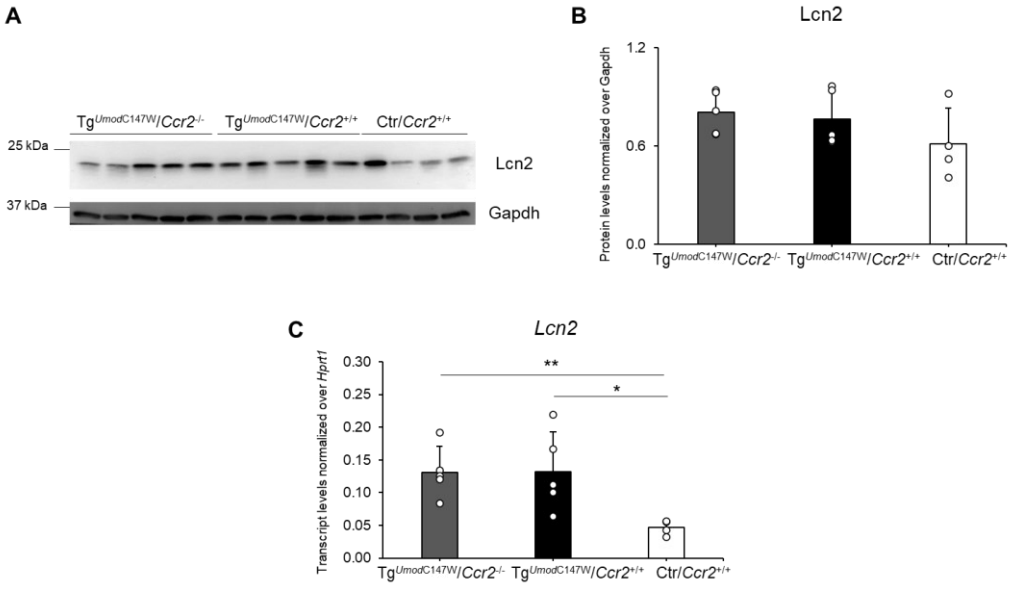


Figure 12. Tubular damage in kidneys of 1-week-old Tg^{UmodC147W}/Ccr2$^{-/-}$ mice. *A) Western blot analysis of Lipocalin-2 in kidneys of Tg^{UmodC147W}/Ccr2$^{-/-}$, Tg^{UmodC147W}/Ccr2$^{+/+}$ and Ctr/Ccr2$^{+/+}$ mice. B) Quantification of Lcn2 protein levels, normalized over Gapdh. C) Real-time RT-qPCR analysis of Lcn2 expression level. N=4-5 animals/group. Data are expressed as mean ± s.d. *P<0.05; ***P<0.005 (unpaired t-test).*

3.1.2 Characterization of 6-week-old Tg^{UmodC147W}/Ccr2$^{-/-}$ mice

We then investigated the effect of *Ccr2* targeting on disease phenotype in 6-week-old Tg$^{Umod\text{C147W}}$ mice, when inflammatory and pro-fibrotic pathways are robustly induced (Trudu *et al*, 2017).

We confirmed *Ccr2* ablation in kidneys of Tg$^{Umod\text{C147W}}$/Ccr2$^{-/-}$ mice (**Figure 13A**) and verified that uromodulin was expressed at similar levels in kidneys of Tg$^{Umod\text{C147W}}$/Ccr2$^{-/-}$ and Tg$^{Umod\text{C147W}}$/Ccr2$^{+/+}$ mice (**Figure 13B**). Also at this time point, mutant uromodulin is clearly ER retained, in a comparable way in kidneys of Tg$^{Umod\text{C147W}}$ mice independently of their *Ccr2* genotype (**Figure 13C, D**).

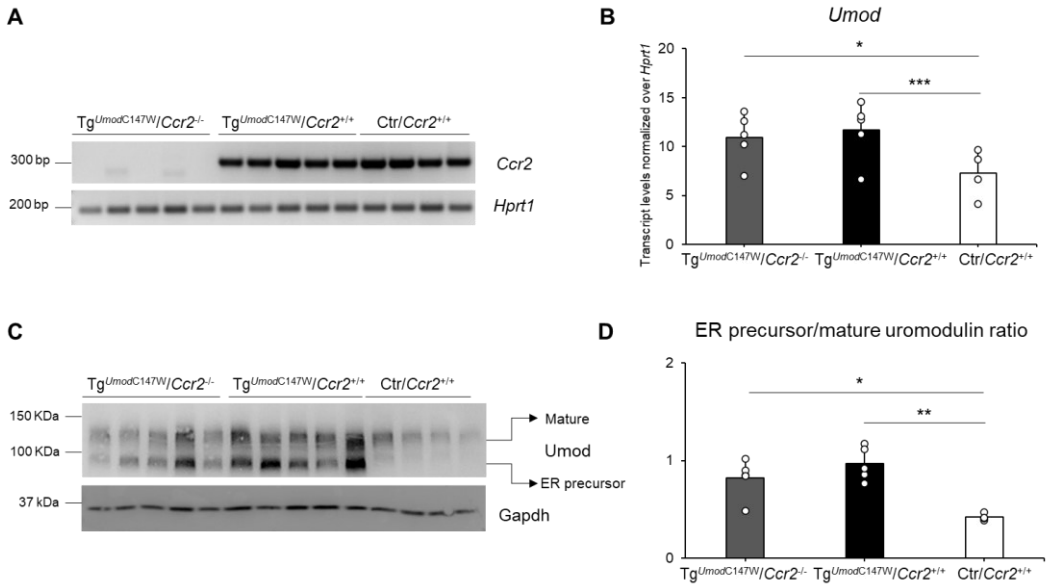


Figure 13. Characterization of 6-week-old Tg^{UmodC147W}/Ccr2$^{-/-}$ mice. *A) Semiquantitative RT-PCR showing the absence of Ccr2 expression in kidneys of Tg^{UmodC147W}/Ccr2$^{-/-}$ mice. Hprt1 expression is reported as a normalizer. B) Analysis by Real-time RT-qPCR of uromodulin expression. C) Western blot using anti-uromodulin antibody showing the enrichment of the lower band, corresponding to the immature ER precursor in kidneys of Tg^{UmodC147W}/Ccr2$^{-/-}$ and Tg^{UmodC147W}/Ccr2$^{+/+}$compared to Ctr/Ccr2$^{+/+}$. Gapdh is reported as loading control. D) Quantification of the ratio ER precursor/mature uromodulin. N=4-5 animals/group. Data are expressed as mean ± s.d. *P<0.05; ***P<0.005 (unpaired t-test).*

Next, we characterized inflammation in mouse kidneys. Compared to wild type, mice expressing mutant uromodulin displayed increased kidney expression levels of inflammatory cell markers and chemokines that were not reduced by *Ccr2* ablation (**Figure 14A**). This is further corroborated by similar F4/80^{+} area in kidneys of Tg^{Umod}C147W/*Ccr2*$^{-/-}$ and Tg^{Umod}C147W/*Ccr2*$^{+/+}$, that shows the expected increase in kidney macrophage infiltration, compared to control group (**Figure 14B, C**).

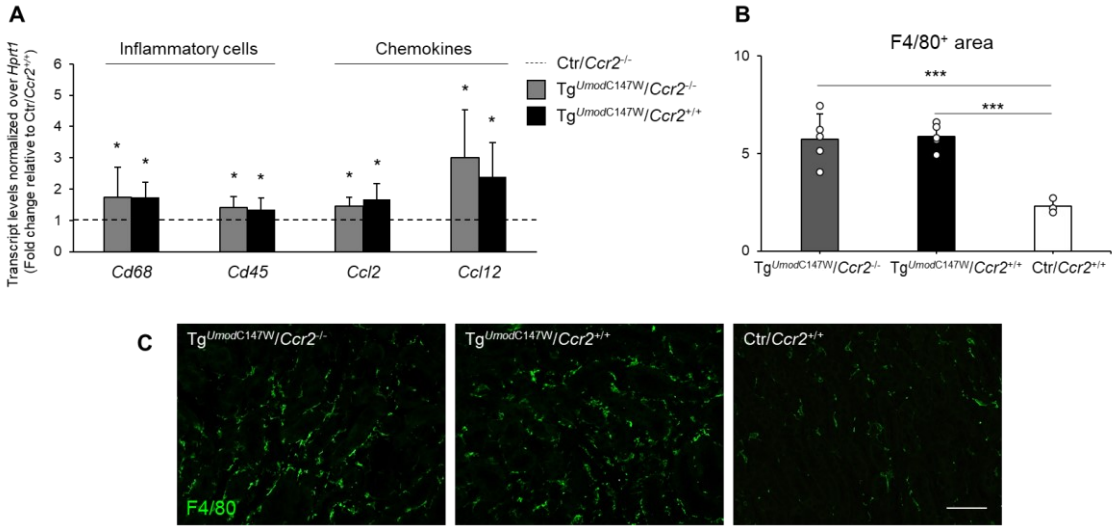


Figure 14. Inflammation in kidneys of 6-week-old Tg^{UmodC147W}/Ccr2$^{-/-}$ mice. *A) Expression level detected by real-time RT-qPCR of marker of macrophages (Cd68) and leukocytes (Cd45) and chemokines (Ccl2, Ccl12). Data are reported as fold changes compared to age- and sex-matched Ctr/Ccr2$^{+/+}$ mice (dashed line). B) Quantification of F4/80 positive area in kidneys of Tg^{UmodC147W}/Ccr2$^{-/-}$, Tg^{UmodC147W}/Ccr2$^{+/+}$ and Ctr/Ccr2$^{+/+}$ mice. C) Representative images of immunofluorescence staining for the monocyte/macrophage marker F4/80 (Bar=100 µm). N=4-5 animals/group. Data are expressed as mean ± s.d. *P<0.05; ***P<0.005 (unpaired t-test).*

We also assessed kidney fibrosis by measuring expression of vimentin. Real-time RT-qPCR analysis revealed similar, increased expression of *Vim1* in kidneys of Tg^{Umod}C147W/*Ccr2*$^{-/-}$ and Tg^{Umod}C147W/*Ccr2*$^{+/+}$ mice compared to wild type animals (**Figure 15A**). This suggests that *Ccr2* ablation is not effective in preventing fibrosis induction in our model, as further demonstrated by comparable, increased levels of vimentin deposition in kidneys of mice expressing mutant uromodulin, irrespective of their *Ccr2* genotype (**Figure 15B, C**).

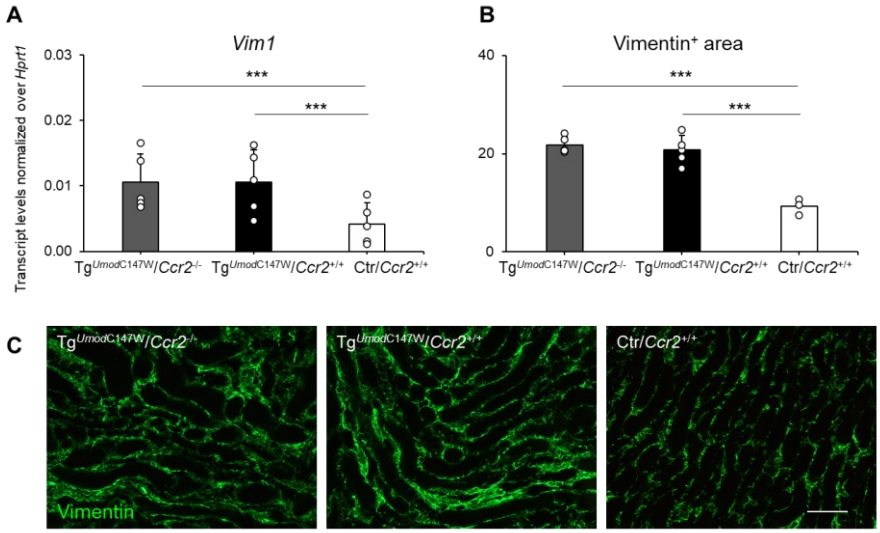


Figure 15. Fibrosis in kidneys of 6-week-old Tg^{UmodC147W}/Ccr2$^{-/-}$ mice. *A) Real-time RT-qPCR analysis of Vim1 (encoding for the fibrosis marker Vimentin). Tg^{UmodC147}/Ccr2$^{-/-}$ were compared to age- and sex-matched Tg^{UmodC147W}/Ccr2$^{+/+}$ and Ctr/Ccr2$^{+/+}$ mice. B) Quantification of Vimentin positive area in kidneys of Tg^{UmodC147W}/Ccr2$^{-/-}$, Tg^{UmodC147W}/Ccr2$^{+/+}$ and Ctr/Ccr2$^{+/+}$ mice. C) Representative images of immunofluorescence staining for Vimentin (Bar=100 µm). N=4-5 animals/group. Data are expressed as mean ± s.d. ***P<0.005 (unpaired t-test).*

We also checked *Lcn2* expression. The analysis revealed significant up-regulation of this stress marker both at protein (**Figure 16A, B**) and at transcript levels (**Figure 16C**) in kidneys of mice expressing transgenic mutant uromodulin, compared to non-transgenic mice. However, no significant difference was observed in Tg$^{Umod\text{C147W}}$/*Ccr2*$^{-/-}$ compared to Tg$^{Umod\text{C147W}}$/*Ccr2*$^{+/+}$, suggesting that also at this later time points *Ccr2* inactivation is not sufficient to rescue tubular damage in kidneys of mutant mice.

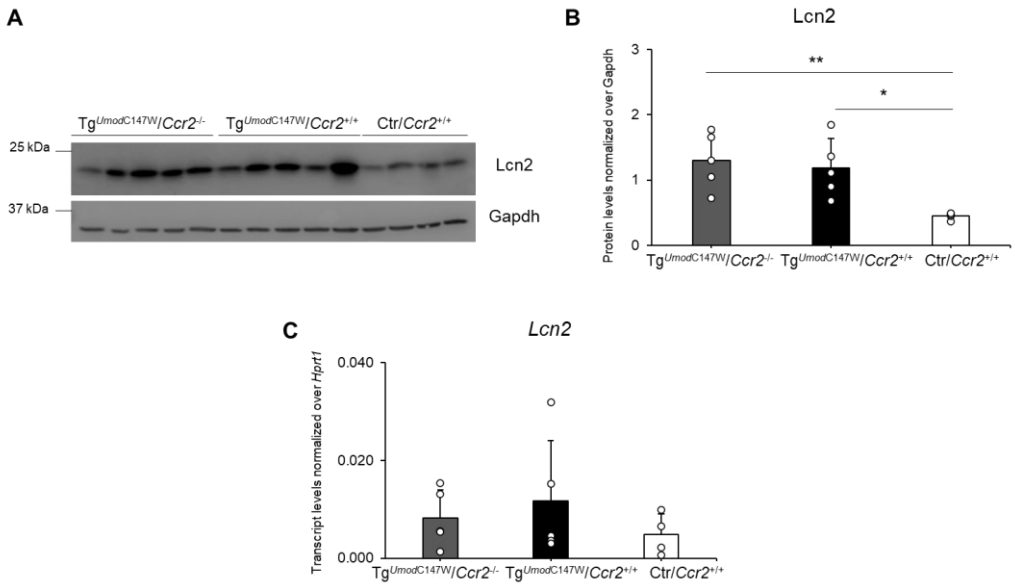


Figure 16. Tubular damage in kidneys of 6-week-old Tg^{UmodC147W}/Ccr2$^{-/-}$ mice. *A) Western blot analysis of Lipocalin-2. B) Quantification of Lcn2 protein levels, normalized over Gapdh. C) Real-time RT-qPCR analysis of Lcn2 expression level. N=4-5 animals/group. Data are expressed as mean ± s.d. *P<0.05; **P<0.001 (unpaired t-test).*

3.1.3 Characterization of 14-week-old Tg^{UmodC147W}/Ccr2$^{-/-}$ mice

To gain insight on the role of Ccr2 axis on disease progression, we characterized 14-week-old Tg^{Umod}C147W/*Ccr2*$^{-/-}$ mice. At this age mutant mice display kidney histological alterations typical of ADTKD-*UMOD*, i.e., focal areas of interstitial inflammatory cell infiltration and fibrosis (Bernascone *et al*, 2010).

After verifying *Ccr2* ablation (**Figure 17A**), we confirmed by real-time RT-qPCR that uromodulin expression was not influenced by the receptor ablation, as demonstrated by comparable expression levels of *Umod* in kidneys from Tg^{Umod}C147W/*Ccr2*$^{-/-}$ and Tg^{Umod}C147W/*Ccr2*$^{+/+}$ mice (**Figure 17B**). **Figure 17C** reports uromodulin analysis by Western blot to assess mutant uromodulin trafficking in kidneys of Tg^{Umod}C147W mice at this time-point. *Ccr2* ablation does not have impact on mutant uromodulin ER retention, as demonstrated by similar ratio of ER form/mature uromodulin in kidneys from Tg^{Umod}C147W/*Ccr2*$^{-/-}$ and Tg^{Umod}C147W/*Ccr2*$^{+/+}$ mice (**Figure 17D**). However, we observed that mutant uromodulin ER retention was rescued in kidneys from a single Tg^{Umod}C147W/*Ccr2*$^{-/-}$ mouse (indicated with # in **Figure 17C**).

This mouse has been further characterized and results will be described in *Paragraph 3.2*.

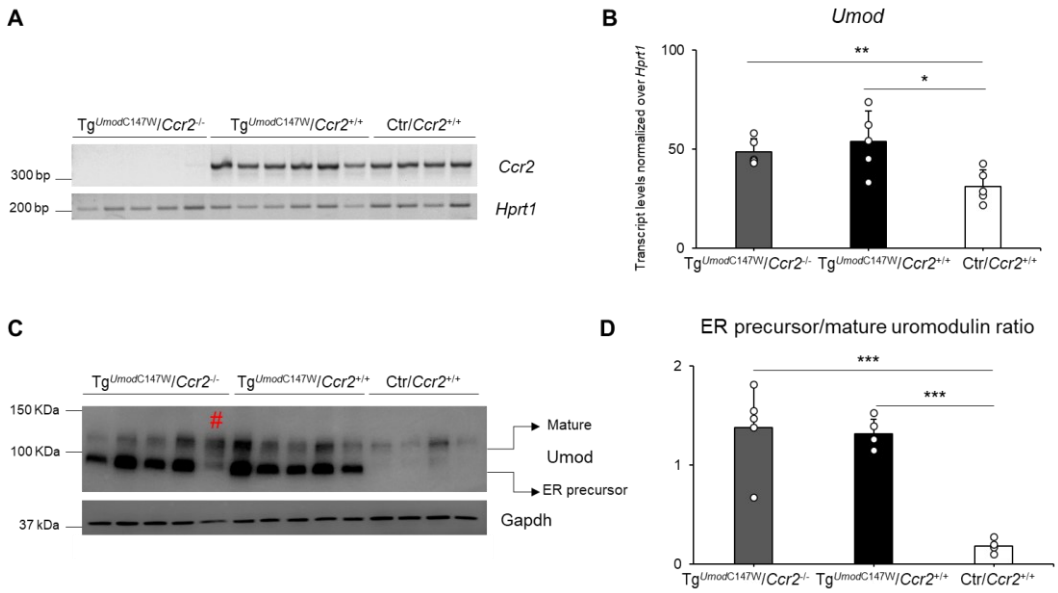


Figure 17. Characterization of 14-week-old Tg^{UmodC147W}/Ccr2$^{-/-}$ mice. *A) Semiquantitative RT-PCR confirming Ccr2 ablation in kidneys of Tg^{UmodC147W}/Ccr2$^{-/-}$ mice. Hprt1 expression is shown as a normalizer. B) Analysis by real-time RT-qPCR of uromodulin expression. C) Western blot using anti-uromodulin antibody showing the enrichment of the lower band, corresponding to the immature ER precursor in kidneys of Tg^{UmodC147W}/Ccr2$^{-/-}$ and Tg^{UmodC147W}/Ccr2$^{+/+}$ compared to Ctr/Ccr2$^{+/+}$mice. Gapdh is reported as loading control. The animal indicated with # shows rescue of mutant uromodulin ER retention. D) Quantification of the ratio ER form/mature form of uromodulin in kidney lysates from Tg^{UmodC147W}/Ccr2$^{-/-}$, Tg^{UmodC147W}/Ccr2$^{+/+}$ and Ctr/Ccr2$^{+/+}$. N=4-5 animals/group. Data are expressed as mean ± s.d. *P<0.05; **P<0.01; ***P<0.005 (unpaired t-test).*

To characterize kidney inflammation, we measured the expression level of markers of inflammatory cells (*Cd68*, *Cd45*) and chemokines (*Ccl2*, *Ccl12*) (**Figure 18A**). Moreover, we assessed macrophage infiltration, by quantifying F4/80^{+} area (**Figure 18B, C**). Also at 14 weeks of age, the analysis revealed induction of inflammation in Tg^{Umod}C147W mice compared to Ctr/Ccr2$^{+/+}$ animals that is not rescued by ablation of *Ccr2*.

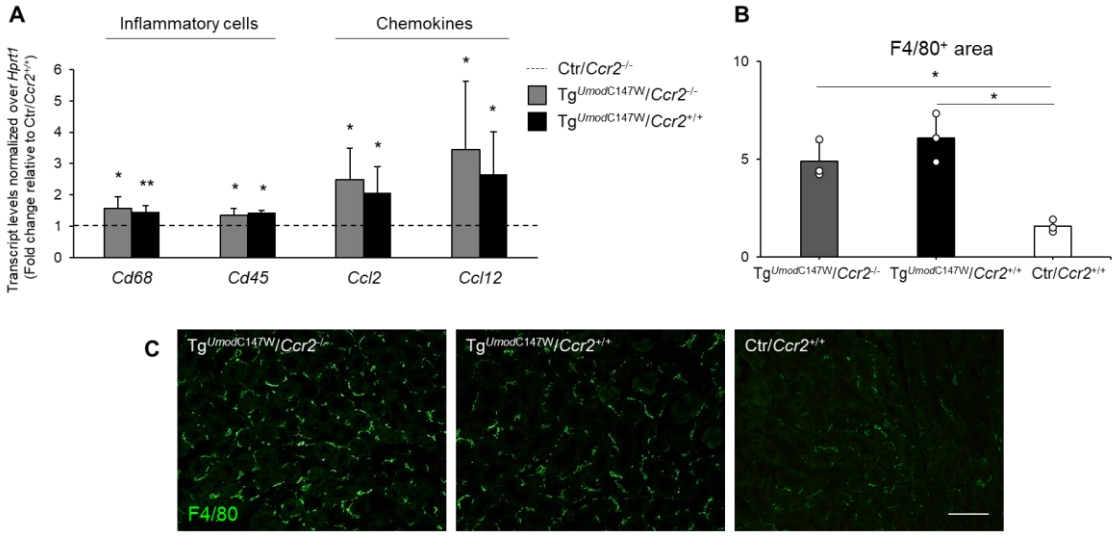


Figure 18. Inflammation in kidneys of 14-week-old $Tg^{UmodC147W}/Ccr2^{-/-}$ mice. *A) Cd68, Cd45, Ccl2 and Ccl12 expression analyzed by real-time RT-qPCR. Histograms represent fold changes relative to expression in age- and sex-matched non-transgenic mice, indicated by the dashed line. B) Quantification of F4/80 positive area in kidneys of $Tg^{UmodC147W}/Ccr2^{-/-}$, $Tg^{UmodC147W}/Ccr2^{+/+}$ and $Ctr/Ccr2^{+/+}$ mice. C) Representative images of immunofluorescence staining for monocyte/macrophage marker (F4/80) (Bar=100 µm). N=4-5 animals/group. Data are expressed as mean ± s.d. *P<0.05; **P<0.01 (unpaired t-test).*

Similar results were obtained from the analysis of fibrosis marker vimentin. Indeed, kidneys of $Tg^{Umod\text{C147W}}$ animals displayed increased *Vim1* expression (**Figure 19A**) and increased vimentin deposition (**Figure 19B, C**) compared to wild type mice, that is not reduced by *Ccr2* ablation.

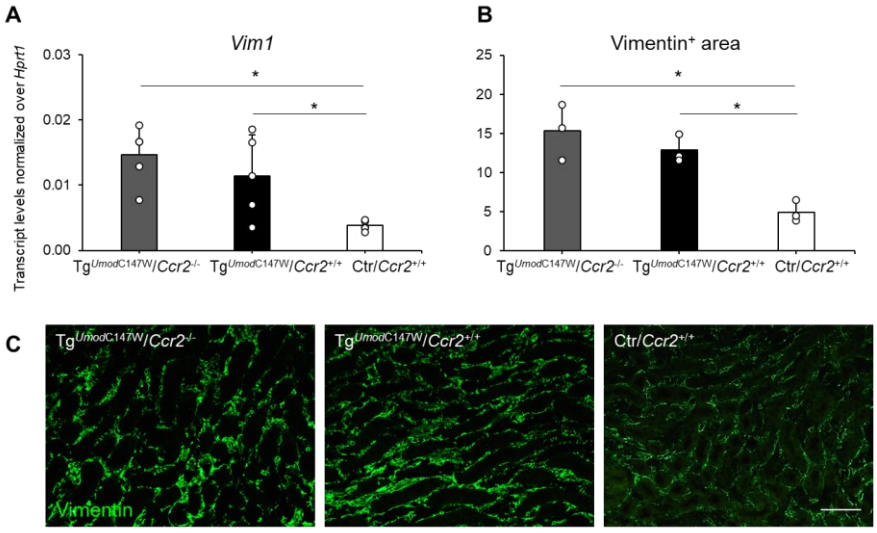


Figure 19. Fibrosis in kidneys of 14-week-old Tg^{UmodC147W}/Ccr2$^{-/-}$ mice. *A) Real-time RT-qPCR analysis of Vim1 (encoding for the fibrosis marker Vimentin). Tg^{UmodC147}/Ccr2$^{-/-}$ were compared to age- and sex-matched Tg^{UmodC147}/Ccr2$^{+/+}$ and Ctr/Ccr2$^{+/+}$ mice. B) Quantification of Vimentin positive area in kidneys of Tg^{UmodC147W}/Ccr2$^{-/-}$, Tg^{UmodC147W}/Ccr2$^{+/+}$ and Ctr/Ccr2$^{+/+}$ mice. C) Representative images of immunofluorescence staining for Vimentin (Bar=100 µm). N=4-5 animals/group. Data are expressed as mean ± s.d. ***P<0.005 (unpaired t-test).*

Finally, we evaluated tubular damage in 14-week-old Tg$^{Umod\text{C147W}}$ mice. Lcn2 was significantly and comparably up-regulated both at protein (**Figure 20A, B**) and transcript (**Figure 20C**) levels in Tg$^{Umod\text{C147W}}$/*Ccr2*$^{-/-}$ and Tg$^{Umod\text{C147W}}$/*Ccr2*$^{+/+}$ compared to control mice, showing that Ccr2 ablation does not ameliorate tubular damage in kidneys of mutant mice also at this later time point.

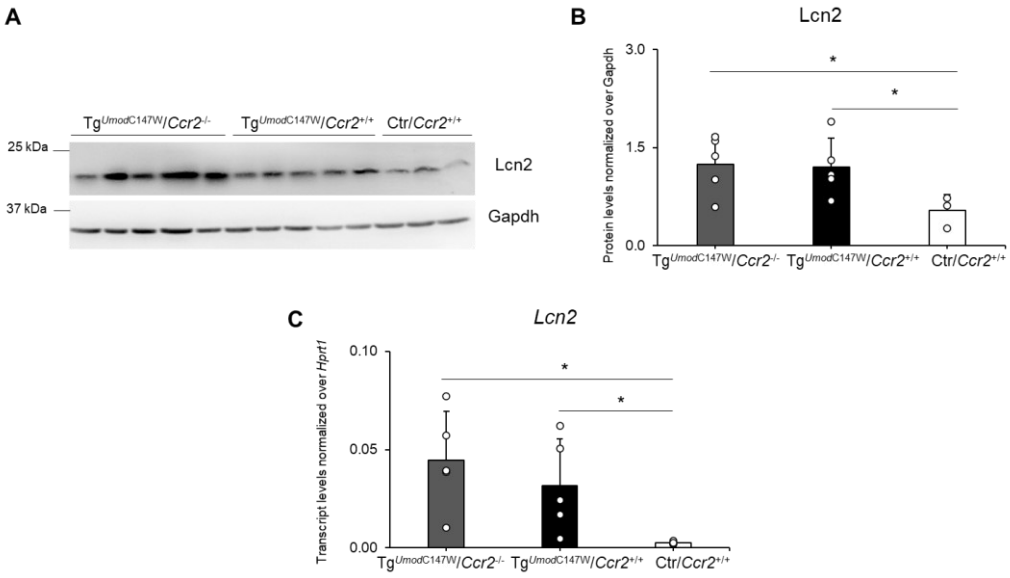


Figure 20. Tubular damage in kidneys of 14-week-old Tg^{UmodC147W}/Ccr2$^{-/-}$ mice. *A) Western blot analysis of Lipocalin-2 kidney protein levels. B) Quantification of Lcn2 kidney protein levels, normalized over Gapdh. C) Real-time RT-qPCR analysis of Lcn2 kidney expression. N=4-5 animals/group. Data are expressed as mean ± s.d. *P<0.05 (unpaired t-test).*

3.1.4 Characterization of 24-week-old Tg^{UmodC147W}/Ccr2$^{-/-}$ mice

Finally, we studied the effect of *Ccr2* targeting on disease phenotype at 24 weeks of age when Tg^{Umod}C147W mice show fully-blown disease, with marked tubulointerstitial damage, severe interstitial inflammation and fibrosis and mild renal failure (Bernascone *et al*, 2010).

Also at this time point, we validated *Ccr2* ablation in kidneys of Tg^{Umod}C147W/*Ccr2*$^{-/-}$ mice by semiquantitative RT-PCR (**Figure 21A**) and confirmed unaltered levels of *Umod* expression (**Figure 21B**) and of ER retention of mutant uromodulin in Tg^{Umod}C147W/*Ccr2*$^{-/-}$ and Tg^{Umod}C147W/*Ccr2*$^{+/+}$ mice (**Figure 21C, D**).

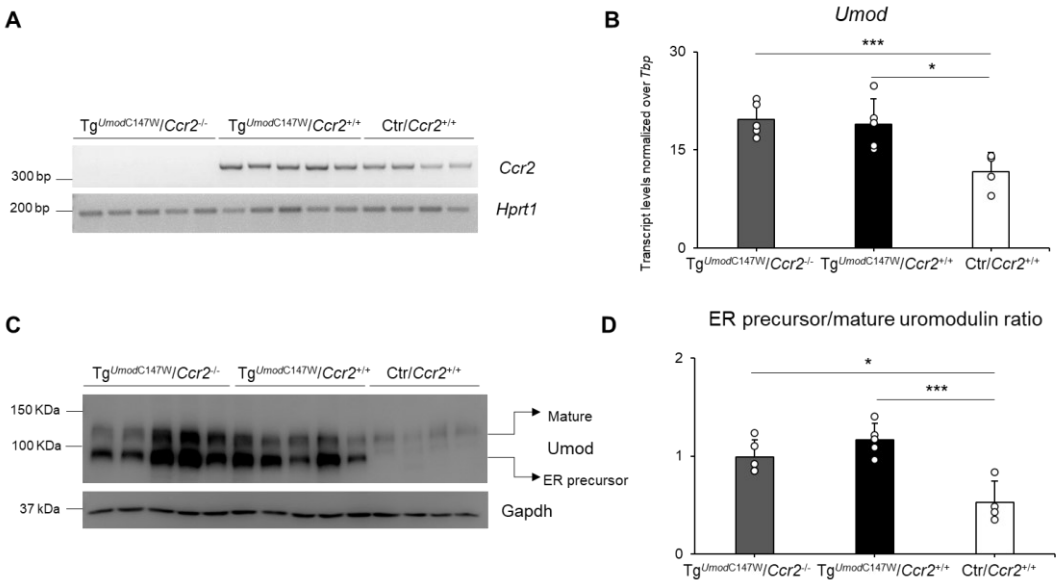


Figure 21. Characterization of 24-week-old Tg^{UmodC147W}/Ccr2$^{-/-}$ mice. *A) Semiquantitative RT-PCR to validate Ccr2 ablation in kidneys of Tg^{UmodC147W}/Ccr2$^{-/-}$ mice. As reference gene, we tested the expression of Hprt1. B) Analysis by real-time RT-qPCR of uromodulin expression. Transcript levels were normalized on Tbp (TATA-box-binding protein). C) Western blot using anti-uromodulin antibody. Gapdh is reported as a loading control. D) Quantification of the ratio ER precursor/mature uromodulin in kidney lysates from Tg^{UmodC147W}/Ccr2$^{-/-}$, Tg^{UmodC147W}/Ccr2$^{+/+}$ and Ctr/Ccr2$^{+/+}$. N=4-5 animals/group. Data are expressed as mean ± s.d. *P<0.05; ***P<0.005 (unpaired t-test).*

24-week-old Tg^{Umod}C147W mice show clear induction of markers of leucocytes (*Cd45*), macrophages (*Cd68*) and of chemokines (*Ccl2*, *Ccl12*), compared to sex- and age-matched non-transgenic mice. However, no significant difference was observed in mutant mice in the presence or absence of *Ccr2* receptor (**Figure 22A**).

We also analyzed kidney macrophage infiltration, by quantifying F4/80^{+} area. We observed no significant differences in Tg^{Umod}C147W/*Ccr2*$^{-/-}$ compared to Tg^{Umod}C147W/*Ccr2*$^{+/+}$ mice, that both showed the expected increase in macrophage infiltration compared to wild type (**Figure 22B, C**). All together these results suggest that *Ccr2* ablation is not sufficient to reduce macrophage infiltration and activation in kidneys of Tg^{Umod}C147W mice at 24 weeks.

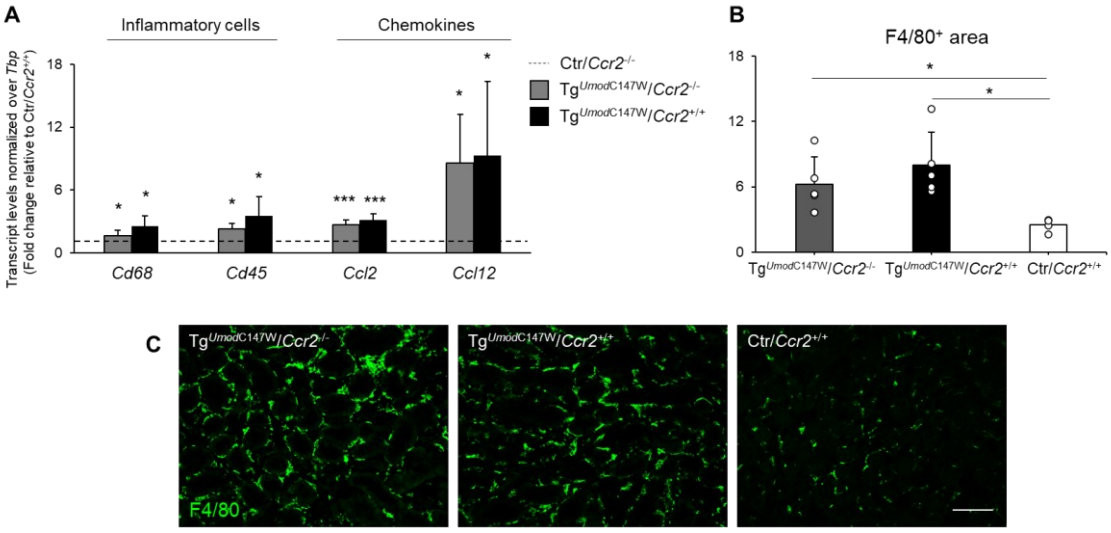


Figure 22. Inflammation in kidneys of 24-week-old Tg^{UmodC147W}/Ccr2$^{-/-}$ mice. *A) Analysis by real-time RT-qPCR of the expression of macrophages marker (Cd68), common leukocytes antigen (Cd45) and chemokines (Ccl2, Ccl12). Data are reported as fold change compared to age- and sex-matched Ctr/Ccr2$^{+/+}$ mice (dashed line). B) The histograms summarize the quantification of F4/80 positive area in kidneys of Tg^{UmodC147W}/Ccr2$^{-/-}$, Tg^{UmodC147W}/Ccr2$^{+/+}$ and Ctr/Ccr2$^{+/+}$ mice. C) Representative images of immunofluorescence staining for monocytes/macrophages marker (F4/80) (Bar=100 µm). N=4-5 animals/group. Data are expressed as mean ± s.d. *P<0.05; ***P<0.005 (unpaired t-test).*

Results on inflammation were reflected by absence of amelioration of fibrotic phenotype in kidneys of Tg^{Umod}C147W/*Ccr2*$^{-/-}$, as demonstrated by comparable levels of *Vim1* levels and vimentin deposition relative to Tg^{Umod}C147W/Ccr2$^{+/+}$ mice. However, as expected, at this age Tg^{Umod}C147W mice showed notable fibrosis induction compared to Ctr mice (**Figure 23**).

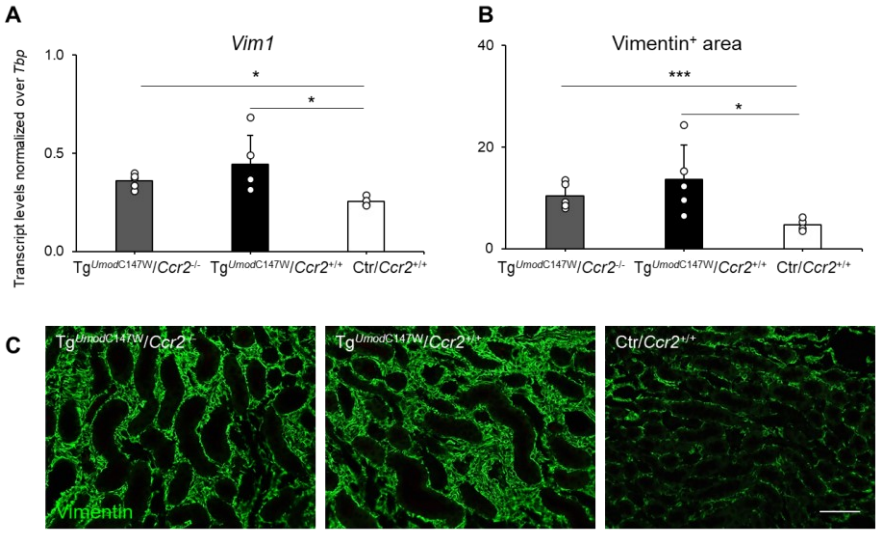


Figure 23. Fibrosis in kidneys of 24-week-old Tg^{UmodC147W}/Ccr2$^{-/-}$ mice. *A) Real-time RT-qPCR analysis of Vim1 (encoding for the fibrosis marker Vimentin). Transcript levels are normalized over Tbp. B) Quantification of Vimentin positive area in kidneys of Tg^{UmodC147W}/Ccr2$^{-/-}$, Tg^{UmodC147W}/Ccr2$^{+/+}$ and wild type mice and C) representative images of immunofluorescence showing increased Vimentin deposition in kidneys of Tg^{UmodC147W} mice. (Bar=100 µm). N=4-5 animals/group. Data are expressed as mean ± s.d. ***P<0.005 (unpaired t-test).*

To assess tubular damage, we measured *Lcn2* at transcript level in the kidney and at protein level both in kidney and urine from Tg$^{Umod\text{C147W}}$/*Ccr2*$^{-/-}$, Tg$^{Umod\text{C147W}}$/*Ccr2*$^{+/+}$ and Ctr/*Ccr2*$^{+/+}$ mice (**Figure 24**). This analysis revealed strong induction of tubular damage in mutant mice, compared to wild type, but again, no amelioration upon Ccr2 ablation.

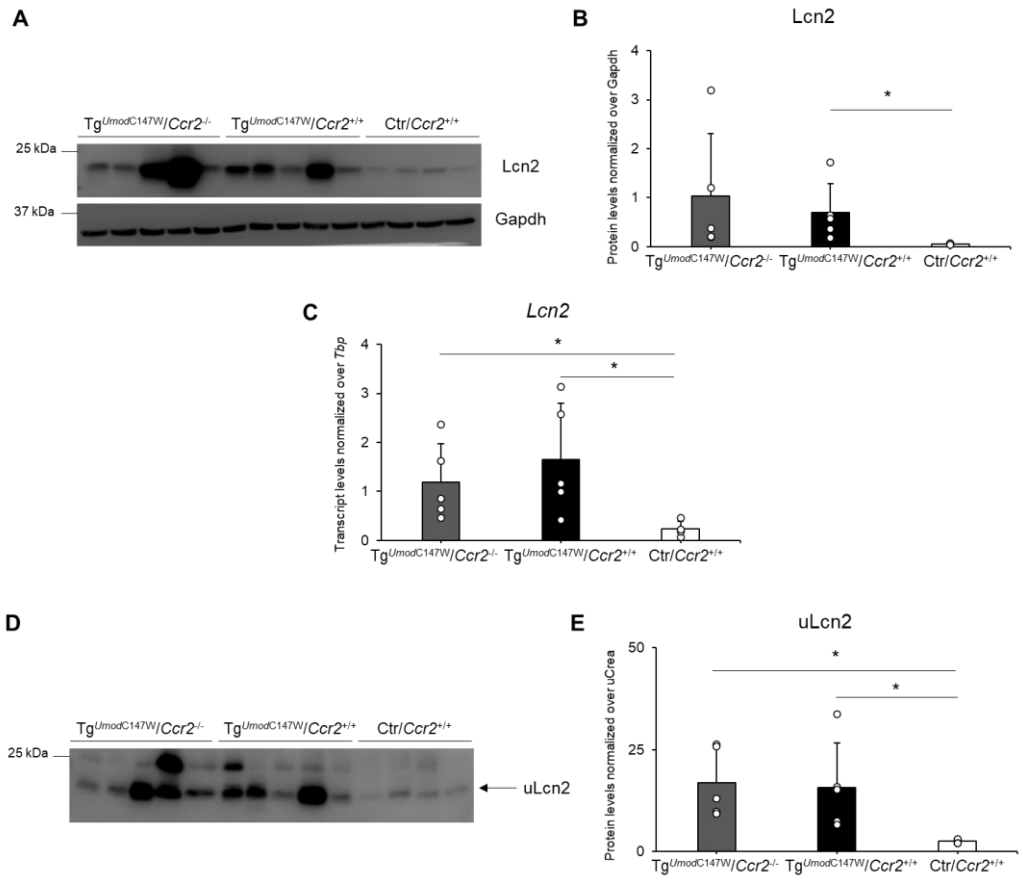


Figure 24.Tubular damage in kidneys of 24-week-old Tg^{UmodC147W}/Ccr2$^{-/-}$ mice. *A) Western blot analysis of Lipocalin-2 in kidney lysates from Tg^{UmodC147W}/Ccr2$^{-/-}$, Tg^{UmodC147W}/Ccr2$^{+/+}$ and wild type mice. B) Quantification of Lcn2 protein levels, normalized over Gapdh. C) Real-time RT-qPCR analysis of Lcn2 expression level. D) Western blot analysis and E) quantification of Lipocalin-2 levels in urines from Tg^{UmodC147W}/Ccr2$^{-/-}$, Tg^{UmodC147W}/Ccr2$^{+/+}$ and Ctr/Ccr2$^{+/+}$ mice. Urines were loaded based on total protein quantification. N=4-5 animals/group. Data are expressed as mean ± s.d. *P<0.05 (unpaired t-test).*

3.1.5 Summary of Tg^{UmodC147W}/Ccr2$^{-/-}$ mouse line characterization

To summarize, all parameters analyzed and already known to be up-regulated in Tg$^{Umod\text{C147W}}$ mice (Bernascone *et al*, 2010; Trudu *et al*, 2017) are induced in mutant mice of both *Ccr2* genotypes (*Ccr2*$^{-/-}$ and *Ccr2*$^{+/+}$) compared to non-transgenic littermates. *Ccr2* ablation in Tg$^{Umod\text{C147W}}$ mice was not effective in blocking initiation of kidney inflammation and thus did not ameliorate disease onset and/or progression in mice expressing mutant uromodulin.

Of note, these data suggest that ADTKD-*UMOD* phenotype in Tg$^{Umod\text{C147W}}$ animals is not affected by mixed genetic background (**Table 2**).

Characterization of Tg$^{Umod C147W}$/*Ccr2*$^{-/-}$ mouse line

	1-week-old		6-weeks-old		14-weeks-old		24-weeks-old	
	vs. Ctr/*Ccr2*$^{+/+}$	vs. Tg$^{Umod C147W}$/*Ccr2*$^{+/+}$	vs. Ctr/*Ccr2*$^{+/+}$	vs. Tg$^{Umod C147W}$/*Ccr2*$^{+/+}$	vs. Ctr/*Ccr2*$^{+/+}$	vs. Tg$^{Umod C147W}$/*Ccr2*$^{+/+}$	vs. Ctr/*Ccr2*$^{+/+}$	vs. Tg$^{Umod C147W}$/*Ccr2*$^{+/+}$
Uromodulin	↑ expression ↑ ER retention	= expression = ER retention	↑ expression ↑ ER retention	= expression = ER retention	↑ expression ↑ ER retention	= expression = ER retention	↑ expression ↑ ER retention	= expression = ER retention
Inflammation	↑ Leucocytes (*Cd45*) ↑ Macrophages (*Cd68*, F4/80+ area) ↑ Chemokines (*Ccl2*, *Ccl12*)	= Leucocytes (*Cd45*) = Macrophages (*Cd68*, F4/80+ area) = Chemokines (*Ccl2*, *Ccl12*)	↑ Leucocytes (*Cd45*) ↑ Macrophages (*Cd68*, F4/80+ area) ↑ Chemokines (*Ccl2*, *Ccl12*)	= Leucocytes (*Cd45*) = Macrophages (*Cd68*, F4/80+ area) = Chemokines (*Ccl2*, *Ccl12*)	↑ Leucocytes (*Cd45*) ↑ Macrophages (*Cd68*, F4/80+ area) ↑ Chemokines (*Ccl2*, *Ccl12*)	= Leucocytes (*Cd45*) = Macrophages (*Cd68*, F4/80+ area) = Chemokines (*Ccl2*, *Ccl12*)	↑ Leucocytes (*Cd45*) ↑ Macrophages (*Cd68*, F4/80+ area) ↑ Chemokines (*Ccl2*, *Ccl12*)	= Leucocytes (*Cd45*) = Macrophages (*Cd68*, F4/80+ area) = Chemokines (*Ccl2*, *Ccl12*)
Fibrosis	↑ *Vim1* ↑ Vimentin deposition	= *Vim1* = Vimentin deposition	↑ *Vim1* ↑ Vimentin deposition	= *Vim1* = Vimentin deposition	↑ *Vim1* ↑ Vimentin deposition	= *Vim1* = Vimentin deposition	↑ *Vim1* ↑ Vimentin deposition	= *Vim1* = Vimentin deposition
Tubular damage	↑ *Lcn2* ↑ Lcn2 kidney levels	= *Lcn2* = Lcn2 kidney levels	↑ *Lcn2* ↑ Lcn2 kidney levels	= *Lcn2* = Lcn2 kidney levels	↑ *Lcn2* ↑ Lcn2 kidney levels	= *Lcn2* = Lcn2 kidney levels	↑ *Lcn2* ↑ Lcn2 kidney levels ↑ Lcn2 urinary levels	= *Lcn2* = Lcn2 kidney levels = Lcn2 urinary levels

Table 2. Characterization of Tg^{UmodC147W}/Ccr2$^{-/-}$ mouse line. *The table summarizes the results obtained from the analysis of different disease parameters (mutant uromodulin ER retention, inflammation, fibrosis and tubular damage) in kidneys of Tg^{UmodC147W}/Ccr2$^{-/-}$. For each time-point analyzed, the comparison of Tg^{UmodC147W}/Ccr2$^{-/-}$ with sex- and age-matched Ctr/Ccr2$^{+/+}$ and Tg^{UmodC147W}/Ccr2$^{+/+}$ mice is reported.*

3.2 Rescue of mutant uromodulin ER retention

As already reported in *Paragraph 3.1.3*, during the characterization of $Tg^{Umod\text{C147W}}/Ccr2^{-/-}$ mouse line, we observed rescue of mutant uromodulin ER retention in kidneys from a 14-week-old $Tg^{Umod\text{C147W}}$ mouse (**Figure 17D** and **Figure 25A**). Western blot analysis of kidney lysates from this animal (blue dashed box in **Figure 25A**) showed a dramatic reduction of uromodulin ER precursor isoform compared to its mutant littermates (e.g., red dashed square in **Figure 25A**). We confirmed biochemical results by performing immunofluorescence staining. Using an anti-HA antibody to specifically stain transgenic mutant uromodulin, we observed the absence of intracellular uromodulin accumulation, that is instead clearly visible in cells expressing mutant uromodulin in kidneys of $Tg^{Umod\text{C147W}}$ mice at this age. Instead, in TAL cells of this mouse, transgenic mutant uromodulin mainly localized at the apical membrane, resembling the typical localization of wild type protein (**Figure 25B**).

Interestingly, at sacrifice this mouse presented with incisors overgrowth causing malocclusion problems and was significantly smaller compared to its mutant littermates (10.5 g vs. an average of 25.5±3.1 g of body weight), suggesting a possible feeding problem.

To exclude genotyping errors or the occurrence of any revertant mutation, we sequenced kidney cDNA from this mouse. The electropherograms reported in **Figure 25C** confirmed transgene expression and the presence of the nucleotide substitution (c.441T>G) leading to p.Cys147Trp uromodulin mutation.

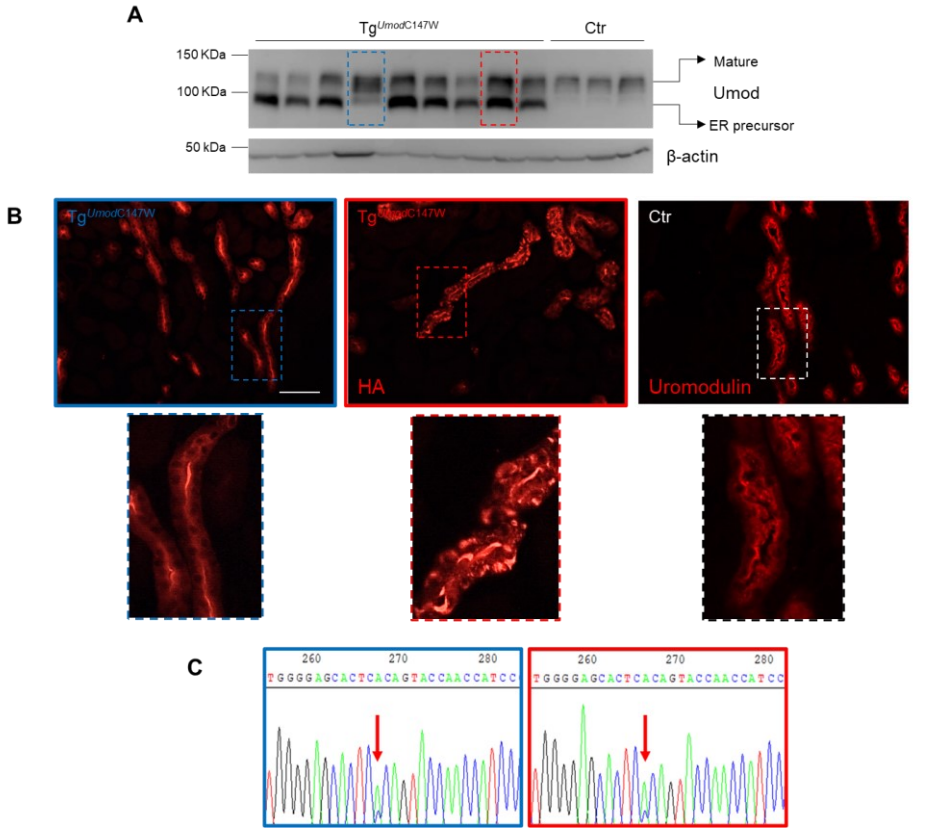


Figure 25. Rescue of mutant uromodulin ER retention in a Tg^{UmodC147W} mouse. *A) Western blot analysis revealed reduction of mutant protein ER retention in one Tg^{UmodC147W} mouse (blue dashed square) compared to other mutant mice (e.g., red square). B-actin is reported as loading control. B) Immunofluorescence staining of transgenic mutant uromodulin (using an anti-HA antibody) confirming biochemical results and showing reduction of intracellular aggregates and increased uromodulin signal at the apical membrane of TAL cells, comparable to what observed in kidney of wild type mice (Ctr, staining performed using and anti-uromodulin antibody). Bar=100 µm. C) Electropherograms obtained by sequencing transgenic uromodulin. The A>C nucleotide substitution corresponding to c.441T>G mutation and leading to Cys147Trp aminoacidic change is indicated by the red arrows.*

Based on these observations, we hypothesized that the rescue in mutant uromodulin ER retention detected in that mouse was due to reduced food intake during its life.

3.3 Proof-of-concept calorie restriction in Tg^{Umod}wt and Tg^{Umod}C147W mice

To test the hypothesis that the effect on uromodulin phenotype observed in the "rescued" mouse was due to food intake reduction, we performed a proof-of-concept

experiment, feeding Tg$^{Umod\text{C147W}}$ mice with a calorie restriction (CR) regimen. In parallel, we also performed CR of age- and sex-matched Tg$^{Umod\text{wt}}$ mice, i.e., animals transgenic for wild type uromodulin, used as control of uromodulin overexpression (Bernascone *et al*, 2010).

The used experimental protocol is schematized in **Figure 26A**. Briefly, starting from 3 weeks of age, at time of weaning, Tg$^{Umod\text{wt}}$ and Tg$^{Umod\text{C147W}}$ were daily allotted with 45% of the food amount that was consumed by age- and sex-matched mice of the same genotype on *ad libitum* (AL) regimen (N=3 mice/group, all females).

During 4 weeks of controlled diet, while animals of both genotypes in the control group grew as expected, Tg$^{Umod\text{wt}}$ and Tg$^{Umod\text{C147W}}$ mice in CR display a loss of body weight corresponding to an average of 21.4 (±3.1)% of their initial body weight (corresponding to 2.7±0.51 g) in the first 2 weeks of diet. Then, body weight was maintained around 9.7 (±0.68) g until the end of diet (**Figure 26B**).

Importantly, body weight of CR mice at sacrifice (7 weeks of age) was comparable to that of the mouse with malocclusion problems (*Paragraph 3.2*), suggesting that this diet could mimic food intake reduction likely occurring for the "rescued" mouse.

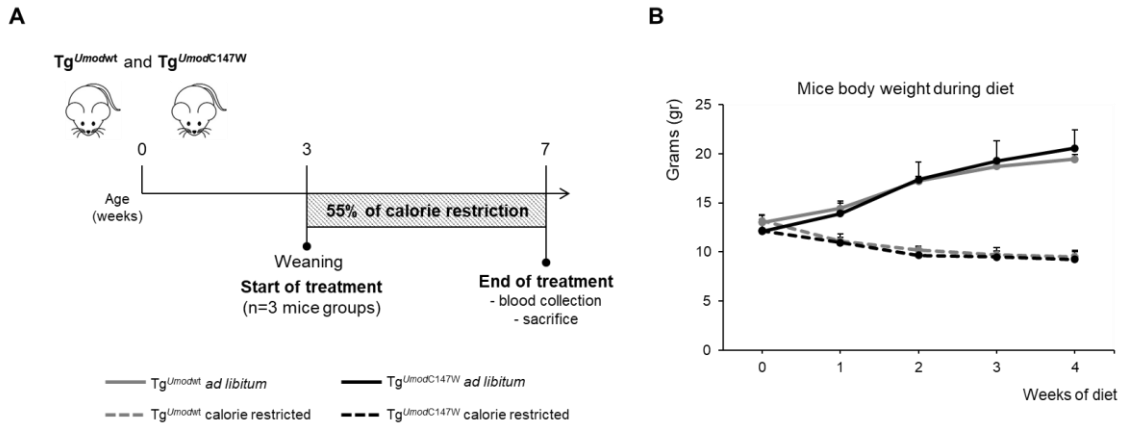


Figure 26. Calorie restriction protocol and mouse body weight during the diet. *A) Graphical representation of calorie restriction protocol. Starting from weaning (3 weeks of age) and for 4 weeks, Tg^{Umodwt} and Tg^{UmodC147W} mice were fed ad libitum or on a 55% CR regimen. B) Body weight of Tg^{Umodwt} and Tg^{UmodC147W} mice on AL or CR regimen. At the end of the protocol, the body weight of CR mice was comparable to the one of the rescued mouse (i.e. about 10 grams). N=3 mice/group.*

3.3.1 Effect of calorie restriction on uromodulin biology

We evaluated the effect of calorie restriction on uromodulin expression and processing in kidneys of Tg*Umod*wt and Tg*Umod*C147W mice. Western blot analysis revealed a clear increase of the upper band, corresponding to fully glycosylated mature uromodulin in mutant CR mice, suggesting an increase in mutant protein folding and trafficking (**Figure 27A**). This is reflected by a strong reduction of mutant uromodulin ER retention in kidneys of Tg*Umod*C147W CR mice compared to Tg*Umod*C147W mice AL, as indicated by reduction of the ratio uromodulin ER/mature forms, that decreases to the levels measured in Tg*Umod*wt AL animals (**Figure 27B**).

Importantly, calorie restriction had no impact on *Umod* expression, as demonstrated by comparable transcript levels among the four experimental groups (**Figure 27C**).

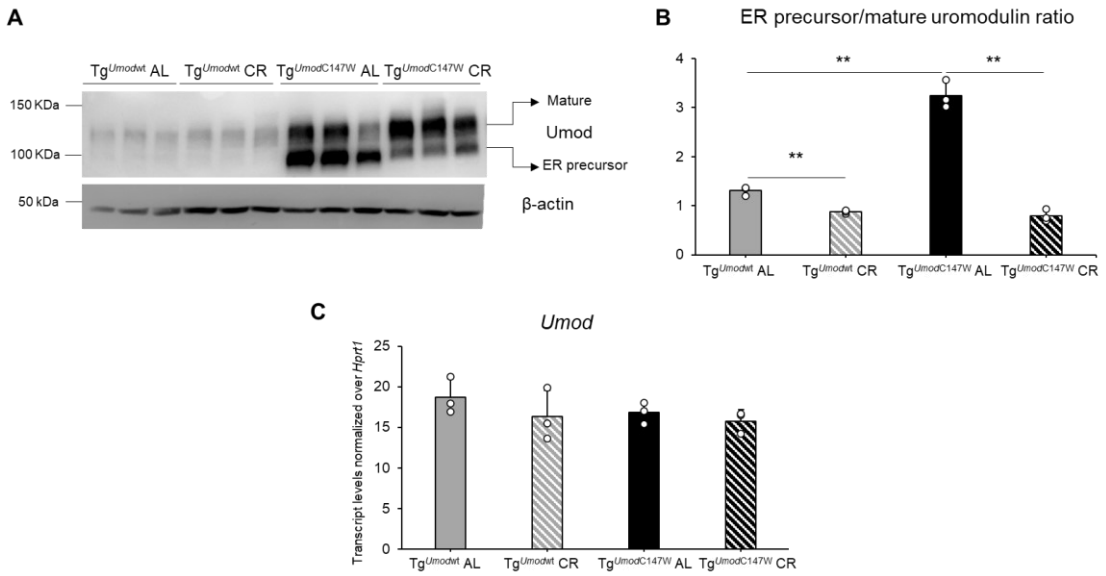


Figure 27. Effect of calorie restriction on mutant uromodulin ER retention and uromodulin expression. *A) Western blot analysis of uromodulin levels in kidneys from Tg^{Umodwt} AL, Tg^{Umodwt} CR, Tg^{UmodC147W} AL and Tg^{UmodC147W} CR mice. B) Quantification of the ratio ER precursor/mature uromodulin forms. C) Analysis by real-time RT-qPCR of Umod expression levels. N=3 animals/group. Data are expressed as mean ± s.d. **P<0.01 (unpaired t-test).*

Immunofluorescence analysis supported the impact of CR on mutant uromodulin folding and maturation. Indeed, staining of transgenic uromodulin (using an anti-HA antibody), shows the presence of the typical large intracellular aggregates in TAL cells of mutant mice fed *ad libitum*, while in mutant CR mice we observed a predominant localization at

the cell apical membrane, resembling the signal observed in mice expressing wild type uromodulin (**Figure 28**).

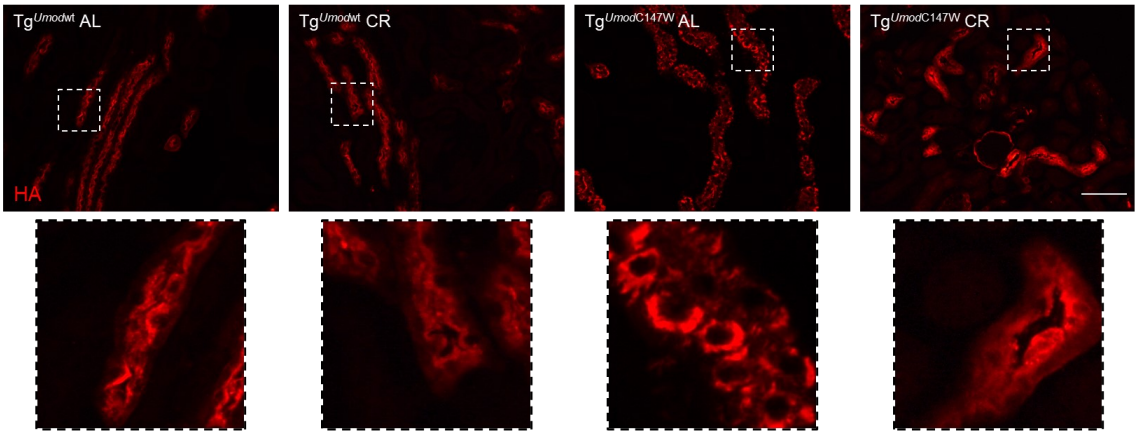


Figure 28. Effect of calorie restriction on uromodulin trafficking. *Immunofluorescence using an anti-HA antibody, showing reduced intracellular localization of mutant uromodulin in kidneys of CR Tg^{UmodC147W}mice, compared to AL ones, and its increased localization at the apical membrane, similar to what observed for Tg^{Umodwt} mice.*

The effect of CR on mutant uromodulin aggregation in the ER was further demonstrated by Western blot analysis in non-reducing conditions. While in Tg$^{Umod\text{wt}}$ mice transgenic uromodulin signal consists of a single band (below 100kDa) corresponding to fully glycosylated mature protein, in Tg$^{Umod\text{C147W}}$ we also detected a lower band (around 75kDa) corresponding to ER immature isoform and a high-molecular-weight signal, likely corresponding to mutant uromodulin aggregates formed by intermolecular disulfide bonds. High molecular weight forms are remarkably reduced in kidneys of CR mutant mice compared to the ones fed AL (**Figure 29A**). Immunofluorescence analysis performed on kidney sections revealed the presence of large intracellular aggregates of mutant uromodulin that co-localize with the ER chaperone calreticulin in AL Tg$^{Umod\text{C147W}}$ mice and that are essentially absent in sections of CR mutant mice (**Figure 29B**).

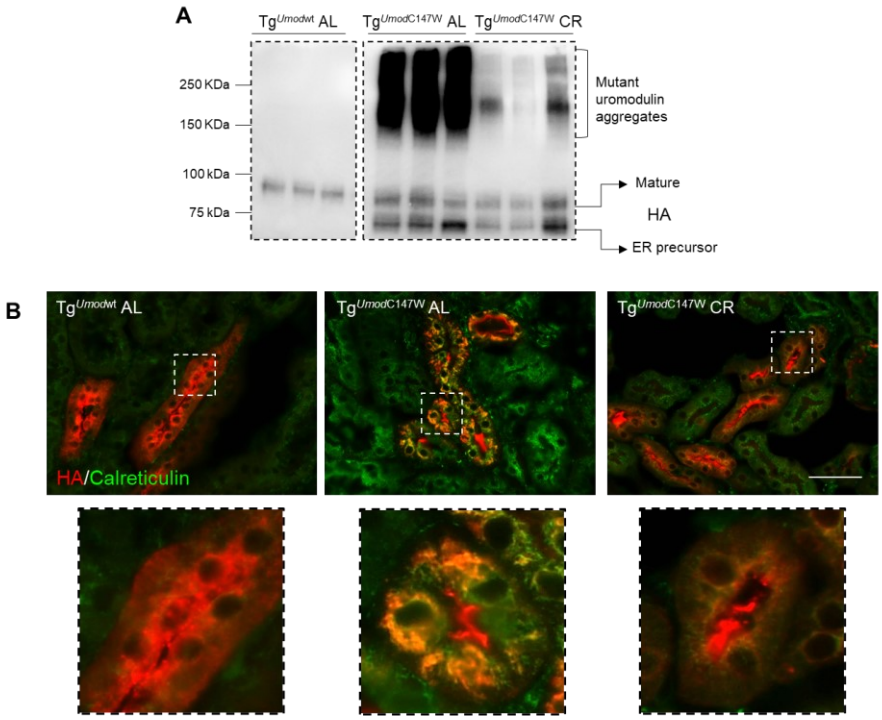


Figure 29. Effect of calorie restriction on mutant uromodulin ER aggregation. *A) Western blot in non-reducing condition using anti-HA antibody.The ~100 kDa band corresponds to mature form of uromodulin and is present both in* Tg^{Umodwt} *and* $Tg^{UmodC147W}$ *mice. The ~75 kDa band corresponds to ER immature uromodulin. High-molecular-weight signal corresponds to mutant uromodulin aggregates. Images are cropped part of the same membrane. B) Dual staining for transgenic uromodulin (HA, in red) and the ER marker calreticulin (in green), in* Tg^{Umodwt}, $Tg^{UmodC147W}$ *AL and* $Tg^{UmodC147W}$ *CR mice. Bar=100µm.*

All together these results demonstrate that CR mimics the effect on uromodulin biology observed in the rescued mouse (*Paragraph 3.2*). This regimen is effective in reducing mutant uromodulin ER retention and aggregation, increasing uromodulin intracellular trafficking and its delivery to the cell plasma membrane, likely because of improved protein folding.

3.3.2 Effect of calorie restriction on inflammation and fibrosis

As already mentioned before, we previously demonstrated early induction of inflammatory pathways downstream of mutant uromodulin ER retention in kidneys of $Tg^{UmodC147W}$ mice that results in fibrosis induction as the disease progresses (Trudu *et al*,

2017 and our unpublished data, *Paragraph 1.6*). Based on these data, we asked if the reduction of uromodulin accumulation in the ER induced by CR could decrease inflammation in kidneys of Tg$^{Umod\text{C147W}}$ mice.

To characterize inflammation, we analyzed the expression level of *Cd68*, confirming significant up regulation of this macrophage marker in Tg$^{Umod\text{C147W}}$ mice at this age and observing a reduction reaching the levels of Tg$^{Umod\text{wt}}$ upon CR. Similar results were obtained from the analysis of pro-inflammatory chemokines *Ccl2* and *Ccl12*, that were strongly down-regulated in kidneys of mutant calorie restricted mice (**Figure 30A**). The reduction in inflammatory cell infiltration was confirmed by immunofluorescence analysis, staining for F4/80 macrophage antigen (**Figure 30B**). The quantification of F4/80^{+} area revealed a significant reduction in macrophage infiltration in kidneys from Tg$^{Umod\text{C147W}}$ CR animals compared to their AL counterpart (**Figure 30D**).

To assess the effect of CR on kidney fibrosis, we next measured *Vim1* expression levels and vimentin deposition. Compared to AL, Tg$^{Umod\text{C147W}}$ CR mice exhibited decreased expression levels of *Vim1* (**Figure 30A**) and decreased vimentin^{+} area (**Figure 30C, E**), showing levels comparable to what observed in Tg$^{Umod\text{wt}}$ animals.

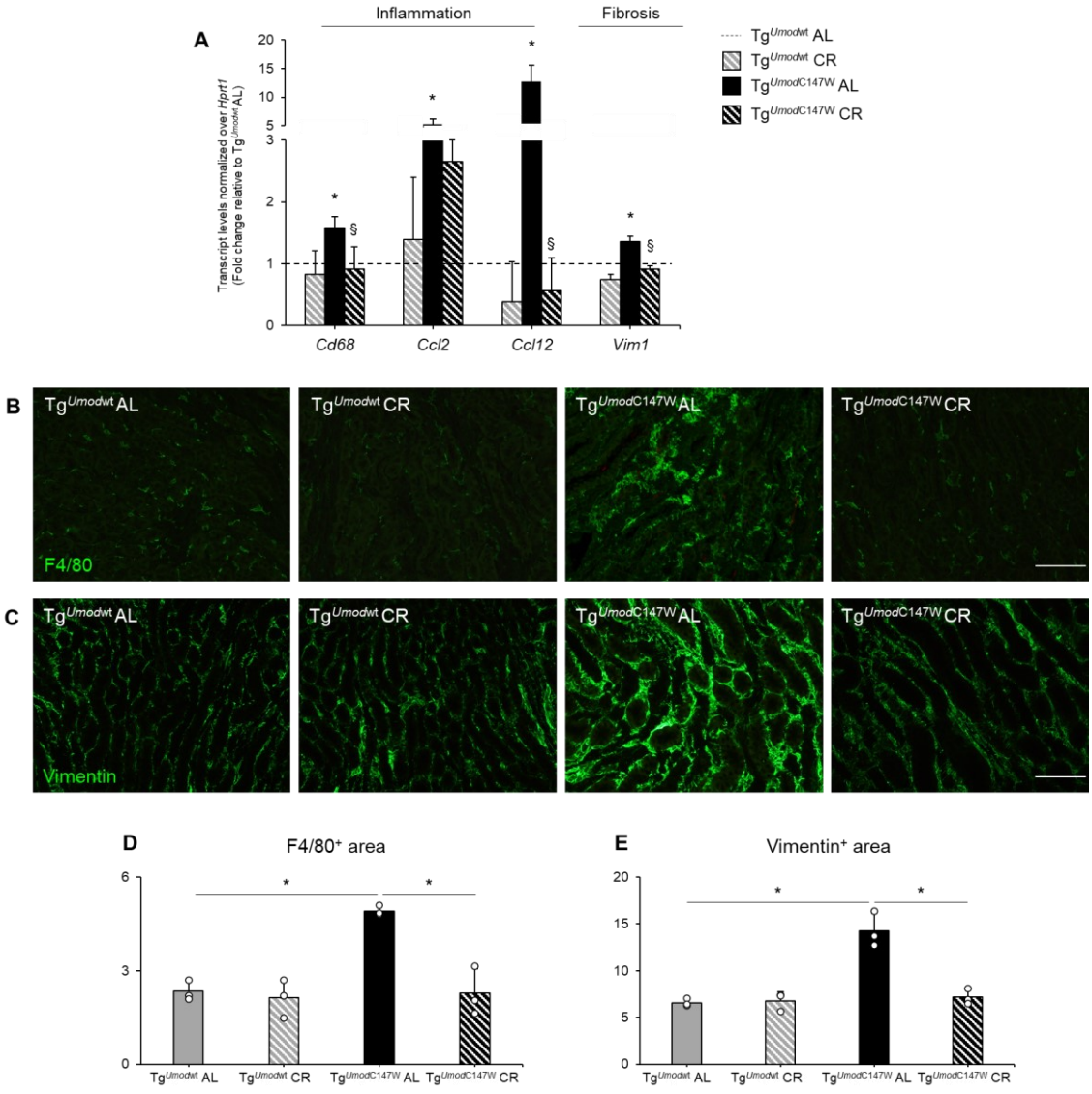


Figure 30. Effect of calorie restriction on inflammation and fibrosis. *A) Analysis by real-time RT-qPCR of the expression of a macrophage marker (Cd68), pro-inflammatory chemokines (Ccl2, Ccl12) and fibrosis marker (Vim1). Data are reported as fold change compared to* Tg^{Umodwt} *AL (dashed line). *P<0.05 compared to* Tg^{Umodwt} *AL;* $^{§}P<0.05$ *compared to* $Tg^{UmodC147W}$ *AL (unpaired t-test). Representative immunofluorescence staining for B) macrophages (F4/80) and C) vimentin in kidneys from* Tg^{Umodwt} *AL,* Tg^{Umodwt} *CR,* $Tg^{UmodC147W}$ *AL and* $Tg^{UmodC147W}$ *CR (Bar=100 µm). The histograms summarize the quantification of D)* $F4/80^{+}$ *area and E)* $Vimentin^{+}$ *area. *P<0.05 (unpaired t-test). C) N=3 animals/group. Data are expressed as mean ± s.d.*

All together these results demonstrate that CR strongly reduces inflammation in kidneys of $Tg^{Umod\text{C147W}}$ mice, likely due to reduced uromodulin retention in the ER. This is reflected by a beneficial effect also on fibrotic phenotype in mutant mice, likely secondary

to reduction of inflammation, corroborating previous observation that in our model inflammation induction precedes fibrosis (Trudu *et al*, 2017).

3.3.3 Effect of calorie restriction on tubular damage

Next, we tested if a decrease in mutant uromodulin retention could attenuate tubular damage, assessing Lcn2 levels in kidneys. Western blot showed increased protein levels in kidneys of Tg$^{Umod\text{C147W}}$ AL, compared to Tg$^{Umod\text{wt}}$. Surprisingly, Lcn2 appeared further increased in both Tg$^{Umod\text{wt}}$ CR and Tg$^{Umod\text{C147W}}$ CR mice compared to their AL counterparts, with levels in Tg$^{Umod\text{C147W}}$ CR mice that are higher compared to Tg$^{Umod\text{wt}}$ CR (**Figure 31A, B**).

Interestingly, immunofluorescence analysis revealed that Lcn2 signal in cells expressing uromodulin is dramatically reduced along with mutant protein aggregates in Tg$^{Umod\text{C147W}}$ CR mice (**Figure 31C**). Instead, the increase observed at total kidney level is due to increased expression of Lcn2 in uromodulin-negative tubules. Further immunofluorescence analysis demonstrated that tubules up-regulating Lcn2 in kidneys of both CR Tg$^{Umod\text{wt}}$ and Tg$^{Umod\text{C147W}}$ animals are proximal tubules, as they are positive for Aquaporin-1 (Aqp1), the principal water-transporting protein enriched in plasma membranes of cells lining this nephron segment (Agarwal *et al*, 2021) (**Figure 31D**).

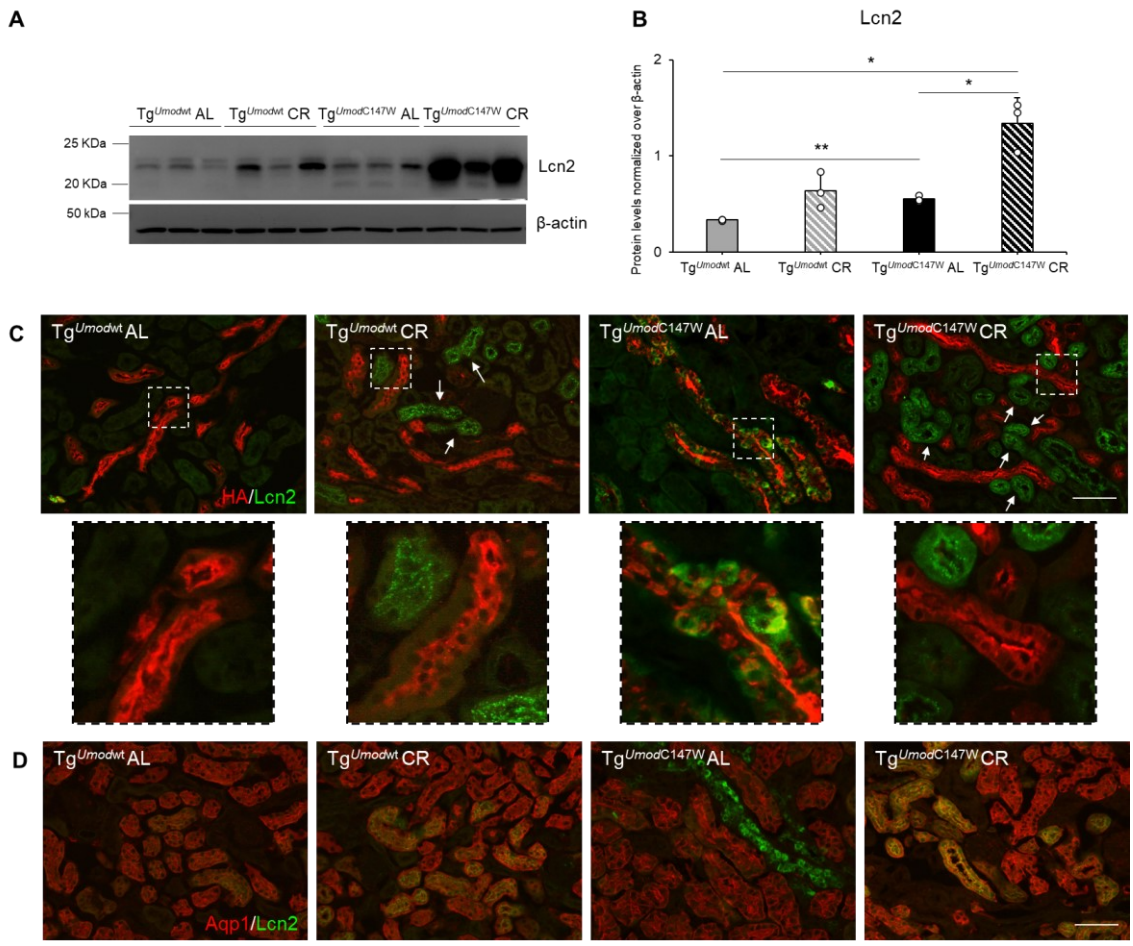


Figure 31. Effect of calorie restriction on tubular damage. *A) Western blot analysis showing increased expression of Lcn2 in kidneys of CR Tg^{Umodwt} and $Tg^{UmodC147W}$ mice, compared to their AL counterparts. B) Histograms represent quantification of Lcn2 protein level normalized over β-actin. C) Immunofluorescence staining showing that Lcn2 (in green) expression is increased in Umod-negative tubules both in Tg^{Umodwt} and $Tg^{UmodC147W}$ mice upon CR, while it is strongly reduced in tubules expressing mutant uromodulin (HA, in red) in $Tg^{UmodC147W}$ mice compared to AL. D) Immunofluorescence analysis showing increased Lcn2 (in green) signal in Aquaporin-1 (Aqp1, in red) positive tubules in CR Tg^{Umodwt} and $Tg^{UmodC147W}$ animals, compared to their AL counterpart. Bar=100 µm. N=3 animals/group. Data are expressed as mean ± s.d. *P<0.05; **P<0.01 (unpaired t-test).*

These results strongly suggest that reducing mutant uromodulin ER retention and aggregation rescues TAL cell damage in $Tg^{UmodC147W}$mice. However, up-regulation of Lcn2 in other tubular segments might indicate induction of metabolic stress in other cellular types within the kidney, likely due to severe caloric restriction.

3.3.4 Effect of calorie restriction on autophagy

To gain insight into the molecular mechanisms induced by calorie restriction and leading to mutant uromodulin aggregate reduction, we analyzed markers of autophagy in kidneys of calorie restricted mice. Studies on different animal models for protein conformational disorders revealed a beneficial role of autophagy up-regulation in slowing down disease progression (Fleming *et al*, 2011; Hidvegi *et al*, 2010) and intriguingly, among a plethora of different inducing effects, calorie restriction was demonstrated to activate autophagy (Chung & Chung, 2019).

Lc3 (or Map1lc3b, Microtubule-associated proteins 1A/1B light chain 3B) is a cytoplasmatic ubiquitin-like protein and a mammalian homologue of yeast Atg8. Lc3-II (active form) is considered a standard marker for autophagosomes and represents the lipidated version of Lc3-I (inactive form). It is generated through conjugation of phospatidylethanolamine (PE) residue to cytosolic Lc3-I on the surface of nascent autophagosomes. The two Lc3 forms can be identified by Western blot. The PE-conjugated form (Lc3-II), although larger in mass, due to its increased hydrophobicity, shows faster electrophoretic mobility in SDS-PAGE gels, consisting of a band of approximately 14-16 kDa. The unconjugated form (Lc3-I) runs approximately around 16-18 kDa (Klionsky *et al*, 2021).

Western blot analysis of the Lc3-II/Lc3-I ratio in kidneys of Tg$^{Umod\text{wt}}$ and Tg$^{Umod\text{C147W}}$ mice revealed no significant difference between AL and CR experimental groups and between different genotypes (**Figure 32A, B**). Instead, the effect of CR on autophagy induction appears clear in liver lysates of the same animals, as we observed increased levels of Lc3-II/Lc3-I ratio in CR Tg$^{Umod\text{wt}}$ and Tg$^{Umod\text{C147W}}$ mice compared to their AL counterparts (**Figure 32C, D**).

These results are in line with previously reported data suggesting decreased response to starvation in kidneys compared with liver (Yamamoto *et al*, 2015; Chung *et al*, 2020).

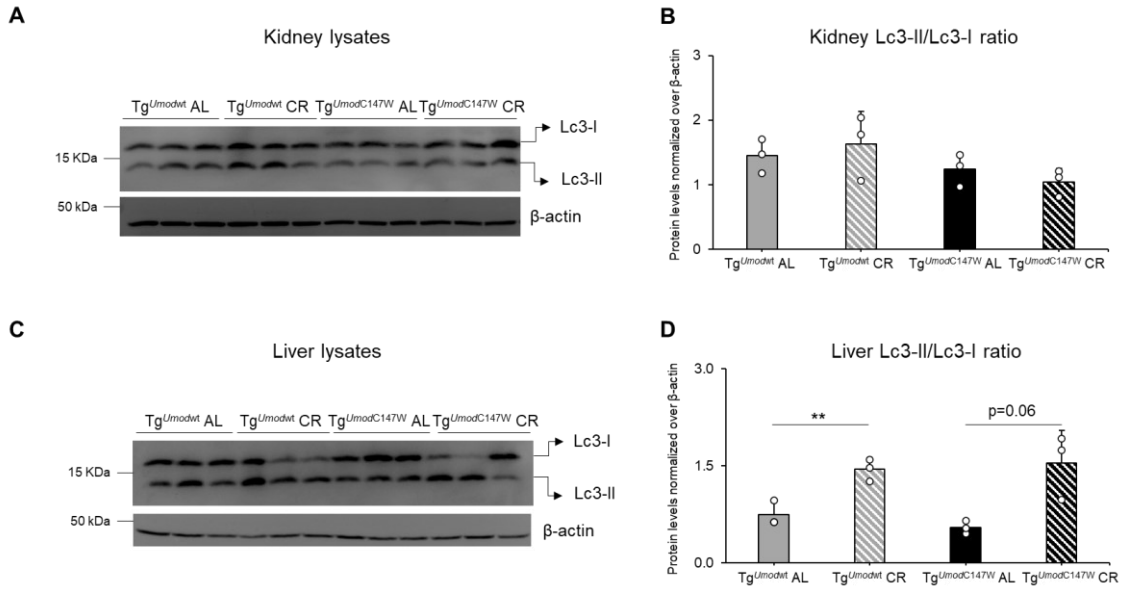


Figure 32. Lc3 ratio in kidneys and liver of Tg^{Umodwt} and Tg^{UmodC147W} AL and CR mice. *Western blot for autophagosome marker Lc3b, in A) kidneys and C) liver lysates from both AL and CR Tg^{Umodwt} and Tg^{UmodC147} animals. Both the active (Lc3-II, ~14kDa) and the inactive (Lc3-I, ~16kDa) forms are detected. The histograms summarize the quantification of active to inactive Lc3 form in B) kidneys and D) livers in all experimental groups. N=3 animals/group. Data are expressed as mean ± s.d. **P<0.01 (unpaired t-test).*

Next, we studied p62 (also called sequestosome-1 or Sqstm1), another key mediator of autophagy. Western blot analysis revealed comparable kidney expression in Tg$^{Umod\text{wt}}$ and Tg$^{Umod\text{C147W}}$ mice both at baseline and after CR (**Figure 33A, B**). However, by analyzing the detergent-insoluble fraction of kidney lysates, we observed that p62 was significantly increased in Tg$^{Umod\text{C147W}}$ mice fed AL, compared to Tg$^{Umod\text{wt}}$ AL ones. Interestingly, increased p62 was reduced to levels comparable to Tg$^{Umod\text{wt}}$ mice by CR (**Figure 33C, D**). Importantly, *Sqstm1* (encoding for p62) transcript levels remain comparable between the experimental groups, suggesting that changes in p62 abundance measured in Tg$^{Umod\text{C147W}}$ mice occur specifically at protein level (**Figure 33E**).

Immunofluorescence staining for p62 on kidney sections confirmed the accumulation of p62 (possibly insoluble) punctae in cells expressing mutant uromodulin, compared to cells expressing the wild type protein, at baseline (**Figure 33F**). p62 is a ubiquitin-binding protein that plays a role as an autophagy scaffold receptor and it takes part in

autophagosome formation (Katsuragi *et al*, 2015). The protein is itself an autophagy-specific substrate and can be used as a reporter of autophagic status of the cells, since its level decreases when autophagy is induced and accumulates when autophagy is blocked (Bjørkøy *et al*, 2009). The presence of p62 punctae in cells expressing mutant uromodulin can thus be regarded as evidence of reduced/impaired autophagy in these cells, a feature already described in another ADTKD-*UMOD* mouse model (Johnson *et al*, 2017).

Interestingly, upon CR, we observed a strong decrease of p62 aggregates in TAL cells of $Tg^{Umod\text{C147W}}$ mice (**Figure 33F**).

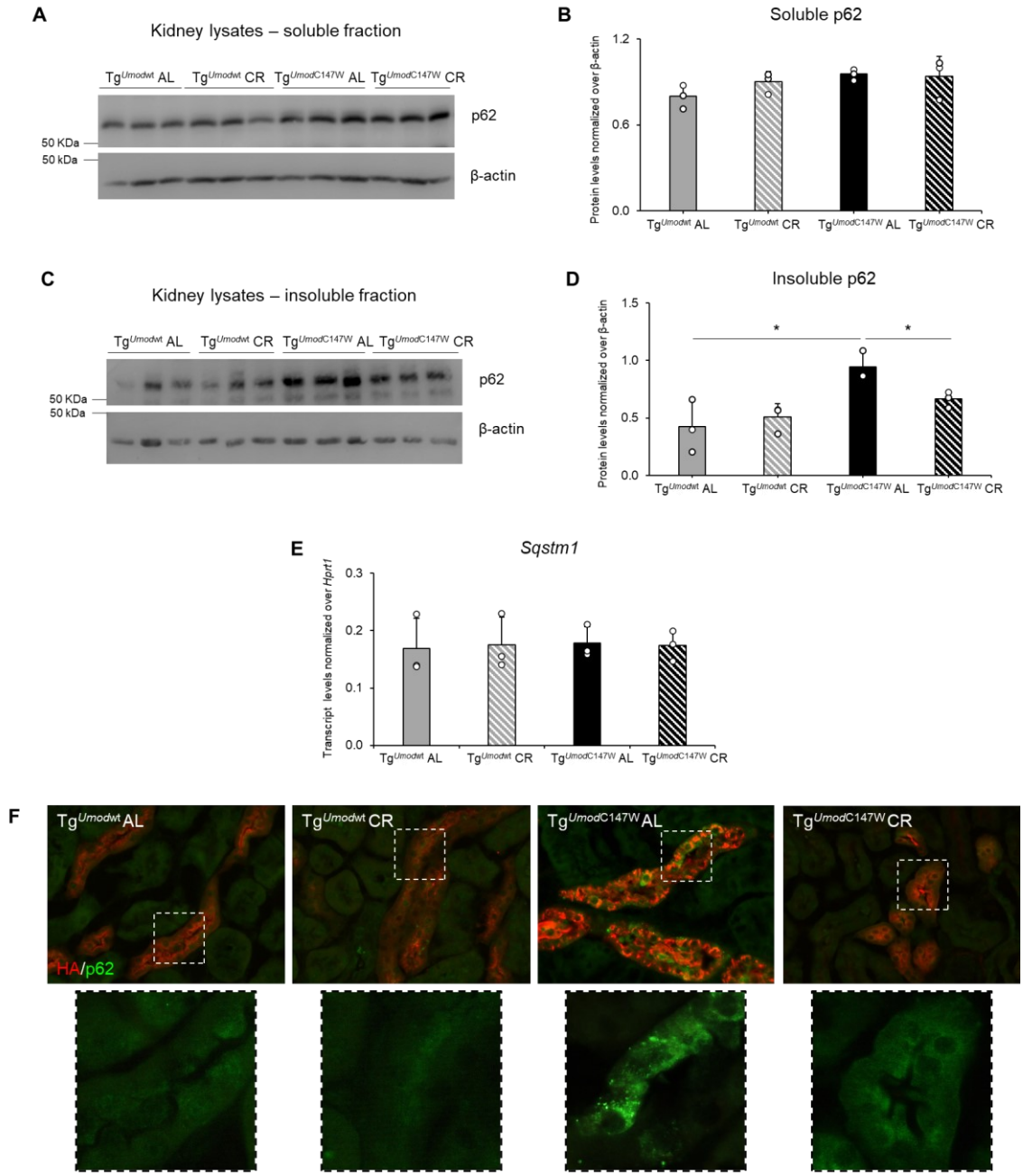


Figure 33. p62 levels in kidneys of Tg^{Umodwt} and Tg^{UmodC147W} mice. *Western blot of p62 in A) soluble and C) insoluble fraction of kidney lysates. Quantification of B) soluble and D) insoluble p62 levels in kidneys of AL or CR Tg^{Umodwt} and Tg^{UmodC147W} animals. E) Analysis by real-time RT-qPCR of Sqstm1 (encoding p62) transcript levels. N=3 animals/group. Data are expressed as mean ± s.d. *P<0.05 (unpaired t-test). F) Immunofluorescence analysis staining for p62 (in green) and transgenic uromodulin (HA, in red) on kidney sections from Tg^{Umodwt} AL, Tg^{Umodwt} CR, Tg^{UmodC147W}AL and Tg^{UmodC147W}CR animals. Bar = 100 µm.*

This suggests an effect of CR in increasing autophagic flux and likely in rescuing the autophagic impairment in cells expressing mutant uromodulin.

3.3.6 Effect of calorie restriction on kidney physiology

Finally, we assessed kidney function by measuring blood urea nitrogen (BUN) in plasma samples collected at the end of the CR protocol. Urea nitrogen is a waste product of protein metabolism in the liver, that is filtered and removed from bloodstream by the kidney. For this reason, its level in the blood is a readout of kidney function.

As compared to Tg$^{Umod\text{wt}}$ AL, Tg$^{Umod\text{C147W}}$ AL mice show a slight but significant increase of plasma urea, that nevertheless is still within the range of normal values (**Figure 34**). This confirms that at this young age (8 weeks) mutant mice are in an early phase of the disease, showing clear signs of inflammation and fibrosis and preserved kidney function (Trudu *et al*, 2017).

While Tg$^{Umod\text{wt}}$ CR mice did not show any significant difference compared to Tg$^{Umod\text{wt}}$ AL mice, BUN levels were increased in Tg$^{Umod\text{C147W}}$ CR, compared to both AL and CR Tg$^{Umod\text{wt}}$ mice (**Figure 34**).

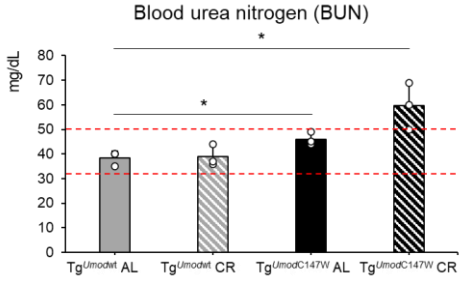


Figure 34. Effect of calorie restriction on blood urea nitrogen levels. *Blood urea nitrogen (BUN) was measured on samples collected from Tg^{Umodwt} AL, Tg^{Umodwt} CR, Tg^{UmodC147W} AL and Tg^{UmodC147W} CR mice at the end of the diet protocol. Red dashed lines indicate the range of reference BUN normal levels. N=3 animals/group. Data are expressed as mean ± s.d. *P<0.05 (unpaired t-test).*

This data, together with the increased level of the marker of kidney damage Lcn2, suggest a detrimental effect of this protocol of extreme CR on kidney function in Tg$^{Umod\text{C147W}}$ mice.

3.4 Testing the efficiency of a milder and prolonged calorie restriction protocol on Tg^{UmodC147W} mice

Based on the interesting results obtained in the proof-of-concept study, we tested the effectiveness of a milder (30%) and prolonged (15 weeks) protocol of calorie restriction (herein referred to as CR-30) in improving ADTKD-*UMOD* disease phenotype, with the aim to test a CR protocol with more translational potential. For this experiment, we used adult pre-symptomatic animals, starting from 8 weeks of age (**Figure 35A**).

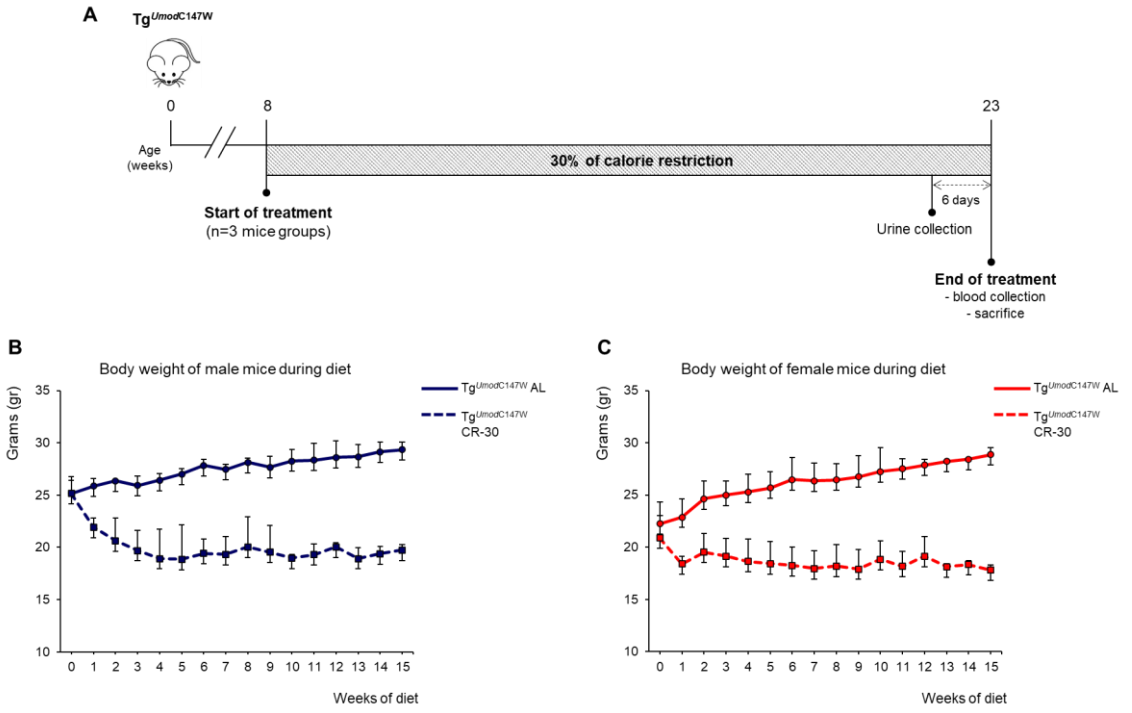


Figure 35. Schematic protocol of milder, prolonged calorie restriction experiment and mice body weight during the diet. *A) Starting from 8 weeks of age Tg^{UmodC147W} mice were fed ad libitum or with a 30% calorie restriction regimen for 15 weeks. Body weight of B) male and C) female Tg^{UmodC147W} mice during the diet. Data are expressed as mean ± s.d. N=3 mice/group.*

To obtain the proper degree of dietary restriction, mice in the CR-30 group were provided once a day with 70% of food amount consumed by sex- and age-matched Tg^{UmodC147W} mice fed *ad libitum*. Both male and female Tg^{UmodC147W} mice were used.

Body weight was evaluated once per week for all the experimental groups (male mice **Figure 35B** and female mice **Figure 35C**). Six days before sacrifice, we performed urine collection through the use of metabolic cages. Mice were sacrificed for phenotyping after 15 weeks of controlled diet when they reached 23 weeks of age, a time point at which Tg$^{Umod\text{C147W}}$ mice show fully-blown disease (Bernascone *et al*, 2010).

3.4.1 Influence of sex on disease severity in Tg^{UmodC147W} mice

During the characterization of the effect of CR-30, we noticed differences in uromodulin expression and processing between male and female mice.

Both Tg$^{Umod\text{wt}}$ and Tg$^{Umod\text{C147W}}$ female mice show higher uromodulin expression levels, as compared to age- and genotype-matched males. Importantly uromodulin expression is comparable in between age- and sex-matched Tg$^{Umod\text{wt}}$ and Tg$^{Umod\text{C147W}}$ mice (**Figure 36**).

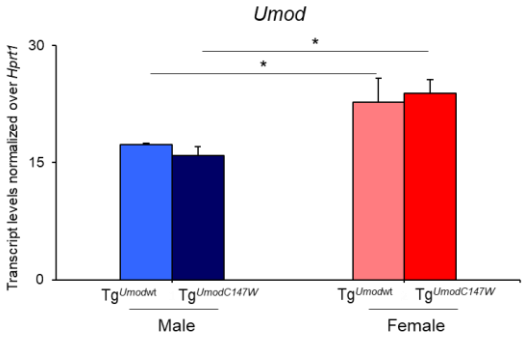


Figure 36. Uromodulin expression in male and female mice. *A) Analysis by Real-time RT-qPCR of Umod expression levels in kidneys from male and female Tg^{Umodwt} and Tg^{UmodC147W} mice showing higher uromodulin expression in female mice of both genotypes. No differences are observed in between sex-matched Tg^{Umodwt} and Tg^{UmodC147W}. N=3 animals/group.*

Both male and female Tg$^{Umod\text{C147W}}$ mice show expected mutant uromodulin ER retention, as demonstrated by co-localization of the transgenic protein with the ER marker calreticulin (**Figure 37A**). We enzymatically digested kidney lysates with Endo H, a recombinant endoglycosidase which cleaves N-linked mannose oligosaccharides from glycoproteins. As shown in **Figure 37B** and already described above, uromodulin

Western blot on Endo H digested samples revealed two bands: the lower band (75 kDa) is Endo H sensitive and corresponds to the ER precursor carrying high-mannose moiety; the upper band (110 kDa) is Endo H insensitive and corresponds to the fully glycosylated mature uromodulin (Bernascone *et al*, 2010). Despite different level of expression, the extent of ER retention is comparable in male and female $Tg^{UmodC147W}$ mice, as demonstrated by similar ER precursor/mature uromodulin ratio in kidneys of both groups (**Figure 37B, C**). Nevertheless, the amount of ER retained uromodulin is remarkably increased in female mice, as also reflected by Western blot analysis in non-reducing conditions showing increased mutant uromodulin aggregates (**Figure 37D**).

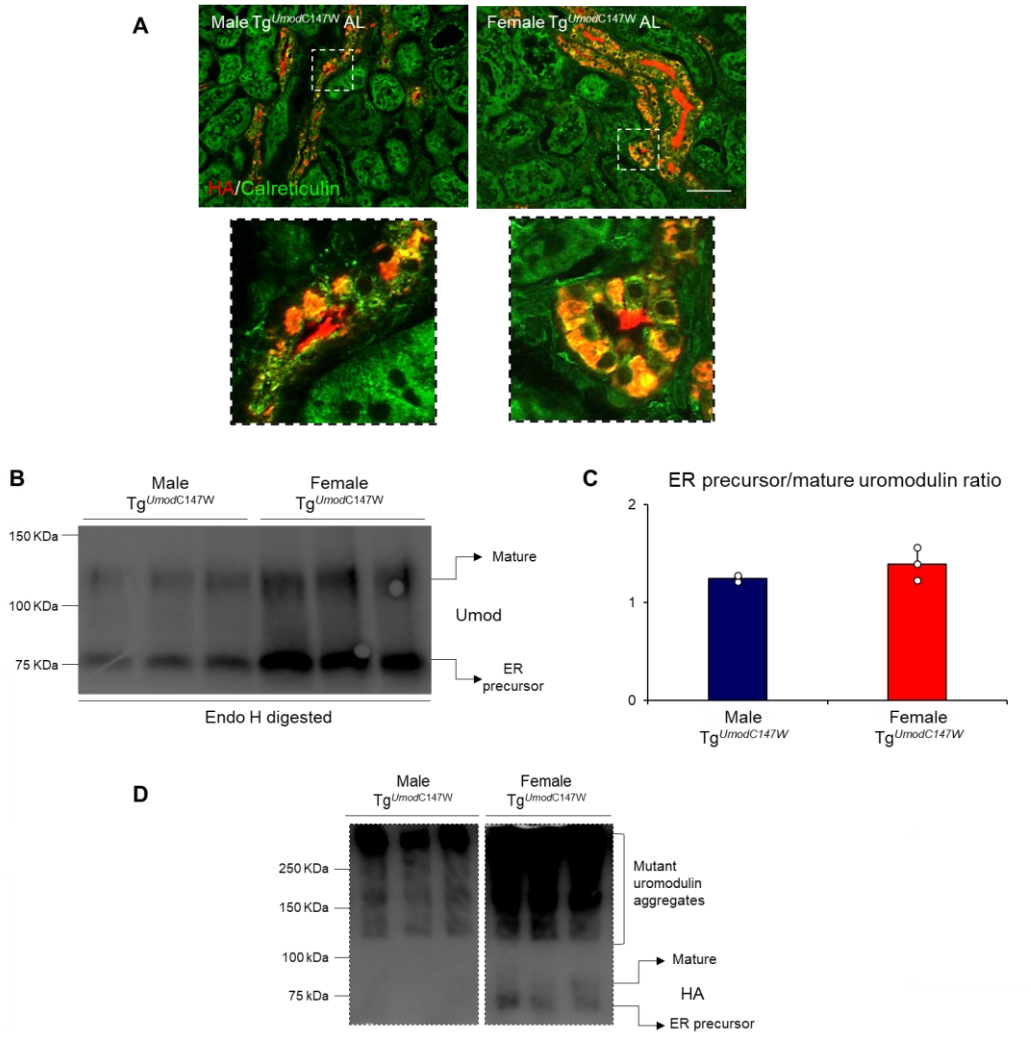


Figure 37. Mutant uromodulin ER retention and aggregation in male and female $Tg^{UmodC147W}$ mice. *A) Dual staining for uromodulin (HA, in red) and the ER marker calreticulin (in green) in kidneys from male and female $Tg^{UmodC147W}$ mice. Bar = 100 µm. B) Western blot analysis in*

*reducing conditions of uromodulin in kidneys from male and female $Tg^{UmodC147W}$ mice. Samples were incubated with Endo H, an enzyme that cleaves high-mannose, ER-type N-glycans from glycoproteins. After digestion, uromodulin detection shows a high molecular weight band (120 kDa), corresponding to fully glycosylated, Endo H-insensitive uromodulin, and a lower band (90 kDa), corresponding to the ER precursor. C) Quantification of the ratio ER precursor/mature uromodulin form in male and female $Tg^{UmodC147W}$ mice. D) Western blot in non-reducing condition using anti-HA antibody to detect. High molecular weight aggregates in male and age-matched female $Tg^{UmodC147W}$ mice. Images are cropped part of the same membrane. Data are expressed as mean ± s.d. *P<0.05 (unpaired t-test). N=3 animals/group.*

This difference in the level of mutant uromodulin expression and ER accumulation and aggregation is reflected by different severity of disease phenotype between female and male $Tg^{UmodC147W}$ mice. As compared to their wild type counterpart, both male and female mutant mice showed induction of genes related to inflammation (*Cd45*, *Cd68*, *Ccl2*, *Ccl12*), fibrosis (*Vim1*) and tubular damage (*Lcn2*). However, induction levels of all these parameters appeared significantly higher in females than in males (**Figure 38**).

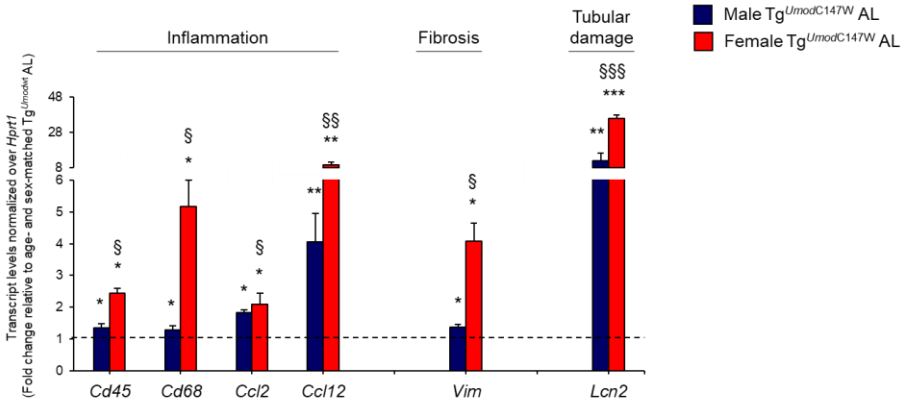


Figure 38. Inflammation, fibrosis and tubular damage in male and female $Tg^{UmodC147W}$ mice. *Analysis by real-time RT-qPCR of the expression levels of genes related to inflammation (Cd45, Cd68, Ccl2, Ccl12), fibrosis (Vim1) and tubular damage (Lcn2) in kidneys of $Tg^{UmodC147W}$ male and female animals. Histograms represent fold changes compared to sex- and age-matched Tg^{Umodwt} (dashed line). Data are expressed as mean ± s.d. *P<0.05, **P<0.01, ***P<0.005 vs. sex- and age-matched Tg^{Umodwt}; §P<0.05, §§P<0.01, §§§P<0.005 $Tg^{UmodC147W}$ males vs females (unpaired t-test). N=3 animals/group.*

These observations strongly suggest that, in our model, ADTKD-*UMOD* phenotype is more severe in females compared to male mice. This is likely due to higher levels of

uromodulin expression leading to increased accumulation and aggregation of mutant uromodulin in kidneys of female mutant animals.

For this reason, results obtained from the characterization of female and mae mice will be presented in two separate sections (*Paragraph 3.4.2* and *Appendix I* respectively).

3.4.2 Effects of CR-30 on ADTKD-UMOD phenotype in female Tg^{UmodC147W} mice

As previously described, the experiment of milder and prolonged calorie restriction was performed on Tg$^{Umod\text{C147W}}$ mice, starting from the age of 8 weeks and for 15 weeks. The initial time point corresponds to an age when mice are in an early phase of disease, displaying features of kidney inflammation and fibrosis (Trudu *et al*, 2017) but preserving kidney function, that in our model, show a decline around 24 weeks of age (Bernascone *et al*, 2010) corresponding to the final time point used in this experiment.

To assess the effect of CR-30 on disease progression and to test its possible role on disease regression, the characterization was performed comparing 23-week-old female Tg$^{Umod\text{wt}}$, Tg$^{Umod\text{C147W}}$ AL and Tg$^{Umod\text{C147W}}$ CR-30, both between them and with Tg$^{Umod\text{wt}}$ and Tg$^{Umod\text{C147W}}$ mice of 8 weeks of age, corresponding to the starting time point of the dietary protocol.

3.4.2.1 Effect of CR-30 on uromodulin biology

After 15 weeks of controlled diet, to characterize the effect of CR-30 on uromodulin biology in female mice, we measured uromodulin transcript and protein levels in the kidney.

As compared to Tg$^{Umod\text{wt}}$ mice, 23-week-old female Tg$^{Umod\text{C147W}}$ mice showed increased kidney levels of uromodulin that were massively reduced upon calorie restriction (**Figure 39A, B**). Importantly, this occurs when *Umod* transcript levels is increased in kidneys of CR mutant mice, compared to both Tg$^{Umod\text{wt}}$ and Tg$^{Umod\text{C147W}}$ AL mice, suggesting that the effect observed at protein level is not due to an effect of CR on gene expression (**Figure 39C**).

Consistent with impaired protein maturation and accumulation in kidney cells, Tg^{UmodC147W} mice showed striking reduction of urinary uromodulin level compared to wild type mice. Of note, reduction of uromodulin level in the kidney was not reflected by increased uromodulin excretion in Tg^{UmodC147W} CR-30 mice, suggesting that the decrease kidney levels are not due to increased secretion (**Figure 39D, E**).

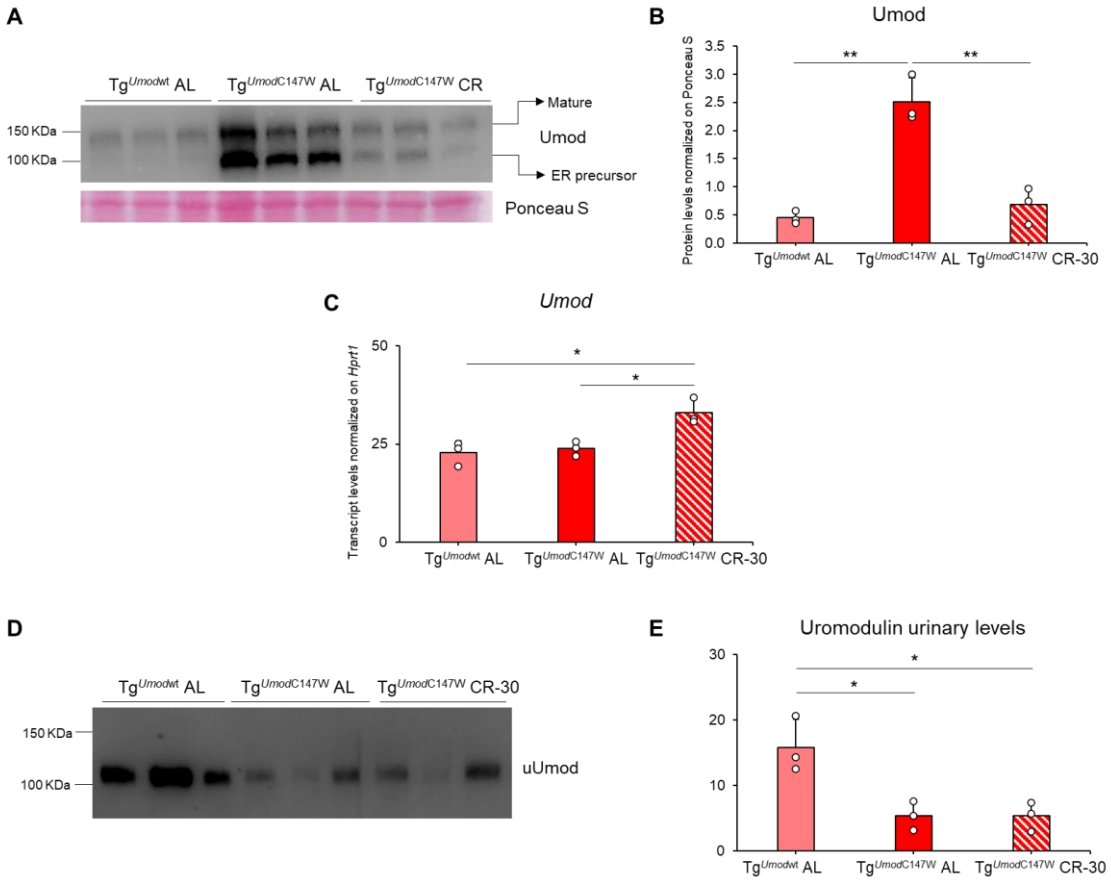


Figure 39. Effect of CR-30 on uromodulin protein and transcript levels in female Tg^{UmodC147W} mice. *A) Analysis of total uromodulin protein levels in whole kidney homogenates of 23-week-old female Tg^{Umodwt} AL, Tg^{UmodC147W} AL and Tg^{UmodC147W} CR-30 mice. Ponceau S is reported as a loading control. B) Quantification of total uromodulin protein levels. C) Umod expression analysis by real-time RT-qPCR in Tg^{Umodwt} AL, Tg^{UmodC147W} AL and Tg^{UmodC147W} CR. D) The same fraction of total urine volume collected from 23-week-old female Tg^{Umodwt} AL, Tg^{UmodC147W} AL and Tg^{UmodC147W} CR-30 mice was loaded on SDS-PAGE to perform Western blot analysis and E) quantification of uromodulin levels in urine (uUmod). Data are expressed as mean ± s.d. *P<0.05, **P<0.01 (unpaired t-test). N=3 animals/group.*

Next, we evaluated the effect of calorie restriction on mutant uromodulin processing by quantifying the ratio of uromodulin ER precursor/mature form after enzymatic digestion

of Tg$^{Umod\text{wt}}$, Tg$^{Umod\text{C147W}}$ AL and Tg$^{Umod\text{C147W}}$ CR-30 kidney lysates with Endo H. Retention of mutant uromodulin in the ER is significantly reduced after 15 weeks of dietary restriction (**Figure 40A, B**) as further confirmed by immunofluorescence, showing dramatic reduction of colocalization of transgenic protein with the ER chaperone calnexin in kidneys of Tg$^{Umod\text{C147W}}$ CR-30 mice, compared to Tg$^{Umod\text{C147W}}$ AL ones (**Figure 40C**).

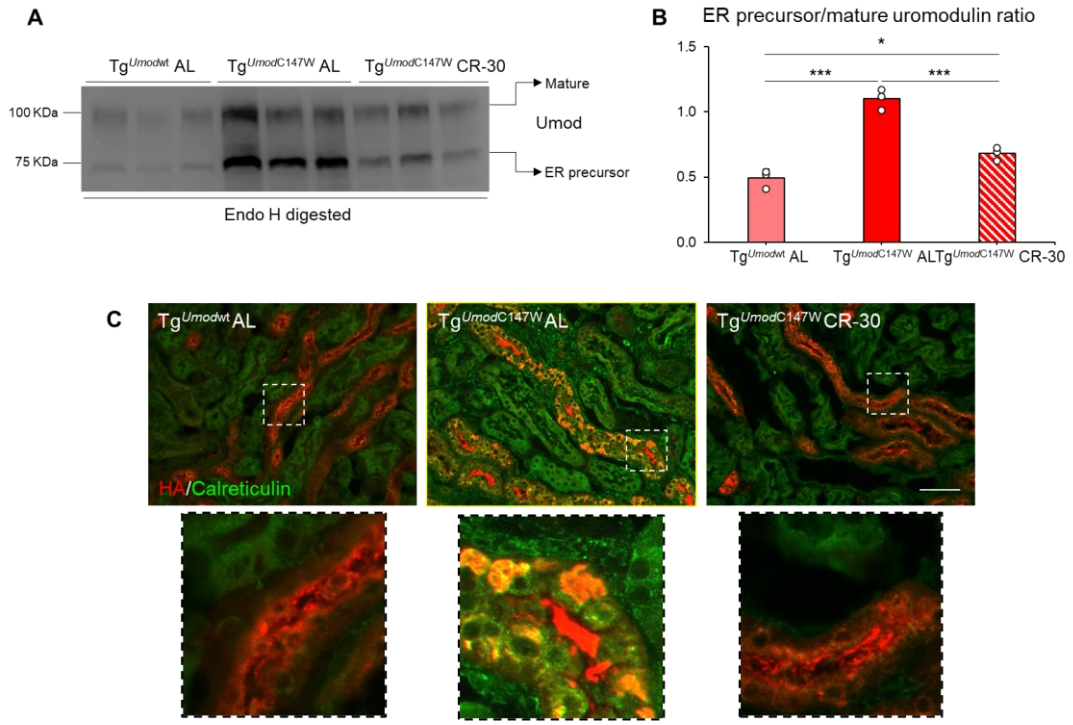


Figure 40. Effect of CR-30 on mutant uromodulin ER retention in female Tg^{UmodC147W} mice. *A) Western blot in reducing conditions, of Endo H digested kidney lysates from Tg^{Umodwt}, Tg^{UmodC147W} AL and Tg^{UmodC147W} CR-30 mice. B) Quantification of the ER precursor/mature uromodulin ratio. Data are expressed as mean ± s.d. *P<0.05, ***P<0.05 (unpaired t-test). N=3 animals/group. C) Immunofluorescence for transgenic uromodulin (HA, in red) and the molecular chaperone calreticulin, used as a marker of the ER (in green) on kidney sections of Tg^{Umodwt} AL, Tg^{UmodC147W} AL and Tg^{UmodC147W} CR-30 mice. Bar = 100 µm.*

Reduction in protein ER retention correlates with a strong decrease of mutant uromodulin aggregation, as demonstrated by non-reducing Western blot showing strongly reduced high molecular weight uromodulin aggregates in kidneys of Tg$^{Umod\text{C147W}}$ CR-30 mice as compared to their age-matched mutant *ad libitum* counterpart (**Figure 41A**). Immunofluorescence staining with anti-HA antibody is consistent with the biochemical results, showing a clear reduction of intracellular aggregates in mutant mice upon CR-30.

Of note, this reduction is also evident when comparing Tg$^{Umod\text{C147W}}$ CR-30 mice with 8-week-old Tg$^{Umod\text{C147W}}$, corresponding to the starting point of the dietary protocol, when intracellular aggregates are already evident in kidneys of mutant mice as compared to age-matched Tg$^{Umod\text{wt}}$ (**Figure 41B**). This is also confirmed by non-reducing Western blot, showing an increase of mutant uromodulin aggregates in kidneys of 23-week-old Tg$^{Umod\text{C147W}}$ AL compared to their 8-week-old counterpart, indicative of disease progression. In Tg$^{Umod\text{C147W}}$ CR-30 mice mutant uromodulin aggregation is reduced to levels that are even lower than the ones observed at the start of the CR-30 protocol (8 weeks of age) (**Figure 41C**).

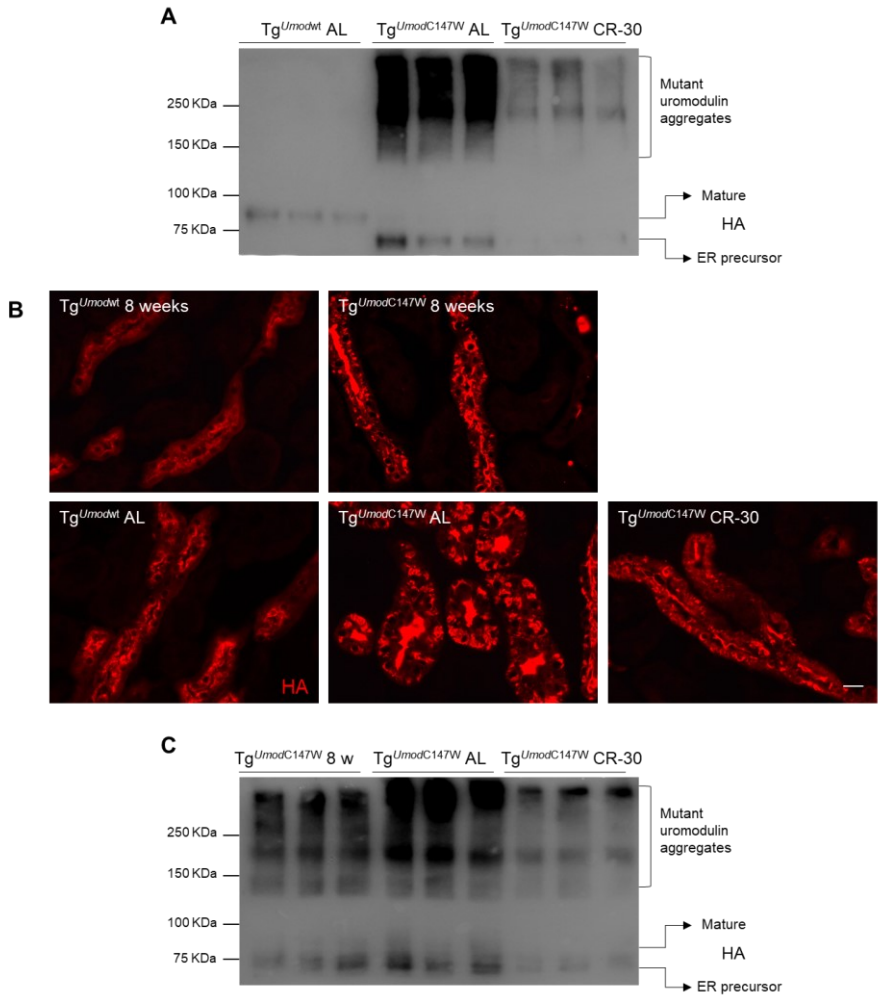


Figure 41. Effect of CR-30 on mutant uromodulin aggregation in female Tg^{UmodC147W} mice. *A) Western blot analysis in non-reducing conditions on whole kidney lysates from 23-week-old Tg^{Umodwt}, Tg^{UmodC147W} AL and Tg^{UmodC147W} CR-30 mice. B) Immunofluorescence analysis staining for transgenic protein (HA, in red) in kidneys of 8-weeks-old Tg^{Umodwt} AL and Tg^{UmodC147W} AL and*

23-week-old Tg^{Umodwt}, $Tg^{UmodC147W}$ AL and $Tg^{UmodC147W}$ CR-30. Bar=100 µm. C) Non-reducing Western blot on kidney samples from 8-week-old $Tg^{UmodC147W}$ and 23-week-old $Tg^{UmodC147W}$ AL and $Tg^{UmodC147W}$ CR-30. N=3 animals/group.

Overall, these results strongly point at calorie restriction as a strategy that is effective in preventing progression of mutant uromodulin accumulation, and in clearing protein aggregates that are already present at the start of treatment.

3.4.2.2 Effect of CR-30 on kidney inflammation

We already demonstrated that inflammation is an early event occurring in kidneys of $Tg^{Umod\text{C147W}}$ mice that progressively increases with age, contributing to kidney damage (Bernascone *et al*, 2010; Trudu *et al*, 2017). To assess the effect of CR-30 on the inflammatory phenotype, we evaluated expression levels of several genes related to inflammation.

No significant changes in the expression levels of inflammatory cells or chemokine genes were observed in 23-week-old $Tg^{Umod\text{wt}}$ compared to 8-week-old $Tg^{Umod\text{wt}}$. On the contrary, all tested parameters increased in 23-week-old $Tg^{Umod\text{C147W}}$ AL compared to 8-week-old $Tg^{Umod\text{C147W}}$, confirming disease progression (**Figure 42A**).

Compared to age-matched *ad libitum* counterpart, $Tg^{Umod\text{C147W}}$ CR-30 mice showed reduced expression of inflammatory cell marker and chemokine genes that returned to the levels observed for $Tg^{Umod\text{wt}}$ and that in some cases (as for *Cd68* and *Ccl12*) were significantly lower than in 8-week-old $Tg^{Umod\text{C147W}}$ mice (**Figure 42A**).

To evaluate macrophage infiltration, we quantified kidney $F4/80^{+}$ area through immunofluorescence analysis. $F4/80^{+}$ area increased in kidneys of mutant mice with age, consistent with gene expression analysis. Interestingly, upon calorie restriction, levels of macrophage infiltration in kidneys of 23-week-old $Tg^{Umod\text{C147W}}$ mice were comparable to what measured in wild type animals and appeared significantly decreased compared to 8-week-old $Tg^{Umod\text{C147W}}$ mice (**Figure 42B, C**).

Finally, we performed histology analysis of kidneys of $Tg^{Umod\text{C147W}}$ mice at 23 weeks of age through H&E staining. We further confirmed improvement of tubulointerstitial

damage in kidney of calorie restricted mutant mice, as demonstrated by strong reduction of area of inflammatory cell infiltrate, decreased tubular dilation and reduction of intratubular casts (**Figure 42D**).

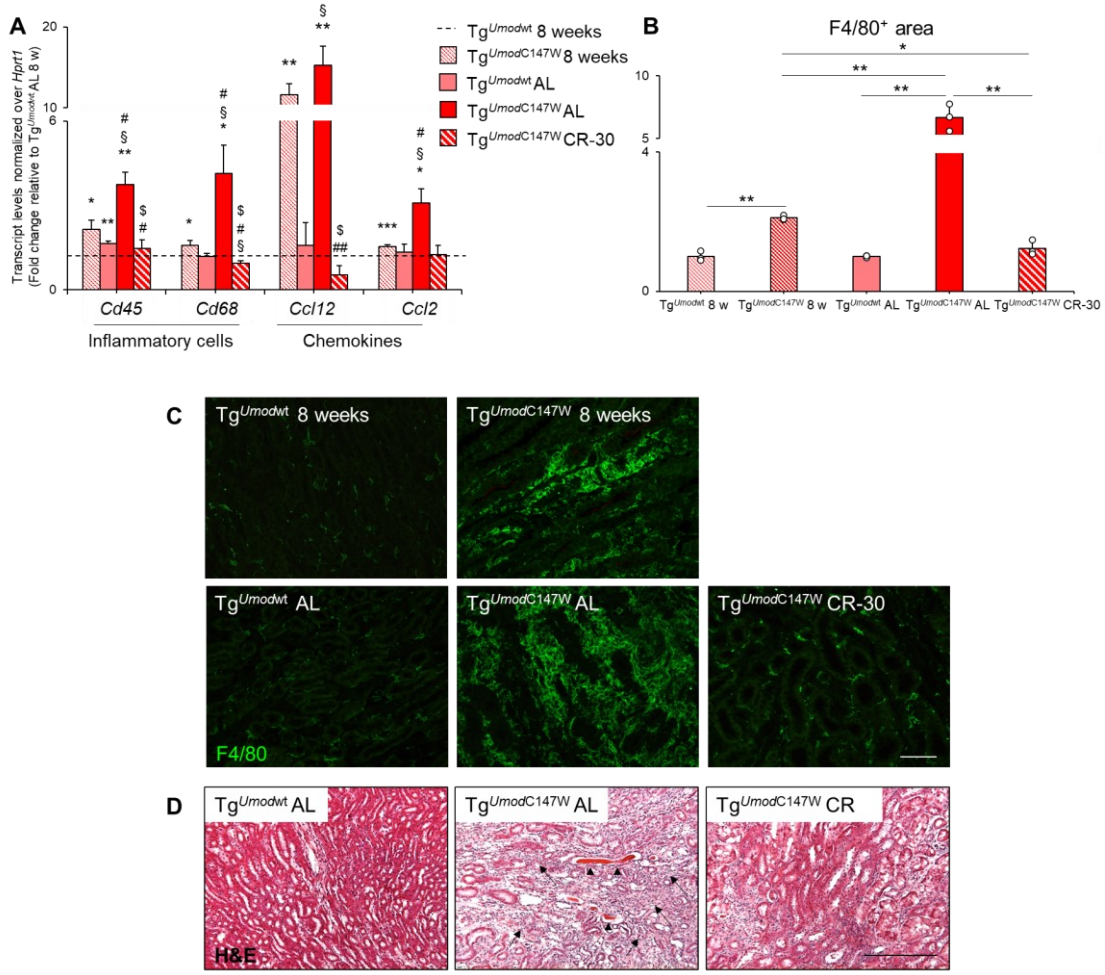


Figure 42. Effect of CR-30 on kidney inflammation in female Tg^{UmodC147W} mice. *A) Cd45, Cd68, Ccl12 and Ccl2 expression levels in kidneys of 8-week-old Tg^{Umodwt} and Tg^{UmodC147W} mice and 23-week-old Tg^{Umodwt}, Tg^{UmodC147W} AL and Tg^{UmodC147W} CR-30 female mice. Data are expressed as mean ± s.d. and presented as fold change relative to 8-week-old Tg^{Umodwt} (dashed line) *P<0.05; **P<0.01; ***P<0.005 vs Tg^{Umodwt} 8w; §P<0.05 vs. Tg^{Umodwt} AL; $^{#}$P<0.05 vs. Tg^{UmodC147W} 8w; $^{$}$P<0.05 Tg^{UmodC147W} AL vs. Tg^{UmodC147W} CR-30 (unpaired t-test). B) Quantification of F4/80^{+} area. Data are expressed as mean ± s.d. *P<0.05; **P<0.01 (unpaired t-test). N=3 animals/group. C) Representative immunofluorescence staining for F4/80 in kidneys of 8-week-old Tg^{Umodwt} and Tg^{UmodC147W} mice and 23-week-old Tg^{Umodwt}, Tg^{UmodC147W} AL and Tg^{UmodC147W} CR-30 female mice. D) Representative histology images of H&E-stained kidney sections of 23-week-old Tg^{Umodwt}, Tg^{UmodC147W} AL and Tg^{UmodC147W} CR-30. Black arrows indicate areas of increased cell infiltration and black arrowheads indicate intraluminal casts in Tg^{UmodC147W} AL mice. Bar = 100 µm.*

All together these data demonstrate that calorie restriction is effective not only in preventing progression of inflammation, but also in ameliorating the already established inflammatory phenotype in kidneys of Tg$^{Umod\text{C147W}}$ mice.

3.4.2.3 Effect of CR-30 on kidney fibrosis

We then assessed if reduction of inflammation has an impact on tubulointerstitial fibrosis, one of the key phenotypes of ADTKD-*UMOD* that is recapitulated in our mouse model. We characterized the effect of CR-30 on kidney fibrosis in Tg$^{Umod\text{C147W}}$ female mice by analyzing vimentin transcript and protein expression levels.

As already described in our previous work (Trudu *et al*, 2017) kidney fibrosis is already established in Tg$^{Umod\text{C147W}}$ at 8 weeks of age and it progresses with time, as demonstrated by further significant increase of *Vim1* expression (**Figure 43A**) and vimentin deposition (**Figure 43B**, **C**) in kidneys of Tg$^{Umod\text{C147W}}$ mice at 23 weeks of age compared to younger mutant mice.

Vimentin expression and deposition in the kidney were significantly reduced in Tg$^{Umod\text{C147W}}$ CR-30 mice compared to age-matched mutant mice fed *ad libitum* (**Figure 43A-C**). Of note, *Vim1* expression and vimentin deposition are significantly reduced in Tg$^{Umod\text{C147W}}$ CR-30 kidneys compared to 8 weeks-old Tg$^{Umod\text{C147W}}$ mice and comparable to what observed in Tg$^{Umod\text{wt}}$ mice (**Figure 43**).

We also performed histological analysis, by staining kidney sections with Picrosirius Red. This is a specific staining for extracellular matrix, allowing to visualize collagen I and collagen III. As it can be observed in the representative images reported in **Figure 43D**, compared to Tg$^{Umod\text{wt}}$ mice, kidneys of 23-week-old Tg$^{Umod\text{C147W}}$ AL mice have areas of increased signal corresponding to local collagen deposition, that are strongly reduced in Tg$^{Umod\text{C147W}}$ CR-30 kidneys.

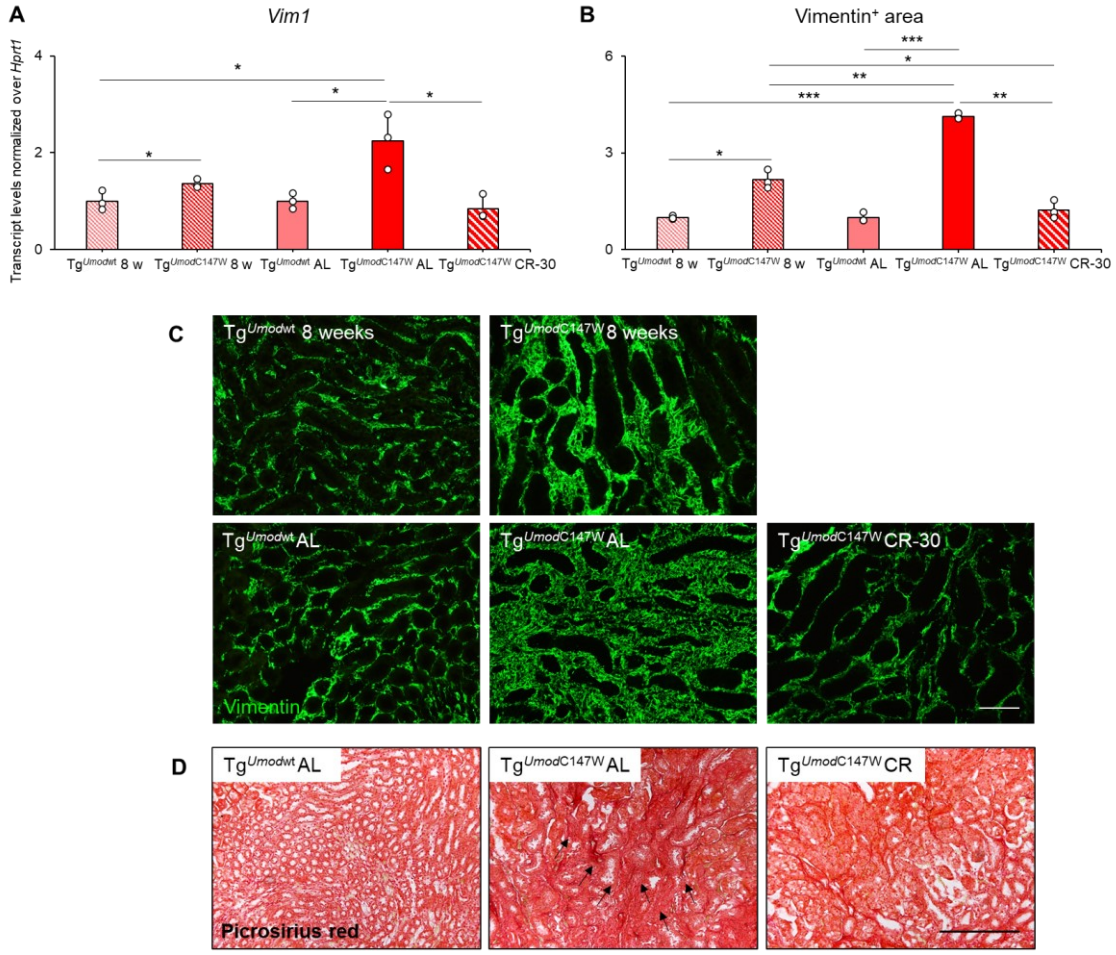


Figure 43. Effect of CR-30 on kidney fibrosis in female Tg^{UmodC147W} mice. *A) Gene expression levels of Vim1, encoding for vimentin, in kidneys of 8-week-old Tg^{Umodwt} and Tg^{UmodC147W} and 23-week-old Tg^{Umodwt} AL, Tg^{UmodC147W} AL and Tg^{UmodC147W} CR-30 mice. B) Quantification of Vimentin^{+} area in kidneys. Data are expressed as mean ± s.d. *P<0.05; **P<0.01; ***P<0.005 (unpaired t-test). N=3 animals/group. C) Representative images of immunofluorescence staining for Vimentin in kidneys of 8-week-old Tg^{Umodwt} and Tg^{UmodC147W} and 23-week-old Tg^{Umodwt} AL, Tg^{UmodC147W} AL and Tg^{UmodC147W} CR-30 mice. D) Representative kidney histological analysis staining collagens with Picrosirius red in 23-week-old Tg^{Umodwt} AL, Tg^{UmodC147W} AL and Tg^{UmodC147W} CR-30 mice. Black arrows indicate areas of increased collagens deposition in Tg^{UmodC147W} AL mice. Bar = 100 µm.*

These results show a significant effect of the CR-30 protocol in reducing kidney fibrosis in Tg$^{Umod\text{C147W}}$ mice. Since fibrosis is likely downstream of the inflammatory process (Trudu *et al*, 2017) these data suggest that resolving inflammation could prevent disease progression and rescue fibrotic phenotype in kidneys of Tg$^{Umod\text{C147W}}$ animals.

3.4.2.4 Effect of CR-30 on tubular damage

Tubular damage is an early event occurring in Tg$^{Umod\text{C147W}}$ mice, as we reported lipocalin-2 induction already at 1 week of age in mutant mice. Its expression remains at high levels in adult mice, and it represents one of the most up-regulated genes identified by kidney transcriptional profiling (Trudu *et al*, 2017).

To investigate the effect of calorie restriction on tubular damage in female Tg$^{Umod\text{C147W}}$ mice, we hence examined Lcn2 levels in TAL cells by immunofluorescence analysis and measured Lcn2 levels in kidneys and urines.

Immunofluorescence analysis revealed that Lcn2 signal is dramatically reduced in TAL cells of Tg$^{Umod\text{C147W}}$ CR-30 female mice, corroborating previous data obtained in the proof-of-concept experiment, and confirming that the reduction of mutant protein ER retention rescues TAL cell stress (**Figure 44A**).

Interestingly, and in contrast with what obtained with the 55% CR protocol, Western blot analysis revealed a significant reduction of Lcn2 also in total kidney (**Figure 44B, C**) and in urine (**Figure 44D, E**) of female Tg$^{Umod\text{C147W}}$ CR-30 mice, compared their *ad libitum* counterpart.

Lcn2 reduction is also confirmed by gene expression analysis. Indeed, real-time RT-qPCR shows strong down-regulation of *Lcn2* in kidneys of Tg$^{Umod\text{C147W}}$ CR-30 mice compared to Tg$^{Umod\text{C147W}}$ AL. Moreover, although *Lcn2* expression did not diminish to the levels measured in Tg$^{Umod\text{wt}}$ mice, it was comparable to 8-week-old Tg$^{Umod\text{C147W}}$ mice (**Figure 44F**).

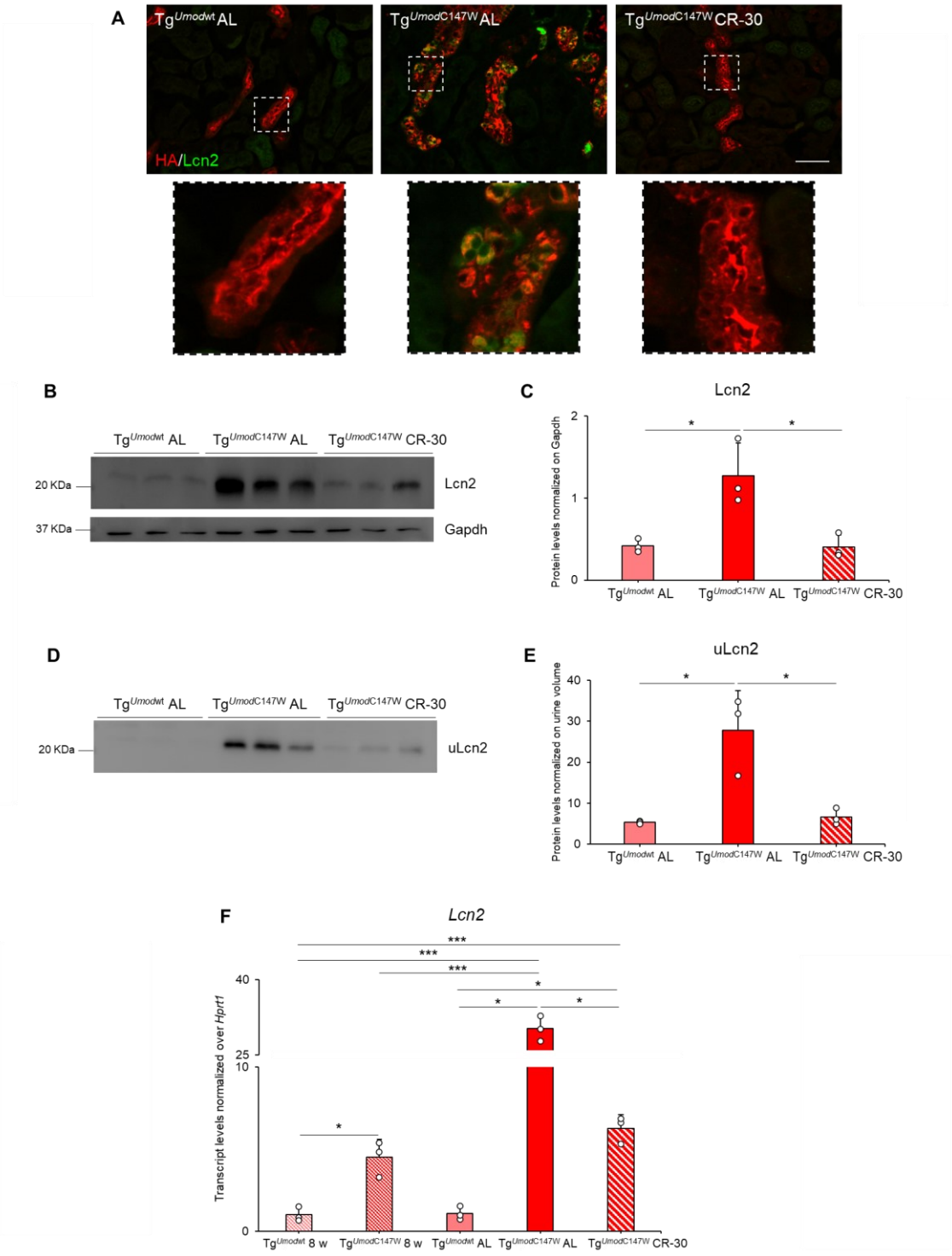


Figure 44. Effect of CR-30 on tubular damage in female Tg^{UmodC147W} mice. *A) Immunofluorescence staining for transgenic uromodulin (HA, in red) and lipocalin-2 (Lcn2, in green) in kidney sections from 23-week-old female Tg^{Umodwt} AL, Tg^{Umod147W} AL and Tg^{UmodC147W} CR-30 mice. Bar = 100 µm. Western blot analysis of Lipocalin-2 in B) kidney and D) urine sample (uLcn2) from 23-week-old female Tg^{Umodwt} AL, Tg^{Umod147W} AL and Tg^{UmodC147W} CR-30 mice. Histograms summarize quantification of C) total kidney (normalized over Gapdh) and E) urinary Lcn2 levels. F) Real-time RT-qPCR analysis of kidney Lcn2 expression in 8-week-old Tg^{Umodwt} AL*

*and $Tg^{Umod147W}$ AL and 23-week-old female Tg^{Umodwt} AL, $Tg^{Umod147W}$ AL and $Tg^{UmodC147W}$ CR-30 female animals. Data are expressed as mean ± s.d. *P<0.05; ***P<0.05 (unpaired t-test).*

All together these results suggest that by decreasing mutant uromodulin accumulation, calorie restriction rescues TAL cell damage in female $Tg^{UmodC147W}$ mice. Importantly, Lcn2 reduction at total kidney level suggests that the CR-30 protocol does not induce overall cellular stress, as observed in the proof-of-concept study with 55% CR.

3.4.2.5 Effect of CR-30 on lipid metabolism

We previously reported that while inflammation and fibrosis are among the most up-regulated pathways in kidneys of 8-week-old $Tg^{UmodC147W}$ mice, down-regulated ones are mostly related to lipid metabolism (Trudu *et al*, 2017). Interestingly, defective fatty acid oxidation in kidney tubular epithelial cells has been associated with progression of kidney damage both in humans and in different models of tubulointerstitial fibrosis (Kang et al, 2015).

To assess if calorie restriction could have an impact also on this disease feature, we measured the expression levels of three representative lipid metabolism genes: *Acox3*, encoding for the peroxisomal protein Acyl-Coenzyme A oxidase 3; *Cyp4b1*, encoding for a member of the Cytochrome P450 family enzymes and *Ehhadh*, encoding for enoyl-CoA hydratase and 3-Hydroxyacyl CoA dehydrogenase, an enzyme involved in the peroxisomal beta-oxidation pathway (**Figure 45**).

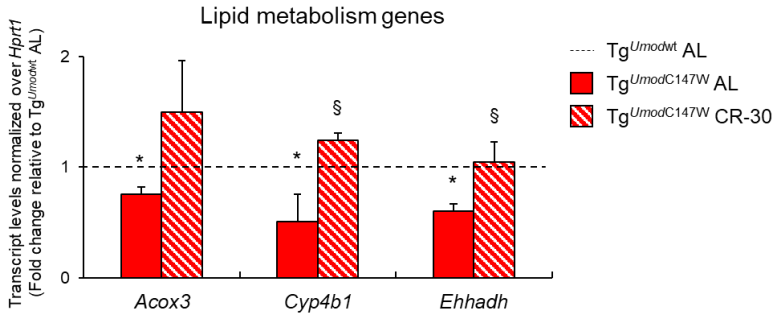


Figure 45. Effect of CR-30 on lipid metabolism in female $Tg^{UmodC147W}$ mice. *Analysis by real-time RT-qPCR of gene related to lipid metabolism (Acox3, Cyp4b1 and Ehhadh) in kidneys of 23-week-old $Tg^{UmodC147W}$ AL and $Tg^{UmodC147W}$ CR-30 compared to age- and sex-matched Tg^{Umodwt}.*

*Histograms represent fold change relative to Tg^{Umodwt} (dashed line). Data are expressed as mean ± s.d. *P<0.05 vs. Tg^{Umodwt}; §P<0.05 vs. Tg^{UmodC147W} AL (unpaired t-test).*

This analysis confirmed that, even at a later time point (23-weeks) all these genes are significantly down-regulated in kidneys of *ad libitum* mutant mice compared to Tg^{Umod}wt ones and revealed that their expression was increased to wild type levels in Tg^{Umod}C147W CR-30 mice, suggesting that calorie restriction is also effective in rescuing lipid metabolism deregulation observed in mutant mice.

3.4.2.6 Effect of CR-30 on kidney physiology

The effect of calorie restriction on kidney physiology in 23-week-old female mutant mice was assessed by evaluating diuresis and serum urea nitrogen levels.

Tg^{Umod}C147W animals showed increased diuresis levels compared to wild type counterpart, in line with previously reported data describing mild kidney failure and polyuria in mutant mice at this age (Bernascone *et al*, 2010). Interestingly, although not significant, diuresis levels showed a trend towards reduction in Tg^{Umod}C147W mice upon 15 weeks of 30% CR *(***Figure 46A**).

Tg^{Umod}C147W mice showed a slight but significant increase of BUN levels already at 8 weeks, although still within normal range. While Tg^{Umod}wt mice maintain stable BUN levels, mutant mice showed an increase at 23-week of age, demonstrating a decline in kidney function as disease progresses. Of note, as compared to age-matched mutant mice fed *ad libitum*, Tg^{Umod}C147W CR-30 mice showed lower BUN values that remain similar to what measured in mutant mice at 8 weeks (**Figure 46B**).

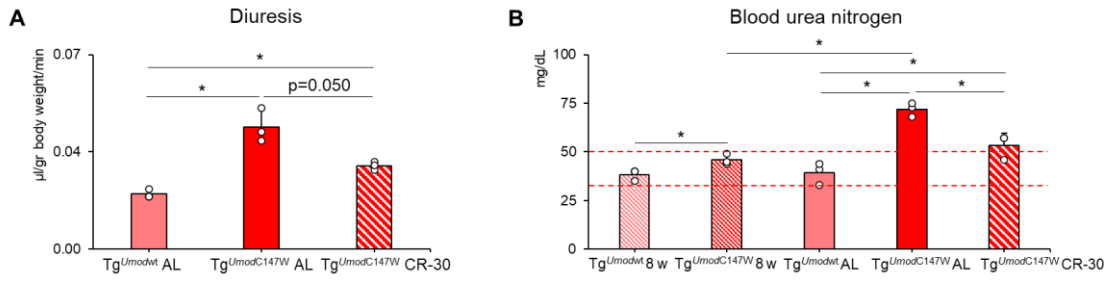


Figure 46. Effect of CR-30 on kidney physiology of female $Tg^{UmodC147W}$ mice. *A) Diuresis of 23-week-old female Tg^{Umodwt}, $Tg^{UmodC147W}$ and $Tg^{UmodC147W}$ CR-30 mice. B) Urea nitrogen levels in blood samples collected from 8-week-old Tg^{Umodwt} AL, $Tg^{UmodC147W}$ AL and 23-week-old Tg^{Umodwt} AL, $Tg^{UmodC147W}$ AL and $Tg^{UmodC147W}$ CR-30 mice. Red dashed lines indicate range of reference levels of BUN (35-50 mg/dL). N=3 animals/group. Data are expressed as mean ± s.d. *P<0.05 (unpaired t-test).*

These results suggest that calorie restriction, by blocking disease progression and ameliorating kidney damage can prevent decline of kidney function in $Tg^{Umod\text{C147W}}$ mice.

3.4.2.7 Molecular mechanisms induced by CR-30

To characterize the molecular mechanisms induced by calorie restriction and causing the reduction of mutant uromodulin aggregates, we evaluated marker of autophagy in kidneys of $Tg^{Umod\text{C147W}}$ CR-30 mice.

At 23 weeks of age, *ad libitum* $Tg^{Umod\text{C147W}}$ mice clearly display signatures of defective autophagy in kidneys, as demonstrated by increased ratio between Lc3b-II (active form) and Lc3b-I (inactive form) compared to $Tg^{Umod\text{wt}}$ mice (**Figure 47A, B**). Noteworthy, upon calorie restriction Lc3-II/Lc3-I ratio is reduced in total kidney of mutant mice compared to their *ad libitum* counterpart.

Moreover, immunofluorescence staining showed massive accumulation of p62 punctae in TAL cells in female mutant mice at 23-weeks (**Figure 47C**). At this age, increased levels of p62 were also detectable at total kidney level in $Tg^{Umod\text{C147W}}$ mice, as demonstrated by Western blot analysis (**Figure 47D, E**). Importantly, this increase occurred when expression of *Sqstm1*, encoding for p62, showed similar levels (**Figure 47F**), suggesting reduction in its degradation rate, rather than increased synthesis. Total kidney levels of p62 are significantly reduced in female 23-week-old $Tg^{Umod\text{C147W}}$ mice upon calorie restriction, and p62 aggregates remained evident only in few cells expressing mutant uromodulin, recapitulating the effect already observed with strong dietary restriction protocol (**Figure 33F**).

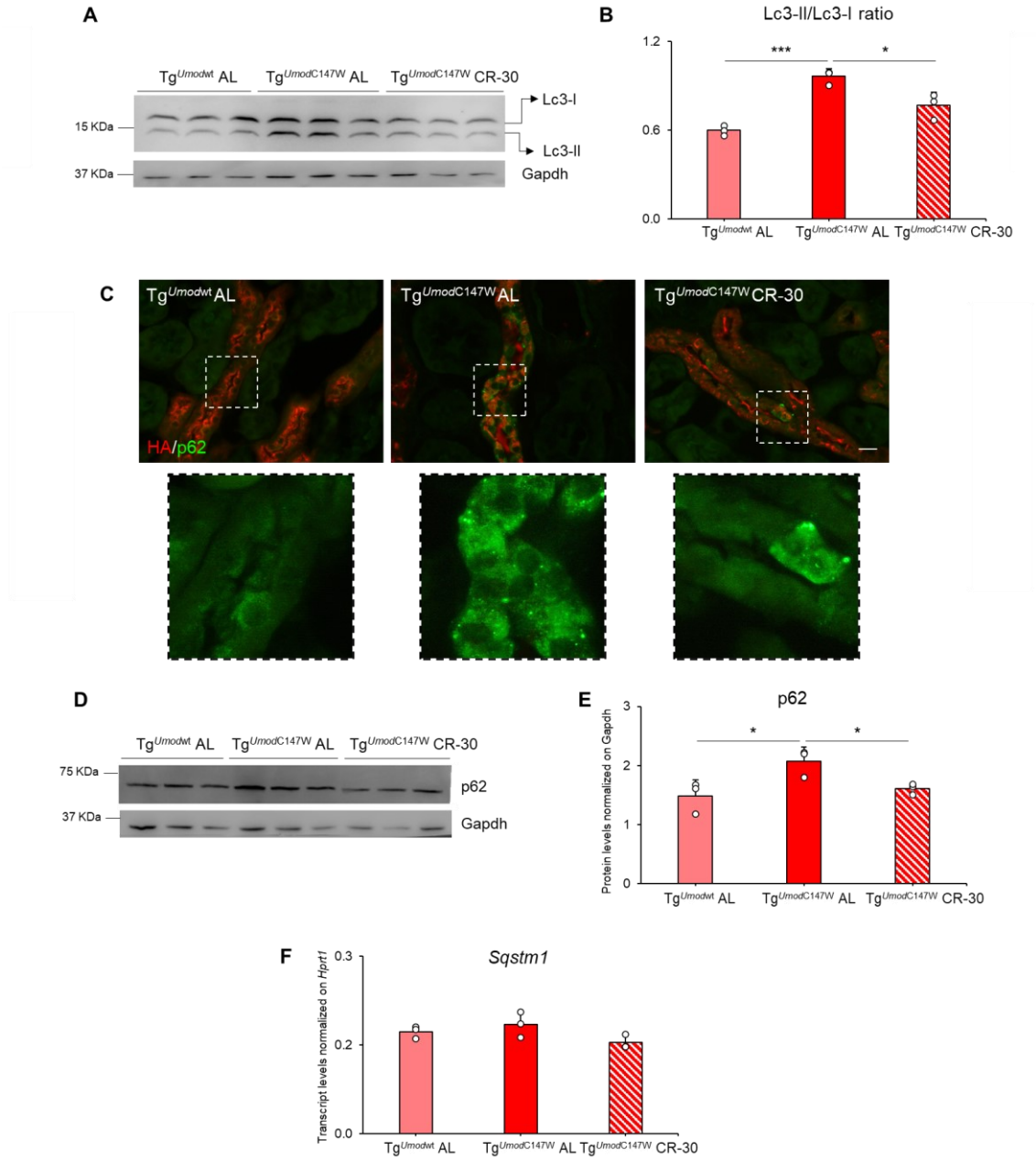


Figure 47. Effect of CR-30 on autophagy in kidney of female Tg^{UmodC147W} mice. *A) Western blot analysis of Lc3, autophagosome marker, shows increased Lc3-II/Lc3-I ratio in kidneys of Tg^{UmodC147W} AL mice compared to Tg^{Umodwt}, that decreases after 15 weeks under CR. B) Quantification of Lc3-II/Lc3-I ratio. C) Immunofluorescence staining for p62 (in green) and transgenic uromodulin (HA, in red) showing reduction of p62 aggregates in mutant uromodulin expressing cells in kidneys of Tg^{UmodC147W} CR-30 mice. Bar = 100 µm. D) and E) Western blot analysis showing increased p62 levels in kidneys of Tg^{UmodC147W} AL mice. F) Analysis of Sqstm1 (encoding p62) expression by real-time RT-qPCR, showing similar levels in all experimental groups. N=3 animals/group. Data are expressed as mean ± s.d. *P<0.05; ***P<0.005 (unpaired t-test).*

As already mentioned above, accumulation of both Lc3 active form and p62 are hallmarks of autophagy impairment, described in our mice as well as in other ADTKD-*UMOD* mouse models (Johnson *et al*, 2017). Rescue of both features strongly suggests that calorie restriction rescues autophagy in TAL cells, thus allowing degradation of mutant uromodulin aggregates.

Calorie restriction can indeed stimulate autophagy through the canonical pathway, as nutrient depletion can lead to inactivation of mTOR (Ferreira-Marques *et al*, 2021). To assess the potential involvement of mTOR signaling pathway in CR-induced autophagy in our model, we tested by Western blot analysis phosphorylation of its downstream target, ribosomal protein S6 (S6RP). Interestingly, this analysis revealed elevated levels of phospho-S6RP in kidneys of $Tg^{UmodC147W}$ mice that were recovered to wild type levels after calorie restriction (**Figure 48**).

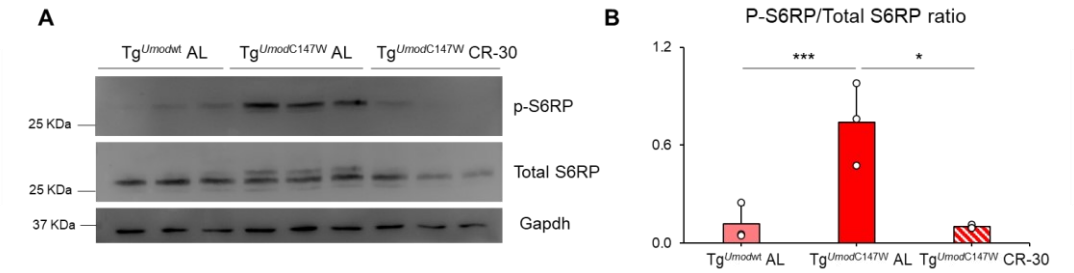


Figure 48. Calorie restriction reduces mTOR activation in $Tg^{UmodC147W}$ mice. *A) Western blot analysis on total kidney lysates from Tg^{Umodwt}, $Tg^{UmodC147W}$ AL and $Tg^{UmodC147W}$ CR-30 mice for phosphorylated and total S6 ribosomal protein (S6RP), downstream target of mTOR. B) Quantification of ratio phosphorylated/total isoforms of S6RP. Data are expressed as mean ± s.d. *P<0.05; ***P<0.005 (unpaired t-test).*

This result suggests that calorie restriction could rescue autophagy impairment by inhibiting mTOR overactivation in mice expressing mutant uromodulin.

Given the reduction of ER-retained mutant uromodulin in TAL cells, we wondered if CR induced ER-phagy as a main degradative pathway. ER-phagy (or reticulophagy) defines a form of autophagy, mediated by selective receptors (or adaptors), that specifically degrades portions of the ER (Reggiori & Molinari, 2022).

By real-time RT-qPCR we tested the expression levels of genes encoding for 8 out of the 11 ER-phagy receptors to date described in mammals (**Figure 49A**) (Mochida & Nakatogawa, 2022).

Retreg2 (encoding for Fam134a), *Retreg3* (encoding for Fam134c), *Rtn3* (encoding for the reticulon family protein Rtn3) and *Atl3* (encoding for Atlastin3) displayed similar levels among the experimental groups. We observed decreased expression levels of *Ccpg1* in Tg$^{Umod\text{C147W}}$ mice compared to Tg$^{Umod\text{wt}}$. Even if a slight increase compared to mutant mice *ad libitum* was observed after calorie restriction, expression was not rescued to the basal levels (**Figure 49A**).

Instead, *Sec62, Tex264* and *Retreg1*, whose expression was down-regulated in Tg$^{Umod\text{C147W}}$ kidneys at baseline, showed restored (or even up-regulated, when compared to Tg$^{Umod\text{wt}}$ mice) levels after calorie restriction (**Figure 49A**).

Importantly, Sec62 was found to mediate autophagic degradation of the ER membranes during the recovery from ER stress, named recov-ER-phagy (Fumagalli et al, 2016). Tex264 was implicated in ER remodeling during nutrient stress (An *et al*, 2019). Fam134b (encoded by *Retreg1*) was the first discovered ER-phagy adaptor in mammals and it is implicated in both constitutive and starvation-enhanced ER-phagy (Khaminets *et al*, 2015). Interestingly, the mTORC1-TFEB/TFE3 axis was reported to be responsible for the transcriptional regulation of Fam134b in response to nutrient starvation (Cinque *et al*, 2020). In the mouse liver, a N-terminal-truncated isoform of Fam134b (Fam134b-2) has been identified and demonstrated to be transcriptionally enhanced by starvation to regulate starvation-induced ER-phagy (Kohno *et al*, 2019). This observation was confirmed also in our model. Indeed, through real-time RT-PCR, using specific primer sets, we tested the expression of both Fam134b isoforms (Kohno *et al*, 2019). Both Fam134b isoforms are down-regulated in kidneys of Tg$^{Umod\text{C147W}}$ mice at basal levels and Fam134b-2, but not Fam134b-1 (encoding the full-length protein), was up-regulated in kidneys of Tg$^{Umod\text{C147W}}$ after calorie restriction (**Figure 49B**).

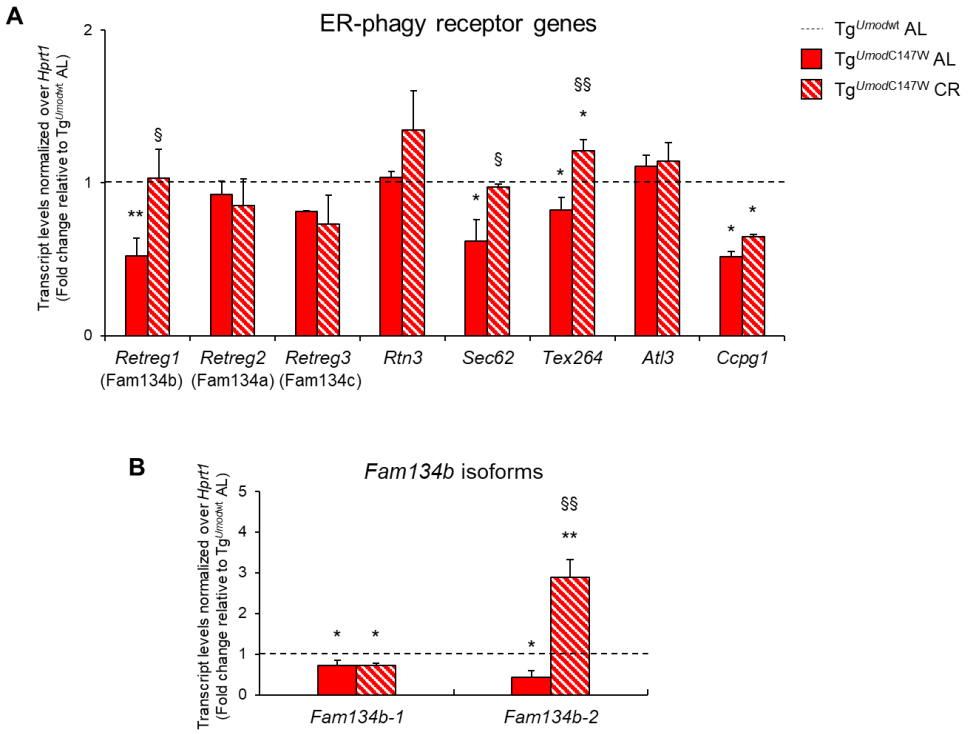


Figure 49. Effect of CR-30 on ER-phagy in female Tg^{UmodC147W} mice. *A) Analysis by real-time RT-qPCR of ER-phagy receptors genes Retreg1 (encoding Fam134b), Retreg2 (Fam134a), Retreg3 (Fam134c), Rtn3, Sec62, Tex264, Atl3, Ccpg1 in kidneys of Tg^{Umodwt}, Tg^{UmodC147W} AL and Tg^{UmodC147W} CR-30 mice. B) Transcript levels of Fam134b-1 and Fam134b-2in kidneys of Tg^{Umodwt}, Tg^{UmodC147W} AL and Tg^{UmodC147W} CR-30 female mice. Histograms represent fold change relative to Tg^{Umodwt} (dashed line). Data are expressed as mean ± s.d. *P<0.05 **P<0.01 versus Tg^{Umodwt}; §P<0.05 §§P<0.01 Tg^{UmodC147W} AL versus Tg^{UmodC147W} CR (unpaired t-test).*

These data suggest a role of calorie restriction in rescuing the expression of key ER-adaptors, thus restoring ER-phagy and allowing degradation of mutant uromodulin ER aggregates in TAL cells of Tg$^{Umod\text{C147W}}$ mice.

Similar results, obtained from the characterization of the effect of CR-30 on male Tg$^{Umod\text{C147W}}$ mice are presented in *Appendix I.*

4. DISCUSSION

ADTKD-*UMOD* is a rare but underdiagnosed inherited cause of CKD, caused by mutation in the *UMOD* gene. Research on ADTKD-*UMOD* has clarified some aspects of its molecular genetics, establishing a main gain-of-function effect of *UMOD* mutations, and proving that their common primary effect is retention of mutant misfolded protein within the ER of expressing cells. However, the downstream molecular mechanisms of pathogenesis are still largely unknown, and no effective therapeutic strategy is currently available.

This work aimed at dissecting the pathogenic events linking mutant uromodulin ER retention to kidney disease and underlying ADTKD-*UMOD* onset and progression.

To this end, we took advantage of a transgenic mouse model expressing mutant p.Cys147Trp uromodulin isoform ($Tg^{UmodC147W}$), previously generated in our laboratory and recapitulating the main features of the human disease (Bernascone *et al,* 2010). Kidney transcriptional profiling of young pre-symptomatic (4 and 8 weeks of age) $Tg^{UmodC147W}$ mice, identified strong activation of pathways related to inflammation and fibrosis, in absence of evident histological and functional alteration (Trudu *et al,* 2017). Further analysis at one week of age demonstrated that inflammation precedes fibrosis, and is coupled with ER retention of mutant uromodulin, tubular damage and induction of cellular stress (Trudu *et al,* 2017). ER retention of mutant uromodulin and cellular stress are already observed at one day *post-natal*. The analysis of kidney expression of a panel of 84 inflammatory genes at this very early time point, well before any functional or histological sign of renal damage, revealed a significant induction of transcripts for key chemokines as *Ccl2*, *Ccl7* and *Ccl12*.

This suggests that these chemokines could play a key role in disease onset as they may represent the early pro-inflammatory signals triggering the inflammation process (our unpublished data, *Paragraph 1.6*).

4.1 C-C chemokine receptor type 2 and chemokines

All the up-regulated chemokines observed at p1 are ligands of the same receptor, C-C chemokine receptor type 2 (Ccr2). We decided to clarify the role of early induction of Ccr2 axis in ADTKD-*UMOD* onset and progression using a genetic approach. We generated a Tg$^{Umod\text{C147W}}$/*Ccr2*$^{-/-}$ mouse line and characterized it at different time points, corresponding to previously characterized stages of the disease in Tg$^{Umod\text{C147W}}$ mice (1 week, 6 weeks, 14 weeks and 24 weeks of age) (Bernascone *et al*, 2010; Trudu *et al*, 2017). At each time point we verified that *Ccr2* ablation did not affect *Umod* expression levels nor the level of mutant uromodulin ER retention and analyzed markers of inflammation, fibrosis, and tubular damage, already known to be up-regulated in the kidneys of Tg$^{Umod\text{C147W}}$ (Trudu *et al,* 2017). The analysis revealed induction of all tested disease parameters in kidneys of transgenic mutant mice compared to age-matched non-transgenic littermates (Ctr/*Ccr2*$^{+/+}$), confirming previous results and excluding any impact of the mixed genetic background on disease onset. However, *Ccr2* ablation did not ameliorate disease onset and/or progression in mice expressing mutant uromodulin.

Numerous evidence has been reported, demonstrating that, irrespective of the initial injury, kidney inflammation plays a key role for in the initiation and progression of kidney fibrosis, suggesting its targeting as a possible therapeutic option (Lv *et al*, 2018). The potential therapeutic relevance of inflammation targeting has been also reported in a murine model of ADTKD-*UMOD* (*Umod*$^{\text{C147W}}$) demonstrating delayed progression of the disease upon treatment with a TNF- α signalling inhibitor (Johnson *et al*, 2017). Several studies on models of kidney damage showed how inflammation is induced by different types of injury to activate, recruit and retain macrophages in the interstitium (Wang *et al*, 2021). Here, macrophages can polarize to phenotypes with different function. The M1 “classically activated”, that are generally regarded as pro-inflammatory macrophages, can promote kidney injury by expressing stimulating inflammatory mediators and reactive oxygen intermediates (Tang *et al*, 2019). M2 “alternatively activated” macrophages have instead anti-inflammatory and pro-reparative properties participating in tissue remodelling, wound healing and repair once the primary injury has resolved (Braga et al, 2015). M1-to-M2 transition is crucial in damaged kidney to induce

tissue repair and when damage and injury are unresolved, M1 macrophages persist in the kidney interstitium mediating and promoting kidney fibrosis (Tang *et al*, 2019).

Ccr2 (also known as CD192) is a seven transmembrane domain protein belonging to the G-protein coupled receptor family (Boring *et al*, 1996). It is prevalently expressed by circulating monocytes and macrophages, but also by other cells of the immune system, such as dendritic cells, activated T cell lymphocytes and basophils (Frade et al, 1997; Nieto et al, 1998; Bakos et al, 2017). Ccr2 is activated through the binding of some high-affinity ligands belonging to the monocyte chemoattractant protein (MCP) family of chemokines, such as CCL2 (also known as MCP1), CCL7 (MCP3), CCL8 (MCP2), CCL12 (MCP5), CCL13 (MCP4) and CCL16 (**Figure 50**, White et al, 2013). Chemokines are cytokines with potent chemotactic properties, that can mediate egress of circulant monocytes from the bone marrow and their accumulation in the site of inflammation, triggering the immune response (Wynn *et al*, 2013). CCL2 and CCL12 are exclusively ligands of CCR2, with CCL2 representing the main, high-affinity ligand, while CCL7, CCL8 and CCL13 can also bind other receptors as CCR1, CCR3 and CCR5 (White *et al*, 2013).

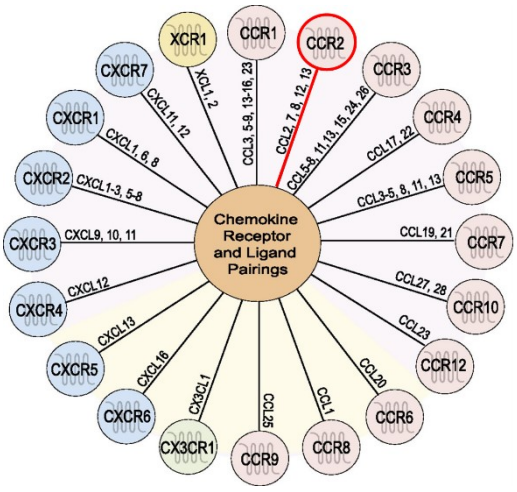


Figure 50. Chemokine receptor and ligand pairings. *C-C motif chemokine receptor 2 (Ccr2) can be bound and activated by chemokines CCL2, CCL7, CCL8, CCL12 and CCL13 (indicated in red) (from* White et al, 2013*).*

Generation and characterization of a *Ccr2* knockout mouse model (*Ccr2*$^{-/-}$) revealed the major role of Ccr2 signalling in recruitment of myeloid cells, particularly monocytes and macrophages. Indeed, *Ccr2*-/- mice displayed diminished migration of inflammatory monocytes from bone marrow to the circulation, resulting in reduced macrophage infiltration to the inflamed site (Boring *et al*, 1997).

A crucial role for Ccr2 axis in the activation and accumulation of macrophages in the kidney interstitium in response to different types of damage, as IRI (Yang *et al*, 2019; Xu *et al*, 2019), renal artery stenosis (RAS) (Kashyap *et al*, 2016) and UUO (Awad *et al*, 2011; Braga *et al*, 2018) has been reported. Interestingly, upon different types of injury, tubular epithelial cells can directly mediate chemotaxis and infiltration of Ccr2 positive monocytes in the kidney, producing and releasing Ccl2 before the accumulation of inflammatory cells (Kashyap *et al*, 2016; Lv *et al*, 2018). The observation that in Tg$^{Umod\text{C147W}}$ mice up-regulation of *Ccl2*, *Ccl12* and *Ccl7* at one day *postnatal* occurs in the absence of inflammatory cell infiltration might suggest a similar situation in our model, pointing at TAL epithelium as the source of pro-inflammatory signals downstream of cell stress induced by ER retention of mutant uromodulin. However, further analysis is required to test this hypothesis.

In different settings of kidney injury *Ccr2* genetic ablation or the use of specific antagonist of this receptor appeared protective, leading to a significative reduction of macrophage infiltration and resulting in a milder fibrotic phenotype (Kitagawa *et al*, 2004; Xia *et al*, 2013; Kashyap *et al*, 2016). Upon UUO, *Ccr2*$^{-/-}$ mice showed a more robust protection to fibrosis development compared to mice lacking other CCR receptors (*Ccr4*$^{-/-}$ and *Ccr5*$^{-/-}$), demonstrating a major role of Ccr2 signalling in monocyte recruitment in the damaged kidney (Braga *et al*, 2018). However, in other experiments, either genetic or pharmacologic block of Ccr2 signalling results in only partial attenuation of inflammation (Saito *et al*, 2018; Xu *et al*, 2019). This is in line with our results as, in the setting of ADTKD-*UMOD*, targeting of Ccr2 does not block disease onset nor it delays disease progression. No significant differences in the studied parameters were, indeed, detected between Tg$^{Umod\text{C147W}}$ mice carrying *Ccr2*-/- or *Ccr2*+/+ genotype at the different time points.

It is worth to mention that in a model of unilateral IRI, macrophage infiltrate is reduced but not abolished in *Ccr2*$^{-/-}$ mice, suggesting that other pathways might play a role in the onset of kidney inflammation (Xu *et al*, 2019). The screening of other key chemokine/receptor pairings such as *Ccl3/Ccr1*, *Ccl8/Ccr3*, *Cxcl12/Cxcr4*, *Cx3cl1/Cx3cr1*, and *Csf1/Csf1* revealed a significant up-regulation of the CCL8(MCP2)/CCR3 pathway, suggesting a possible compensatory response to the loss of CCL2/CCR2 signalling (Xu *et al*, 2019).

Based on this information, we carried out a preliminary analysis in Tg$^{Umod\text{C147W}}$/*Ccr2*$^{-/-}$ mice to assess possible induction of compensatory pathways of inflammation also in our model. We tested expression levels of *Ccl8* (Ccr3 ligand), *Ccr1* and *Ccr5* in kidneys of Tg$^{Umod\text{C147W}}$/*Ccr2*$^{-/-}$, Tg$^{Umod\text{C147W}}$/*Ccr2*$^{+/+}$ and Ctr/*Ccr2*$^{+/+}$ mice at early (1 week) and late (23 weeks) stages of disease (**Figure 51**). As opposed to the previously cited study, *Ccl8* is significantly down-regulated in Tg$^{Umod\text{C147W}}$/*Ccr2*$^{-/-}$ mice compared to Tg$^{Umod\text{C147W}}$/Ccr2$^{+/+}$ ones at all tested time points. However, compared to mutant mice expressing *Ccr2*, Tg$^{Umod\text{C147W}}$/*Ccr2*$^{-/-}$ mice showed increased *Ccr5* expression at 23-weeks of age and slight but significant up-regulation of *Ccr1* at 1 week that progressively increased at 23 weeks of age (**Figure 51**).

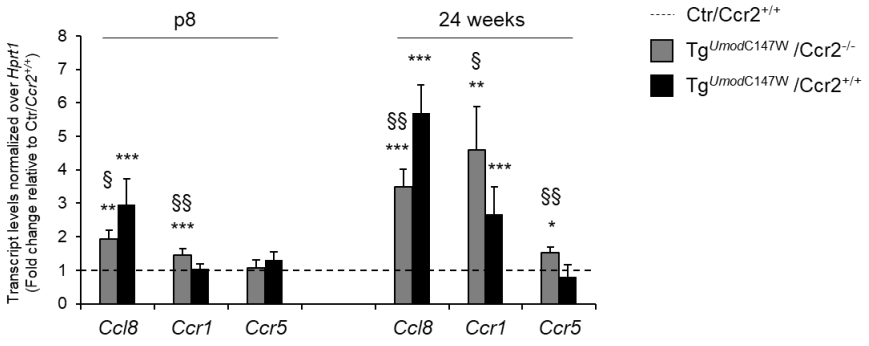


Figure 51. Early and late compensatory effects induced by Ccr2 deletion in kidneys of Tg^{UmodC147W} mice. *Analysis by semiquantitative RT-PCR of the expression levels of Ccl8, Ccr1 and Ccr5 in kidneys of 1-week and 23-week-old Tg$^{UmodC147W/}$Ccr2$^{-/-}$, Tg^{UmodC147W}/Ccr2$^{+/+}$ and Ctr/Ccr2$^{+/+}$ mice. Data are expressed as mean ± s.d and reported as fold changes compared to age- and sex-matched Ctr/Ccr2$^{+/+}$ mice (dashed line). N=3-5 animals/group. *P<0.05, **P<0.01, ***P<0.005 vs. Ctr/Ccr2$^{+/+}$; §P<0.05, §§P<0.01 Tg$^{UmodC147W/}$Ccr2$^{-/-}$ vs. Tg^{UmodC147W}/Ccr2$^{+/+}$ (unpaired t-test).*

Although preliminary, these data suggest that *Ccr2* ablation can induce compensatory activation of inflammatory pathways contributing to disease onset (*Ccr1*) and sustainment (*Ccr5*) in Tg$^{Umod\text{C147W}}$/Ccr2$^{-/-}$ mice.

Characterization of a mouse line carrying a compound deletion of *Ccr1*, *Ccr2*, *Ccr3* and *Ccr5* (iCCR) revealed evidence for context-dependent redundancy of these receptors in controlling monocytic and eosinophilic recruitment in resting conditions in different tissues such as the lung and the skin. Ccr2 appeared as the dominant receptor mediating myelomonocytic cells recruitment at the inflamed site (Dyer *et al*, 2019). Nevertheless, in an air-pouch model of inflammation the authors identified a residual subpopulation of monocytes which is recruited in inflamed tissues also in absence of Ccr2 signalling and that, intriguingly, show high expression levels of *Ccr1* and *Ccr3* receptors (Dyer *et al*, 2019). Although analysing tissues other than the kidney, this study might support the hypothesis of redundant and compensatory mechanisms that may play a role also in Tg$^{Umod\text{C147W}}$/*Ccr2*$^{-/-}$ mice. Strategies to obtain compound deletion of Ccr receptors or the use of specific inhibitors as for instance α-Ccr2 or α-Ccl2 antibodies, could be envisaged as alternatively ways to clarify the significance of early induction of Ccr2 signalling in disease pathogenesis, possibly avoiding compensatory effects.

However, we cannot exclude the possibility that the lack of beneficial effect of Ccr2 ablation in Tg$^{Umod\text{C147W}}$/*Ccr2*$^{-/-}$ mice is due to the role of other, yet unidentified, pro-inflammatory molecules. Indeed, up-regulated expression of *Ccl2*, *Ccl12* and *Ccl7* at p1 was detected testing a large but limited number (84) of pro-inflammatory molecules (*1.6 Preliminary results*). Future experiments aimed at characterizing the overall composition of mononuclear infiltrating cells in kidneys of Tg$^{Umod\text{C147W}}$ mice at different stage of the disease will be instrumental to gain further insight into the role of inflammation in ADTKD-*UMOD* onset and evolution and to identify novel targets for therapeutic strategies.

Overall, we demonstrated that ablation of Ccr2 signaling is not sufficient to prevent the onset or delay the progression of ADTKD in Tg$^{Umod\text{147W}}$ mice. This is likely due to the induction of compensatory pathways recruiting monocytes and triggering inflammatory response in kidneys of mice expressing mutant uromodulin.

4.2 Calorie restriction

During phenotyping of Tg$^{Umod\text{C147W}}$/*Ccr2*$^{-/-}$ mouse line, in kidneys from a single 14-week-old Tg$^{Umod\text{C147W}}$ mouse, we noticed full rescue of mutant uromodulin ER retention and its increased localization at the apical membrane of TAL cells, resembling the one of wild type protein. At sacrifice this animal presented with lower body weight compared to littermates and a malocclusion problem due to incisors overgrowth. After excluding the occurrence of a reverting mutation, we hypothesized that the observed effect on mutant uromodulin trafficking was due to reduced food intake.

To test our hypothesis, we designed a proof-of-concept experiment mimicking food intake reduction observed in the "rescued" mouse. In this experiment Tg$^{Umod\text{C147W}}$ mice were subjected to a short term (4 weeks) severe (55%) calorie restriction regimen (CR-55) starting from weaning (p21) until 7 weeks of age, when mutant mice are in a pre-symptomatic stage of the disease (Trudu *et al*, 2017). The results obtained were in line with the original observation, confirming the effect of CR on mutant uromodulin trafficking.

Based on these interesting results, we next tested the therapeutic potential of a milder (30%) and prolonged (15 weeks) protocol of CR (CR-30) at a later stage of disease, starting from 8-week-old Tg$^{Umod\text{C147W}}$ mice until 23 weeks of age, when they reached mild renal failure (Bernascone *et al*, 2010). This protocol was effective in reducing mutant uromodulin ER retention and aggregation and ameliorating ADTKD-*UMOD* phenotype in Tg$^{Umod\text{C147W}}$ mice.

CR is defined as the reduction of total calorie intake, providing an adequate intake of essential micro- and macro-nutrients and avoiding malnutrition. It is regarded as the most powerful and reproducible non-genetic intervention to delay age-associated pathologies and extend lifespan in a large variety of species including yeast, worm, fly, rodent, non-human primates and human beings (Fontana *et al*, 2010; Longo & Anderson, 2022). This health-promoting action of CR is mediated by its action on a plethora of molecular mechanisms, including autophagy induction, improvement of cell survival and mitochondrial fitness, modulation of nutrient-sensing and reduction of pro-inflammatory signals and oxidative stress (Fontana & Partridge, 2015; Zhang *et al*, 2021) (**Figure 52**).

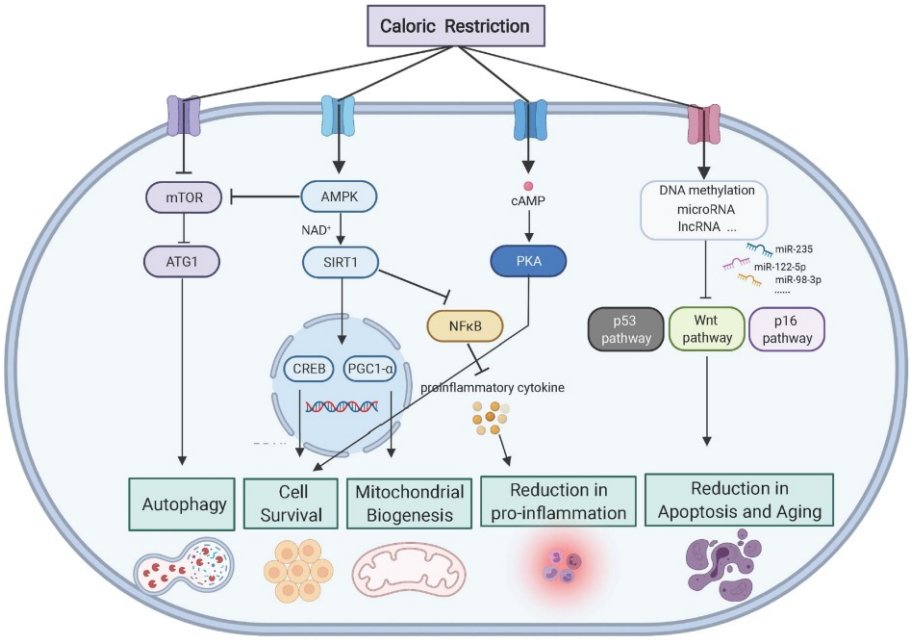


Figure 52.Cellular and molecular mechanisms controlled by calorie restriction *(from Zang et al, 2021. Open access).*

There is an increasing amount of evidence also describing the beneficial role of CR in diseases that are caused by protein accumulation and inflammation, both in humans and in different pre-clinical models (see below).

A role of CR in kidney protection has also been investigated (Wang *et al*, 2018). In a rat model of kidney aging, CR decreased proteinuria, delayed tubular epithelial cell senescence and epithelial-to-mesenchymal transition (Dong *et al*, 2017). Preconditioning with short-term CR protects mice from ischemia/reperfusion induced kidney damage (Mitchell *et al*, 2010; Johnsen *et al*, 2020). Mild to moderate (10-40%) CR has been described as effective in ameliorating ADPKD development in mice, reducing cyst area, kidney fibrosis, inflammation, and injury in a dose-dependent manner and through a mechanism that likely involves activation of LKB1-AMPK and suppression of mTOR pathway (Warner *et al*, 2016).

In $Tg^{UmodC147W}$ mice, in absence of any effect on *UMOD* expression, CR-55 led to a striking reduction of ER retained mutant uromodulin and to a remarkable increase of uromodulin localization at the plasma membrane. The fact that a significant proportion

of mutant protein is detected as mature protein suggests that the effect of CR on reducing ER retention and aggregation, likely relieves the load on the ER folding machinery and rescues uromodulin trafficking along the secretory pathway. The increase of protein folding capacity and enhanced proteostasis might also be a direct effect of CR. Indeed, a study on skeletal muscle samples from humans following long-term (3-15 years) CR (about 30%) regimen revealed increased levels of chaperones HSP70 and GRP78 compared to age-matched controls (Yang *et al*, 2016). Increased levels of these chaperones were also observed in rat and mouse models subjected to a CR diet (Selsby *et al*, 2005; Arumugam *et al*, 2010; Manzanero *et al*, 2011). The milder CR-30 protocol recapitulates the effect in reducing mutant uromodulin ER accumulation and aggregation without affecting uromodulin transcript levels. However, this is not reflected by an increase in protein maturation. This discrepancy might reflect different or additional mechanisms induced by the severe CR protocol compared to the milder one. Alternatively, differences on mutant uromodulin maturation could be due to the different age of mice at the start of the two experiments (p21 in CR-55 vs 8-weeks in CR-30), indicating that CR, either directly or indirectly, is effective in rescuing mutant uromodulin trafficking only at earlier time points, when ER aggregation of mutant uromodulin is less pronounced.

Our CR experiments also showed a dramatic reduction of the expression of *Lcn2* in TAL cells expressing mutant uromodulin, indicating that TAL cell stress, likely induced by ER retention of mutant uromodulin, can be resolved by reducing mutant uromodulin intracellular accumulation and aggregation. However, upon CR-55 *Lcn2* expression appeared strongly increased in proximal tubules of Tg$^{Umod\text{C147W}}$ CR-55 mice and, to a lower extent, also in Tg$^{Umod\text{wt}}$ CR-55 mice, suggesting an impact of CR on these cells. In Tg$^{Umod\text{C147W}}$ mice kidney transcriptomic analysis revealed up-regulation of the proximal tubule damage marker *Havrc1* at this age (8-weeks). Similarly, up-regulation of stress related genes specifically was observed in the proximal tubule in a second ADTKD-*UMOD* mouse model, suggesting an impact of *UMOD* mutations also on these cells (Trudu *et al*, 2017; Horsch *et al*, 2014). The higher expression of *Lcn2* in proximal tubules of Tg$^{Umod\text{C147W}}$ CR-55 compared to Tg$^{Umod\text{wt}}$ CR-55 mice might hence indicate that the severe dietary regimen applied exacerbates the already present proximal tubular damage in Tg$^{Umod\text{C147W}}$ mice. As opposed to the proof-of-concept experiment, in 23-weeks-old

Tg$^{Umod\text{C147W}}$ CR-30 mice *Lcn2* expression is not only decreased in TAL cells along with mutant uromodulin aggregates, but also reduced at total kidney level, and not increased in proximal tubules, confirming an impact of the milder CR in ameliorating overall tubular damage in kidneys of Tg$^{Umod\text{C147W}}$ mice.

Inflammation is an early event of pathogenesis occurring in kidneys of Tg$^{Umod\text{C147W}}$ mice. It is likely activated downstream of TAL cell stress and increases with age contributing to progressive kidney damage (Trudu *et al*, 2017). CR significantly ameliorates inflammation in mice expressing mutant uromodulin. This anti-inflammatory effect of CR in Tg$^{Umod\text{C147W}}$ mice could be an indirect consequence of reduced TAL cell stress, following reduction of mutant uromodulin retention and aggregation in the ER. However, a synergistic effect due to the direct anti-inflammatory role of CR is likely to play a role. Indeed, several studies demonstrated the potent efficacy of CR in reducing inflammation in different settings, ranging from inflammaging to inflammation of metabolic disorders and chronic diseases (Kökten *et al*, 2021; Fontana *et al*, 2021). In multiple sclerosis (MS) a neurodegenerative disease characterized by central nervous system inflammation, demyelination and axonal damage, CR demonstrated a protective role by reducing inflammation, oxidative damage and favoring neuroprotection and remyelination (Mojaverrostami *et al*, 2020; Fontana *et al*, 2021). Interestingly, in a pre-clinical murine model of MS, reduction of dietary intake has been reported to impact on the circulating pool of inflammatory monocytes, reducing monocyte infiltration in the inflamed spinal cord. This is due to increased AMPK pathway activation in the liver, eventually leading to reduced *Ccl2* systemic levels and consequent reduced mobilization of monocytes from bone marrow. This effect of CR seems restricted to chronic inflammation, as it did not impact on monocyte mobilization during acute infection (Jordan *et al*, 2019). The beneficial effect of CR was also reported in a mouse model of atherosclerosis where it ameliorated disease phenotype by reducing macrophage infiltration and vascular calcification (Yang *et al*, 2020).

We also described a beneficial effect of CR on fibrotic phenotype in Tg$^{Umod\text{C147W}}$ mice, likely downstream to reduced inflammation. This is in line with previous observation that in our model inflammation precedes fibrosis (Trudu *et al*, 2017) and demonstrates that resolving inflammation is effective in rescuing induction of tubulointerstitial fibrosis and preventing disease progression. The observation that in 23-week-old Tg$^{Umod\text{C147W}}$ CR-30

mice inflammatory and fibrotic markers are reduced to levels that are even lower than the ones observed at the start of dietary protocol (8 weeks), and comparable to wild type mice, suggests a reversal of ADTKD-*UMOD* phenotype induced by CR. Interestingly, kidney plasticity and its ability to repair structural changes and regenerate have been recently reported in a mouse model of ADPKD, showing a reversal of disease phenotype following re-expression of *Pkd* genes. In this model, recovery of kidney function appeared complete when re-expression of *Pkd* occurred at early stage of disease, but only partial, with persisting signs of kidney scarring, if re-expression was induced at later time points (Dong *et al*, 2021). Our CR-30 experiment was performed on Tg$^{Umod\text{C147W}}$ mice at an early stage of the disease, when inflammation and fibrosis were already strongly induced but mice still maintain normal kidney function. It will be important to test the effectiveness of CR in ameliorating disease progression and/or inducing ADTKD reversal when started at later disease stages.

In kidneys of Tg$^{Umod\text{C147W}}$ mice both at early (7-weeks) and later time point (23-weeks) we observed an accumulation of p62 puncta specifically in TAL cells, that, at least at later time points, occurs in the presence of increased total kidney levels of Lc3-II/Lc3-I ratio. P62 is a ubiquitin-binding scaffold protein that plays a role as autophagy receptor for ubiquitinated proteins and that is itself degraded along with the substrate, thus representing a readout of autophagic flux (Bjørkøy *et al*, 2009; Katsuragi *et al*, 2015). The presence of p62 aggregates in cells expressing mutant uromodulin can be considered as evidence of reduced/impaired autophagy in these cells, a feature described in other diseases such as non-alcoholic fatty liver disease and already reported in another ADTKD-*UMOD* mouse model (González-Rodríguez *et al*, 2014; Johnson *et al*, 2017). We also observed increased levels of phosho-S6RP, a downstream target of mTOR signaling pathway, in kidneys of Tg$^{Umod\text{C147W}}$ mice. Upon CR phosho-S6RP levels are restored to wild type levels in kidneys of Tg$^{Umod\text{C147W}}$ mice and p62 aggregates are strongly decreased in TAL cells along with mutant uromodulin aggregates. These results indicate that CR, by inhibiting mTOR overactivation, can restore autophagy in TAL cells of Tg$^{Umod\text{C147W}}$ mice leading to the clearance of mutant uromodulin aggregates. The observation that starvation or treatment with mTOR inhibitors (i.e., rapamycin and Torin 1) by enhancing autophagy stimulates intracellular removal of aggregates in cellular models expressing different mutant uromodulin isoforms, strongly supports our results

(Schiano *et al*, 2022; Johnson *et al*, 2017). A beneficial role of CR in ameliorating disease phenotype by inducing autophagy and reducing protein accumulation has been described in other disease settings. In two mouse models of Alzheimer's disease both long-term (40% CR for 68 weeks) and periodic (3 cycles of 2 weeks of 40% CR followed by 9 days of AL diet) CR attenuate neuropathology by reducing hippocampal β-amyloid plaques through autophagy stimulation (Müller *et al*, 2021; Gregosa *et al*, 2019). In a mouse model of Huntington disease, autophagy induced by intermittent fasting has been reported effective in reducing mutant huntingtin accumulation in the brain (Ehrnhoefer *et al*, 2018).

The relevant toxic role of uromodulin aggregates in the progression of ADTKD-*UMOD* has been recently described in two newly generated knock-in mouse models expressing p.Cys171Tyr (*Umod*^{C171Y}) and p.Arg186Ser (*Umod*^{R186S}) *Umod* mutations. These two mutations differently impact on uromodulin trafficking and propensity to aggregate, and this associates with different disease severity in *Umod*^{C171Y} and *Umod*^{R186S} mice, recapitulating ADTKD features observed in patients carrying the corresponding *UMOD* mutations (Schiano *et al*, 2022). In our model a similar situation is observed when comparing disease phenotype in male and female Tg$^{Umod C147W}$ mice. In female mice, increased *Umod* expression is reflected by a higher amount of mutant uromodulin aggregates within the ER that lead to a more pronounced induction of inflammation, fibrosis and tubular damage, resulting in a more severe disease phenotype. Hence, strategies aimed at degrading mutant uromodulin aggregates could be a valuable therapeutic option in the context of ADTKD-*UMOD*.

A clinical trial envisaging CR is currently ongoing for MS patients. The current therapies are only partially effective in controlling the relapsing-remitting phases of this disease and as mentioned before, CR in MS models showed promising results. The trial includes 120 participants with a mild restriction of 15-20% (of the ideal diet for the individual) or a mild restriction of 15-20% without cow's milk and gluten (https://clinicaltrials.gov; Identifier: NCT04042415; estimated study completion date: September 2023). The aim is to improve the outcome of the relapsing-remitting MS and the efficacy of drugs used as first line treatment using CR as an adjuvant therapy to alter the metabolic state andre-equilibrate immune/inflammatory response of patients.

Some of the numerous effects induced by CR could be mimicked by using pharmaceutical agents, such as salicylic acid, resveratrol, rapamycin, metformin, 2-deoxy-D-glucose that are collectively referred to as caloric restriction mimetics (CRMs). The targets of CRMs include pathways as glycolysis, mTOR, AMPK, sirtuins and insulin/insulin-like grow factor (Madeo *et al*, 2019; Hofer *et al*, 2021). The use of CRMs may hence be envisaged as an alternative strategy to ameliorate disease phenotype without reducing caloric intake also in the context of ADTKD-*UMOD*.

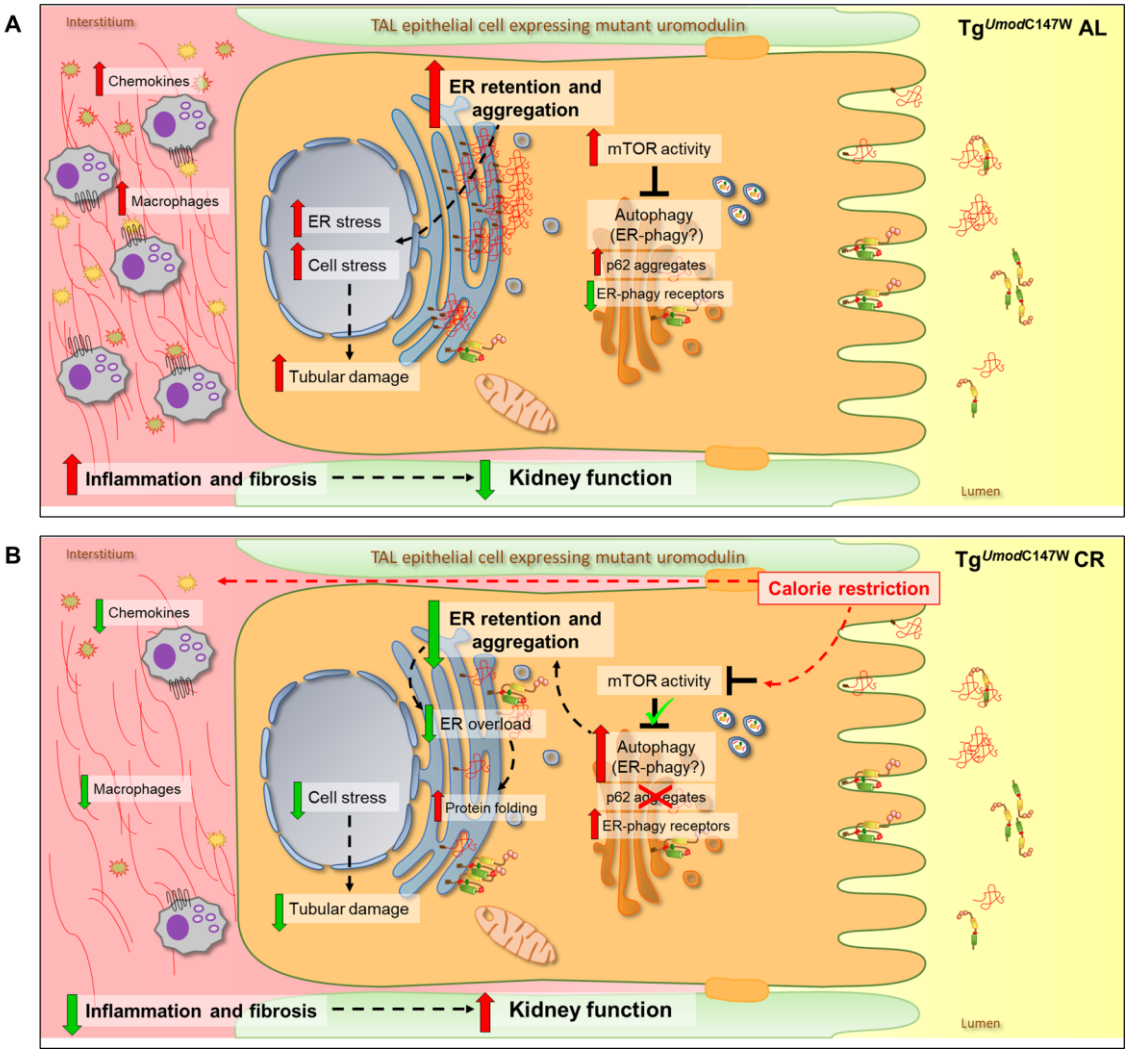


Figure 53. Working model: effect of calorie restriction on ADTKD-UMOD pathogenesis. *A) Molecular effects induced by mutant uromodulin expression in kidneys of* $Tg^{UmodC147W}$ *mice fed ad libitum (AL). B) Molecular effects induced by calorie restriction (CR) in kidneys of* $Tg^{UmodC147W}$ *mice.*

In sum, we demonstrated that calorie restriction-restored autophagy is effective in inducing degradation of mutant uromodulin aggregates in the ER. This rescues TAL epithelial cell stress and blocks the induction of the inflammatory process. This, likely in synergy with the direct anti-inflammatory role of CR, eventually prevents fibrosis, progressive kidney damage and decline of kidney function in $Tg^{Umod C147W}$ mice (**Figure 53**).

Overall, our results establish the proof of principle that rescuing the primary effect of *UMOD* mutations can prevent ADTKD-*UMOD* onset and progression.

5. MATERIALS AND METHODS

5.1 Animal models

All animals used in the presented study were housed in a light- and temperature-controlled room with free access to tap water and standard chow (Diet VRF1 (P), SDS Diets, France) except otherwise indicated. All procedures were carried out in accordance with the *San Raffaele Institutional Animal Care and Use Committee* (IACUC) guidelines.

5.1.1 $Tg^{UmodC147W}$ and Tg^{Umodwt} mouse lines

Transgenic mouse lines expressing mutant ($Tg^{Umod\text{C147W}}$) or wild type ($Tg^{Umod\text{wt}}$) uromodulin were previously generated and characterized in our laboratory (Bernascone *et al*, 2010; Trudu *et al*, 2017). Both these mouse lines are on the FVB background.

The mutant and wild type transgenes comprise a fragment (2.9 kb) of the mouse *Umod* gene promoter, the first non-coding exon and intron, the remaining coding sequence from exon 2 to exon 11 and the entire 3' UTR. An HA-tag was inserted at the N-terminus, between the leader peptide and the first EGF-like domain (i.e., between p.Ser26 and p.Thr27) to discriminate transgenic uromodulin from the endogenous one. Uromodulin mutant transgene encodes for the p.Cys147Trp mutant uromodulin, homologous to the p.Cys148Trp patient mutation (Rampoldi *et al*, 2003; Bernascone *et al*, 2010).

5.1.2 Generation of $Tg^{UmodC147W}/Ccr2^{-/-}$ mouse line

$Ccr2^{-/-}$ animals are a mouse line on the C57BL/6J background with a targeted disruption of C-C Chemokine Receptor 2 (Ccr2), previously generated and described by Boring et al, (Boring *et al*, 1997) and kindly provided by Prof. Iannacone (Dynamics of immune responses Unit, San Raffaele Scientific Institute, Milan).

To obtain the animals used for the characterization, $Tg^{Umod\text{C147W}}$ mice were crossed with *$Ccr2^{-/-}$* mice. $Tg^{Umod\text{C147W}}/Ccr2^{+/-}$ and Ctr/*$Ccr2^{+/-}$* animals obtained in the F1 were backcrossed to generate $Tg^{Umod\text{C147W}}/Ccr2^{-/-}$, $Tg^{Umod\text{C147W}}/Ccr2^{+/+}$ and Ctr/*$Ccr2^{+/+}$* mice used in the experiments.

$Tg^{Umod\text{C147W}}/Ccr2^{-/-}$ female mice were compared with age- and sex- matched $Tg^{Umod\text{C147W}}/Ccr2^{+/+}$ and Ctr/*$Ccr2^{+/+}$* (animals that do not carry the transgene) littermates and sacrificed at 1 week, 6 weeks, 14 weeks or 24 weeks of age (n=4/5 animals per

genotype at each age) to assess the effect of *Ccr2* targeting on disease phenotype at different time points.

At the assigned time point mice were sacrificed by cervical dislocation after blood collection by retro-orbital bleeding and kidneys were collected and stored for subsequent analysis. Urine samples were collected from 24-week-old mice using metabolic cage after appropriate training period.

5.1.3 Protocol of 55% calorie restriction

Starting from weaning (21 days of age), female Tg$^{Umod\text{C147W}}$ and Tg$^{Umod\text{wt}}$ mice were fed *ad libitum* (n=3 animals/genotype) or with a 55% calorie restriction (CR) regimen (n=3 animals/genotype), for 4 weeks. The restriction was performed by providing to CR mice once daily 45% of the amount of food consumed by mice on *ad libitum* regimen (AL). Mice were single-housed, food intake and body weight were assessed daily. Immediately before sacrifice, blood was collected from retro-orbital bleeding. At sacrifice, kidney and liver were collected, properly processed and stored for subsequent characterization.

5.1.4 Protocol of 30% calorie restriction

For this experiment both male and female Tg$^{Umod\text{C147W}}$ mice were used. Starting from 2 months of age (pre-symptomatic stage), Tg$^{Umod\text{C147W}}$ mice were individually housed to measure the exact food intake and fed AL or with 30% CR regimen (n=3 mice/sex for each dietary regimen). Food intake of animals in the *ad libitum* group was daily measured and CR mice were allotted once daily 70% of the amount of food consumed by mice on AL regimen. Body weight of each animal was assessed weekly. 23-week-old Tg$^{Umod\text{wt}}$ mice were used as control group (n=3/sex). Six days before sacrifice, animals were subjected to urine collection using metabolic cage. Immediately before sacrifice, blood was collected by retro-orbital bleeding. After 15 weeks of controlled diet Tg$^{Umod\text{C147W}}$ AL and Tg$^{Umod\text{C147W}}$ 30-CR mice were sacrificed and kidney and liver were collected, properly processed and stored for following analysis.

5.1.5 Metabolic cage for urine collection

Urine samples were collected using individual metabolic cages (Techniplast, Varese, Italy) that provide immediate and perfect separation of urine from feces. Mice were accommodated in metabolic cages for two non-consecutive days, representing the training period. After appropriate training, urine was collected for 15-hours during night period.

During the period in metabolic cages mice were provided with free access to tap water and *ad libitum* or rationed food according to experimental group. Once collected, urine samples were spun at 1000 x g for 5 minutes to remove food remnants and stored at -80°C for subsequent analysis.

For the analysis of uromodulin and Lcn2 urinary levels, the same fraction of total urine volume collected the third day of metabolic cage were subjected to western blot analysis as described below.

5.1.6 Serum samples collection

Prior to sacrifice, up to 500µl of blood were collected from mice by retro-orbital bleeding using heparinized capillary tubes, upon anaesthetization with avertin (200 µg/gr body weight). Blood samples were then centrifuged at 3000 x g for 5 minutes and serum collected and stored at -20°C for subsequent analysis. Blood urea nitrogen levels were measured by the Core Facility of Animal Biochemistry, San Raffaele Scientific Institute, Milan, using the automatic biochemistry analyser iLab Aries (ANTISEL, Athens, Greece).

5.1.7 Mouse tissues collection

Mouse tissues collected from animals sacrified by cervical dislocation were stored at -80°C for subsequent RNA or protein extraction.

For immunofluorescence and histological staining, kidneys were fixed with a 4% paraformaldehyde (PFA) solution for 16 hours, incubated for 16 hours in 30% sucrose (w/v in PBS) and embedded in optimum cutting temperature embedding medium (OCT) (Bio-Optica, Milan, Italy), snap-frozen in a mixture of isopropanol and dry ice and stored at -80°C.

5.2 Genomic DNA extraction and genotyping

Genomic DNA (gDNA) was extracted from tail biopsies. Tissue was incubated overnight at 56 °C in 500µl of Tail solution (100 mM Tris pH 8.5, 5 mM EDTA, 0.2% SDS, 200 mM NaCl, 0.1 ng/ml Proteinase K (Promega, Madison, WI, USA)). After 10 min of centrifugation at 17,900 x g, the supernatant was added to 1 mL of a 1:1 ethanol: isopropanol solution to precipitate DNA. DNA pellet was washed in 70% EtOH, and then

resuspended in water. gDNA concentration was quantified using Nanodrop 8000 spectrophotometer (Thermofisher, Waltham, MA, USA).

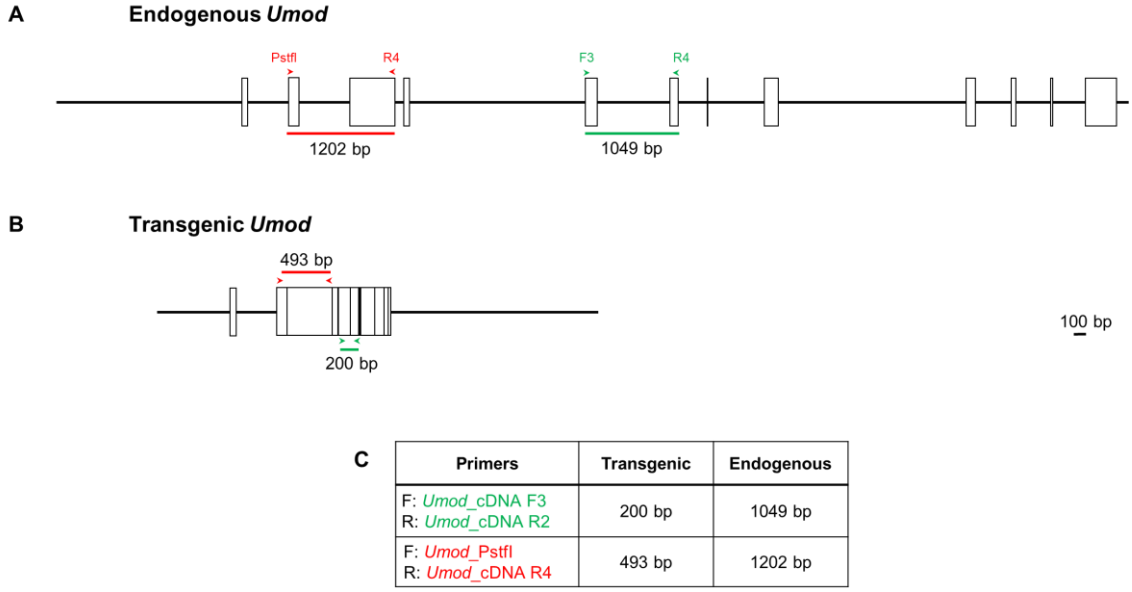
Mice genotype was assessed by PCR analysis using the GoTaq® Green Master Mix 2X (Promega) supplemented with 0.25 µM of primer forward and reverse (see details below) and using 100 ng of gDNA as template.

5.2.1 Uromodulin genotyping

Presence of uromodulin transgene was verified through 2 PCRs using two different combinations of primers (Umod_cDNA_F3 with Umod_cDNA_R2 and Umod_PstfI forward with Umod_cDNA_R4 (**Figure 54**, primer sequences are reported in **Table 7**) with the following amplification program (30 cycles):

Table 3. PCR protocol reaction for transgene detection.

	Temperature	Time	Cycle
Denaturation	94°C	2 min	1
Deneturation	94°C	20 sec	30
Annealing	60°C	20 sec	
Extension	72°C	20 sec	



C

Primers	Transgenic	Endogenous
F: *Umod_cDNA F3* R: *Umod_cDNA R2*	200 bp	1049 bp
F: *Umod_PstfI* R: *Umod_cDNA R4*	493 bp	1202 bp

Figure 54. Uromodulin genotyping. *Schematic representation of A) endogenous Umod and B) transgenic uromodulin construct. Red arrowheads represent the annealing site of UMOD_PstfI forward and UMOD_cDNA R4, green arrows are the site of UMOD_cDNA F3 and*

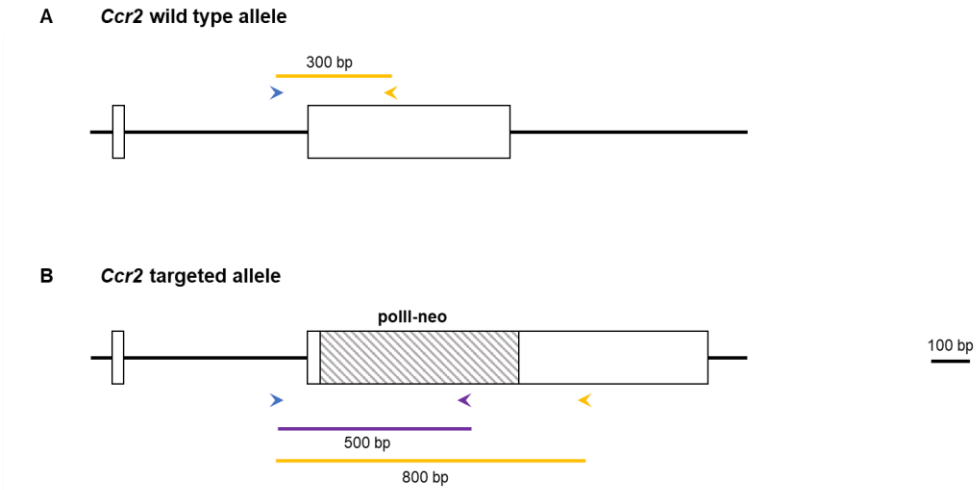
UMOD_cDNA R2 on both endogenous and transgenic uromodulin. Product size for each set of primers on both transgenic and endogenous gene are reported in C.

5.2.2 Ccr2 genotyping

Two PCRs were performed to assess *Ccr2* genotyping, using a common *Ccr2* forward primer (Ccr2 common) with two different reverse primers annealing on *Ccr2* exon 2 (Ccr2 wt) or on the PolII-neo cassette (Ccr2 KO) (see **Table 7** for sequences) whose insertion causes *Ccr2* allele targeting (**Figure 55**). The following PCR program was used (40 cycles):

Table 4. PCR protocol reaction for Ccr2 genotyping.

	Temperature	Time	Cycle
Denaturation	94°C	2 min	1
Denaturation	94°C	20 sec	40
Annealing	55°C	20 sec	
Extension	72°C	20 sec	



C

Primers	Wild type	Knockout
F: Ccr2 common R: Ccr2 wt	300 bp	800 bp
F: Ccr2 common R: Ccr2 KO	No product	500 bp

Figure 55. Ccr2 genotyping. *Schematic representation of A) Ccr2 wild type and B) targeted (knockout) allele that contains the polII-neo cassette in exon 2 indicated by dashed box. Blue*

arrowhead represents the common Ccr2 forward primer used in both PCRs, yellow arrowhead the Ccr2 WT and purple arrowhead the Ccr2 KO reverse primers.

5.3 Purification of PCR product from agarose gel and sequencing

To sequence the transgene, we performed a PCR using the combination of primers UMOD_PstfI forward and UMOD cDNA_R3 (see **Table 7** for sequences) and kidney cDNA (1:10 dilution) as template, obtaining a fragment of 829 bp of uromodulin transgene. This set amplifies also a 793 bp product on endogenous uromodulin. The PCR product of the expected size was extracted from agarose gel using QIAquick Gel Extraction Kit (Qiagen, Hilden, Germany) following the manufacturer's instructions. DNA was eluted in nuclease-free water and analysed on agarose gel for quantification. 400 ng of purified PCR product were used as template for Sanger Sequencing reaction, using the reverse UMOD cDNA_R3 primer, to assess the presence of nucleotide substitution in heterozygosity.

5.4 Protein extraction

For protein extraction, half kidneys (total kidney for 1-week-old mice) were homogenized on ice using Potter (Tissue Grinder, 2 ml, Potter – Elvehejem, Wheaton) in a buffer containing 50mM Tris-HCl pH 7.4, 150 mM sodium chloride, 10 mM sodium fluoride, 1 mM sodium orthovanadate, 1 mM Glycerol Phosphate, 1:1000 Protease-Inhibitor Cocktail (Sigma-Aldrich, St Louis, MO, USA), 1% Triton X-100, 0.5% SDS and 60 mM n-octyl-β-D-glucopyranoside, a non-ionic detergent used for the solubilization and the extraction of membrane-bound and GPI-anchored proteins. Kidney homogenates were incubated at 4°C for 60 min, under rotation to allow protein extraction and then centrifuged for 10 min at 17,900 x g to separate the insoluble material (pellet). Protein concentration was assessed using Bradford protein assay (Biorad, Hercules, CA, USA).

5.5 Endo Hf Digestion

Endo Hf (New England® BioLabs, Ipswich, MA, USA) is a recombinant fusion protein of Endoglycosidase H and maltose binding protein that specifically cleaves high-mannose, ER-type N-glycans from glycoproteins. After denaturation by incubation for 15 min at 55°C in the denaturation buffer (10X), 20 µg of proteins was digested with 1 units of Endo Hf in Glycobuffer 3 (10X) for 90 min at 37°C. At the end of digestion, the enzyme was inactivated by incubation at 55°C for 15 min and samples analysed by western blot.

5.6 Western blot

Protein lysates or urine samples were separated by SDS-polyacrylamide gel electrophoresis (PAGE) in reducing (using a loading buffer containing 50 mM Tris HCl pH 6.8, 2% SDS, 0.2% bromophenol blue, 10% glycerol and 100 mM dithiothreitol (DTT) as reducing agent) or non-reducing (using the same loading buffer without DTT) condition at constant voltage (80 V for protein stacking and then 120V for protein separation) and transferred on nitrocellulose membrane (GE-Heltcare, Chicago, IL, USA). After blocking, the indicated primary antibody (**Table 6**) was added to the membrane and incubated overnight at 4°C. Horseradish peroxidase-conjugated secondary antibodies (1:7500 dilution, GE-Heltcare, **Table 6**) were added and incubated for 90 min at room temperature. Protein bands were visualized with the Immobilon Western Chemiluminescent Horseradish Peroxidase Substrate kit (Millipore, Billerica, MA, USA) at Uvitec (Alliance mini HD9, Uvitec Cabridge). Quantification of the optical band densities was performed using the gel analysis option of ImageJ software (Schneider *et al*, 2012). The optical density of proteins of interest was normalized on the one of Gapdh or Actin (loading controls) run on the same gel.

5.7 Immunofluorescence

7 µm-thick kidney sections were permeabilized twice for 15 min at room temperature in PBS + 0.1% Tween 20 and then blocked for 60 min at room temperature with 10% of donkey serum in PBS with 0.1% Tween 20. Then, the sections were

incubated overnight at 4 °C with primary antibodies (**Table 6**) diluted in PBS with 1% donkey serum + 0.1% Tween 20. After 3 washes with PBS-0.1% Tween 20 at room temperature, the proper fluorescent-conjugated secondary antibody (dilution 1:500 Alexa Fluor, Thermofisher, **Table 6**) was incubated for 90 min at room temperature. Nuclei were counterstained with diamidino-2-phenylindole (DAPI) and then the slides were mounted using FluorSave Reagent (Calbiochem, San Diego, CA, USA).

All tissue sections were visualized under a DM 5000B fluorescence upright microscope (Leica DFC480 camera, Leica DFC Twain Software, 20x/0.75 lens; Leica Microsystems, Deerfield, IL, USA) and identical acquisition parameters were ensured for the visualization of the same antibody in different kidney sections.

Quantification of the fluorescent positive area was performed by adjusting the threshold with a specific function of ImageJ software and then measured with analyse tools (Schneider *et al*, 2012).

5.8 Histological staining

7 µm-thick sections obtained from OCT-embedded kidneys were prepared to perform histological staining. The samples were incubated for 3 min at -20°C with acetone, for 5 min at 4°C with methanol and for 10 min at room temperature in deionized water.

Hematoxylin (Bio-Optica) and Eosin (Bio-Optica) staining and Picrosirius Red (Abcam, Cambridge, UK) stainings were carried out following the manufacturer's instructions, to evaluate kidney inflammation and collagen deposition on three representative sections from $Tg^{Umod\text{wt}}$, $Tg^{Umod\text{C147W}}$ AL and $Tg^{Umod\text{C147W}}$ CR-30 mice (n=1 animal/genotype/dietary regimen). Representative pictures of kidney morphology were acquired in bright field, using DM 5000B fluorescence upright microscope (Leica DFC480 camera, Leica DFC Twain Software, 20x/0.75 lens; Leica Microsystems, Deerfield, IL, USA).

5.9 RNA extraction and isolation

Total RNA was extracted by homogenization of half kidney (total kidney for 1-week-old animals) in 1 mL of TRiFast II RNA isolation solution (Euroclone, Pero, Italy) and incubated at room temperature for 5 min. 200µl of chloroform were added to the sample that was mixed by vortexing for 15 sec. The sample was incubated at room temperature for 3 min. Then, it was centrifuged at 12,000 *x g* for 15 min at 4°C to separate the three phases; the upper one colourless and aqueous containing RNA was transferred to a new centrifuge tube. 500µl of isopropanol was added to precipitate RNA. After 10 min of incubation at room temperature, RNA was pelleted by centrifugation at 12,000 *x g* for 10 min at 4°C, washed with 1 mL ice-cold 75% ethanol, centrifuged at 12,000 *x g* for 10 min and dried at room temperature for 3 min before resuspension in nuclease-free water. RNA concentration was determined by using Nanodrop 8000 spectrophotometer (Thermofisher) and RNA quality was checked on 1% agarose gel (w/v).

5.10 Reverse transcription and Real-Time qPCR analysis

Reverse transcription was performed using iScript™ gDNA Clear cDNA Synthesis Kit (BioRad) following the manufacturer's instructions. Briefly, 1µg of RNA was incubated with DNase for 5 min at 25 °C to allow gDNA digestion and then 5 min at 75 °C to inactivate DNase. Then iScript Reverse Transcription Supermix, containing RNase H, Moloney murine leukaemia virus (MMLV) reverse transcriptase, dNTPs, oligo(dT), random primers and RNase inhibitor, was added in each sample and the reaction was incubated in a thermal cycler as follows: 5 min at 25 °C (priming), 20 min at 46 °C (reverse transcription) and 1 min at 95 °C (reverse transcriptase inactivation). The obtained cDNA was diluted 1:10 in nuclease free-water and used as template to perform gene expression analysis by Real Time RT-qPCR on CFX96™ Touch Real-time PCR (BioRad) using the qPCR Core kit for SYBR® Green I No ROX (Eurogentec, Liège, Belgium). Specific primers (see **Table 8** for sequences) were designed by using Primer 3 and the amplification efficiency for each couple of primers was determined by dilution curves. Expression of genes of interest was normalized to *Hprt1* or *Tbp*. The relative mRNA expression was calculated following the ΔΔCT method (Pfaffl, 2001).

5.11 Semiquantitative RT-PCR analysis

Ccr2 targeting and *Ccl8*, *Ccr1* and *Ccr5* expression were tested by semiquantitative RT-PCR using a 25 µl mix composed by GoTaq® Green Master Mix 2X (Promega), 0.25 µM of each primer (see **Table 8** for sequences) and 5µl of 1:10 diluted cDNA as template.

Table 5. Protocol of semiquantitative RT-PCR reaction.

	Temperature	Time	Cycle
Denaturation	94°C	2 min	1
Denaturation	94°C	20 sec	40 (for *Ccr2)*
Annealing	60°C	20 sec	30 (for *Ccl8*, *Ccr1*, *Ccr5*)
Extension	72°C	20 sec	

5.12 Antibodies

Table 6. List of antibodies used for western blot and/or immunofluorescence experiments.

Target	Host	Dilution	Company	Code	Use
Primary antibodies					
Uromodulin	Sheep	1:2000	US Biological	T0850-02B	WB
		1:500			IF
HA	Rat	1:500	Roche	#11867423001	IF
HA	Rabbit	1:1000	Sigma	H6908	WB
		1:500			IF
Lipocalin-2	Goat	1:500	R&D System	AF1857	WB
		1:100			IF
Vimentin	Rabbit	1:1000	Abcam	Ab92549	IF
F4/80	Rat	1:100	BioRad	MCA497GA	IF
p62	Rabbit	1:1000	Sigma	P0067	WB
		1:100			IF
Lc3b	Rabbit	1:100	Cell signalling	#2775	WB
β-actin	Mouse	1:10000	Sigma	A2228	WB
Gapdh	Mouse	1:1000	Santa Cruz Biotechnology	sc-32233	WB

Calreticulin	Rabbit	1:1000	Sigma	C4606	IF
phospho-S6RP (Ser235/236)	Rabbit	1:1000	Cell Signalling	#2211	WB
S6 Ribosomal Protein	Rabbit	1:1000	Cell Signalling	#2317	WB
HRP-conjuged secondary antibodies					
Sheep IgG	Donkey	1:7500	Abcam	ab6900	WB
Rabbit IgG	Donkey	1:7500	GE-Healthcare	NA934V	WB
Mouse IgG	Sheep	1:7500	GE-Healthcare	NA931V	WB
Goat IgG	Rabbit	1:7500	Agilent	P0449	WB
Fluorescent-conjuged secondary antibodies					
Rabbit IgG 488	Donkey	1:500	Thermofisher	A21206	IF
Rabbit IgG 594	Donkey	1:500	Thermofisher	A21207	IF
Rat IgG 488	Donkey	1:500	Thermofisher	A21208	IF
Rat IgG 594	Donkey	1:500	Thermofisher	A21209	IF
Goat IgG 488	Donkey	1:500	Thermofisher	A11055	IF

5.13 Primers

Table 7. List and sequences of primers used for *UMOD* and *Ccr2* genotyping.

Name	Primer forward (5' to 3')	Primer reverse (5' to 3')
***Umod* genotyping**		
***Umod* cDNA_F3**	GACAATGCTCAGGCTTCAGTG	
***Umod* cDNA_R2**		GTCCAGAGGGTAAGAGCATTC
***Umod* cDNA PstI**	AAACTGCAGACCTAACCCATCCTTGCCTTTG	
***Umod* cDNA R4**		AAGTAGTCGCCTTCTGTGTTG
***Ccr2* genotyping**		
***Ccr2* common**	ATGGCGCAAGGCTATTTG	
***Ccr2* wt**		GCCCACAAAACCAAAGATGA
***Ccr2* KO**		CTCGTGCTTTACGGTATCGC

Table 8. List and sequences of primers used for gene expression analysis.

Gene	Primer forward (5' to 3')	Primer reverse (5' to 3')	Species

Acox3	GCTCACTTCACAAGCCCTCT	TAGCAAACAAGCCAGCGGTA	mouse
Asns	CTGAAGAAGGCATTCAGGCCC	AAGATCACCACGCTGTCTGTG	mouse
Atf3	CAGAAGTCAGTGCGACCGCC	TCGCCGCCTCCTTTTCCTCTCA	mouse
Atl3	GTATCAGTGGCTGGTGCTTTTCG	ATCAGAGCCTCCTCGCCATGAA	mouse
Ccl2	TTCACCAGCAAGATGATCCCA	ACCTCTCTCTTGAGCTTGGTG	mouse
Ccl8	GCTGCTCATAGCTGTCCCTG	AGCTTTTCAGCACCCGAAGG	mouse
Ccl12	CATCAGTCCTCAGGTATTGGCTGGA	CTTGGGGTCAGCACAGATCTCCTT	mouse
Ccpg1	CCACGAAGATGAGCTGGATGGT	CAGTAACGGTCCAACACCTCTC	mouse
Ccr1	GCCCAGAAACAAAGTCTGTGTGGA	TGGCATGGAGTGGAGTCCCCAT	mouse
Ccr2	AGAGGGCATTGGATTCACCAC	AGTATGCCGTGGATGAACTGAG	mouse
Cd45	GTTCTGGGCTCCTTCCTCTT	GGAGACCAGGAAGTCTGTGC	mouse
Ccr5	GTGAGACATCCGTTCCCCCTACA	AGGAGCTGAGCCGCAATTTGT	mouse
Cd68	CTGACAAGGGACACTTCGGG	AGGCCAATGATGAGAGGCAG	mouse
Cyp4b1	CCAGCTCAGCAAGCCAGTAA	GTGGGTCAAAGACCTCTGGG	mouse
Ehhadh	ACCACTGGCTTCTGGTATCG	GCCATAGTGATCTGTGGAGCA	mouse
Fam134b-1	CTGCTCACCTTCCTGGGTG	TTCCCAGCTTTCAGTGAGGC	mouse
Fam134b-2	CATAATAGTCCACTCCTCGGCTTC	CTCAGTCTGGCTCTTTCATCTG	mouse
Hprt1	CTGGTGAAAAGGACCTCTCGAAG	CCAGTTTCACTAATGACACAAACG	mouse
Lcn2	TCCCCCTGCAGCCAGACTTCC	AGTAGCGACAGCCCTGGTCCTG	mouse
Retreg1	AGACTGAGCCAGTGCATTGCAG	ACACTGCAGACCAGGAGGCAAA	mouse
Retreg2	CTCTGAGCTGTCAGATGAGGAG	TCTCGGTTCAGAGCCTCTTCTG	mouse
Retreg3	CTTCAGTGTCCGTGGCTACATG	CTGAGGACAGAAGGCAGCAAGT	mouse
Rtn3	CATAACCCTGACCCTACAACAC	GGAGCGTCTACTCTGTCCTTG	mouse
Sec62	TTCTACGTGCCAGAGGTGAAGG	GCGAACATCCAGGCTCACAGAA	mouse
Sqstm1	CGGCTTCCAGGCGCACTACC	CCACAGGCCCGTTGCAACCA	mouse
Tbp	AGCTCTGGAATTGTACCGCA	TGACTGCAGCAAATCGCTTG	mouse
Tex264	GTGTGGATCTATGACCCAGTTCA	CACCTACTCTCATTTCTGCTGGC	mouse
Umod	ATGGGGGTGACTTGTCCCGG	AATCGGGCCTGAGATGACTCG	mouse
Vim1	GGATCAGCTCACCAACGACA	GGTCAAGACGTGCCAGAGAA	mouse

5.14 Statistical Analysis

Data are expressed as mean ± standard deviation. Comparisons between the experimental groups were performed using two-tailed unpaired Student's *t*-test analysis, using as threshold of statistical significance a value of $P < 0.05$.

6. REFERENCES

Adam J, Bollée G, Fougeray S, Noël L-H, Antignac C, Knebelman B & Pallet N (2012) Endoplasmic Reticulum Stress in UMOD-Related Kidney Disease: A Human Pathologic Study. *American Journal of Kidney Diseases* 59: 117–121

Agarwal S, Sudhini YR, Polat OK, Reiser J & Altintas MM (2021) Renal cell markers: lighthouses for managing renal diseases. *American Journal of Physiology-Renal Physiology* 321: F715–F739

Akwo EA, Chen H-C, Liu G, Triozzi JL, Tao R, Yu Z, Chung CP, Giri A, Ikizler TA, Stein CM, *et al* (2022) Phenome-Wide Association Study of UMOD Gene Variants and Differential Associations With Clinical Outcomes Across Populations in the Million Veteran Program a Multiethnic Biobank. *Kidney Int Rep* 7: 1802–1818

Alelign T & Petros B (2018) Kidney Stone Disease: An Update on Current Concepts. *Adv Urol* 2018: 3068365

Alesutan I, Luong TTD, Schelski N, Masyout J, Hille S, Schneider MP, Graham D, Zickler D, Verheyen N, Estepa M, *et al* (2021) Circulating uromodulin inhibits vascular calcification by interfering with pro-inflammatory cytokine signalling. *Cardiovasc Res* 117: 930–941

Algharably EAH, Bolbrinker J, Lezius S, Reibis R, Wegscheider K, Völler H & Kreutz R (2017) Uromodulin associates with cardiorenal function in patients with hypertension and cardiovascular disease. *J Hypertens* 35: 2053–2058

Almeida LF, Tofteng SS, Madsen K & Jensen BL (2020) Role of the renin–angiotensin system in kidney development and programming of adult blood pressure. *Clin Sci* 134: 641–656

An H, Ordureau A, Paulo JA, Shoemaker CJ, Denic V & Harper JW (2019) TEX264 Is an Endoplasmic Reticulum-Resident ATG8-Interacting Protein Critical for ER Remodeling during Nutrient Stress. *Mol Cell* 74: 891-908.e10

Arumugam T v., Phillips TM, Cheng A, Morrell CH, Mattson MP & Wan R (2010) Age and energy intake interact to modify cell stress pathways and stroke outcome. *Ann Neurol* 67: 41–52

Awad AS, Kinsey GR, Khutsishvili K, Gao T, Bolton WK & Okusa MD (2011) Monocyte/macrophage chemokine receptor CCR2 mediates diabetic renal injury. *American Journal of Physiology-Renal Physiology* 301: F1358–F1366

Ayasreh N, Bullich G, Miquel R, Furlano M, Ruiz P, Lorente L, Valero O, García-González MA, Arhda N, Garin I, *et al* (2018) Autosomal Dominant Tubulointerstitial Kidney Disease: Clinical Presentation of Patients With ADTKD-UMOD and ADTKD-MUC1. *American Journal of Kidney Diseases* 72: 411–418

Bachmann S, Koeppen-Hagemann I & Kriz W (1985) Ultrastructural localization of Tamm-Horsfall glycoprotein (THP) in rat kidney as revealed by protein A-gold immunocytochemistry. *Histochemistry* 83: 531–538

Bachmann S, Mutig K, Bates J, Welker P, Geist B, Gross V, Luft FC, Alenina N, Bader M, Thiele BJ, *et al* (2005) Renal effects of Tamm-Horsfall protein (uromodulin) deficiency in mice. *Am J Physiol Renal Physiol* 288: F559-67

Bakos E, Thaiss CA, Kramer MP, Cohen S, Radomir L, Orr I, Kaushansky N, Ben-Nun A, Becker-Herman S & Shachar I (2017) CCR2 Regulates the Immune Response by Modulating the Interconversion and Function of Effector and Regulatory T Cells. *The Journal of Immunology* 198: 4659–4671

Bates JM, Raffi HM, Prasadan K, Mascarenhas R, Laszik Z, Maeda N, Hultgren SJ & Kumar S (2004) Tamm-Horsfall protein knockout mice are more prone to urinary tract infection Rapid Communication. *Kidney Int* 65: 791–797

Bayer ME (1964) AN ELECTRON MICROSCOPE EXAMINATION OF URINARY MUCOPROTEIN AND ITS INTERACTION WITH INFLUENZA VIRUS. *Journal of Cell Biology* 21: 265–274

Beck BB, Trachtman H, Gitman M, Miller I, Sayer JA, Pannes A, Baasner A, Hildebrandt F & Wolf MTF (2011) Autosomal Dominant Mutation in the Signal Peptide of Renin in a Kindred With Anemia, Hyperuricemia, and CKD. *American Journal of Kidney Diseases* 58: 821–825

Benting JH, Rietveld AG & Simons K (1999) N-Glycans Mediate the Apical Sorting of a Gpi-Anchored, Raft-Associated Protein in Madin-Darby Canine Kidney Cells. *Journal of Cell Biology* 146: 313–320

Bernascone I, Janas S, Ikehata M, Trudu M, Corbelli A, Schaeffer C, Rastaldi MP, Devuyst O & Rampoldi L (2010) A transgenic mouse model for uromodulin-associated kidney diseases shows specific tubulo-interstitial damage, urinary concentrating defect and renal failure. *Hum Mol Genet* 19: 2998–3010

Bernascone I, Vavassori S, di Pentima A, Santambrogio S, Lamorte G, Amoroso A, Scolari F, Ghiggeri GM, Casari G, Polishchuk R, *et al* (2006) Defective intracellular trafficking of uromodulin mutant isoforms. *Traffic* 7: 1567–1579

Bingham C, Ellard S, van't Hoff WG, Simmonds HA, Marinaki AM, Badman MK, Winocour PH, Stride A, Lockwood CR, Nicholls AJ, *et al* (2003) Atypical familial juvenile hyperuricemic nephropathy associated with a hepatocyte nuclear factor-1β gene mutation. *Kidney Int* 63: 1645–1651

Bjørkøy G, Lamark T, Pankiv S, Øvervatn A, Brech A & Johansen T (2009) Chapter 12 Monitoring Autophagic Degradation of p62/SQSTM1. In pp 181–197.

Bleyer AJ, Hart TC, Shihabi Z, Robins V & Hoyer JR (2004) Mutations in the uromodulin gene decrease urinary excretion of Tamm-Horsfall protein. *Kidney Int* 66: 974–977

Bleyer AJ, Kidd K, Živná M & Kmoch S (2017) Autosomal Dominant Tubulointerstitial Kidney Disease. *Adv Chronic Kidney Dis* 24: 86–93

Bleyer AJ, Zivná M, Hulková H, Hodanová K, Vyletal P, Sikora J, Zivný J, Sovová J, Hart TC, Adams JN, *et al* (2010) Clinical and molecular characterization of a family with a dominant renin gene mutation and response to treatment with fludrocortisone. *Clin Nephrol* 74: 411–422

Blumenstiel B, DeFelice M, Birsoy O, Bleyer AJ, Kmoch S, Carter TA, Gnirke A, Kidd K, Rehm HL, Ronco L, *et al* (2016) Development and Validation of a Mass Spectrometry–Based Assay for the Molecular Diagnosis of Mucin-1 Kidney Disease. *The Journal of Molecular Diagnostics* 18: 566–571

Boder P, Mary S, Mark PB, Leiper J, Dominiczak AF, Padmanabhan S, Rampoldi L & Delles C (2021) Mechanistic interactions of uromodulin with the thick ascending limb: perspectives

in physiology and hypertension. *J Hypertens* 39: 1490–1504 doi:10.1097/HJH.0000000000002861 [PREPRINT]

Bokhove M, Nishimura K, Brunati M, Han L, de Sanctis D, Rampoldi L & Jovine L (2016) A structured interdomain linker directs self-polymerization of human uromodulin. *Proceedings of the National Academy of Sciences* 113: 1552–1557

Bolar NA, Golzio C, Živná M, Hayot G, Van Hemelrijk C, Schepers D, Vandeweyer G, Hoischen A, Huyghe JR, Raes A, *et al* (2016) Heterozygous Loss-of-Function SEC61A1 Mutations Cause Autosomal-Dominant Tubulo-Interstitial and Glomerulocystic Kidney Disease with Anemia. *The American Journal of Human Genetics* 99: 174–187

Bollée G, Dahan K, Flamant M, Morinière V, Pawtowski A, Heidet L, Lacombe D, Devuyst O, Pirson Y, Antignac C, *et al* (2011) Phenotype and Outcome in Hereditary Tubulointerstitial Nephritis Secondary to *UMOD* Mutations. *Clinical Journal of the American Society of Nephrology* 6: 2429–2438

Boring L, Gosling J, Chensue SW, Kunkel SL, Farese R v., Broxmeyer HE & Charo IF (1997) Impaired monocyte migration and reduced type 1 (Th1) cytokine responses in C-C chemokine receptor 2 knockout mice. *Journal of Clinical Investigation* 100: 2552–2561

Boring L, Gosling J, Monteclaro FS, Lusis AJ, Tsou C-L & Charo IF (1996) Molecular Cloning and Functional Expression of Murine JE (Monocyte Chemoattractant Protein 1) and Murine Macrophage Inflammatory Protein 1α Receptors. *Journal of Biological Chemistry* 271: 7551–7558

Braga TT, Agudelo JSH & Camara NOS (2015) Macrophages During the Fibrotic Process: M2 as Friend and Foe. *Front Immunol* 6

Braga TT, Correa-Costa M, Silva RC, Cruz MC, Hiyane MI, da Silva JS, Perez KR, Cuccovia IM & Camara NOS (2018) CCR2 contributes to the recruitment of monocytes and leads to kidney inflammation and fibrosis development. *Inflammopharmacology* 26: 403–411

Brunati M, Perucca S, Han L, Cattaneo A, Consolato F, Andolfo A, Olinger E, Peng J, Santambrogio S, Perrier R, *et al* (2015) The serine protease hepsin mediates urinary secretion and polymerisation of Zona Pellucida domain protein uromodulin.

Cavallone D, Malagolini N & Serafini-Cessi F (2001) Mechanism of release of urinary Tamm-Horsfall glycoprotein from the kidney GPI-anchored counterpart. *Biochem Biophys Res Commun* 280: 110–4

Chaiyarit S & Thongboonkerd V (2022) Oxidized forms of uromodulin promote calcium oxalate crystallization and growth, but not aggregation. *Int J Biol Macromol* 214: 542–553

Chan SC, Zhang Y, Shao A, Avdulov S, Herrera J, Aboudehen K, Pontoglio M & Igarashi P (2018) Mechanism of Fibrosis in *HNF1B* -Related Autosomal Dominant Tubulointerstitial Kidney Disease. *Journal of the American Society of Nephrology* 29: 2493–2509

Chen H-D, Yu C-C, Yang I-H, Hung C-C, Kuo M-C, Tarng D-C, Chang J-M & Hwang D-Y (2022) UMOD Mutations in Chronic Kidney Disease in Taiwan. *Biomedicines* 10: 2265

Chen W, Zhang Z, Zhang S, Zhu P, Ko JK-S & Yung KK-L (2021) MUC1: Structure, Function, and Clinic Application in Epithelial Cancers. *Int J Mol Sci* 22: 6567

Choi SW, Ryu OH, Choi SJ, Song IS, Bleyer AJ & Hart TC (2005) Mutant Tamm-Horsfall Glycoprotein Accumulation in Endoplasmic Reticulum Induces Apoptosis Reversed by Colchicine and Sodium 4-Phenylbutyrate. *Journal of the American Society of Nephrology* 16: 3006–3014

Chung HY, Kim DH, Bang E & Yu BP (2020) Impacts of Calorie Restriction and Intermittent Fasting on Health and Diseases: Current Trends. *Nutrients* 12: 2948

Chung KW & Chung HY (2019) The Effects of Calorie Restriction on Autophagy: Role on Aging Intervention. *Nutrients* 11: 2923

Cinque L, Leonibus C, Iavazzo M, Krahmer N, Intartaglia D, Salierno FG, de Cegli R, di Malta C, Svelto M, Lanzara C, *et al* (2020) MiT/ TFE factors control ER -phagy via transcriptional regulation of FAM 134B . *EMBO J* 39

Connor TM, Hoer S, Mallett A, Gale DP, Gomez-Duran A, Posse V, Antrobus R, Moreno P, Sciacovelli M, Frezza C, *et al* (2017) Mutations in mitochondrial DNA causing tubulointerstitial kidney disease. *PLoS Genet* 13: e1006620

Cormican S, Connaughton DM, Kennedy C, Murray S, Živná M, Kmoch S, Fennelly NK, O'Kelly P, Benson KA, Conlon ET, *et al* (2019) Autosomal dominant tubulointerstitial kidney disease (ADTKD) in Ireland. *Ren Fail* 41: 832–841

Cornec-Le Gall E, Olson RJ, Besse W, Heyer CM, Gainullin VG, Smith JM, Audrézet M-P, Hopp K, Porath B, Shi B, *et al* (2018) Monoallelic Mutations to DNAJB11 Cause Atypical Autosomal-Dominant Polycystic Kidney Disease. *The American Journal of Human Genetics* 102: 832–844

Cui Z, Li Y, Liu G & Jiang Y (2022) miR-103a-3p Silencing Ameliorates Calcium Oxalate Deposition in Rat Kidney by Activating the UMOD/TRPV5 Axis. *Dis Markers* 2022: 1–15

Dahan K, Devuyst O, Smaers M, Vertommen D, Loute G, Poux J-M, Viron B, Jacquot C, Gagnadoux M-F, Chauveau D, *et al* (2003) A Cluster of Mutations in the UMOD Gene Causes Familial Juvenile Hyperuricemic Nephropathy with Abnormal Expression of Uromodulin. *Journal of the American Society of Nephrology* 14: 2883–2893

Darisipudi MN, Thomasova D, Mulay SR, Brech D, Noessner E, Liapis H & Anders H-J (2012) Uromodulin Triggers IL-1β–Dependent Innate Immunity *via* the NLRP3 Inflammasome. *Journal of the American Society of Nephrology* 23: 1783–1789

Dawnay AB & Cattell WR (1981) Serum Tamm-Horsfall glycoprotein levels in health and in renal disease. *Clin Nephrol* 15: 5–8

Devuyst O, Olinger E & Rampoldi L (2017) Uromodulin: from physiology to rare and complex kidney disorders. *Nat Rev Nephrol* 13: 525–544

Devuyst O, Olinger E, Weber S, Eckardt KU, Kmoch S, Rampoldi L & Bleyer AJ (2019) Autosomal dominant tubulointerstitial kidney disease. *Nat Rev Dis Primers* 5 doi:10.1038/s41572-019-0109-9 [PREPRINT]

Donald ASR, Yates AD, Soh CPC, Morgan WTJ & Watkins WM (1983) A blood group Sda-active pentasaccharide isolated from Tamm-Horsfall urinary glycoprotein. *Biochem Biophys Res Commun* 115: 625–631

Dong D, Cai G, Ning Y, Wang J, Lv Y, Hong Q, Cui S, Fu B, Guo Y & Chen X (2017) Alleviation of senescence and epithelial-mesenchymal transition in aging kidney by short-term caloric restriction and caloric restriction mimetics via modulation of AMPK/mTOR signaling. *Oncotarget* 8: 16109–16121

Dong K, Zhang C, Tian X, Coman D, Hyder F, Ma M & Somlo S (2021) Renal plasticity revealed through reversal of polycystic kidney disease in mice. *Nat Genet* 53: 1649–1663

Dubois-Laforgue D, Cornu E, Saint-Martin C, Coste J, Bellanné-Chantelot C & Timsit J (2018) Response to Comment on Dubois-Laforgue et al. Diabetes, Associated Clinical Spectrum, Long-term Prognosis, and Genotype/Phenotype Correlations in 201 Adult Patients With Hepatocyte Nuclear Factor 1B (*HNF1B*) Molecular Defects. Diabetes Care 2017;40:1436–1443. *Diabetes Care* 41: e8–e9

Dvela-Levitt M, Kost-Alimova M, Emani M, Kohnert E, Thompson R, Sidhom E-H, Rivadeneira A, Sahakian N, Roignot J, Papagregoriou G, *et al* (2019) Small Molecule Targets TMED9 and Promotes Lysosomal Degradation to Reverse Proteinopathy. *Cell* 178: 521-535.e23

Dyer DP, Medina-Ruiz L, Bartolini R, Schuette F, Hughes CE, Pallas K, Vidler F, Macleod MKL, Kelly CJ, Lee KM, *et al* (2019) Chemokine Receptor Redundancy and Specificity Are Context Dependent. *Immunity* 50: 378-389.e5

Easton RL, Patankar MS, Clark GF, Morris HR & Dell A (2000) Pregnancy-associated Changes in the Glycosylation of Tamm-Horsfall Glycoprotein. *Journal of Biological Chemistry* 275: 21928–21938

Eckardt KU, Alper SL, Antignac C, Bleyer AJ, Chauveau D, Dahan K, Deltas C, Hosking A, Kmoch S, Rampoldi L, *et al* (2015) Autosomal dominant tubulointerstitial kidney disease: Diagnosis, classification, and management - A KDIGO consensus report. *Kidney Int* 88: 676–683

Econimo L, Schaeffer C, Zeni L, Cortinovis R, Alberici F, Rampoldi L, Scolari F & Izzi C (2022) Autosomal Dominant Tubulointerstitial Kidney Disease: An Emerging Cause of Genetic CKD. *Kidney Int Rep* 7: 2332–2344

Ehrnhoefer DE, Martin DDO, Schmidt ME, Qiu X, Ladha S, Caron NS, Skotte NH, Nguyen YTN, Vaid K, Southwell AL, *et al* (2018) Preventing mutant huntingtin proteolysis and intermittent fasting promote autophagy in models of Huntington disease. *Acta Neuropathol Commun* 6: 16

Ekici AB, Hackenbeck T, Morinière V, Pannes A, Buettner M, Uebe S, Janka R, Wiesener A, Hermann I, Grupp S, *et al* (2014) Renal fibrosis is the common feature of autosomal dominant tubulointerstitial kidney diseases caused by mutations in mucin 1 or uromodulin. *Kidney Int* 86: 589–599

El-Achkar TM, McCracken R, Liu Y, Heitmeier MR, Bourgeois S, Ryerse J & Wu X-R (2013) Tamm-Horsfall protein translocates to the basolateral domain of thick ascending limbs, interstitium, and circulation during recovery from acute kidney injury. *American Journal of Physiology-Renal Physiology* 304: F1066–F1075

El-Achkar TM & Wu X-R (2012) Uromodulin in Kidney Injury: An Instigator, Bystander, or Protector? *American Journal of Kidney Diseases* 59: 452–461

El-Achkar TM, Wu X-R, Rauchman M, McCracken R, Kiefer S & Dagher PC (2008) Tamm-Horsfall protein protects the kidney from ischemic injury by decreasing inflammation and altering TLR4 expression. *American Journal of Physiology-Renal Physiology* 295: F534–F544

Fedak D, Kuźniewski M, Fugiel A, Wieczorek-Surdacka E, Przepiórkowska-Hoyer B, Jasik P, Miarka P, Dumnicka P, Kapusta M, Solnica B, *et al* (2016) Serum uromodulin concentrations correlate with glomerular filtration rate in patients with chronic kidney disease. *Pol Arch Med Wewn* 126: 995–1004

Ferrè S & Igarashi P (2019) New insights into the role of HNF-1β in kidney (patho)physiology. *Pediatric Nephrology* 34: 1325–1335

Ferreira-Marques M, Carvalho A, Cavadas C & Aveleira CA (2021) PI3K/AKT/MTOR and ERK1/2-MAPK signaling pathways are involved in autophagy stimulation induced by caloric restriction or caloric restriction mimetics in cortical neurons. *Aging* 13: 7872–7882

Fleming A, Noda T, Yoshimori T & Rubinsztein DC (2011) Chemical modulators of autophagy as biological probes and potential therapeutics. *Nat Chem Biol* 7: 9–17

Fontana L, Ghezzi L, Cross AH & Piccio L (2021) Effects of dietary restriction on neuroinflammation in neurodegenerative diseases. *Journal of Experimental Medicine* 218

Fontana L & Partridge L (2015) Promoting Health and Longevity through Diet: From Model Organisms to Humans. *Cell* 161: 106–118

Fontana L, Partridge L & Longo VD (2010) Extending Healthy Life Span—From Yeast to Humans. *Science (1979)* 328: 321–326

Frade JM, Mellado M, del Real G, Gutierrez-Ramos JC, Lind P & Martinez-A C (1997) Characterization of the CCR2 chemokine receptor: functional CCR2 receptor expression in B cells. *J Immunol* 159: 5576–84

Fumagalli F, Noack J, Bergmann TJ, Cebollero E, Pisoni GB, Fasana E, Fregno I, Galli C, Loi M, Soldà T, *et al* (2016) Translocon component Sec62 acts in endoplasmic reticulum turnover during stress recovery. *Nat Cell Biol* 18: 1173–1184

Garimella PS, Bartz TM, Ix JH, Chonchol M, Shlipak MG, Devarajan P, Bennett MR & Sarnak MJ (2017) Urinary Uromodulin and Risk of Urinary Tract Infections: The Cardiovascular Health Study. *American Journal of Kidney Diseases* 69: 744–751

Gast C, Marinaki A, Arenas-Hernandez M, Campbell S, Seaby EG, Pengelly RJ, Gale DP, Connor TM, Bunyan DJ, Hodaňová K, *et al* (2018) Autosomal dominant tubulointerstitial kidney disease-UMOD is the most frequent non polycystic genetic kidney disease. *BMC Nephrol* 19: 301

Ghirotto S, Tassi F, Barbujani G, Pattini L, Hayward C, Vollenweider P, Bochud M, Rampoldi L & Devuyst O (2016) The uromodulin gene locus shows evidence of pathogen adaptation through human evolution. *Journal of the American Society of Nephrology* 27: 2983–2996

González-Rodríguez Á, Mayoral R, Agra N, Valdecantos MP, Pardo V, Miquilena-Colina ME, Vargas-Castrillón J, lo Iacono O, Corazzari M, Fimia GM, *et al* (2014) Impaired autophagic flux is associated with increased endoplasmic reticulum stress during the development of NAFLD. *Cell Death Dis* 5: e1179–e1179

GOTTSCHALK A (1952) Carbohydrate Residue of a Urine Mucoprotein inhibiting Influenza Virus Hæmagglutination. *Nature* 170: 662–663

Graham LA, Padmanabhan S, Fraser NJ, Kumar S, Bates JM, Raffi HS, Welsh P, Beattie W, Hao S, Leh S, *et al* (2014) Validation of Uromodulin as a Candidate Gene for Human Essential Hypertension. *Hypertension* 63: 551–558

Gregosa A, Vinuesa Á, Todero MF, Pomilio C, Rossi SP, Bentivegna M, Presa J, Wenker S, Saravia F & Beauquis J (2019) Periodic dietary restriction ameliorates amyloid pathology and cognitive impairment in PDAPP-J20 mice: Potential implication of glial autophagy. *Neurobiol Dis* 132: 104542

Gresh L, Fischer E, Reimann A, Tanguy M, Garbay S, Shao X, Hiesberger T, Fiette L, Igarashi P, Yaniv M, *et al* (2004) A transcriptional network in polycystic kidney disease. *EMBO J* 23: 1657–1668

Gribouval O, Gonzales M, Neuhaus T, Aziza J, Bieth E, Laurent N, Bouton JM, Feuillet F, Makni S, Amar H ben, *et al* (2005) Mutations in genes in the renin-angiotensin system are associated with autosomal recessive renal tubular dysgenesis. *Nat Genet* 37: 964–968

Groopman EE, Marasa M, Cameron-Christie S, Petrovski S, Aggarwal VS, Milo-Rasouly H, Li Y, Zhang J, Nestor J, Krithivasan P, *et al* (2019) Diagnostic Utility of Exome Sequencing for Kidney Disease. *New England Journal of Medicine* 380: 142–151

Gudbjartsson DF, Holm H, Indridason OS, Thorleifsson G, Edvardsson V, Sulem P, de Vegt F, d'Ancona FCH, den Heijer M, Franzson L, *et al* (2010) Association of Variants at UMOD with Chronic Kidney Disease and Kidney Stones—Role of Age and Comorbid Diseases. *PLoS Genet* 6: e1001039

Hai T, Wolfgang CD, Marsee DK, Allen AE & Sivaprasad U (1999) ATF3 and stress responses. *Gene Expr* 7: 321–35

Hajarnis SS, Patel V, Aboudehen K, Attanasio M, Cobo-Stark P, Pontoglio M & Igarashi P (2015) Transcription Factor Hepatocyte Nuclear Factor-1β (HNF-1β) Regulates MicroRNA-200 Expression through a Long Noncoding RNA. *Journal of Biological Chemistry* 290: 24793–24805

Hanisch F-G & Muller S (2000) MUC1: the polymorphic appearance of a human mucin. *Glycobiology* 10: 439–449

Hart TC (2002) Mutations of the UMOD gene are responsible for medullary cystic kidney disease 2 and familial juvenile hyperuricaemic nephropathy. *J Med Genet* 39: 882–892

Heidet L, Decramer S, Pawtowski A, Morinière V, Bandin F, Knebelmann B, Lebre A-S, Faguer S, Guigonis V, Antignac C, *et al* (2010) Spectrum of *HNF1B* Mutations in a Large Cohort of Patients Who Harbor Renal Diseases. *Clinical Journal of the American Society of Nephrology* 5: 1079–1090

Hidvegi T, Ewing M, Hale P, Dippold C, Beckett C, Kemp C, Maurice N, Mukherjee A, Goldbach C, Watkins S, *et al* (2010) An Autophagy-Enhancing Drug Promotes Degradation of Mutant α_1-Antitrypsin Z and Reduces Hepatic Fibrosis. *Science (1979)* 329: 229–232

Hiesberger T, Bai Y, Shao X, McNally BT, Sinclair AM, Tian X, Somlo S & Igarashi P (2004) Mutation of hepatocyte nuclear factor–1β inhibits Pkhd1 gene expression and produces renal cysts in mice. *Journal of Clinical Investigation* 113: 814–825

Hofer SJ, Davinelli S, Bergmann M, Scapagnini G & Madeo F (2021) Caloric Restriction Mimetics in Nutrition and Clinical Trials. *Front Nutr* 8

Horikawa Y, Iwasaki N, Hara M, Furuta H, Hinokio Y, Cockburn BN, Lindner T, Yamagata K, Ogata M, Tomonaga O, *et al* (1997) Mutation in hepatocyte nuclear factor–1β gene (TCF2) associated with MODY. *Nat Genet* 17: 384–385

Horsch M, Beckers J, Fuchs H, Rie Gailus-Durner V, Hrabě De Angelis M, Rathkolb B, Wolf E, Aigner B & Kemter E (2014) Uromodulin Retention in Thick Ascending Limb of Henle's Loop Affects SCD1 in Neighboring Proximal Tubule: Renal Transcriptome Studies in Mouse Models of Uromodulin-Associated Kidney Disease.

Horton JK, Davies M, Topley N, Thomas D & Williams JD (1990) Activation of the inflammatory response of neutrophils by Tamm-Horsfall glycoprotein. *Kidney Int* 37: 717–726

Imai T, Miyazaki H, Hirose S, Hori H, Hayashi T, Kageyama R, Ohkubo H, Nakanishi S & Murakami K (1983) Cloning and sequence analysis of cDNA for human renin precursor. *Proceedings of the National Academy of Sciences* 80: 7405–7409

Izzi C, Dordoni C, Econimo L, Delbarba E, Grati FR, Martin E, Mazza C, Savoldi G, Rampoldi L, Alberici F, *et al* (2020) Variable Expressivity of HNF1B Nephropathy, From Renal Cysts and Diabetes to Medullary Sponge Kidney Through Tubulo-interstitial Kidney Disease. *Kidney Int Rep* 5: 2341–2350

Johnsen M, Kubacki T, Yeroslaviz A, Späth MR, Mörsdorf J, Göbel H, Bohl K, Ignarski M, Meharg C, Habermann B, *et al* (2020) The Integrated RNA Landscape of Renal Preconditioning against Ischemia-Reperfusion Injury. *Journal of the American Society of Nephrology* 31: 716–730

Johnson BG, Dang LT, Marsh G, Roach AM, Levine ZG, Monti A, Reyon D, Feigenbaum L & Duffield JS (2017) Uromodulin p.Cys147Trp mutation drives kidney disease by activating ER stress and apoptosis. *Journal of Clinical Investigation* 127: 3954–3969

Jordan S, Tung N, Casanova-Acebes M, Chang C, Cantoni C, Zhang D, Wirtz TH, Naik S, Rose SA, Brocker CN, *et al* (2019) Dietary Intake Regulates the Circulating Inflammatory Monocyte Pool. *Cell* 178: 1102-1114.e17

Joseph CB, Mariniello M, Yoshifuji A, Schiano G, Lake J, Marten J, Richmond A, Huffman JE, Campbell A, Harris SE, *et al* (2022) Meta-GWAS Reveals Novel Genetic Variants Associated with Urinary Excretion of Uromodulin. *Journal of the American Society of Nephrology* 33: 511–529

Jovine L, Qi H, Williams Z, Litscher E & Wassarman PM (2002) The ZP domain is a conserved module for polymerization of extracellular proteins. *Nat Cell Biol* 4: 457–461

Kang HM, Ahn SH, Choi P, Ko Y-A, Han SH, Chinga F, Park ASD, Tao J, Sharma K, Pullman J, *et al* (2015) Defective fatty acid oxidation in renal tubular epithelial cells has a key role in kidney fibrosis development. *Nat Med* 21: 37–46

Kashyap S, Warner GM, Hartono SP, Boyilla R, Knudsen BE, Zubair AS, Lien K, Nath KA, Textor SC, Lerman LO, *et al* (2016) Blockade of CCR2 reduces macrophage influx and development of chronic renal damage in murine renovascular hypertension. *American Journal of Physiology-Renal Physiology* 310: F372–F384

Katsura K, Nakano Y, Zhang Y, Shemirani R, Li W & den Besten P (2022) WDR72 regulates vesicle trafficking in ameloblasts. *Sci Rep* 12: 2820

Katsuragi Y, Ichimura Y & Komatsu M (2015) p62/SQSTM1 functions as a signaling hub and an autophagy adaptor. *FEBS Journal* 282: 4672–4678

Kemter E, Fröhlich T, Arnold GJ, Wolf E & Wanke R (2017) Mitochondrial Dysregulation Secondary to Endoplasmic Reticulum Stress in Autosomal Dominant Tubulointerstitial Kidney Disease – UMOD (ADTKD-UMOD). *Sci Rep* 7: 42970

Kemter E, Prueckl P, Sklenak S, Rathkolb B, Habermann FA, Hans W, Gailus-Durner V, Fuchs H, Hrabě de Angelis M, Wolf E, *et al* (2013) Type of uromodulin mutation and allelic status influence onset and severity of uromodulin-associated kidney disease in mice. *Hum Mol Genet* 22: 4148–4163

Kemter E, Sklenak S, Rathkolb B, Hrabě de Angelis M, Wolf E, Aigner B & Wanke R (2014) No Amelioration of Uromodulin Maturation and Trafficking Defect by Sodium 4-Phenylbutyrate in Vivo. *Journal of Biological Chemistry* 289: 10715–10726

Khaminets A, Heinrich T, Mari M, Grumati P, Huebner AK, Akutsu M, Liebmann L, Stolz A, Nietzsche S, Koch N, *et al* (2015) Regulation of endoplasmic reticulum turnover by selective autophagy. *Nature* 522: 354–358

Kidd K, Vylet'al P, Schaeffer C, Olinger E, Živná M, Hodaňová K, Robins V, Johnson E, Taylor A, Martin L, *et al* (2020) Genetic and Clinical Predictors of Age of ESKD in Individuals With Autosomal Dominant Tubulointerstitial Kidney Disease Due to UMOD Mutations. *Kidney Int Rep* 5: 1472–1485

Kim Y, Wang Z, Li C, Kidd K, Wang Y, Johnson BG, Kmoch S, Morrissey JJ, Bleyer AJ, Duffield JS, *et al* (2021) Ultrabright plasmonic fluor nanolabel-enabled detection of a urinary ER stress biomarker in autosomal dominant tubulointerstitial kidney disease. *American Journal of Physiology-Renal Physiology* 321: F236–F244

Kirby A, Gnirke A, Jaffe DB, Barešová V, Pochet N, Blumenstiel B, Ye C, Aird D, Stevens C, Robinson JT, *et al* (2013) Mutations causing medullary cystic kidney disease type 1 lie in a large VNTR in MUC1 missed by massively parallel sequencing. *Nat Genet* 45: 299–303

Kitagawa K, Wada T, Furuichi K, Hashimoto H, Ishiwata Y, Asano M, Takeya M, Kuziel WA, Matsushima K, Mukaida N, *et al* (2004) Blockade of CCR2 Ameliorates Progressive Fibrosis in Kidney. *Am J Pathol* 165: 237–246

Klionsky DJ, Kamal Abdel-Aziz A, Abdelfatah S, Abdellatif M, Abdoli A, Abel S, Abeliovich H, Abildgaard MH, Princely Abudu Y, Acevedo-Arozena A, *et al* (2021) Guidelines for the use and interpretation of assays for monitoring autophagy (4th edition) 1

Knaup KX, Hackenbeck T, Popp B, Stoeckert J, Wenzel A, Büttner-Herold M, Pfister F, Schueler M, Seven D, May AM, *et al* (2018) Biallelic Expression of Mucin-1 in Autosomal Dominant Tubulointerstitial Kidney Disease: Implications for Nongenetic Disease Recognition. *Journal of the American Society of Nephrology* 29: 2298–2309

Kohno S, Shiozaki Y, Keenan AL, Miyazaki-Anzai S & Miyazaki M (2019) An N-terminal–truncated isoform of FAM134B (FAM134B-2) regulates starvation-induced hepatic selective ER-phagy. *Life Sci Alliance* 2: e201900340

Kökten T, Hansmannel F, Ndiaye NC, Heba A-C, Quilliot D, Dreumont N, Arnone D & Peyrin-Biroulet L (2021) Calorie Restriction as a New Treatment of Inflammatory Diseases. *Advances in Nutrition* 12: 1558–1570

Kompatscher A, de Baaij JHF, Aboudehen K, Hoefnagels APWM, Igarashi P, Bindels RJM, Veenstra GJC & Hoenderop JGJ (2017) Loss of transcriptional activation of the potassium channel Kir5.1 by HNF1β drives autosomal dominant tubulointerstitial kidney disease. *Kidney Int* 92: 1145–1156

Köttgen A, Glazer NL, Dehghan A, Hwang SJ, Katz R, Li M, Yang Q, Gudnason V, Launer LJ, Harris TB, *et al* (2009) Multiple loci associated with indices of renal function and chronic kidney disease. *Nat Genet* 41: 712–717

Köttgen A, Pattaro C, Böger CA, Fuchsberger C, Olden M, Glazer NL, Parsa A, Gao X, Yang Q, Smith A v, *et al* (2010) New loci associated with kidney function and chronic kidney disease. *Nat Genet* 42: 376–384

LaFavers KA, Macedo E, Garimella PS, Lima C, Khan S, Myslinski J, McClintick J, Witzmann FA, Winfree S, Phillips CL, *et al* (2019) Circulating uromodulin inhibits systemic oxidative stress by inactivating the TRPM2 channel. *Sci Transl Med* 11

LaFavers KA, Micanovic R, Sabo AR, Maghak LA & El-Achkar TM (2022) Evolving Concepts in Uromodulin Biology, Physiology, and Its Role in Disease: a Tale of Two Forms. *Hypertension* 79: 2409–2418

Laouari D, Burtin M, Phelep A, Martino C, Pillebout E, Montagutelli X, Friedlander G & Terzi F (2011) TGF-α Mediates Genetic Susceptibility to Chronic Kidney Disease. *Journal of the American Society of Nephrology* 22: 327–335

Lau W-H, Leong W-S, Ismail Z & Gam L-H (2008) Qualification and application of an ELISA for the determination of Tamm Horsfall Protein (THP) in human urine and its use for screening of Kidney Stone Disease. *Int J Biol Sci*: 215–222

Li Y, Cheng Y, Consolato F, Schiano G, Chong MR, Pietzner M, Nguyen NQH, Scherer N, Biggs ML, Kleber ME, *et al* (2022) Genome-wide studies reveal factors associated with circulating uromodulin and its relationships to complex diseases. *JCI Insight* 7

Linxweiler M, Schick B & Zimmermann R (2017) Let's talk about Secs: Sec61, Sec62 and Sec63 in signal transduction, oncology and personalized medicine. *Signal Transduct Target Ther* 2: 17002

Liu H, Ren H & Spear BT (2011a) The Mouse Alpha-Albumin (Afamin) Promoter Is Differentially Regulated by Hepatocyte Nuclear Factor 1α and Hepatocyte Nuclear Factor 1β. *DNA Cell Biol* 30: 137–147

Liu X, Strable MS & Ntambi JM (2011b) Stearoyl CoA Desaturase 1: Role in Cellular Inflammation and Stress. *Advances in Nutrition* 2: 15–22

Liu Y, El-Achkar TM & Wu X-R (2012) Tamm-Horsfall Protein Regulates Circulating and Renal Cytokines by Affecting Glomerular Filtration Rate and Acting as a Urinary Cytokine Trap. *Journal of Biological Chemistry* 287: 16365–16378

Liu Y, Goldfarb DS, El-Achkar TM, Lieske JC & Wu X-R (2018) Tamm-Horsfall protein/uromodulin deficiency elicits tubular compensatory responses leading to hypertension and hyperuricemia. *American Journal of Physiology-Renal Physiology* 314: F1062–F1076

Liu Y, Mo L, Goldfarb DS, Evan AP, Liang F, Khan SR, Lieske JC & Wu X-R (2010) Progressive renal papillary calcification and ureteral stone formation in mice deficient for Tamm-Horsfall protein. *American Journal of Physiology-Renal Physiology* 299: F469–F478

Loffing J, Loffing-Cueni D, Valderrabano V, Kläusli L, Hebert SC, Rossier BC, Hoenderop JGJ, Bindels RJM & Kaissling B (2001) Distribution of transcellular calcium and sodium transport pathways along mouse distal nephron. *American Journal of Physiology-Renal Physiology* 281: F1021–F1027

Longo VD & Anderson RM (2022) Nutrition, longevity and disease: From molecular mechanisms to interventions. *Cell* 185: 1455–1470

Lv W, Booz GW, Wang Y, Fan F & Roman RJ (2018) Inflammation and renal fibrosis: Recent developments on key signaling molecules as potential therapeutic targets. *Eur J Pharmacol* 820: 65–76

Ma L, Liu Y, El-Achkar TM & Wu XR (2012) Molecular and cellular effects of Tamm-Horsfall protein mutations and their rescue by chemical chaperones. *Journal of Biological Chemistry* 287: 1290–1305

Ma L, Liu Y, Landry NK, El-Achkar TM, Lieske JC & Wu XR (2017) Point mutation in D8C domain of Tamm-Horsfall protein/uromodulin in transgenic mice causes progressive renal damage and hyperuricemia. *PLoS One* 12

Mabillard H, Sayer JA & Olinger E (2021) Clinical and genetic spectra of autosomal dominant tubulointerstitial kidney disease. *Nephrology Dialysis Transplantation*

Madeo F, Carmona-Gutierrez D, Hofer SJ & Kroemer G (2019) Caloric Restriction Mimetics against Age-Associated Disease: Targets, Mechanisms, and Therapeutic Potential. *Cell Metab* 29: 592–610

Manzanero S, Gelderblom M, Magnus T & Arumugam T v (2011) Calorie restriction and stroke. *Exp Transl Stroke Med* 3: 8

Marakala V (2022) Neutrophil gelatinase-associated lipocalin (NGAL) in kidney injury - A systematic review. *Clin Chim Acta* 536: 135–141

Marshall JL, Noel T, Wang QS, Chen H, Murray E, Subramanian A, Vernon KA, Bazua-Valenti S, Liguori K, Keller K, *et al* (2022) High-resolution Slide-seqV2 spatial transcriptomics enables discovery of disease-specific cell neighborhoods and pathways. *iScience* 25

Maydan O, McDade PG, Liu Y, Wu X-R, Matsell DG & Eddy AA (2018) Uromodulin deficiency alters tubular injury and interstitial inflammation but not fibrosis in experimental obstructive nephropathy. *Physiol Rep* 6: e13654

McCallum L, Brooksbank K, McConnachie A, Aman A, Lip S, Dawson J, MacIntyre IM, MacDonald TM, Webb DJ & Padmanabhan S (2021) Rationale and Design of the Genotype-Blinded Trial of Torasemide for the Treatment of Hypertension (BHF UMOD). *Am J Hypertens* 34: 92–99

Mendel DB, Hansen LP, Graves MK, Conley PB & Crabtree GR (1991) HNF-1 alpha and HNF-1 beta (vHNF-1) share dimerization and homeo domains, but not activation domains, and form heterodimers in vitro. *Genes Dev* 5: 1042–1056

Micanovic R, Chitteti BR, Dagher PC, Srour EF, Khan S, Hato T, Lyle A, Tong Y, Wu X-R & El-Achkar TM (2015) Tamm-Horsfall Protein Regulates Granulopoiesis and Systemic Neutrophil Homeostasis. *Journal of the American Society of Nephrology* 26: 2172–2182

Micanovic R, Khan S, Janosevic D, Lee ME, Hato T, Srour EF, Winfree S, Ghosh J, Tong Y, Rice SE, *et al* (2018) Tamm-Horsfall Protein Regulates Mononuclear Phagocytes in the Kidney. *Journal of the American Society of Nephrology* 29: 841–856

Micanovic R, LaFavers KA, Patidar KR, Ghabril MS, Doud EH, Mosley AL, Sabo AR, Khan S & El-Achkar TM (2022) The kidney releases a nonpolymerizing form of uromodulin in the urine and circulation that retains the external hydrophobic patch domain. *American Journal of Physiology-Renal Physiology* 322: F403–F418

Mills KT, Stefanescu A & He J (2020) The global epidemiology of hypertension. *Nat Rev Nephrol* 16: 223–237

Mitchell JR, Verweij M, Brand K, van de Ven M, Goemaere N, van den Engel S, Chu T, Forrer F, Müller C, de Jong M, *et al* (2010) Short-term dietary restriction and fasting precondition against ischemia reperfusion injury in mice. *Aging Cell* 9: 40–53

Mo L, Liaw L, Evan AP, Sommer AJ, Lieske JC & Wu X-R (2007) Renal calcinosis and stone formation in mice lacking osteopontin, Tamm-Horsfall protein, or both. *American Journal of Physiology-Renal Physiology* 293: F1935–F1943

Mo L, Zhu X-H, Huang H-Y, Shapiro E, Hasty DL & Wu X-R (2004) Ablation of the Tamm-Horsfall protein gene increases susceptibility of mice to bladder colonization by type 1-fimbriated *Escherichia coli*. *American Journal of Physiology-Renal Physiology* 286: F795–F802

Mochida K & Nakatogawa H (2022) ER -phagy: selective autophagy of the endoplasmic reticulum . *EMBO Rep* 23

Mojaverrostami S, Pasbakhsh P, Madadi S, Nekoonam S, Zarini D, Noori L, Shiri E, Salama M, Zibara K & Kashani IR (2020) Calorie restriction promotes remyelination in a Cuprizone-Induced demyelination mouse model of multiple sclerosis. *Metab Brain Dis* 35: 1211–1224

Morris AP, Le TH, Wu H, Akbarov A, van der Most PJ, Hemani G, Smith GD, Mahajan A, Gaulton KJ, Nadkarni GN, *et al* (2019) Trans-ethnic kidney function association study reveals putative causal genes and effects on kidney-specific disease aetiologies. *Nat Commun* 10: 29

Moskowitz JL, Piret SE, Lhotta K, Kitzler TM, Tashman AP, Velez E, Thakker R v. & Kotanko P (2013) Association between Genotype and Phenotype in Uromodulin-Associated Kidney Disease. *Clinical Journal of the American Society of Nephrology* 8: 1349–1357

Muchmore A v. & Decker JM (1985) Uromodulin: A Unique 85-Kilodalton Immunosuppressive Glycoprotein Isolated from Urine of Pregnant Women. *Science (1979)* 229: 479–481

Müller L, Power Guerra N, Stenzel J, Rühlmann C, Lindner T, Krause BJ, Vollmar B, Teipel S & Kuhla A (2021) Long-Term Caloric Restriction Attenuates β-Amyloid Neuropathology and Is Accompanied by Autophagy in APPswe/PS1delta9 Mice. *Nutrients* 13: 985

Mutig K, Kahl T, Saritas T, Godes M, Persson P, Bates J, Raffi H, Rampoldi L, Uchida S, Hille C, *et al* (2011) Activation of the Bumetanide-sensitive Na+,K+,2Cl− Cotransporter (NKCC2) Is Facilitated by Tamm-Horsfall Protein in a Chloride-sensitive Manner. *Journal of Biological Chemistry* 286: 30200–30210

Nagano C, Morisada N, Nozu K, Kamei K, Tanaka R, Kanda S, Shiona S, Araki Y, Ohara S, Matsumura C, *et al* (2019) Clinical characteristics of HNF1B-related disorders in a Japanese population. *Clin Exp Nephrol* 23: 1119–1129

Niborski LL, Paces-Fessy M, Ricci P, Bourgeois A, Magalhães P, Kuzma-Kuzniarska M, Lesaulnier C, Reczko M, Declercq E, Zürbig P, *et al* (2021) *Hnf1b* haploinsufficiency differentially affects developmental target genes in a new renal cysts and diabetes mouse model. *Dis Model Mech* 14

Nie M, Bal MS, Liu J, Yang Z, Rivera C, Wu X-R, Hoenderop JGJ, Bindels RJM, Marciano DK & Wolf MTF (2018) Uromodulin regulates renal magnesium homeostasis through the ion channel transient receptor potential melastatin 6 (TRPM6). *Journal of Biological Chemistry* 293: 16488–16502

Nieto M, Navarro F, Perez-Villar JJ, del Pozo MA, González-Amaro R, Mellado M, Frade JM, Martínez-A C, López-Botet M & Sánchez-Madrid F (1998) Roles of chemokines and receptor polarization in NK-target cell interactions. *J Immunol* 161: 3330–9

Nijenhuis T, Hoenderop JGJ, van der Kemp AWCM & Bindels RJM (2003) Localization and Regulation of the Epithelial Ca $^{2+}$ Channel TRPV6 in the Kidney. *Journal of the American Society of Nephrology* 14: 2731–2740

Okorn C, Goertz A, Vester U, Beck BB, Bergmann C, Habbig S, König J, Konrad M, Müller D, Oh J, *et al* (2019) HNF1B nephropathy has a slow-progressive phenotype in childhood—with the exception of very early onset cases: results of the German Multicenter HNF1B Childhood Registry. *Pediatric Nephrology* 34: 1065–1075

Olden M, Corre T, Hayward C, Toniolo D, Ulivi S, Gasparini P, Pistis G, Hwang S-J, Bergmann S, Campbell H, *et al* (2014) Common Variants in *UMOD* Associate with Urinary Uromodulin Levels: A Meta-Analysis. *Journal of the American Society of Nephrology* 25: 1869–1882

Olinger E, Hofmann P, Kidd K, Dufour I, Belge H, Schaeffer C, Kipp A, Bonny O, Deltas C, Demoulin N, *et al* (2020) Clinical and genetic spectra of autosomal dominant tubulointerstitial kidney disease due to mutations in UMOD and MUC1. *Kidney Int* 98: 717–731

Olinger E, Schaeffer C, Kidd K, Elhassan EAE, Cheng Y, Dufour I, Schiano G, Mabillard H, Pasqualetto E, Hofmann P, *et al* (2022) An intermediate-effect size variant in *UMOD* confers risk for chronic kidney disease. *Proceedings of the National Academy of Sciences* 119

Ørskov I, Ferencz A & Ørskov F (1980) TAMM-HORSFALL PROTEIN OR UROMUCOID IS THE NORMAL URINARY SLIME THAT TRAPS TYPE 1 FIMBRIATED ESCHERICHIA COLI. *The Lancet* 315: 887

Otterpohl KL, Busselman BW, Ratnayake I, Hart RG, Hart KR, Evans CM, Phillips CL, Beach JR, Ahrenkiel P, Molitoris BA, *et al* (2020) Conditional Myh9 and Myh10 inactivation in adult mouse renal epithelium results in progressive kidney disease. *JCI Insight* 5

Padmanabhan S, Melander O, Johnson T, di Blasio AM, Lee WK, Gentilini D, Hastie CE, Menni C, Monti MC, Delles C, *et al* (2010) Genome-Wide Association Study of Blood Pressure Extremes Identifies Variant near UMOD Associated with Hypertension. *PLoS Genet* 6: e1001177

Pang S, Urquhart P & Hooper NM (2004) N-Glycans, not the GPI anchor, mediate the apical targeting of a naturally glycosylated, GPI-anchored protein in polarised epithelial cells. *J Cell Sci* 117: 5079–5086

Paragas N, Qiu A, Zhang Q, Samstein B, Deng S-X, Schmidt-Ott KM, Viltard M, Yu W, Forster CS, Gong G, *et al* (2011) The Ngal reporter mouse detects the response of the kidney to injury in real time. *Nat Med* 17: 216–222

Pattaro C, Köttgen A, Teumer A, Garnaas M, Böger CA, Fuchsberger C, Olden M, Chen M-H, Tin A, Taliun D, *et al* (2012) Genome-wide association and functional follow-up reveals new loci for kidney function. *PLoS Genet* 8: e1002584

Patton S, Gendler SJ & Spicer AP (1995) The epithelial mucin, MUC1, of milk, mammary gland and other tissues. *Biochimica et Biophysica Acta (BBA) - Reviews on Biomembranes* 1241: 407–423

Pennica D, Kohr WJ, Kuang W-J, Glaister D, Aggarwal BB, Chen EY & Goeddel D v. (1987) Identification of Human Uromodulin as the Tamm-Horsfall Urinary Glycoprotein. *Science (1979)* 236: 83–88

Pfaffl MW (2001) A new mathematical model for relative quantification in real-time RT-PCR. *Nucleic Acids Res* 29: 45e–445

Pfistershammer K, Klauser C, Leitner J, Stöckl J, Majdic O, Weichhart T, Sobanov Y, Bochkov V, Säemann M, Zlabinger G, *et al* (2008) Identification of the scavenger receptors SREC-I, Cla-1 (SR-BI), and SR-AI as cellular receptors for Tamm-Horsfall protein. *J Leukoc Biol* 83: 131–138

Piret SE, Olinger E, Reed AAC, Nesbit MA, Hough TA, Bentley L, Devuyst O, Cox R & Thakker R v. (2017) Mouse model for inherited renal fibrosis associated with endoplasmic reticulum stress. *Dis Model Mech*

Popp B, Ekici AB, Knaup KX, Schneider K, Uebe S, Park J, Bafna V, Meiselbach H, Eckardt K-U, Schiffer M, *et al* (2022) Prevalence of hereditary tubulointerstitial kidney diseases in the

German Chronic Kidney Disease study. *European Journal of Human Genetics* 30: 1413–1422

Porter KR & Tamm I (1955) Direct visualization of a mucoprotein component of urine. *J Biol Chem* 212: 135–40

Pruijm M, Ponte B, Ackermann D, Paccaud F, Guessous I, Ehret G, Pechère-Bertschi A, Vogt B, Mohaupt MG, Martin P-Y, *et al* (2016) Associations of Urinary Uromodulin with Clinical Characteristics and Markers of Tubular Function in the General Population. *Clinical Journal of the American Society of Nephrology* 11: 70–80

Raffi H, Bates JM, Laszik Z & Kumar S (2006) Tamm–Horsfall protein knockout mice do not develop medullary cystic kidney disease. *Kidney Int* 69: 1914–1915

Rampoldi L, Caridi G, Santon D, Boaretto F, Bernascone I, Lamorte G, Tardanico R, Dagnino M, Colussi G, Scolari F, *et al* (2003) Allelism of MCKD, FJHN and GCKD caused by impairment of uromodulin export dynamics. *Hum Mol Genet* 12: 3369–3384

Reggiori F & Molinari M (2022) ER-phagy: mechanisms, regulation, and diseases connected to the lysosomal clearance of the endoplasmic reticulum. *Physiol Rev* 102: 1393–1448

Renigunta A, Renigunta V, Saritas T, Decher N, Mutig K & Waldegger S (2011) Tamm-Horsfall Glycoprotein Interacts with Renal Outer Medullary Potassium Channel ROMK2 and Regulates Its Function. *Journal of Biological Chemistry* 286: 2224–2235

Rezende-Lima W, Parreira KS, García-González M, Riveira E, Banet JF & Lens XM (2004) Homozygosity for uromodulin disorders: FJHN and MCKD-type 2. *Kidney Int* 66: 558–563

Rhodes DC (2006) Importance of carbohydrate in the interaction of Tamm-Horsfall protein with complement 1q and inhibition of classical complement activation. *Immunol Cell Biol* 84: 357–365

Romero MC, Nocera S & Nesse AB (1997) Decreased Tamm-Horsfall protein in lithiasic patients. *Clin Biochem* 30: 63–67

van Rooijen JJM, Voskamp AF, Kamerling JP & Vliegenthart JFG (1999) Glycosylation sites and site-specific glycosylation in human Tamm-Horsfall glycoprotein. *Glycobiology* 9: 21–30

Saito H, Tanaka T, Tanaka S, Higashijima Y, Yamaguchi J, Sugahara M, Ito M, Uchida L, Hasegawa S, Wakashima T, *et al* (2018) Persistent expression of neutrophil gelatinase-associated lipocalin and M2 macrophage markers and chronic fibrosis after acute kidney injury. *Physiol Rep* 6: e13707

Saji T, Kikuchi R, Kusuhara H, Kim I, Gonzalez FJ & Sugiyama Y (2008) Transcriptional Regulation of Human and Mouse Organic Anion Transporter 1 by Hepatocyte Nuclear Factor 1 α/β. *Journal of Pharmacology and Experimental Therapeutics* 324: 784–790

Santambrogio S, Cattaneo A, Bernascone I, Schwend T, Jovine L, Bachi A & Rampoldi L (2008) Urinary uromodulin carries an intact ZP domain generated by a conserved C-terminal proteolytic cleavage. *Biochem Biophys Res Commun* 370: 410–413

Satanovskij R, Bader A, Block M, Herbst V, Schlumberger W, Haack T, Nockher WA, Heemann U, Renders L, Schmaderer C, *et al* (2017) A new missense mutation in UMOD gene leads to severely reduced serum uromodulin concentrations — A tool for the diagnosis of uromodulin-associated kidney disease. *Clin Biochem* 50: 155–158

Savige J & Harraka P (2021) Pathogenic Variants in the Genes Affected in Alport Syndrome (COL4A3–COL4A5) and Their Association With Other Kidney Conditions: A Review. *American Journal of Kidney Diseases* 78: 857–864

Schaeffer C, Cattaneo A, Trudu M, Santambrogio S, Bernascone I, Giachino D, Caridi G, Campo A, Murtas C, Benoni S, *et al* (2012) Urinary secretion and extracellular aggregation of mutant uromodulin isoforms. *Kidney Int* 81: 769–778

Schaeffer C, Devuyst O & Rampoldi L (2021) Uromodulin: Roles in Health and Disease. *Annual Review of Physiology Annu Rev Physiol 2021* 83: 477–501

Schaeffer C, Izzi C, Vettori A, Pasqualetto E, Cittaro D, Lazarevic D, Caridi G, Gnutti B, Mazza C, Jovine L, *et al* (2019) Autosomal Dominant Tubulointerstitial Kidney Disease with Adult Onset due to a Novel Renin Mutation Mapping in the Mature Protein. *Sci Rep* 9

Schaeffer C, Merella S, Pasqualetto E, Lazarevic D & Rampoldi L (2017) Mutant uromodulin expression leads to altered homeostasis of the endoplasmic reticulum and activates the unfolded protein response. *PLoS One* 12

Schaeffer C, Santambrogio S, Perucca S, Casari G & Rampoldi L (2009) Analysis of Uromodulin Polymerization Provides New Insights into the Mechanisms Regulating ZP Domain-mediated Protein Assembly. *Mol Biol Cell* 20: 589–599

Scherberich JE, Gruber R, Nockher WA, Christensen EI, Schmitt H, Herbst V, Block M, Kaden J & Schlumberger W (2018) Serum uromodulin—a marker of kidney function and renal parenchymal integrity. *Nephrology Dialysis Transplantation* 33: 284–295

Schiano G, Glaudemans B, Olinger E, Goelz N, Müller M, Loffing-Cueni D, Deschenes G, Loffing J & Devuyst O (2019) The Urinary Excretion of Uromodulin is Regulated by the Potassium Channel ROMK. *Sci Rep* 9: 19517

Schiano G, Lake J, Mariniello M, Schaeffer C, Harvent M, Rampoldi L, Olinger E & Devuyst O (2022) Allelic and Gene Dosage Effects Involving Uromodulin Aggregates Drive Autosomal Dominant Tubulointerstitial Kidney Disease. *bioRxiv*

Schmid M, Prajczer S, Gruber LN, Bertocchi C, Gandini R, Pfaller W, Jennings P & Joannidis M (2010) Uromodulin Facilitates Neutrophil Migration Across Renal Epithelial Monolayers. *Cellular Physiology and Biochemistry* 26: 311–318

Schneider CA, Rasband WS & Eliceiri KW (2012) NIH Image to ImageJ: 25 years of image analysis. *Nat Methods* 9: 671–675

Schubert D, Klein M-C, Hassdenteufel S, Caballero-Oteyza A, Yang L, Proietti M, Bulashevska A, Kemming J, Kühn J, Winzer S, *et al* (2018) Plasma cell deficiency in human subjects with heterozygous mutations in Sec61 translocon alpha 1 subunit (SEC61A1). *Journal of Allergy and Clinical Immunology* 141: 1427–1438

Schulz C-A, Engström G, Christensson A, Nilsson PM, Melander O & Orho-Melander M (2019) Genetic Predisposition for Renal Dysfunction and Incidence of CKD in the Malmö Diet and Cancer Study. *Kidney Int Rep* 4: 1143–1151

Scolari F, Caridi G, Rampoldi L, Tardanico R, Izzi C, Pirulli D, Amoroso A, Casari G & Ghiggeri GM (2004) Uromodulin storage diseases: Clinical aspects and mechanisms. *American Journal of Kidney Diseases* 44: 987–999

Selsby JT, Judge AR, Yimlamai T, Leeuwenburgh C & Dodd SL (2005) Life long calorie restriction increases heat shock proteins and proteasome activity in soleus muscles of Fisher 344 rats. *Exp Gerontol* 40: 37–42

Serafini-Cessi F, Malagolini N & Cavallone D (2003) Tamm-Horsfall glycoprotein: biology and clinical relevance. *American Journal of Kidney Diseases* 42: 658–676

Serafinicessi F, Malagolini N, Hoops TC & Rindler MJ (1993) Biosynthesis and Oligosaccharide Processing of Human Tamm-Horsfall Glycoprotein Permanently Expressed in HeLa Cells. *Biochem Biophys Res Commun* 194: 784–790

Serafini-Cessi F, Monti A & Cavallone D (2005) N-Glycans carried by Tamm-Horsfall glycoprotein have a crucial role in the defense against urinary tract diseases. *Glycoconj J* 22: 383–394

Sicking M, Živná M, Bhadra P, Barešová V, Tirincsi A, Hadzibeganovic D, Hodaňová K, Vyleťal P, Sovová J, Jedličková I, *et al* (2022) Phenylbutyrate rescues the transport defect of the Sec61α mutations V67G and T185A for renin. *Life Sci Alliance* 5: e202101150

Simons K & Ikonen E (1997) Functional rafts in cell membranes. *Nature* 387: 569–572

Sparks MA, Crowley SD, Gurley SB, Mirotsou M & Coffman TM (2014) Classical Renin-Angiotensin System in Kidney Physiology. In *Comprehensive Physiology* pp 1201–1228. Wiley

Spicer AP, Rowse GJ, Lidner TK & Gendler SJ (1995) Delayed Mammary Tumor Progression in Muc-1 Null Mice. *Journal of Biological Chemistry* 270: 30093–30101

Stanisich JJ, Zyla DS, Afanasyev P, Xu J, Kipp A, Olinger E, Devuyst O, Pilhofer M, Boehringer D & Glockshuber R (2020) The cryo-EM structure of the human uromodulin filament core reveals a unique assembly mechanism. *Elife* 9

van der Starre WE, van Nieuwkoop C, Thomson U, Zijderveld-Voshart MSM, Koopman JPR, van der Reijden TJK, van Dissel JT & van de Vosse E (2015) Urinary Proteins, Vitamin D and Genetic Polymorphisms as Risk Factors for Febrile Urinary Tract Infection and Relation with Bacteremia: A Case Control Study. *PLoS One* 10: e0121302

Steubl D, Block M, Herbst V, Nockher WA, Schlumberger W, Satanovskij R, Angermann S, Hasenau A-L, Stecher L, Heemann U, *et al* (2016) Plasma Uromodulin Correlates With Kidney Function and Identifies Early Stages in Chronic Kidney Disease Patients. *Medicine* 95: e3011

Stsiapanava A, Xu C, Brunati M, Zamora-Caballero S, Schaeffer C, Bokhove M, Han L, Hebert H, Carroni M, Yasumasu S, *et al* (2020) Cryo-EM structure of native human uromodulin, a zona pellucida module polymer. *EMBO J* 39

Stsiapanava A, Xu C, Nishio S, Han L, Yamakawa N, Carroni M, Tunyasuvunakool K, Jumper J, de Sanctis D, Wu B, *et al* (2022) Structure of the decoy module of human glycoprotein 2 and uromodulin and its interaction with bacterial adhesin FimH. *Nat Struct Mol Biol* 29: 190–193

Tamm I & Horsfall FL (1950) Characterization and Separation of an Inhibitor of Viral Hemagglutination Present in Urine. *Exp Biol Med* 74: 108–114

Tamm I & Horsfall FL (1952) A MUCOPROTEIN DERIVED FROM HUMAN URINE WHICH REACTS WITH INFLUENZA, MUMPS, AND NEWCASTLE DISEASE VIRUSES. *Journal of Experimental Medicine* 95: 71–97

Tang PM-K, Nikolic-Paterson DJ & Lan H-Y (2019) Macrophages: versatile players in renal inflammation and fibrosis. *Nat Rev Nephrol* 15: 144–158

Thomas DBL, Davies M & Williams JD (1993) Release of Gelatinase and Superoxide from Human Mononuclear Phagocytes in Response to Particulate Tamm Horsfall Protein

Thornley C, Dawnay A & Cattell WR (1985a) Human Tamm-Horsfall glycoprotein: urinary and plasma levels in normal subjects and patients with renal disease determined by a fully validated radioimmunoassay. *Clin Sci* 68: 529–535

Thornley C, Dawnay A & Cattell WR (1985b) Human Tamm-Horsfall glycoprotein: urinary and plasma levels in normal subjects and patients with renal disease determined by a fully validated radioimmunoassay. *Clin Sci* 68: 529–535

Tokonami N, Olinger E, Debaix H, Houillier P & Devuyst O (2018) The excretion of uromodulin is modulated by the calcium-sensing receptor. *Kidney Int* 94: 882–886

Torffvit O, Melander O & Hultén UL (2004) Urinary Excretion Rate of Tamm-Horsfall Protein Is Related to Salt Intake in Humans. *Nephron Physiol* 97: p31–p36

Trudu M, Janas S, Lanzani C, Debaix H, Schaeffer C, Ikehata M, Citterio L, Demaretz S, Trevisani F, Ristagno G, *et al* (2013) Common noncoding UMOD gene variants induce salt-sensitive hypertension and kidney damage by increasing uromodulin expression. *Nat Med* 19: 1655–1660

Trudu M, Schaeffer C, Riba M, Ikehata M, Brambilla P, Messa P, Martinelli-Boneschi F, Rastaldi MP & Rampoldi L (2017) Early involvement of cellular stress and inflammatory signals in the pathogenesis of tubulointerstitial kidney disease due to UMOD mutations. *Sci Rep* 7

Valluru MK, Chung NK, Gilchrist M, Butland L, Cook J, Takou A, Dixit A, Weedon MN & Ong ACM (2022) A founder *UMOD* variant is a common cause of hereditary nephropathy in the British population. *J Med Genet*: jmedgenet-2022-108704

Viau A, el Karoui K, Laouari D, Burtin M, Nguyen C, Mori K, Pillebout E, Berger T, Mak TW, Knebelmann B, *et al* (2010) Lipocalin 2 is essential for chronic kidney disease progression in mice and humans. *Journal of Clinical Investigation* 120: 4065–4076

Vylet'al P, Kublová M, Kalbáčová M, Hodaňová K, Barešová V, Stibůrková B, Sikora J, Hůlková H, živný J, Majewski J, *et al* (2006) Alterations of uromodulin biology: a common denominator of the genetically heterogeneous FJHN/MCKD syndrome. *Kidney Int* 70: 1155–1169

Walter P & Ron D (2011) The Unfolded Protein Response: From Stress Pathway to Homeostatic Regulation. *Science (1979)* 334: 1081–1086

Wang S-Y, Cai G-Y & Chen X-M (2018) Energy restriction in renal protection. *British Journal of Nutrition* 120: 1149–1158

Wang X, Chen J, Xu J, Xie J, Harris DCH & Zheng G (2021) The Role of Macrophages in Kidney Fibrosis. *Front Physiol* 12

Warner G, Hein KZ, Nin V, Edwards M, Chini CCS, Hopp K, Harris PC, Torres VE & Chini EN (2016) Food Restriction Ameliorates the Development of Polycystic Kidney Disease. *Journal of the American Society of Nephrology* 27: 1437–1447

Weiss GL, Stanisich JJ, Sauer MM, Lin CW, Eras J, Zyla DS, Trück J, Devuyst O, Aebi M, Pilhofer M, *et al* (2020) Architecture and function of human uromodulin filaments in urinary tract infections. *Science (1979)* 369: 1005–1010

Wenzel A, Altmueller J, Ekici AB, Popp B, Stueber K, Thiele H, Pannes A, Staubach S, Salido E, Nuernberg P, *et al* (2018) Single molecule real time sequencing in ADTKD-MUC1

allows complete assembly of the VNTR and exact positioning of causative mutations. *Sci Rep* 8: 4170

White GE, Iqbal AJ & Greaves DR (2013) CC Chemokine Receptors and Chronic Inflammation—Therapeutic Opportunities and Pharmacological Challenges. *Pharmacol Rev* 65: 47–89

Wiggins RC (1987) Uromucoid (Tamm-Horsfall glycoprotein) forms different polymeric arrangements on a filter surface under different physicochemical conditions. *Clinica Chimica Acta* 162: 329–340

Wolf MTF, Wu X-R & Huang C-L (2013) Uromodulin upregulates TRPV5 by impairing caveolin-mediated endocytosis. *Kidney Int* 84: 130–137

Wolf MTF, Zhang J & Nie M (2019) Uromodulin in mineral metabolism. *Curr Opin Nephrol Hypertens* 28: 481–489

Wopperer FJ, Knaup KX, Stanzick KJ, Schneider K, Jobst-Schwan T, Ekici AB, Uebe S, Wenzel A, Schliep S, Schürfeld C, *et al* (2022) Diverse molecular causes of unsolved autosomal dominant tubulointerstitial kidney diseases. *Kidney Int* 102: 405–420

Wuttke M, Li Y, Li M, Sieber KB, Feitosa MF, Gorski M, Tin A, Wang L, Chu AY, Hoppmann A, *et al* (2019) A catalog of genetic loci associated with kidney function from analyses of a million individuals. *Nat Genet* 51: 957–972

Wynn TA, Chawla A & Pollard JW (2013) Macrophage biology in development, homeostasis and disease. *Nature* 496: 445–455

Xia Y, Entman ML & Wang Y (2013) CCR2 Regulates the Uptake of Bone Marrow-Derived Fibroblasts in Renal Fibrosis. *PLoS One* 8

Xu L, Sharkey D & Cantley LG (2019) Tubular GM-CSF promotes late MCP-1/CCR2-mediated fibrosis and inflammation after ischemia/reperfusion injury. *Journal of the American Society of Nephrology* 30: 1825–1840

Yamamoto J, Kamata S, Miura A, Nagata T, Kainuma R & Ishii I (2015) Differential adaptive responses to 1- or 2-day fasting in various mouse tissues revealed by quantitative PCR analysis. *FEBS Open Bio* 5: 357–368

Yamamoto S, Kaimori J-Y, Yoshimura T, Namba T, Imai A, Kobayashi K, Imamura R, Ichimaru N, Kato K, Nakaya A, *et al* (2017) Analysis of an ADTKD family with a novel frameshift mutation in MUC1 reveals characteristic features of mutant MUC1 protein. *Nephrology Dialysis Transplantation* 32: 2010–2017

Yang J, Zeng P, Liu L, Yu M, Su J, Yan Y, Ma J, Hu W, Yang X, Han J, *et al* (2020) Food with calorie restriction reduces the development of atherosclerosis in apoE-deficient mice. *Biochem Biophys Res Commun* 524: 439–445

Yang L, Licastro D, Cava E, Veronese N, Spelta F, Rizza W, Bertozzi B, Villareal DT, Hotamisligil GS, Holloszy JO, *et al* (2016) Long-Term Calorie Restriction Enhances Cellular Quality-Control Processes in Human Skeletal Muscle. *Cell Rep* 14: 422–428

Yang Q, Wang Y, Pei G, Deng X, Jiang H, Wu J, Zhou C, Guo Y, Yao Y, Zeng R, *et al* (2019) Bone marrow-derived Ly6C− macrophages promote ischemia-induced chronic kidney disease. *Cell Death Dis* 10: 291

Ying W-Z & Sanders PW (1998) Dietary salt regulates expression of Tamm-Horsfall glycoprotein in rats. *Kidney Int* 54: 1150–1156

Yoshida T, Sugiura H, Mitobe M, Tsuchiya K, Shirota S, Nishimura S, Shiohira S, Ito H, Nobori K, Gullans SR, *et al* (2008) ATF3 protects against renal ischemia-reperfusion injury. *J Am Soc Nephrol* 19: 217–24

Zaidan M, Burtin M, Zhang JD, Blanc T, Barre P, Garbay S, Nguyen C, Vasseur F, Yammine L, Germano S, *et al* (2020) Signaling pathways predisposing to chronic kidney disease progression. *JCI Insight* 5

Zhang L, Xu H, Ding N, Li X, Chen X & Chen Z (2021) Beneficial Effects on Brain Micro-Environment by Caloric Restriction in Alleviating Neurodegenerative Diseases and Brain Aging. *Front Physiol* 12

Živná M, Hůlková H, Matignon M, Hodaňová K, Vylet'al P, Kalbáčová M, Barešová V, Sikora J, Blažková H, Živný J, *et al* (2009) Dominant Renin Gene Mutations Associated with Early-Onset Hyperuricemia, Anemia, and Chronic Kidney Failure. *The American Journal of Human Genetics* 85: 204–213

Živná M, Kidd K, Přistoupilová A, Barešová V, DeFelice M, Blumenstiel B, Harden M, Conlon P, Lavin P, Connaughton DM, *et al* (2018) Noninvasive Immunohistochemical Diagnosis and Novel *MUC1* Mutations Causing Autosomal Dominant Tubulointerstitial Kidney Disease. *Journal of the American Society of Nephrology* 29: 2418–2431

Živná M, Kidd K, Zaidan M, Vyleťal P, Barešová V, Hodaňová K, Sovová J, Hartmannová H, Votruba M, Trešlová H, *et al* (2020) An international cohort study of autosomal dominant tubulointerstitial kidney disease due to mutations identifies distinct clinical subtypes. *Kidney Int* 98: 1589–1604

APPENDIX

I. Effects of CR-30 on ADTKD-UMOD phenotype in male Tg^{UmodC147W} mice

I.1 Effect of CR-30 on uromodulin biology

We assessed the effect of 15 weeks of CR-30 on uromodulin expression and protein levels in kidneys of male Tg$^{Umod\text{C147W}}$ mice.

Western blot analysis revealed decreased levels of total uromodulin in Tg$^{Umod\text{C147W}}$ CR-30 mice, compared to Tg$^{Umod\text{C147W}}$ fed AL, that in turn show the expected increase compared to Tg$^{Umod\text{wt}}$, caused by mutant uromodulin intracellular accumulation (**Figure I.1A, B**). Also in male mice, the decrease in protein level is not due to down-regulation of *Umod* gene expression, that appeared on the contrary up-regulated in Tg$^{Umod\text{C147W}}$ mice upon calorie restriction (**Figure I.1C**). Confirming results obtained in female mice, decreased kidney levels of uromodulin in male Tg$^{Umod\text{C147W}}$ CR-30 mice is not reflected by increased urinary levels, suggesting that reduction of uromodulin accumulation caused by calorie restriction is not explained by increased secretion (**Figure I.1D, E**).

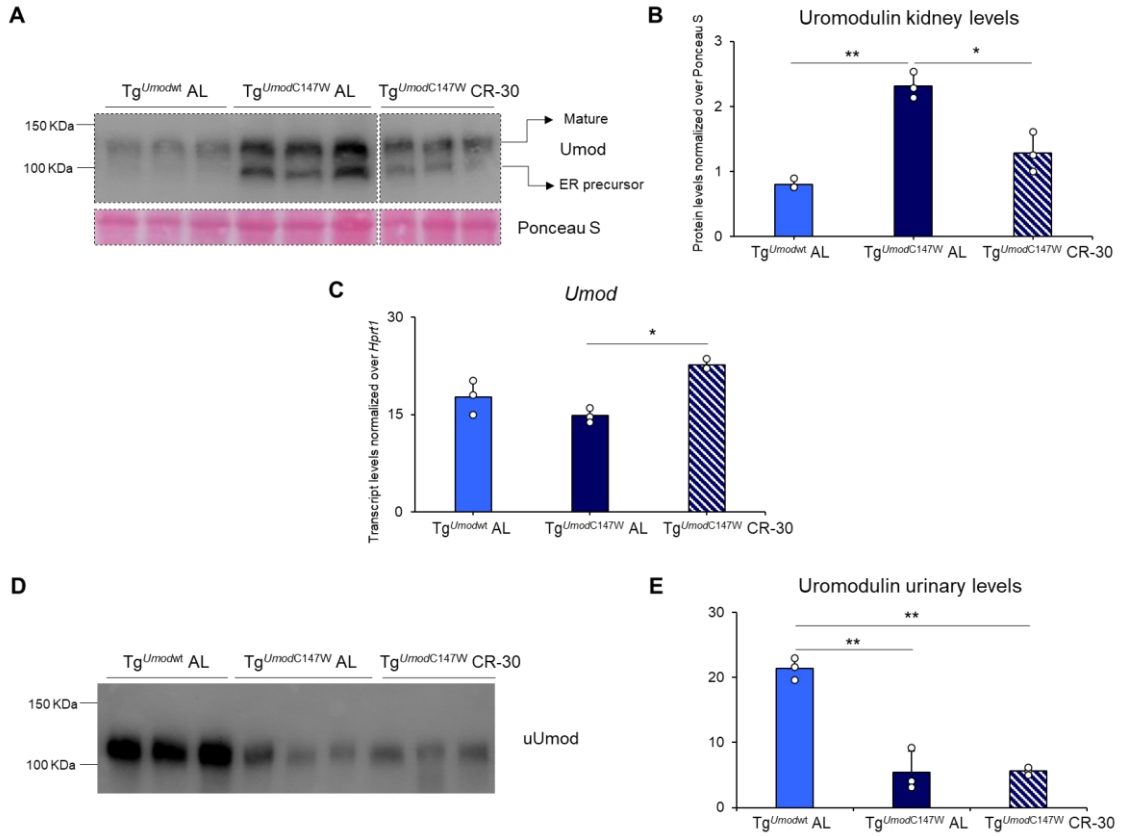


Figure I.1. Effect of CR-30 on uromodulin protein and transcript levels in male Tg^{UmodC147W} mice. *A) Analysis of uromodulin protein abundance in whole kidney homogenates of 23-week-old male Tg^{Umodwt} AL, Tg^{UmodC147W} AL and Tg^{UmodC147W} CR-30 mice. Images are cropped part of the same membrane. Ponceau S is reported as a loading control. B) Quantification of total uromodulin showing a reduction of uromodulin accumulation in kidneys of Tg^{UmodC147W} mice after 15 weeks of 30% CR. C) Gene expression analysis by real-time RT-qPCR suggests that reduction at protein level is not due to gene down-regulation, as Tg^{UmodC147W} CR-30 mice show instead increased Umod expression compared to age- and sex-matched Tg^{Umodwt} AL and Tg^{UmodC147W} AL mice. D) The same fraction of total urine volume collected from 23-week-old male Tg^{Umodwt} AL, Tg^{UmodC147W} AL and Tg^{UmodC147W} CR-30 mice the third day of metabolic cage were loaded on SDS-PAGE to perform Western blot analysis and E) quantification of uromodulin levels in urine (uUmod). Data are expressed as mean ± s.d. *P<0.05, **P<0.01 (unpaired t-test). N=3 animals/group.*

The ratio between ER precursor/fully glycosylated uromodulin was reduced in Tg^{Umod}C147W CR-30 mice, compared to Tg^{Umod}C147W AL mice, confirming also in male mice the effect of milder and prolonged CR protocol on mutant uromodulin ER retention (**Figure I.2A, B**). These biochemical data are consistent with immunofluorescence analysis, since colocalization of transgenic uromodulin with the ER marker calreticulin,

that is increased in Tg$^{Umod\text{C147W}}$ mice compared to Tg$^{Umod\text{wt}}$, is strongly reduced in TAL cells of mutant mice after CR (**Figure I.2C**).

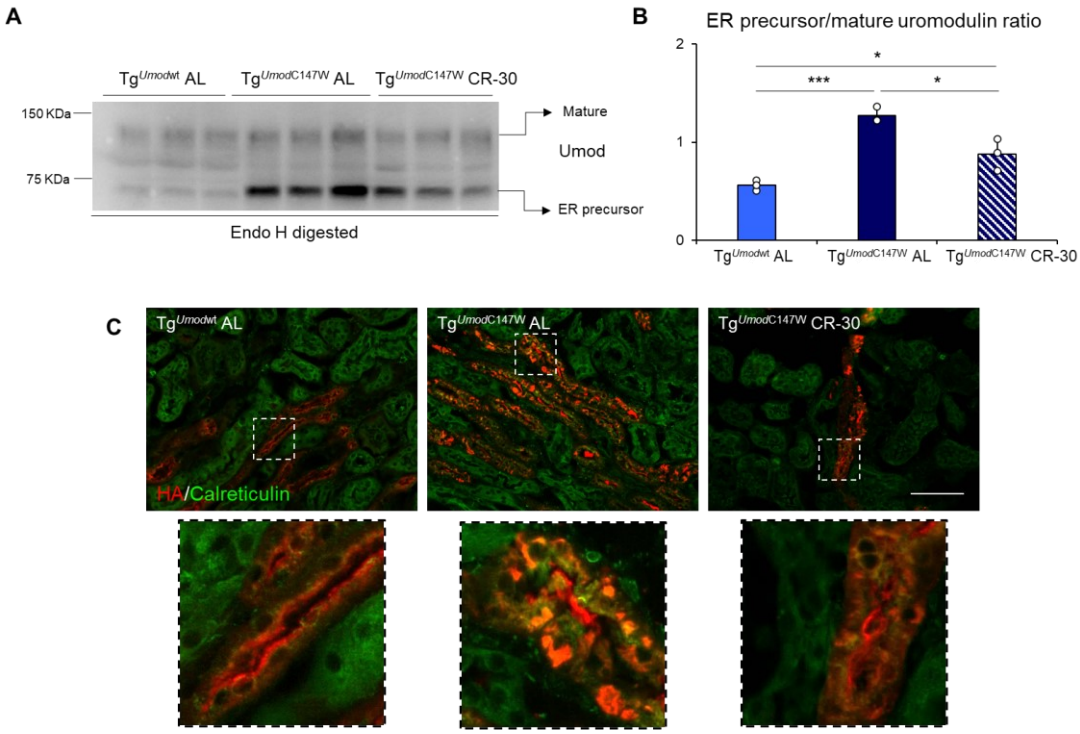


Figure I.2. Effect of CR-30 on mutant uromodulin ER retention in male Tg^{UmodC147W} mice. *A) Western blot in reducing conditions, showing total uromodulin, in kidney lysates of Tg^{Umodwt} AL, Tg^{UmodC147W} AL and Tg^{UmodC147W} mice. Lysates were subjected to enzymatic digestion by EndoH to separate the Endo H-sensitive uromodulin ER precursor (lower band) from the Endo H-insensitive fully glycosylated uromodulin (upper band). B) Quantification of the ratio between ER retained and mature uromodulin glycoforms. Data are expressed as mean ± s.d. *P<0.05, **P<0.01 (unpaired t-test). N=3 animals/group. C) Dual staining for transgenic uromodulin (HA, in red) and the ER marker calreticulin (in green) on kidney sections from Tg^{Umodwt} AL, Tg^{UmodC147W} AL and Tg^{UmodC147W} CR-30 mice. Bar = 100 µm.*

The reduction in protein retention in the ER correlates with a dramatic reduction of mutant uromodulin aggregates, as demonstrated by non-reducing Western blot of kidney lysates (**Figure I.3A**) and by immunofluorescence analysis of the transgenic protein (**Figure I.3B**). In both experiments, mutant uromodulin aggregates are clearly reduced in Tg$^{Umod\text{C147W}}$ CR-30 mice compared to AL ones.

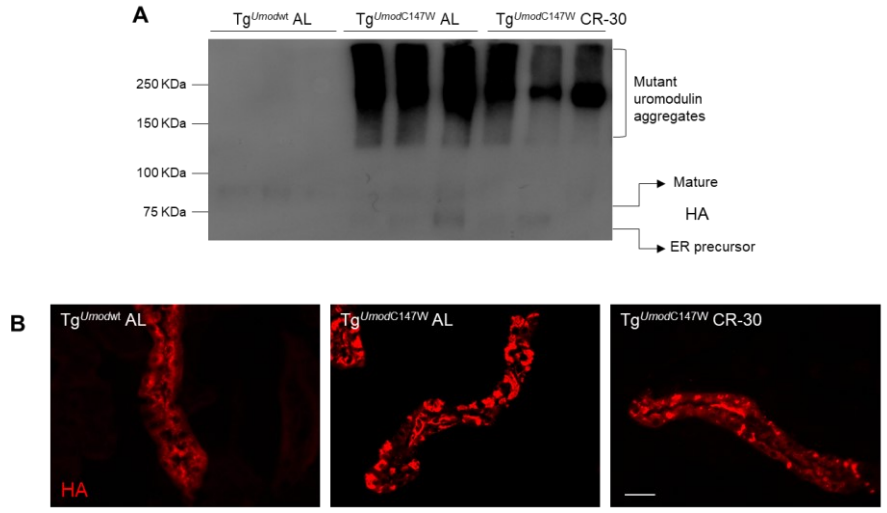


Figure I.3. Effect of CR-30 on mutant uromodulin aggregation in male Tg^{UmodC147W} mice. *A) Western blot analysis in non-reducing conditions and B) immunofluorescence analysis staining for transgenic protein (HA, in red) on kidney sections from Tg^{Umodwt} AL, Tg^{UmodC147W} AL and Tg^{UmodC147W} CR-30 mice. Bar = 100 µm. N=3 animals/group.*

I.2 Effect of CR-30 on kidney inflammation

We assessed the effect of the CR-30 protocol on inflammatory phenotype in male Tg$^{Umod\text{C147W}}$ mice by measuring the expression levels of genes related to inflammation, strongly induced in kidneys of our mouse model at this age.

As expected, markers of inflammatory cells (*Cd45* and *Cd68*) and pro-inflammatory chemokines (*Ccl2*, *Ccl12*) were indeed up-regulated in mutant animals fed AL, and their expression was significantly reduced to Tg$^{Umod\text{wt}}$ AL levels in Tg$^{Umod\text{C147W}}$ CR-30 mice (**Figure I.4A**).

Reduced inflammatory cell infiltration in kidneys of mice expressing mutant uromodulin upon calorie restriction was also demonstrated by decreased F4/80^{+} area (**Figure I.4B, C**) and by kidney histology (hematoxylin and eosin, H&E) showing clear reduction of infiltrating inflammatory cells in kidneys of Tg$^{Umod\text{C147W}}$ CR-30 mice compared to their AL counterpart (**Figure I.4D**).

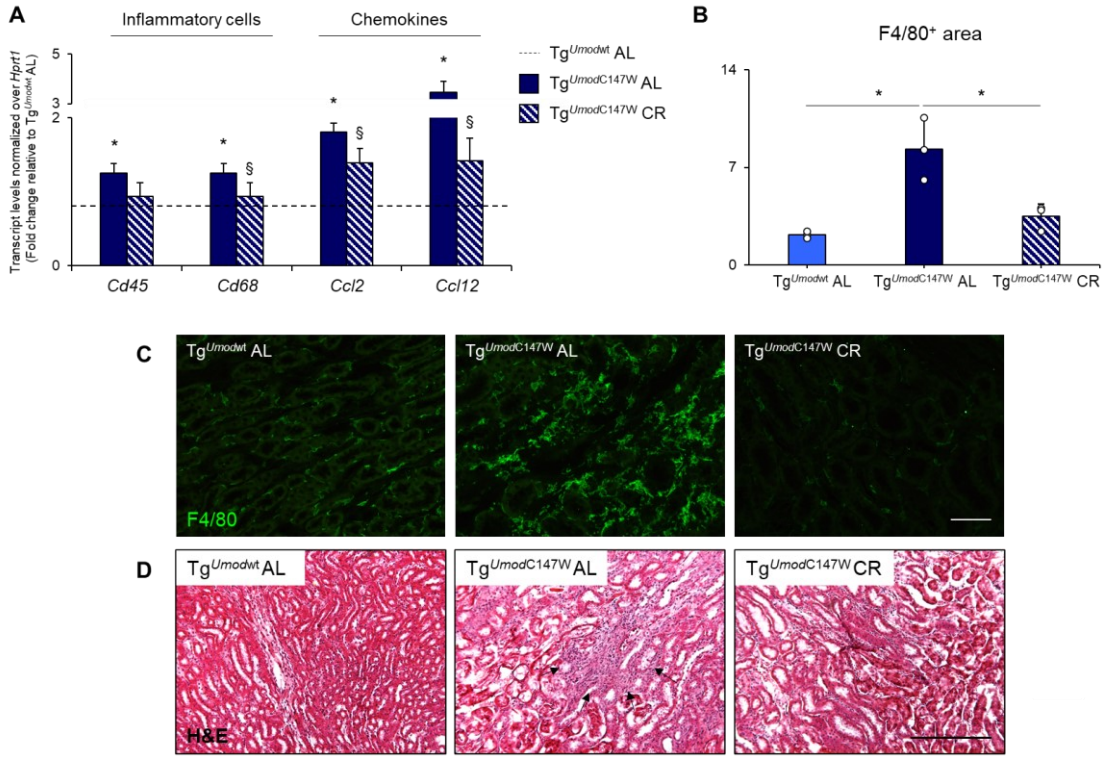


Figure I.4. Effect of CR-30 on kidney inflammation in male $Tg^{UmodC147W}$ mice. *A) Expression level of genes for inflammatory cells (Cd45, Cd68) and pro-inflammatory chemokines (Ccl2, Ccl12) in kidneys of 23-week-old male Tg^{Umodwt} AL, $Tg^{UmodC147W}$ AL and $Tg^{UmodC147W}$ CR-30 mice. Data are expressed as mean ± s.d. relative to Tg^{Umodwt} (dashed line) *P<0.05 vs Tg^{Umodwt}; §P<0.05 $Tg^{UmodC147W}$ AL vs $Tg^{UmodC147W}$ CR-30 (unpaired t-test). B) Quantification of F4/80+ area in the three experimental groups. Data are expressed as mean ± s.d. *P<0.05 (unpaired t-test). N=3 animals/group. C) Representative immunofluorescence staining for F4/80 in kidneys of Tg^{Umodwt}, $Tg^{UmodC147W}$ AL and $Tg^{UmodC147W}$ CR-30 mice. D) Representative histology images of H&E-stained kidney sections of Tg^{Umodwt}, $Tg^{UmodC147W}$ AL and $Tg^{UmodC147W}$ CR-30 mice. Black arrows indicate areas of increased inflammatory cells infiltration in $Tg^{UmodC147W}$ AL mice. Bar = 100 µm.*

All these results demonstrate that the CR-30 protocol is effective in reducing inflammation in kidneys of 23-week-old mice expressing mutant uromodulin.

I.3 Effect of CR-30 on kidney fibrosis

To evaluate fibrosis, we measured vimentin gene expression and protein levels in kidneys of Tg^{Umodwt} AL, $Tg^{UmodC147W}$ AL and $Tg^{UmodC147W}$ CR-30 mice. *Vim1* expression as well as vimentin deposition are increased in kidneys of male mutant mice AL, while they are reduced to levels comparable to wild type animals in $Tg^{UmodC147W}$ CR-30 mice (**Figure I.5A-C**). Amelioration of fibrosis was further demonstrated by Picrosirius red staining,

showing increased area of collagen deposition in kidney interstitium of 23-week-old Tg^{UmodC147W} AL that are reduced upon calorie restriction (**Figure I.5D**).

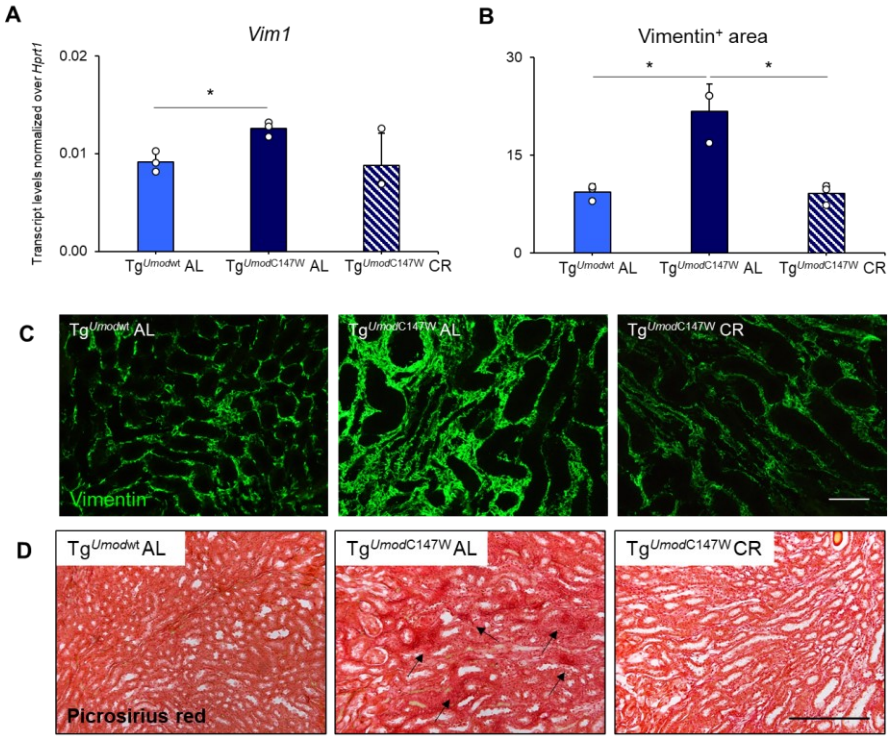


Figure I.5. Effect of CR-30 on kidney fibrosis in male Tg^{UmodC147W} mice. *A) Real-time RT-qPCR of Vim1, encoding for Vimentin, in kidneys of Tg^{Umodwt} AL, Tg^{UmodC147W} AL and Tg^{UmodC14W7} CR-30 mice. B) The graph summarizes quantification of Vimentin^{+} area in kidneys of Tg^{Umodwt} AL, Tg^{UmodC147W} AL and Tg^{UmodC147} CR-30 mice. Data are expressed as mean ± s.d. *P<0.05 (unpaired t-test). N=3 animals/group. C) Representative immunofluorescence staining for vimentin in kidneys of Tg^{Umodwt}, Tg^{UmodC147W} AL and Tg^{UmodC147W} CR-30 mice. D) Representative histological analysis staining collagens with Picrosirius red to assess degree of renal fibrosis. Black arrows indicate areas of increased collagens deposition in Tg^{UmodC147W} AL mice. Bar = 100 µm.*

To summarize, reduction of 30% of calorie intake ameliorated fibrotic phenotype in Tg^{UmodC147W} mice and recapitulated the effect obtained in female mice. This effect is likely secondary to effective reduction of kidney inflammation in CR-30 mutant mice.

I.4 Effect of CR-30 on tubular damage

Next, we studied lipocalin-2 to assess the effect of calorie restriction on tubular damage. Lcn2 expression in kidneys was measured by real-time RT-qPCR (**Figure I.6A**) and

Western blot analysis (**Figure I.6B, C**). Tubular damage is induced in mutant mice, compared to wild type, and is not reduced by calorie restriction. Nevertheless, immunofluorescence staining for Lcn2 in kidneys revealed strong reduction of Lcn2 signal in TAL cells expressing uromodulin in $Tg^{UmodC147W}$ CR-30 mice (**Figure I.6D**). These data are in line with previous observation showing that calorie restriction, by rescuing mutant uromodulin aggregation, attenuates cellular stress in TAL segments.

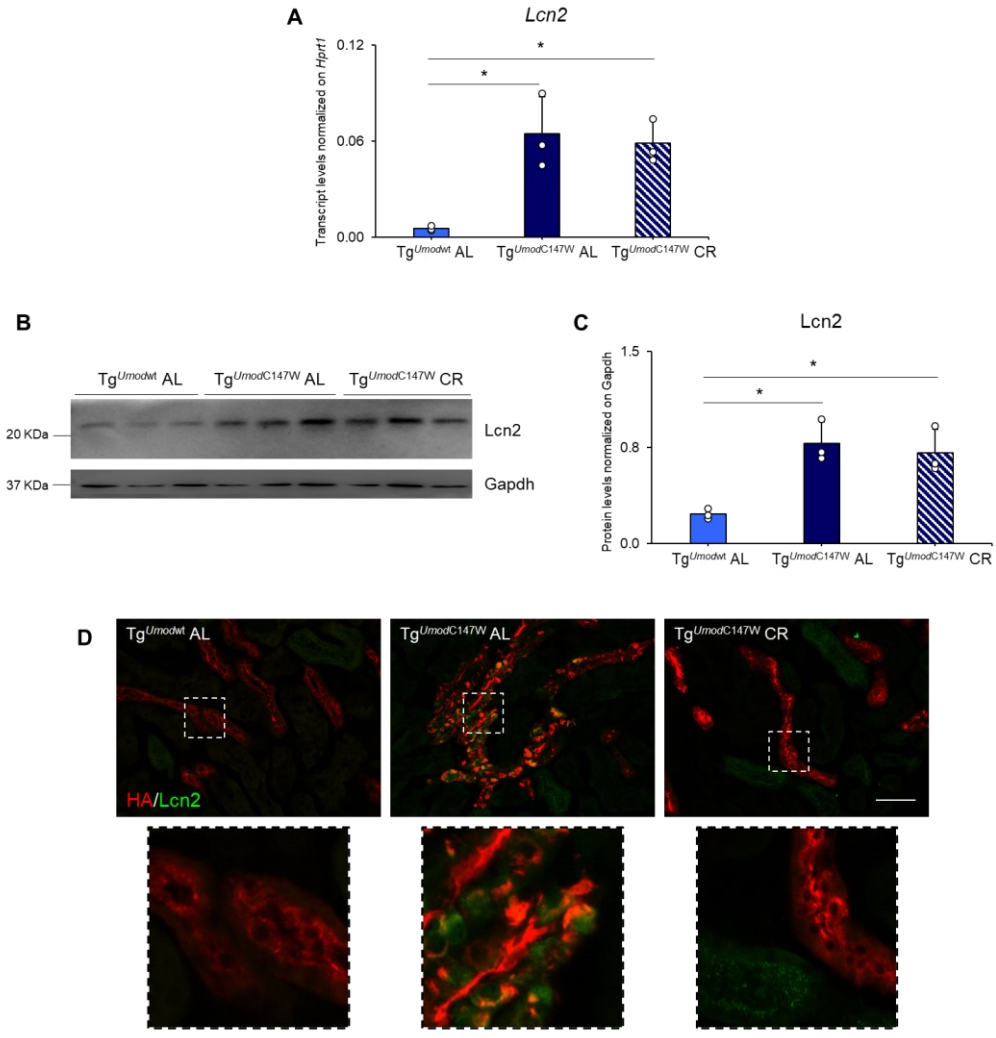


Figure I.6. Effect of CR-30 on tubular damage in male $Tg^{UmodC147W}$ mice. *A) Real-time RT-qPCR of Lcn2 expression levels in kidneys of Tg^{Umodwt}, $Tg^{UmodC147W}$ AL and $Tg^{UmodC147W}$ CR-30 mice. B) Western blot analysis showing increased Lcn2 levels in kidneys of $Tg^{UmodC147W}$ AL mice compared to wild type mice, that however are not reduced by CR. C) Histograms represent quantification of Lcn2 protein level normalized over Gapdh. Data are expressed as mean ± s.d. *P<0.05 (unpaired t-test). N=3 animals/group. D) Immunofluorescence staining showing that Lcn2 (in green) expression is strongly reduced in tubules expressing mutant uromodulin (HA, in*

red) in $Tg^{UmodC147W}$ CR-30 mice compared to their AL counterpart. Bar=100 μm. N=3 animals/group.

Although CR-30 did not reduce total Lcn2 to the levels of wild type animals, we did not observe any increase of its levels in kidneys of mutant mice as seen with the strong dietary restriction (55% CR). Instead we observed its decreased expression in uromodulin expressing cells.

I.5 Effect of CR-30 on kidney autophagy

We then focused on the molecular mechanisms induced by dietary restriction in kidneys of 23-week-old male $Tg^{Umod\text{C147W}}$ mice and leading to reduction of mutant uromodulin aggregates, focusing our attention on autophagy induction.

As observed in age-matched female mice, we detected increased Lc3-II/Lc3-I ratio in kidneys of 23-week-old mutant male mice relative to wild type, that was significantly reduced in $Tg^{Umod\text{C147W}}$ CR-30 mice (**Figure I.7A, B**). The strong accumulation of p62 puncta in cells expressing mutant uromodulin is clearly visible also in 23-weeks-old male $Tg^{Umod\text{C147W}}$ mice and its signal remained detectable only in few cells within TAL segments upon CR-30 (**Figure I.7C**).

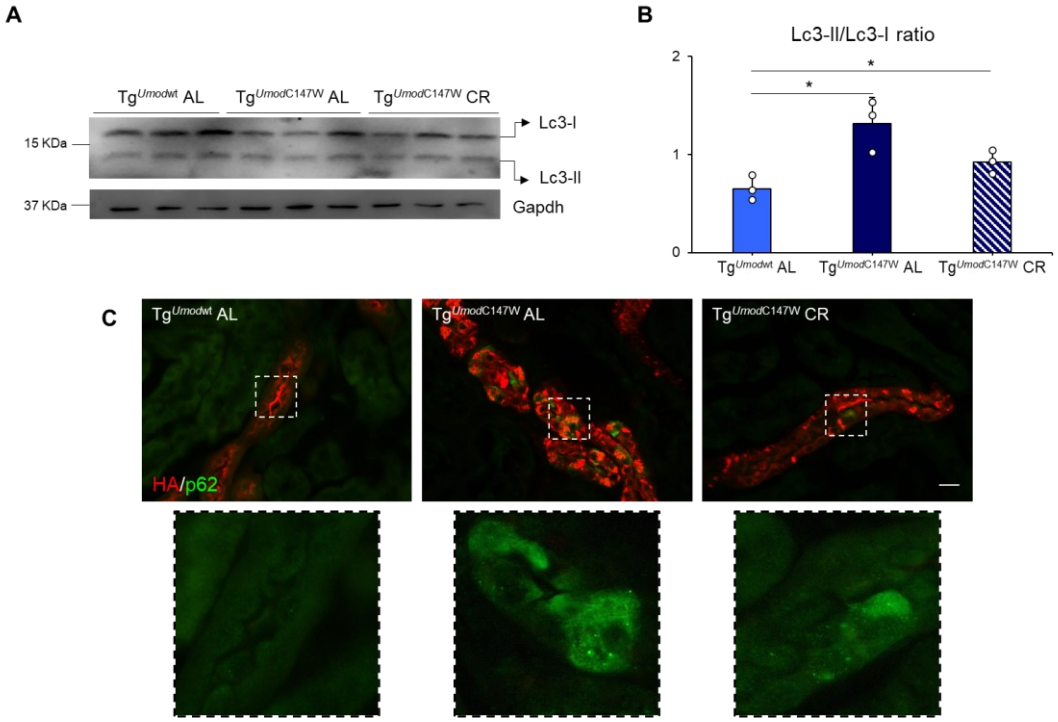


Figure I.7. Effect of CR-30 on autophagy in kidney of male Tg^{UmodC147W} mice. *A) Western blot for Lc3b (autophagosome marker) in kidneys lysates from Tg^{Umodwt} AL, Tg^{UmodC147W} AL and Tg^{UmodC147W} CR-30 animals. B) The histograms summarize the quantification of active (Lc3-II, lower band) to inactive Lc3 (Lc3-I, upper band) form in all the experimental groups. N=3 animals/group. Data are expressed as mean ± s.d. *P<0.05 (unpaired t-test). C) Immunofluorescence staining for p62 (in green) and transgenic uromodulin (HA, in red) in kidney sections from Tg^{Umodwt} AL, Tg^{UmodC147W} AL and Tg^{UmodC147W} CR-30 mice. Bar = 100 µm.*

Confirming what observed in female mice, these experiments suggest that 30% calorie restriction, likely by restoring autophagy in TAL cells, leads to degradation of mutant protein resulting in a decrease of mutant uromodulin ER retention and aggregation in Tg$^{Umod\text{C147W}}$ CR-30 mice.

I.6 Effect of CR-30 on kidney physiology

To evaluate the effect of 15 weeks of 30% dietary restriction on kidney physiology, we measured diuresis and urea nitrogen in blood samples from male Tg$^{Umod\text{wt}}$, Tg$^{Umod\text{C147W}}$ AL and Tg$^{Umod\text{C147W}}$ CR-30 mice.

23-week-old Tg$^{Umod\text{C147W}}$ male mice showed normal values of BUN and levels of diuresis comparable to what observed for age- and sex-matched wild type mice and both these parameters remained stable after 15 weeks of dietary restriction (**Figure I.8A, B**).

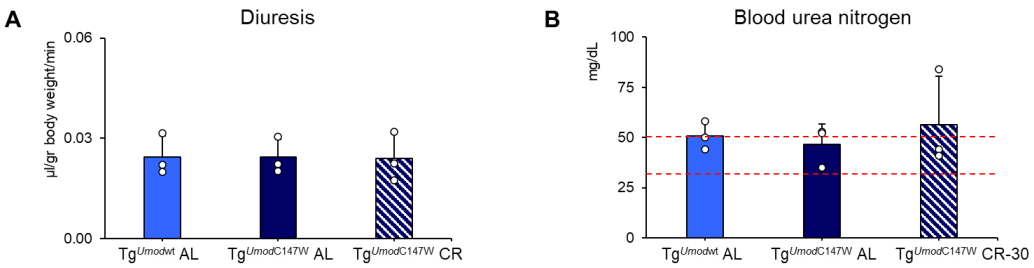


Figure I.8. Effect of CR-30 on kidney physiology of male Tg^{UmodC147W} mice. *A) Diuresis levels in 23-week-old male mice were calculated as volume of urine collected overnight normalized over mice body weight. B) Plasma urea nitrogen levels in blood samples collected from Tg^{Umodwt} AL, Tg^{UmodC147W} AL and Tg^{UmodC147W} CR-30 mice at the end of the calorie restriction protocol. Red dashed lines indicate the range of values considered as normal level of BUN (35-50 mg/dL). N=3 animals/group. Data are expressed as mean ± s.d. *P<0.05 (unpaired t-test).*

These results showed that kidney function is still preserved in male mutant mice at 23 weeks of age despite presence of inflammation and fibrosis. This confirmed the different degree of disease severity between male and female mutant mice in our model, that is likely due to different quantity of intracellularly accumulated mutant uromodulin.